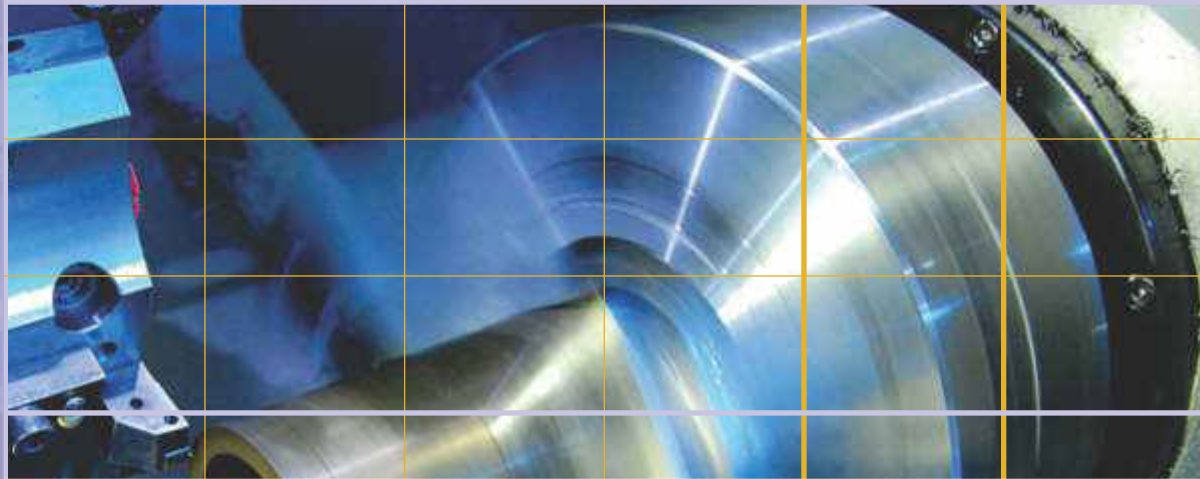


No. 4/2017

# HIDRAULICA

HYDRAULICS-PNEUMATICS-TRIBOLOGY-ECOLOGY-SENSORICS-MECHATRONICS



<http://hidraulica.fluidas.ro>



ISSN 1453 - 7303  
ISSN-L 1453 - 7303

## CONTENTS

<b>EDITORIAL: On criteria</b>	
Ph.D. <b>Petrin DRUMEA</b>	
<ul style="list-style-type: none"> <li>• <b>Optimal Shapes of the Cylindrical Pressurized Fuel Tanks</b></li> </ul>	6 - 17
Prof. PhD. Eng. <b>Marin BICĂ</b> , Assoc. Prof. PhD. Eng. <b>Mihai ȚĂLU</b> , Assoc. Prof. PhD. Eng. <b>Ștefan ȚĂLU</b>	
<ul style="list-style-type: none"> <li>• <b>Considerations on the Calculation of Ventilation Systems for Special Ships</b></li> </ul>	18 - 24
PhD std. Eng. <b>Octavian - Narcis VOLINTIRU</b> , Prof. PhD. Eng. <b>Anastase PRUIU</b> , PhD. Eng. <b>Ionut Cristian SCURTU</b>	
<ul style="list-style-type: none"> <li>• <b>Researches regarding the Behavior of CuAl10.5Ni5Fe4.8Mn1.5 at Erosion Generated by Vibratory Cavitation</b></li> </ul>	25 - 33
PhD. Student eng. <b>Iosif LAZAR</b> , Prof. PhD.eng. <b>Ilare BORDEASU</b> , Prof. PhD.eng. <b>Mircea O. POPOVICIU</b> , Lect. PhD.eng. <b>Lavinia Madalina MICU</b>	
<ul style="list-style-type: none"> <li>• <b>The Influence of Deviation from Circularity on the Stress of a Pressurized Fuel Cylindrical Tank</b></li> </ul>	34 - 45
Assoc. Prof. PhD. Eng. <b>Ștefan ȚĂLU</b> , Assoc. Prof. PhD. Eng. <b>Mihai ȚĂLU</b>	
<ul style="list-style-type: none"> <li>• <b>Distributed Hardware and Software Architecture for Monitoring and Control of Hydraulic Drives</b></li> </ul>	46 - 50
PhD.std. Eng. <b>Ioana ILIE</b> , PhD. Eng. <b>Marian BLEJAN</b>	
<ul style="list-style-type: none"> <li>• <b>Specific Methods for Acquiring Controlled Atmosphere for Clean Rooms Used in Industrial and Medical Domains</b></li> </ul>	51 - 56
Assistant professor <b>Fănel Dorel ȘCHEAUA</b>	
<ul style="list-style-type: none"> <li>• <b>The CAD Analyses of a Torospheric Head Cover of a Pressurized Cylindrical Fuel Tank after the Crash Test</b></li> </ul>	57 - 66
Prof. PhD. Eng. <b>Daniela VINTILĂ</b> , Assoc. Prof. PhD. Eng. <b>Mihai ȚĂLU</b> , Assoc. Prof. PhD. Eng. <b>Ștefan ȚĂLU</b>	
<ul style="list-style-type: none"> <li>• <b>Testing Means of Piston-Type Seals</b></li> </ul>	67 - 72
PhD. Eng. <b>Gabriela MATAACHE</b> , PhD. Eng. <b>Gheorghe ȘOVĂIALĂ</b> , Dipl. Eng. <b>Alina Iolanda POPESCU</b> , Res. Assist. <b>Ana-Maria POPESCU</b>	
<ul style="list-style-type: none"> <li>• <b>Operational Management with Application on Streamline Sewage Treatment Stations</b></li> </ul>	73 - 83
Prof. Dr. Eng. <b>Mariana PANAITESCU</b> , Prof. Dr. Eng. <b>Fanel-Viorel PANAITESCU</b>	
<ul style="list-style-type: none"> <li>• <b>Mobile Equipment for Testing the Power Steering of Cars</b></li> </ul>	84 - 88
Dipl. eng. <b>Alexandru HRISTEA</b> , PhD. eng. <b>Radu RĂDOI</b> , Dipl. eng. <b>Bogdan TUDOR</b> , Eng. <b>Ion BALAN</b>	
<ul style="list-style-type: none"> <li>• <b>The Influence of the Corrosion and Temperature on the Von Mises Stress in the Lateral Cover of a Pressurized Fuel Tank</b></li> </ul>	89 - 97
Assoc. Prof. PhD. Eng. <b>Mihai ȚĂLU</b>	
<ul style="list-style-type: none"> <li>• <b>Examining Fire Pump Metz FP 24/8 on Cavitation</b></li> </ul>	98 - 104
Assist. Prof. PhD. Stud. Eng. <b>Nikolett FECSER</b> , Assist. Prof. PhD. <b>Rajmund KUTI</b>	
<ul style="list-style-type: none"> <li>• <b>Electronic Control Module for Test Stand on the Production Line of Hydraulic Cylinders and Rotary Hydraulic Motors</b></li> </ul>	105 - 108
PhD. Eng. <b>Radu RĂDOI</b> , Dipl. Eng. <b>Alexandru HRISTEA</b> , Dipl. Eng. <b>Bogdan TUDOR</b> , PhD. Stud. Eng. <b>Mihai ALEXE</b>	
<ul style="list-style-type: none"> <li>• <b>Aspects regarding the Use of Digital Hydraulics in P.E.T. Waste Baling Presses</b></li> </ul>	109 - 114
Lect.Ph.D.Eng. <b>Iulian-Claudiu DUȚU</b> , Prof.Ph.D.Eng. <b>Sorin-Ștefan BIRIȘ</b> , Prof.Ph.D.Eng. <b>Edmond MAICAN</b>	
<ul style="list-style-type: none"> <li>• <b>Electronic Module for Data Acquisition and Transmitting for Portable Power Steering Test Equipment</b></li> </ul>	115 - 119
Dipl. Eng. <b>Alexandru HRISTEA</b> , PhD. Eng. <b>Radu RĂDOI</b> , Dipl. Eng. <b>Bogdan TUDOR</b> , Eng. <b>Ion BĂLAN</b>	

**BOARD****DIRECTOR OF PUBLICATION**

- PhD. Eng. Petrin DRUMEA - Hydraulics and Pneumatics Research Institute in Bucharest, Romania

**EDITOR-IN-CHIEF**

- PhD.Eng. Gabriela MATACHE - Hydraulics and Pneumatics Research Institute in Bucharest, Romania

**EXECUTIVE EDITOR, GRAPHIC DESIGN & DTP**

- Ana-Maria POPESCU - Hydraulics and Pneumatics Research Institute in Bucharest, Romania

**EDITORIAL BOARD**

PhD.Eng. Gabriela MATACHE - Hydraulics and Pneumatics Research Institute in Bucharest, Romania

Assoc. Prof. Adolfo SENATORE, PhD. – University of Salerno, Italy

PhD.Eng. Catalin DUMITRESCU - Hydraulics and Pneumatics Research Institute in Bucharest, Romania

Assoc. Prof. Andrei DRUMEA, PhD. – University Politehnica of Bucharest, Romania

PhD.Eng. Radu Iulian RADOI - Hydraulics and Pneumatics Research Institute in Bucharest, Romania

Assoc. Prof. Constantin RANEA, PhD. – University Politehnica of Bucharest; National Authority for Scientific Research and Innovation (ANCSI), Romania

Prof. Aurelian FATU, PhD. – Institute Pprime – University of Poitiers, France

PhD.Eng. Małgorzata MALEC – KOMAG Institute of Mining Technology in Gliwice, Poland

Prof. Mihai AVRAM, PhD. – University Politehnica of Bucharest, Romania

Lect. Ioan-Lucian MARCU, PhD. – Technical University of Cluj-Napoca, Romania

**COMMITTEE OF REVIEWERS**

PhD.Eng. Corneliu CRISTESCU – Hydraulics and Pneumatics Research Institute in Bucharest, Romania

Assoc. Prof. Pavel MACH, PhD. – Czech Technical University in Prague, Czech Republic

Prof. Ilare BORDEASU, PhD. – Politehnica University of Timisoara, Romania

Prof. Valeriu DULGHERU, PhD. – Technical University of Moldova, Chisinau, Republic of Moldova

Assist. Prof. Krzysztof KĘDZIA, PhD. – Wrocław University of Technology, Poland

Prof. Dan OPRUTA, PhD. – Technical University of Cluj-Napoca, Romania

PhD.Eng. Teodor Costinel POPESCU - Hydraulics and Pneumatics Research Institute in Bucharest, Romania

PhD.Eng. Marian BLEJAN - Hydraulics and Pneumatics Research Institute in Bucharest, Romania

Ph.D. Amir ROSTAMI – Georgia Institute of Technology, USA

Prof. Adrian CIOCANEA, PhD. – University Politehnica of Bucharest, Romania

Prof. Carmen-Anca SAFTA, PhD. - University Politehnica of Bucharest, Romania

Assoc. Prof. Mirela Ana COMAN, PhD. – Technical University of Cluj-Napoca, North University Center of Baia Mare, Romania

Prof. Ion PIRNA, PhD. – The National Institute of Research and Development for Machines and Installations Designed to Agriculture and Food Industry - INMA Bucharest, Romania

Assoc. Prof. Constantin CHIRITA, PhD. – “Gheorghe Asachi” Technical University of Iasi, Romania

**Published by:**

**Hydraulics and Pneumatics Research Institute, Bucharest-Romania**

Address: 14 Cuțitul de Argint, district 4, Bucharest, 040558, Romania

Phone: +40 21 336 39 91; Fax: +40 21 337 30 40; e-Mail: [ihp@fluidas.ro](mailto:ihp@fluidas.ro); Web: [www.ihp.ro](http://www.ihp.ro)

**with support from:**

**National Professional Association of Hydraulics and Pneumatics in Romania - FLUIDAS**

e-Mail: [fluidas@fluidas.ro](mailto:fluidas@fluidas.ro); Web: [www.fluidas.ro](http://www.fluidas.ro)

**HIDRAULICA Magazine** is indexed by international databases



ISSN 1453 – 7303; ISSN – L 1453 – 7303

## EDITORIAL

### On criteria

Many years ago, during my studentship, I was walking slowly together with a colleague towards the botanical garden. Suddenly, he shows me a car and tells me that it belongs to Professor X, the greatest specialist in combustion engines in our country and even in Europe. To my naive question, which were the engines designed and put into production by the great specialist, I received a rough answer, namely that the named Professor is a specialist, not a researcher or a technical designer.



Ph.D.Eng. Petrin DRUMEA  
MANAGING EDITOR

In the latest years I have found out to my surprise that the great engineers have papers written and published in some “quoted” journals, not patents or new products designed and put into production. Currently, the self-declared specialists of our domain hold no patents, no technical design projects, and they glare contempt at laboratory research and even worse at technical design, although on their diploma there is still written “engineer”. Basically, I would not mind this situation too much, but I am deeply disturbed by the fact that these “specialists” are extremely noisy, sometimes even aggressive, managing to impose their assessment criteria which state the supremacy of words on practical achievements. I am curious how A. Saligny or G. Constantinescu would now be appreciated.

Should we still be surprised by the fact that the economy and especially local industry continue to lower their technical level, that Romanian engineers leave the country to work abroad and the only hope relates to the possible penetration of foreign companies regarded as able to reconnect us to the international production circuit? I personally am not surprised by this course of things, I am just concerned. I would like that all the specialists in the field, from time to time, to be placed face-to-face with the specialized research laboratories and industrial level commissioning activities, and only after that they should afford to give advice, set criteria and assess research and researchers. Is it that difficult?

## Optimal Shapes of the Cylindrical Pressurized Fuel Tanks

Prof. PhD. Eng. **Marin BICĂ**<sup>1</sup>, Assoc. Prof. PhD. Eng. **Mihai ȚĂLU**<sup>2,\*</sup>,  
Assoc. Prof. PhD. Eng. **Ștefan ȚĂLU**<sup>3</sup>

<sup>1</sup> University of Craiova, Faculty of Mechanics, Department of Applied Mechanics and Civil Engineering, Calea București Street, no. 107, 200512 Craiova, Dolj county, Romania. E-mail: marinbica52@gmail.com

<sup>2</sup> University of Craiova, Faculty of Mechanics, Department of Applied Mechanics and Civil Engineering, Calea București Street, no. 107, 200512 Craiova, Dolj county, Romania. Corresponding author\* e-mail: mihai\_talu@yahoo.com

<sup>3</sup> Technical University of Cluj-Napoca, The Directorate of Research, Development and Innovation Management (DMCDI), Constantin Daicoviciu Street, no. 15, Cluj-Napoca, 400020, Cluj county, Romania. E-mail: stefan\_ta@yahoo.com

§: All authors contributed equally to this work.

**Abstract:** *In this paper is made a comparative study of state of stress and linear deformation which appear in a series of pressurized cylindrical tanks with different end caps designed to store the LPG fuel. Initial design data for the tank design are identical, as well as the lateral cylindrical cover. Taking into account the constructive symmetry of the tanks, models with cross sections  $\frac{1}{4}$  for the side cover, with  $\frac{1}{4}$  at the end caps and with section at  $\frac{1}{8}$  in the case of the tank assembly are used. It was taken into consideration in the calculation of linear deformation and stress, the simultaneous effect of the temperature and corrosion variation, which reduces the thickness of the tank shells with the increase of the exploitation period. Details of the geometry and the materials selected are also discussed. Finally, it was established for the analyzed group of tanks at the end of the operating period, for the extreme working temperatures, which is the most advantageous form of tank with the minimum stress state and linear deformation.*

**Keywords:** *Automotive industry, corrosion, crash test, industrial engineering design, optimization, pressurized fuel tank, state of effort*

### 1. Introduction

The optimal design of the pressurized fuel tanks in automotive industry is an important and practical topic which has been explored for decades [1-3]. This is a key to increasing product competitiveness and safety in exploitation through innovative ideas [4, 5].

The cylindrical pressurized fuel tanks are designed using specific rules for the design, construction, inspection, testing and verification according with the major international standards [6-11].

Basic design criteria include information on corrosion, loadings, design methods, thickness, weld joint coefficients and design of welded joints [5]. In addition, there are well established rules for performing calculations for shells, heads, cones, nozzles, flat covers, flanges and tube sheets [5].

In practice, the cylindrical pressurized fuel tanks are generally preferred because of the simple manufacturing problem and make better use of the available storage space [6-11].

Design study for the stress analysis of cylindrical pressurized fuel tanks due to the various loadings involves the study of longitudinal and circumferential stresses and plays an important role in structural optimization and safety of the equipment [4, 5].

Integrated concurrent engineering techniques [12-15] are employed to enrich the design process of the cylindrical pressurized fuel tanks for representing geometry [16-18] and material details with multidimensional visualization techniques [19-31] to find an optimal geometrical solution [32-34] at less cost.

### 2. Design procedure of the cylindrical pressurized fuel tanks

The cylindrical pressurized fuel tanks has been analyzed considering the following head covers: a) torospheric type; b) ellipsoidal type; c) for low pressure; d) connected with circular arcs; e) flat; and f) with back head covers connected with circular arcs. The design data used are:

- the lateral cover has a diameter of  $D = 250$  mm and length  $L = 700$  mm;
- the tank material is AISI 4340 steel;
- the maximum hydraulic test pressure:  $p_{\max} = 30$  bar;
- the working temperature between the limits:  $T = -30$  °C up to  $T = 60$  °C;
- the duration of the tank exploitation:  $n_a = 20$  years;
- the corrosion rate of the material:  $v_c = 0.1$  mm/years;

CAD model generation of the cylindrical pressurized fuel tanks with different types of head covers was done in AutoCAD Autodesk 2017 software [35], (as shown in Figures 1 to 6).

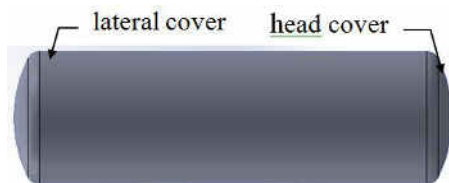


Fig. 1. The tank with torospheric head covers



Fig. 2. The tank with ellipsoidal head covers



Fig. 3. The tank with low pressure head covers



Fig. 4. The tank with head covers connected with circular arcs



Fig. 5. The tank with flat head covers



Fig. 6. The tank with back head covers connected with circular arcs

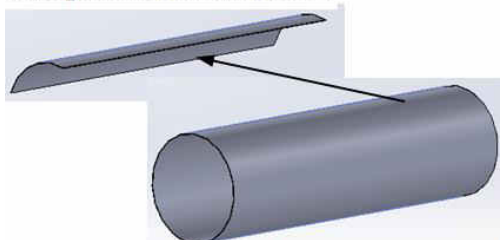
Optimized CAD design of these tanks was imported to SolidWorks 2017 software [36] for analysis with the: Static, Thermal and Design Study modules.

At first, an optimal design of the lateral cover was made, then has been carried out the optimal design of head cover and finally the state of stress and deformation of the whole tank was performed. At the final stage of exploitation the thickness of the cover is minimal due to the corrosion action and appears the biggest solicitations in the pressurized tank.

### 2.1. The CAD design of the cylindrical lateral cover

The parameterized model used in calculus is a section of  $\frac{1}{4}$  from the initial cover (Figure 7) and the corresponding surfaces to which the constraints and restrictions are applied are shown in Figure 8.

The parametric model  $\frac{1}{4}$



The initial parametric model

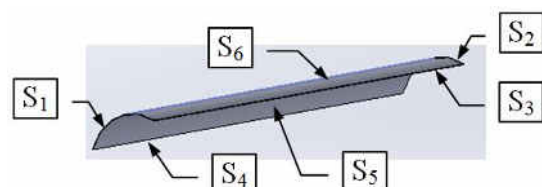


Fig. 7. The parametric model of lateral covers

Fig. 8. The  $\frac{1}{4}$  section of lateral head covers where is made the marking of the exterior surfaces

The following parameters were applied as input parameters to the parametric model (Figure 8):

- the maximum pressure  $p_{\max} = 30$  N/mm<sup>2</sup> on the inner surface  $S_5$ ;
- the temperature between the limits:  $T = -30$  °C to  $T = 60$  °C on the surface  $S_6$ ;

- the opposing and equal traction forces of value of  $F = 36800$  N on the surfaces:  $S_1$  and  $S_2$ , generated by the action of pressure on the inner surfaces of the head covers;
- the surface symmetry on  $S_4$  and  $S_5$ ;
- the canceling the displacement of the cover along to the symmetry axis;
- the material of the lateral cover: AISI 4340 steel.

The applied optimization function is intended to achieve a minimum mass. The variable of optimization is the thickness of the cover with limits in range:  $s = 0.5...3$  mm.

The applied restriction of constraint is that the value of Von Mises effort  $\sigma_{rez} \leq \sigma_a = 710$  N/mm<sup>2</sup> ( $\sigma_a$  - the admissible value of the traction stress of the material).

Applying the optimization procedure, the obtained values are: the thickness  $s = 0.59$  mm for  $T = 60$  °C, with the stress value of the  $\sigma_{rez, max} = 651.86$  N/mm<sup>2</sup> and linear deformation value  $u_{max} = 0.316$  mm. Distributions of linear deformation and state of stress are shown in Figures 9 and 10.

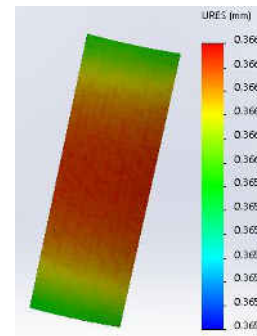
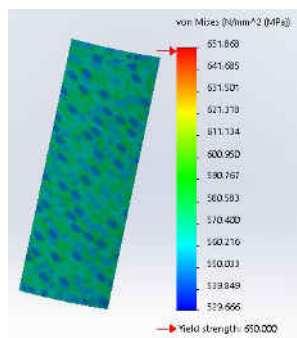


**Fig. 9.** The graph of Von Mises stress of lateral cover **Fig. 10.** The graph of linear deformation of lateral cover

The optimized thickness of the cover was corrected taking into account: the corrosion phenomenon, the tolerance of negative execution of the sheet laminate and the thinning of the sheet in the embossing process. The formula for calculating the thickness is the following:

$$s_{real} = s_{opt} + \Delta s_c + \Delta s_T + \Delta s_{am} = s_{opt} + v_c \cdot n_a + abs(A_i) + 0.1 \cdot s \tag{1}$$

where:  $\Delta s_c$ , loss of thickness by corrosion;  $\Delta s_T$ , addition of thickness due to the negative tolerance of the laminate sheet;  $v_c$ , corrosion velocity of the lateral cover,  $v_c = 0.1$  mm/year;  $n_a$ , number of years of exploitation;  $A_i$ , lower tolerance of the laminate sheet.

Finally, the minimum value of the sheet thickness is determined as:

$$s_{real\ min} = 0.59 + 0.1 \cdot 20 + abs(-0.6) + 0.1 \cdot 4 = 3.59 \text{ mm} \tag{2}$$

A laminate sheet of AISI 4340 steel with a thickness of  $s = 4^{+0.25}_{-0.6}$  mm is chosen for analysis.

## 2.2. The optimized design of the cylindrical pressurized tank with torospheric head covers

The corresponding graphical representations for the optimization of the head cover sectioned to  $1/4$  of the initial model, (as shown in Figure 11 b), and for the parameterized models of tanks sectioned to  $1/8$  (as shown in Figure 11 c) are given below:

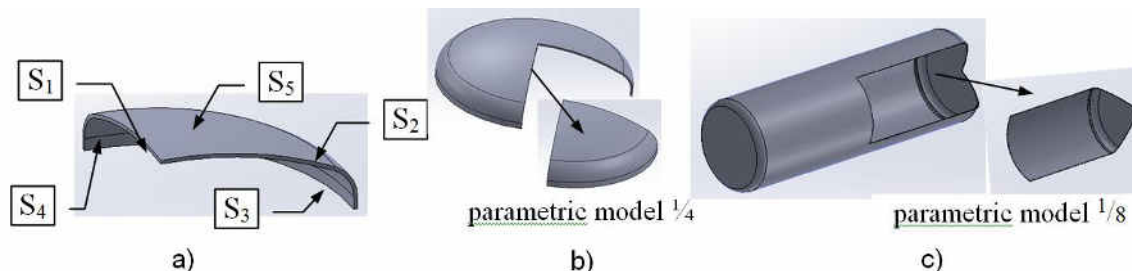


**Fig. 11.** a) The  $1/4$  section of lateral head cover with the corresponding marking of the exterior surfaces; b) The parametric model at  $1/4$  section of head cover; c) The parametric model at  $1/8$  section of tank

The sketch and the parametric shaping of the torospheric head cover according to standard DIN 28011 are shown in Figure 12.

The torospheric head cover 10 % DIN 28011

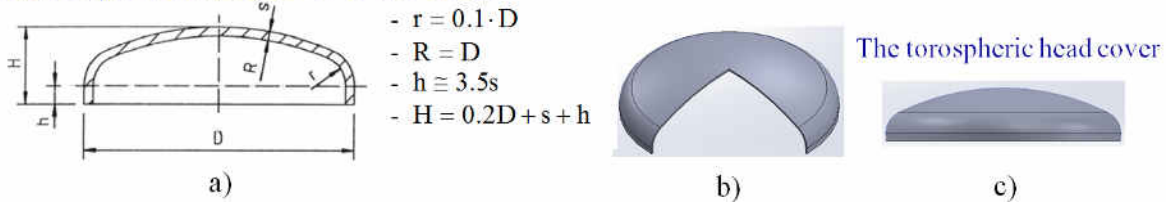


Fig. 12. a) The sketch of torospheric head cover; b) The 3/4 section of parametric model of the torospheric head cover; c) The front view of parametric model of the torospheric head cover

According to Fig. 11 a) and for all the following head covers, the following algorithm was applied:

- the maximum pressure  $p_{max} = 30 \text{ N/mm}^2$  on inner surface  $S_4$ ;
- the temperature between the limits:  $T = -30 \text{ }^\circ\text{C}$  to  $T = 60 \text{ }^\circ\text{C}$ , on the surface  $S_5$ ;
- the symmetry on the surfaces:  $S_1$  and  $S_2$ ;
- the canceling the displacement of the cover along to the symmetry axis.

The cover is optimized to obtain a minimum mass and the effort must be:  $\sigma_{rez} \leq \sigma_a = 710 \text{ N/mm}^2$ .

The sizes to be optimized are: the cover thickness  $s = 2...4 \text{ mm}$  and the height  $h = 8...12 \text{ mm}$ . The values of dimensions  $R = D = 250 \text{ mm}$  and  $r = 0.1 \cdot D = 25 \text{ mm}$ . The obtained values are:  $s = 2.38 \text{ mm}$  and  $h = 8.03 \text{ mm}$  at  $T = -30 \text{ }^\circ\text{C}$  for the maximum effort  $\sigma_{rez, max} = 652.88 \text{ N/mm}^2$ .

The distribution of the stress and linear deformation of the optimal head cover is shown in Figure 13.

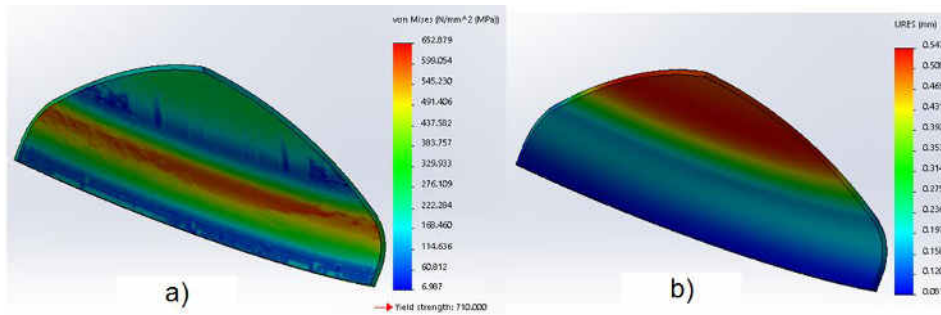


Fig. 13. The graphs for torospheric head cover: a) The Von Mises stress; b) The resultant linear deformation

The correction of the optimal thickness of the cover  $s$  is made with the following formula:

$$s_{real \text{ min}} = 2.38 + 0.1 \cdot 20 + \text{abs}(-0.6) + 0.1 \cdot 5 = 5.48 \text{ mm} \tag{3}$$

A laminate sheet of AISI 4340 steel with a thickness of  $s = 5.5^{+0.25}_{-0.6} \text{ mm}$  it was chosen for the manufacturing process. Next dimensions were obtained for the head cover:  $h \cong 3.5 \cdot s = 20 \text{ mm}$  and  $H = 75.5 \text{ mm}$ .

The pressurized tank must resist to  $n_a = 20$  years and the calculation shows that at temperature  $T = -30 \text{ }^\circ\text{C}$  is the maximum stress and at  $T = 60 \text{ }^\circ\text{C}$  the linear resultant deformation is maximal.

For temperature  $T = -30 \text{ }^\circ\text{C}$  the stress and deformation of the tank are shown in Figures 14a and 14b and for  $T = 60 \text{ }^\circ\text{C}$  in Figures 14c and 14d.

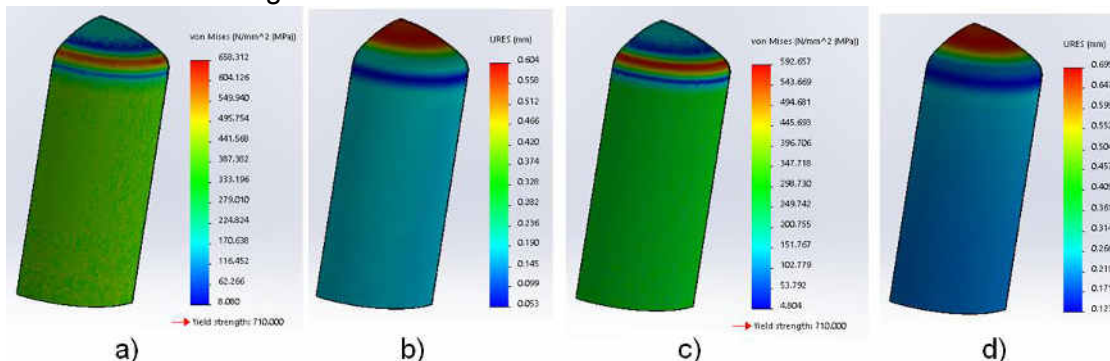
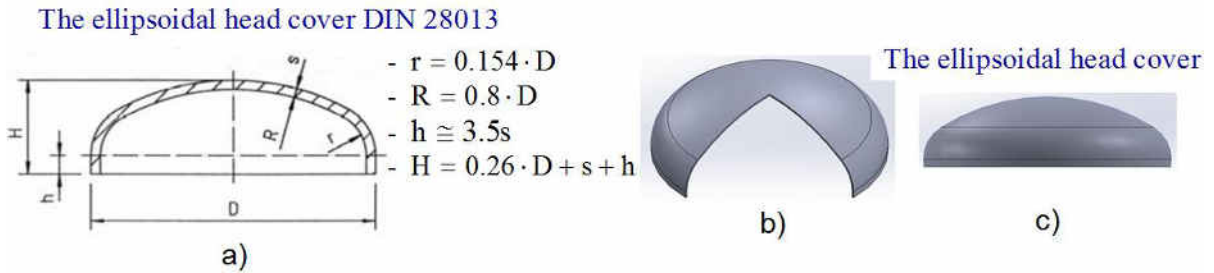


Fig. 14. The graphs for pressurized cylindrical tank with torospheric head covers: a) The Von Mises stress at  $T = -30 \text{ }^\circ\text{C}$ ; b) The resultant linear deformation at  $T = -30 \text{ }^\circ\text{C}$ ; c) The Von Mises stress at  $T = 60 \text{ }^\circ\text{C}$ ; d) The resultant linear deformation at  $T = 60 \text{ }^\circ\text{C}$

**2.3. The optimized design of the cylindrical tank with ellipsoidal head covers**

The sketch and the parametric model of the ellipsoidal cover are shown in Figure 15.



**Fig. 15.** a) The sketch of ellipsoidal head cover; b) The 3/4 section of parametric model of the ellipsoidal head cover; c) The front view of parametric model of the ellipsoidal head cover

The parameters for optimization are: the thickness  $s = 1...4$  mm and the height  $h = 6...10$  mm. The values of geometric dimensions are:  $R = 0.8 \cdot D = 200$  mm and  $r = 0.154 \cdot D = 38.5$  mm. The obtained values are:  $s = 1.445$  mm and  $h = 6.005$  mm with  $\sigma_{rez\ max} = 594.74$  N/mm<sup>2</sup> at  $T = -30$  °C. The corresponding distribution of stress and linear deformation is shown in Figure 16.

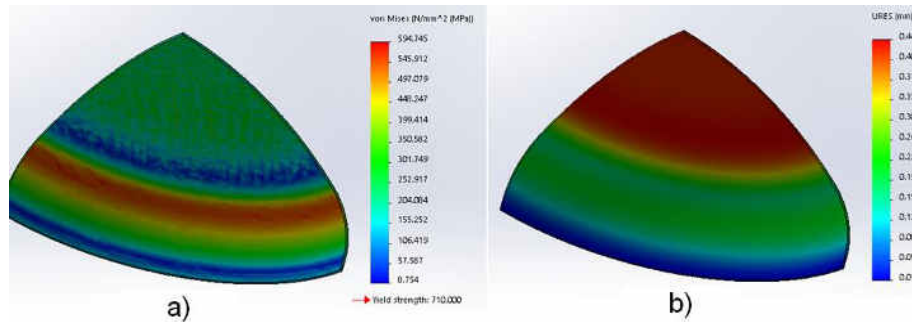


**Fig. 16.** The graphs for elliptical head cover: a) The Von Mises stress; b) The resultant linear deformation

Finally, the minimum thickness of the cover is:

$$s_{real\ min} = 1.45 + 0.1 \cdot 20 + \text{abs}(-0.6) + 0.1 \cdot 4 = 4.45 \text{ mm} \tag{4}$$

A laminate sheet of AISI 4340 steel with a thickness of  $s = 4.5^{+0.25}_{-0.6}$  mm is chosen. For the head cover we have the following dimensions:  $h \approx 3.5 \cdot s = 16$  mm and  $H = 85.5$  mm. The stress and linear deformation of the tank at  $T = -30$  °C are shown in Figures 17a and 17b, and at  $T = 60$  °C in Figures 17c and 17d.

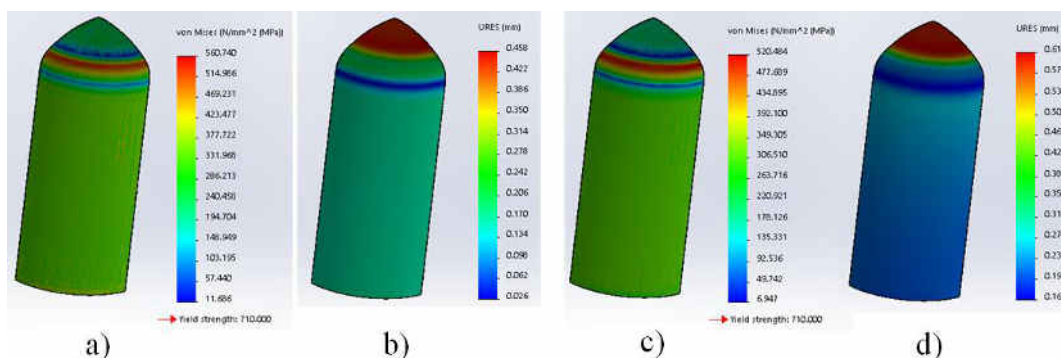


**Fig. 17.** The graphs for pressurized cylindrical tank with elliptical head covers: a) The Von Mises stress at  $T = -30$  °C; b) The resultant linear deformation at  $T = -30$  °C; c) The Von Mises stress at  $T = 60$  °C; b) The resultant linear deformation at  $T = 60$  °C

**2.4. The optimized design of the cylindrical tank with low pressure head covers**

The sketch and the parametric model of the low pressure head cover are shown in Figure 18. The variables subjected to optimization are: thickness  $s = 2...5$  mm, height  $h = 12...16$  mm and radius  $r = 15...40$  mm. The obtained values are:  $s = 3.336$  mm,  $h = 12.056$  mm,  $r = 15$  mm at  $T =$

-30 °C with a maximum stress  $\sigma_{rez. max} = 587.68 \text{ N/mm}^2$  and a linear resultant deformation  $u_{max} = 0.481 \text{ mm}$ .

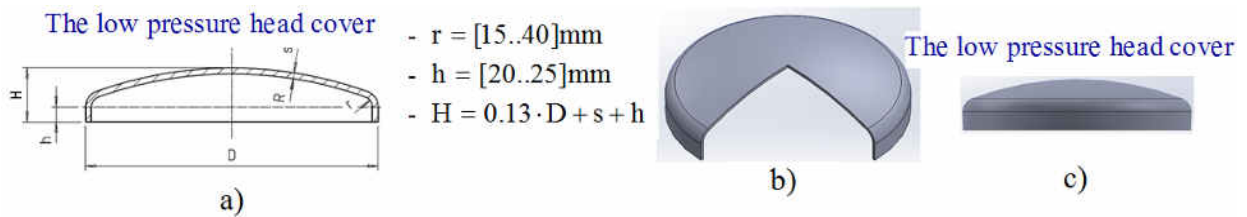


Fig. 18. a) The sketch of the low pressure head cover; b) The 3/4 section of parametric model of the low pressure head cover; c) The front view of parametric model of the low pressure head cover

The corresponding graphs of the stress and the state of the resulting linear deformation of the optimal cover head are shown in Figure 19.

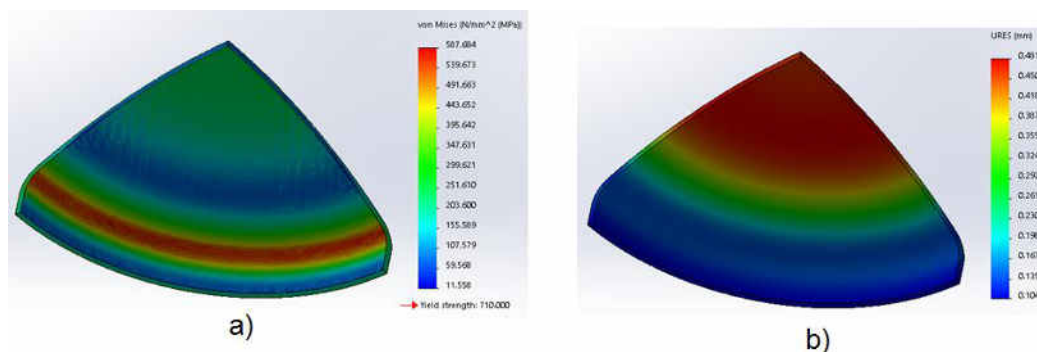


Fig. 19. The graphs for low pressure head cover: a) The Von Mises stress; b) The resultant linear deformation

The minimum real thickness of the cover is:

$$s_{real min} = 3.34 + 0.1 \cdot 20 + \text{abs}(-0.6) + 0.1 \cdot 6 = 6.54 \text{ mm} \tag{5}$$

A laminate sheet of AISI 4340 steel with a thickness of  $s = 6.5^{+0.25}_{-0.6} \text{ mm}$  was chosen.

For the head cover we have the following dimensions:  $h \cong 3.5 \cdot s = 22 \text{ mm}$  and  $H = 61 \text{ mm}$ .

For temperature  $T = -30 \text{ }^\circ\text{C}$  the stress and deformation of the tank are shown in Figures 20a and 20b and for  $T = 60 \text{ }^\circ\text{C}$  in Figures 20c and 20d.

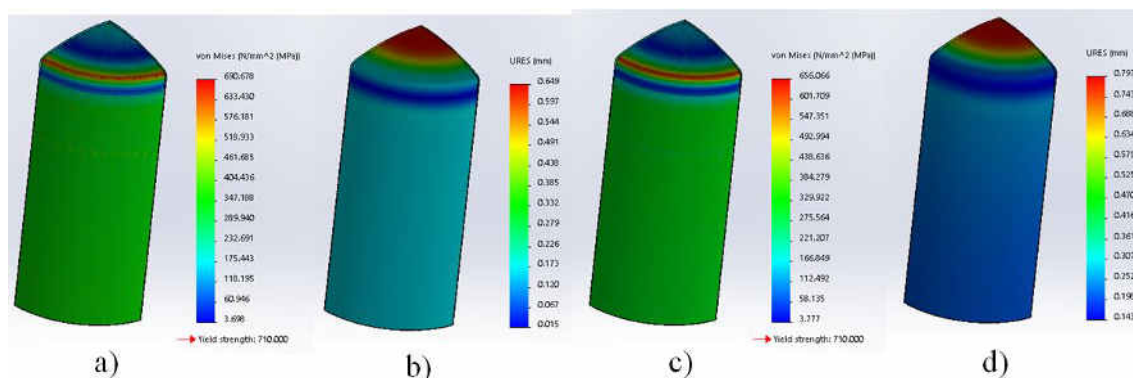
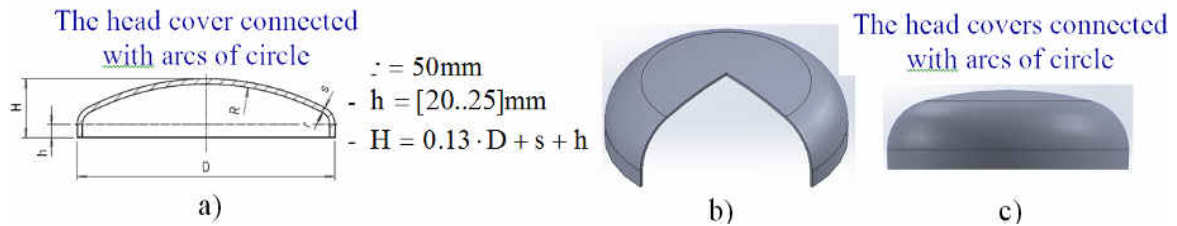


Fig. 20. The graphs for cylindrical tank with low pressure head covers: a) The Von Mises stress at  $T = -30 \text{ }^\circ\text{C}$ ; b) The resultant linear deformation at  $T = -30 \text{ }^\circ\text{C}$ ; c) The Von Mises stress at  $T = 60 \text{ }^\circ\text{C}$ ; b) The resultant linear deformation at  $T = 60 \text{ }^\circ\text{C}$ ;

### 2.5. The optimized design of the cylindrical tank with caps connected with circular arcs

The sketch and the parametric model of the head cover are shown in Figure 21.

The variables subjected to optimization are: the thickness  $s = 2 \dots 5 \text{ mm}$ , the height  $h = 20 \dots 25 \text{ mm}$ , and the radius  $r = 50 \text{ mm}$ . The obtained values are:  $s = 2 \text{ mm}$  and  $h = 12.056 \text{ mm}$  at  $T = -30 \text{ }^\circ\text{C}$ , with a maximum stress  $\sigma_{rez. max} = 659.01 \text{ N/mm}^2$  and a linear deformation  $u_{max} = 0.999 \text{ mm}$ .



**Fig. 21.** a) The sketch of head cover connected with circular arcs; b) The ¼ section of model with the head cover connected with circular arcs; c) The front view model of the head cover connected with circular arcs

The corresponding graphs of the stress and the state of the resulting linear deformation of the optimal cover head are shown in Figure 22.

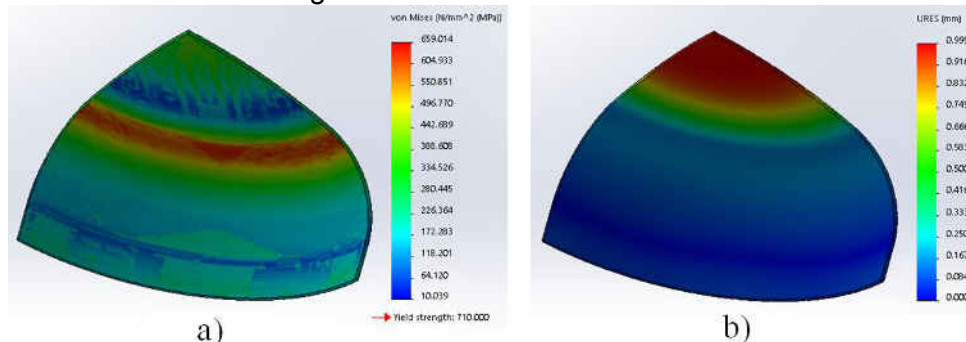


**Fig. 22.** The graphs for low pressure head cover connected with circular arcs: a) The Von Mises stress; b) The resultant linear deformation.

The minimum thickness of the cover connected with circular arcs is:

$$s_{real\ min} = 2 + 0.1 \cdot 20 + \text{abs}(-0.6) + 0.1 \cdot 55 = 5.15\ \text{mm} \quad (6)$$

A laminate sheet of AISI 4340 steel with a thickness of  $s = 5.5^{+0.25}_{-0.6}$  mm is chosen. The stress and linear deformation of the tank at  $T = -30\ ^\circ\text{C}$  are shown in Figures 23a and 23b and at  $T = 60\ ^\circ\text{C}$  in Figures 23c and 23d.

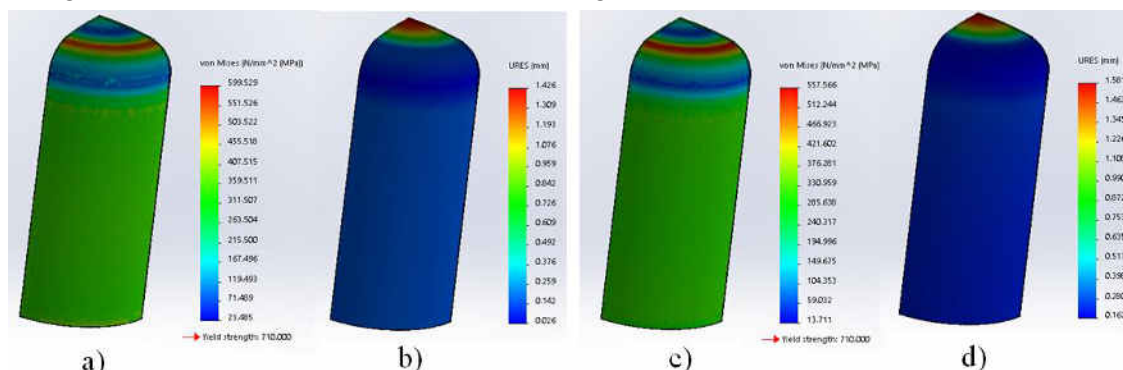


**Fig. 23.** The graphs for pressurized cylindrical tank with head covers connected with circular arcs: a) The Von Mises stress at  $T = -30\ ^\circ\text{C}$ ; b) The resultant linear deformation at  $T = -30\ ^\circ\text{C}$ ; c) The Von Mises stress at  $T = 60\ ^\circ\text{C}$ ; d) The resultant linear deformation at  $T = 60\ ^\circ\text{C}$

## 2.6. The optimized design of the cylindrical tank with flat head covers

The sketch and the parametric modeling of the flat head cover are shown in Figure 24.

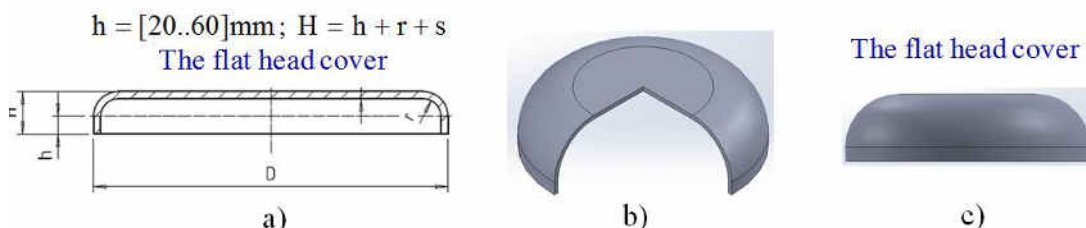


**Fig. 24.** a) The sketch of the flat head cover; b) The ¼ section of parametric model of the flat head cover; c) The front view of parametric model of the flat head cover

The variables subjected to optimization are: thickness  $s = 3...5$  mm, the heights:  $h = 20...60$  mm. and  $H = 30...70$  mm. The obtained values are:  $s = 5$  mm,  $h = 15$  mm,  $H = 70$  mm and radius  $r = 50$  mm at  $T = -30$  °C, with a maximum stress  $\sigma_{rez. max} = 659.01$  N/mm<sup>2</sup> and a linear resultant deformation  $u_{max} = 1.395$  mm. The corresponding graphs of the stress and the state of the resulting linear deformation of the optimal cover head are shown in Figures 25a and 25b.

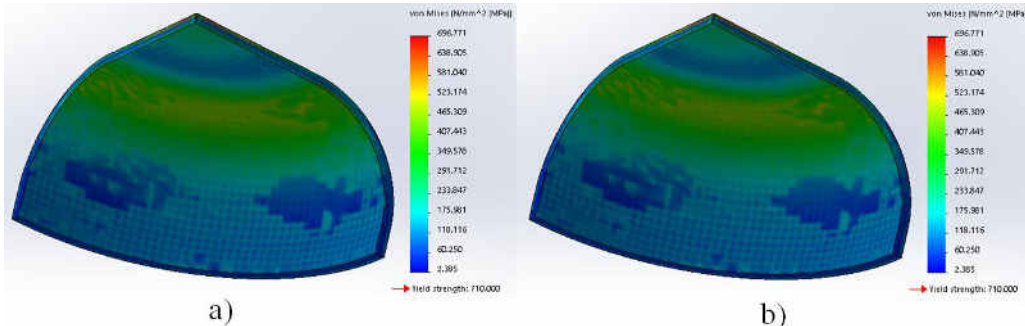


Fig. 25. The graphs for flat head cover a) The Von Mises stress; b) The resultant linear deformation

The minimum thickness of the flat cover is:

$$s_{real min} = 5 + 0.1 \cdot 20 + \text{abs}(-0.6) + 0.1 \cdot 8.5 = 8.45 \text{ mm} \quad (7)$$

A laminate sheet of AISI 4340 steel with a thickness of  $s = 8.5^{+0.25}_{-0.6}$  mm is chosen.

The graphs of stress and linear deformation of tank at  $T = -30$  °C are shown in Figures 26a and 26b and for  $T = 60$  °C in Figures 26c and 26d.

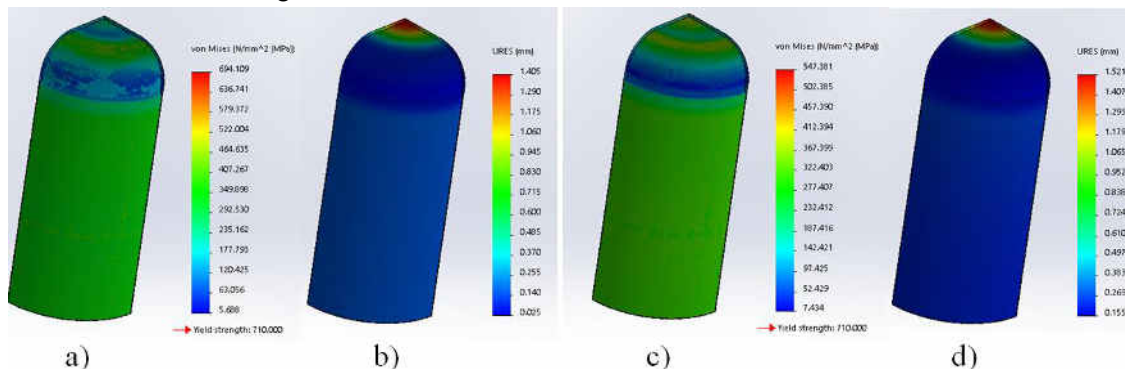


Fig. 26. The graphs for cylindrical tank with flat head covers: a) The Von Mises stress at  $T = -30$  °C; b) The linear deformation at  $T = -30$  °C; c) The Von Mises stress at  $T = 60$  °C; b) The linear deformation at  $T = 60$  °C

### 2.7. The optimized design of the cylindrical tank with back head covers connected with circular arcs

The sketch and the parametric model of the back head cover connected with circular arcs are shown in Figure 27.

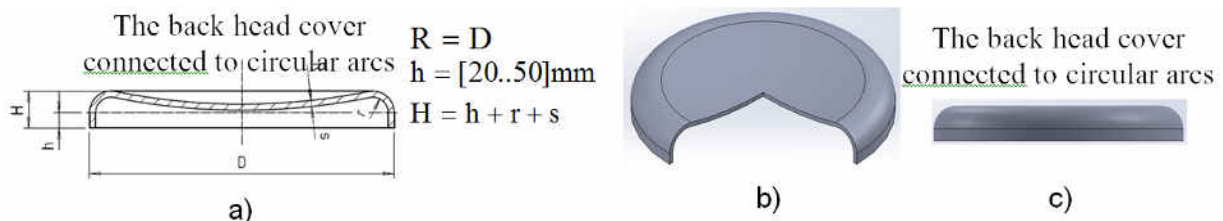


Fig. 27. a) The sketch of the back head cover connected with circular arcs; b) The 3/4 section of parametric model of the back head cover connected with circular arcs; c) The front view of parametric model of the back head cover connected with circular arcs

The variables subjected to optimization are:  $s = 3...6$  mm,  $h = 12...20$  mm and  $H = 30...35$  mm. The obtained values are:  $s = 4.5$  mm,  $r = 22.5$  mm,  $h = 12$  mm and  $H = 34.5$  mm at  $T = -30$  °C with a maximum stress  $\sigma_{rez. max} = 628.27$  N/mm<sup>2</sup> and a linear resultant deformation  $u_{max} = 1.873$  mm.

The corresponding graphs of the stress and the state of the resulting linear deformation of the optimal back head cover are shown in Figures 28a and 28b.

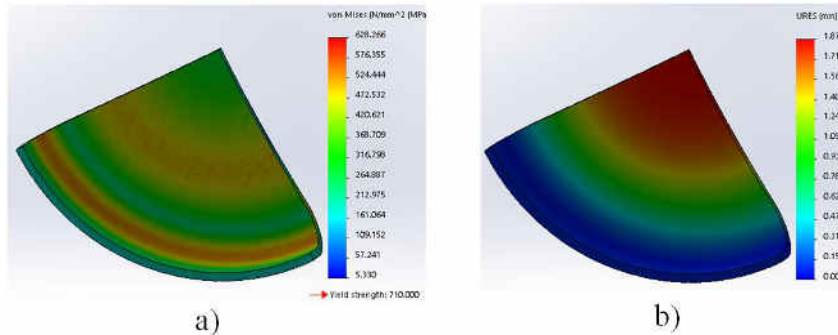


Fig. 28. The graphs for back head cover connected with circular arcs: a) The stress; b) The linear deformation

The minimum real thickness of the back head covers connected with circular arcs is:

$$s_{\text{real min}} = 4.5 + 0.1 \cdot 20 + \text{abs}(-0.6) + 0.1 \cdot 8 = 7.9 \text{ mm} \tag{8}$$

A laminate sheet of AISI 4340 steel with a thickness of  $s = 8^{+0.25}_{-0.6}$  mm was chosen. The corresponding graphs of the stress and the state of the resulting linear deformation of the tank at  $T = -30^\circ\text{C}$  are shown in Figures 29a and 29b and at  $T = 60^\circ\text{C}$  in Figures 29c and 29d.

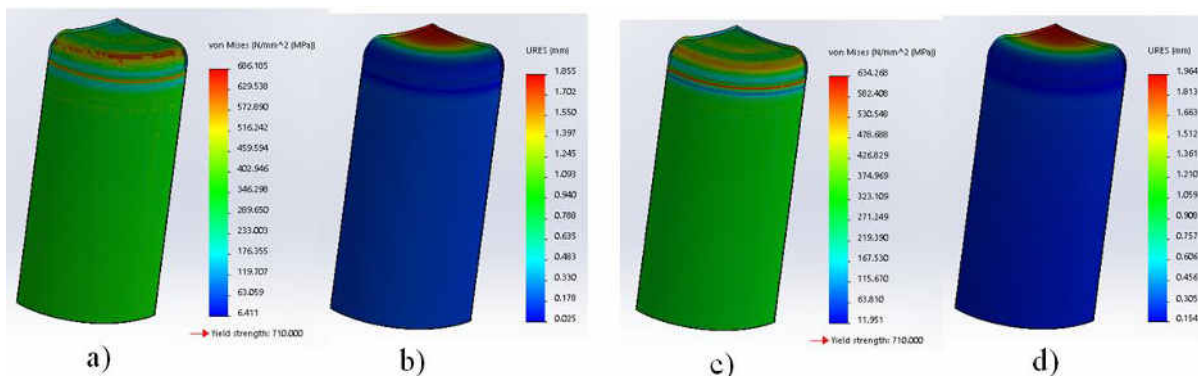


Fig. 29. The graphs for pressurized cylindrical tank with back head covers connected with circular arcs: a) The Von Mises stress at  $T = -30^\circ\text{C}$ ; b) The resultant linear deformation at  $T = -30^\circ\text{C}$ ; c) The Von Mises stress at  $T = 60^\circ\text{C}$ ; d) The resultant linear deformation at  $T = 60^\circ\text{C}$

The numerical values of state of stress and linear resultant deformation of the tanks are given in Table 1.

Table 1: The Von Misses stress and deformation of pressurized cylindrical tanks

No.	The type of pressurized cylindrical tank	$T = -30^\circ\text{C}$		$T = 60^\circ\text{C}$	
		$\sigma$ [MPa]	$u$ [mm]	$\sigma$ [MPa]	$u$ [mm]
1	Tank with torospheric head covers	658.312	0.604	592.657	0.695
2	Tank with ellipsoidal head covers	560.74	0.458	520.484	0.613
3	Tank with low pressure head covers	690.67	0.649	656.07	0.797
4	Tank with head covers connected with circular arcs	599.53	1.426	557.57	1.58
5	Tank with flat head covers	694.11	1.405	547.38	1.521
6	Tank with back head covers connected with circular arcs	686.185	1.855	634.268	1.964

The graphical representations of the Von Mises stress and the resulting linear deformation for  $T = -30^\circ\text{C}$  and  $T = 60^\circ\text{C}$  depending on the number's tank as specified in Table 1, computed for the end of the exploitation period (where  $n_a = 20$  years) are shown in Figures 30 and 31.

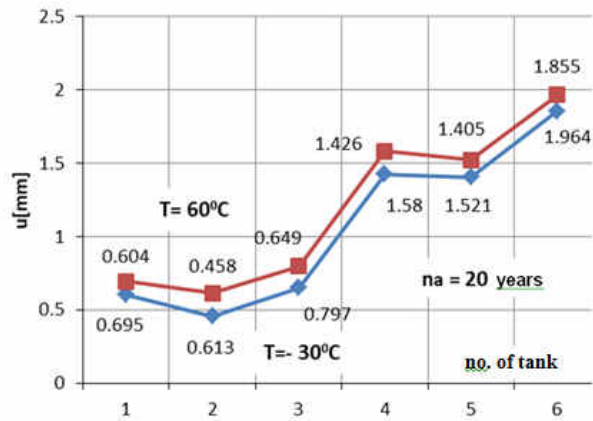
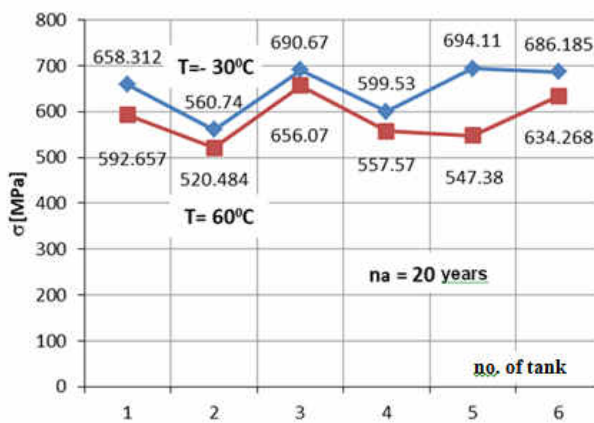


Fig. 30. The graphs for Von Mises stress at  $n_a = 20$  years Fig. 31. The linear deformation at  $n_a = 20$  years

In Figure 32 is shown the percentage variation of the Von Mises stress computed in respect to the admissible stress of material  $\sigma_a = 710$  [MPa] at the temperatures of  $T = -30$  °C and  $T = 60$  °C, depending on the number of tank (as specified in Table 1) at  $n_a = 20$  years of exploitation.

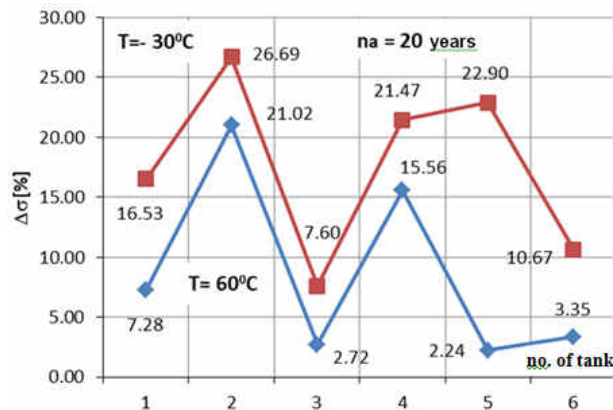


Fig. 32. The graphs for percentage variation of Von Mises stress at  $n_a = 20$  years

### 3. Discussion

From these analyses shown in tables and graphical representations we can say that:

- The tank with ellipsoidal cover is the least loaded at both extreme temperatures, at  $T = -30$  °C,  $\sigma_{max} = 560.74$  MPa and  $T = 60$  °C,  $\sigma_{max} = 520.48$  MPa, according Figures 30 and 31.
- The flat cap tank has the highest stress value  $\sigma_{max} = 694.11$  MPa at  $T = -30$  °C and shows the greatest variation of stress between extreme temperatures,  $\Delta\sigma = 146.73$  MPa, according Figure 30.
- The tank with the low pressure head covers best accomplish for both extreme temperatures the conditions since the difference in admissible value is lower. It results that this tank is optimally dimensioned.
- The tank with head covers connected with circular arcs has the highest linear strain deformation  $u = 1.855$  mm for  $T = 60$  °C and the lowest value is found for the ellipsoidal head cover tank, as shown in Figure 31.
- The tank with low pressure head covers shows the minimum value of the percentage stress deviation  $\Delta\sigma = 7.6$  % at  $T = -30$  °C and  $\Delta\sigma = 2.72$  % for  $T = 60$  °C, that means it is the optimally dimensioned. At the opposite pole, the tank with ellipsoidal head covers has the greatest deviation of  $\Delta\sigma = 26.69$  % at  $T = -30$  °C and  $\Delta\sigma = 21.02$  % for  $T = 60$  °C, as shown in Figure 32.
- At the end of the exploitation period, the tank with the ellipsoidal head covers shows the largest reserve of resistance of stress  $\Delta\sigma = 21.02$  %, while the tank with flat head covers has the lowest resistance capacity  $\Delta\sigma = 2.24$  %, as shown in Figure 32.

#### 4. Conclusions

According to the findings of the present study the following conclusions can be drawn:

- the Von Mises stress state and linear deformation of the tanks is directly influenced by: temperature variation, operating period, loading pressure and tank shape;
- at identical design input dates, for the end of the exploitation period, the tank with ellipsoidal head covers is the least subject to stress, followed in order by: tank with torospheric head covers, tank with low pressure head covers, tank with flat head covers and tank with back head covers connected with circular arcs which is subject to highest stress;
- the state of stress is lower at the maximum positive temperature than at the negative temperature for any type of tank, the stress variation curves for extreme operating temperature have about the same variation, except for this made the curve deviation at the tank with circular arcs;
- the resulting linear deformation is higher at the extreme positive and lower at the negative temperature for all tank types, and the order of increase the deformation is as follows: tank with ellipsoidal head caps, tank with low pressure head covers , tank with head covers connected with circular arcs, tank with flat head covers and the tank with back covers connected with circular arcs;
- from the point of view of stress and deformation, the tank with ellipsoidal head covers has the best shape and the most stressed is the tank with flat head covers;
- it is mentioned the fact that all the studied forms are optimized dimensionally in respect with the stress and deformation for which they were designed and work adequate.

**Financial disclosure:** Neither author has a financial or proprietary interest in any material or method mentioned.

**Competing interests:** The authors declare that they have no significant competing financial, professional or personal interests that might have influenced the performance or presentation of the work described in this manuscript.

#### References

- [1] A.C. Nedelcu, “Romanian automotive industry – analysis made from the intellectual capital perspective“, *Revista Economica*, vol. 67, no. 5, pp. 80-89, 2015;
- [2] G. Matache, C. Cristescu, C. Dumitrescu, V. Miroiu, “Pregătirea specialiștilor în vederea adaptabilității și creșterii competitivității”, *Magazine of Hydraulics, Pneumatics, Tribology, Ecology, Sensorics, Mechatronics (HIDRAULICA)*, no. 3-4, pp. 7-14, 2012. ISSN 1453-7303;
- [3] M. Rusănescu, “Material requirements planning, inventory control system in industry”, *Magazine of Hydraulics, Pneumatics, Tribology, Ecology, Sensorics, Mechatronics (HIDRAULICA)*, no. 1, pp. 21-25, 2014. ISSN 1453-7303;
- [4] R. Khobragade, V. Hiwase, “Design, and analysis of pressure vessel with hemispherical and flat circular end”, *International Journal of Engineering Science and Computing*, vol. 7, no. 5, pp. 12458-12469, 2017;
- [5] D. H. Nash, “UK Rules for unfired pressure vessels”. In: “The Companion guide to ASME boiler and pressure vessel code”, 2008. ASME, Chapter 51. ISBN 9780971902717, <https://strathprints.strath.ac.uk/6502>;
- [6] M.C. Ghiță, A.C. Micu, M. Țălu, Ș. Țălu, “Shape optimization of vehicle's methane gas tank”, *Annals of Faculty of Engineering Hunedoara - International Journal of Engineering, Hunedoara*, Tome X, Fascicule 3, pp. 259-266, 2012;
- [7] M.C. Ghiță, A.C. Micu, M. Țălu, Ș. Țălu, E. Adam, “Computer-Aided Design of a classical cylinder gas tank for the automotive industry“, *Annals of Faculty of Engineering Hunedoara - International Journal of Engineering, Hunedoara*, Tome XI, Fascicule 4, pp. 59-64, 2013;
- [8] M.C. Ghiță, A.C. Micu, M. Țălu, Ș. Țălu, “3D modelling of a gas tank with reversed end up covers for automotive industry“, *Annals of Faculty of Engineering Hunedoara - International Journal of Engineering, Hunedoara*, Tome XI, Fascicule 3, 2013, pp. 195-200, 2013;
- [9] M.C. Ghiță, A.C. Micu, M. Țălu, Ș. Țălu, “3D modelling of a shrink fitted concave ended cylindrical tank for automotive industry“. *Acta Technica Corviniensis – Bulletin of Engineering, Hunedoara, Romania*, Tome VI, Fascicule 4, pp. 87-92, 2013;
- [10] M.C. Ghiță, A.C. Micu, M. Țălu, Ș. Țălu, Shape optimization of a thoroidal methane gas tank for automotive industry, *Annals of Faculty of Engineering Hunedoara - International Journal of Engineering, Hunedoara*, Tome X, Fascicule 3, pp. 295-297, 2012;

- [11] M.C. Ghiță, C.Ș. Ghiță, Ș. Țălu, S. Rotaru, “Optimal design of cylindrical rings used for the shrinkage of vehicle tanks for compressed natural gas”, *Annals of Faculty of Engineering Hunedoara - International Journal of Engineering*, Hunedoara, Tome XII, Fascicule 3, pp. 243-250, 2014;
- [12] C. Bîrleanu, Ș. Țălu, “Organe de mașini. Proiectare și reprezentare grafică asistată de calculator” (Machine elements. Designing and computer assisted graphical representations), Cluj-Napoca, Victor Melenti Publishing house, 2001;
- [13] Ș. Țălu, “Limbajul de programare AutoLISP. Teorie și aplicații”, (AutoLISP programming language. Theory and applications), Cluj-Napoca, Risoprint Publishing house, 2001;
- [14] Ș. Țălu, “Reprezentări grafice asistate de calculator” (Computer assisted graphical representations), Cluj-Napoca, Osama Publishing house, 2001;
- [15] Ș. Țălu, “Grafică tehnică asistată de calculator” (Computer assisted technical graphics), Cluj-Napoca, Victor Melenti Publishing house, 2001;
- [16] Ș. Țălu, M. Țălu, “A CAD study on generating of 2D supershapes in different coordinate systems”, *Annals of Faculty of Engineering Hunedoara - International Journal of Engineering*, Hunedoara, Tome VIII, Fascicule 3, pp. 201-203, 2010;
- [17] Ș. Țălu, M. Țălu, “CAD generating of 3D supershapes in different coordinate systems”, *Annals of Faculty of Engineering Hunedoara - International Journal of Engineering*, Hunedoara, Tome VIII, Fascicule 3, pp. 215-219, 2010;
- [18] Ș. Țălu, “CAD representations of 3D shapes with superellipsoids and convex polyhedrons”, *Annals of Faculty of Engineering Hunedoara - International Journal of Engineering*, Hunedoara, Tome IX, Fascicule 3, 2011, pp. 349-352, 2011;
- [19] Ș. Țălu, “AutoCAD 2005”, Cluj-Napoca, Risoprint Publishing house, 2005;
- [20] Ș. Țălu, M. Țălu, “AutoCAD 2006. Proiectare tridimensională” (AutoCAD 2006. Three-dimensional designing), Cluj-Napoca, MEGA Publishing house, 2007;
- [21] Ș. Țălu, “AutoCAD 2017”, Cluj-Napoca, Napoca Star Publishing house, 2017;
- [22] Ș. Țălu, “Geometrie descriptivă” (Descriptive geometry), Cluj-Napoca, Risoprint Publishing house, 2010;
- [23] A. Florescu-Gligore, M. Orban, Ș. Țălu, “Cotarea în proiectarea constructivă și tehnologică” (Dimensioning in technological and constructive engineering graphics), Cluj-Napoca, Lithography of The Technical University of Cluj-Napoca, 1998;
- [24] A. Florescu-Gligore, Ș. Țălu, D. Noveanu, “Reprezentarea și vizualizarea formelor geometrice în desenul industrial” (Representation and visualization of geometric shapes in industrial drawing), Cluj-Napoca, U. T. Pres Publishing house, 2006;
- [25] Ș. Țălu, C. Racocea, “Reprezentări axonometrice cu aplicații în tehnică” (Axonometric representations with applications in technique), Cluj-Napoca, MEGA Publishing house, 2007;
- [26] C. Racocea, Ș. Țălu, “Reprezentarea formelor geometrice tehnice în axonometrie” (The axonometric representation of technical geometric shapes), Cluj-Napoca, Napoca Star Publishing house, 2011;
- [27] T. Nițulescu, Ș. Țălu, “Aplicații ale geometriei descriptive și graficii asistate de calculator în desenul industrial” (Applications of descriptive geometry and computer aided design in engineering graphics), Cluj-Napoca, Risoprint Publishing house, 2001;
- [28] Ș. Țălu, “Micro and nanoscale characterization of three dimensional surfaces. Basics and applications”, Napoca Star Publishing House, Cluj-Napoca, Romania, 2015;
- [29] M. Țălu, “Calculul pierderilor de presiune distribuite în conducte hidraulice” (Calculation of distributed pressure loss in hydraulic pipelines), Craiova, Universitaria Publishing house, 2016;
- [30] M. Țălu, “Pierderi de presiune hidraulică în conducte tehnice cu secțiune inelară. Calcul numeric și analiză C.F.D.” (Hydraulic pressure loss in technical piping with annular section. Numerical calculation and C.F.D.), Craiova, Universitaria Publishing house, 2016;
- [31] M. Țălu, “Mecanica fluidelor. Curgeri laminare monodimensionale” (Fluid mechanics. The monodimensional laminar flow), Craiova, Universitaria Publishing house, 2016;
- [32] M. Țălu, “The influence of the corrosion and temperature on the Von Mises stress in the lateral cover of a pressurized fuel tank”, *Magazine of Hydraulics, Pneumatics, Tribology, Ecology, Sensorics, Mechatronics (HIDRAULICA)*, no. 4, pp. 89-97, 2017, ISSN 1453-7303;
- [33] Ș. Țălu, M. Țălu, “The influence of deviation from circularity on the stress of a pressurized fuel cylindrical tank”, *Magazine of Hydraulics, Pneumatics, Tribology, Ecology, Sensorics, Mechatronics (HIDRAULICA)*, no. 4, pp. 34-45, 2017, ISSN 1453-7303;
- [34] D. Vintilă, M. Țălu, Ș. Țălu, “The CAD analyses of a torospheric head cover of a pressurized cylindrical fuel tank after the crash test”, *Magazine of Hydraulics, Pneumatics, Tribology, Ecology, Sensorics, Mechatronics (HIDRAULICA)*, no. 4, pp. 57-66, 2017, ISSN 1453-7303;
- [35] \*\*\* Autodesk AutoCAD 2017 software;
- [36] \*\*\* SolidWorks 2017 software.

## Considerations on the Calculation of Ventilation Systems for Special Ships

PhD std. Eng. **Octavian - Narcis VOLINTIRU**<sup>1</sup>, Prof. PhD. Eng. **Anastase PRUIU**<sup>1</sup>,  
PhD. Eng. **Ionut Cristian SCURTU**<sup>1</sup>

<sup>1</sup> Naval Academy “Mircea cel Batran”, Constanta, Romania; scurtucristian@yahoo.com

**Abstract:** *In the normal operation of ships, as a result of heat discharges from different machinery and people, the increase in humidity as well as due to the various releases of gases from the on-board systems or from the goods being carried, the air in the rooms is degraded, with the need for replacement and processing. Artificial microclimate systems have the function of thermally and humidly processing the air so that in the interior of the naval compartments the proper state parameters are maintained: comfort conditions in living spaces, storage conditions, the operation of machines and aggregates.*

**Keywords:** *Ventilation system, citadel system, HVAC, air treatment unit, air filter unit*

### 1. Introduction

HVAC installations include: ventilation installations, heating installations, cooling systems, conditioning plants (complex processing).

Ventilation systems have the function of delivering air without wetting, eliminating heat, NOx and humidity.

Ventilation and conditioning systems provide [1]:

- for surface vessels: complex air humidity processing so that its status parameters are automatically maintained at comfort levels;
- for seagoing and submarine compartments: in addition to the parameters it performs for surface vessels [2], it also provides a chemical composition for filling the oxygen consumed and retaining carbon dioxide released on board.



Fig. 1. Special ship – military ship

### 2. Microclimate condition for special ships compartments

#### 2.1. Microclimate condition for crew rooms

Air conditions in the ship's compartments depend on temperature, humidity and movement. The effect of air on the crew in the compartments is dictated by their metabolism, health, acclimatization, effort and their clothing [3,4].

The temperature graph is based on the results. For example at a temperature of 26 [°C], a value of humidity of 50 [%] and air speed of  $1 \left[ \frac{m}{s} \right]$ , the effective temperature should be 21.2 [°C].

The minimum amount of fresh air / outside air supplied must not be less than 8 liters / second / person. At the same time, it must be at least 40% of the total amount of air introduced into a given space.



- living spaces;
- space of complementary crew on board;
- medical compartments and facilities;
- galleys;
- storage rooms for hazardous materials;
- hangars for aviation;
- warehouses including refrigeration areas.

### 3.3. Risk situations for the ventilation system:

- the ambient conditions provided by the ventilation system are those conditions in which the operation of the machinery will not be significantly degraded or lead to failure;
- unfavorable environmental conditions can endanger personnel;
- the CO<sub>2</sub> level will have to be taken into account. All spaces requiring regular staff visits must be adequately ventilated;
- consideration must be given to the extraction of fire and smoke gases (eg CO<sub>2</sub> and equivalents) in an area that will not harm personnel;
- water inlet through the ventilation holes. Ventilation holes or appropriate locking devices shall be provided to ensure the ship's integrity;
- propagation of fire. The number and location of the stops depend on the type of ship. In all cases, ventilation must be done outside the ventilation space.

## 4. Special HVAC systems

In simple terms, there are three types of subsystems of the artificial microclimate system onboard ship (intake fans, extraction fans and recirculation fans). The compartments of the vessel are either ventilated or air-conditioned. In ventilated compartments, there is an air intake system and an extraction system that returns air to the atmosphere. In the air-conditioned compartments, the air is recirculated, an amount of air in the compartment is evacuated to the atmosphere, and a quantity is replaced by fresh air. Generally, air is introduced into the ship through fans installed in compartments fitted with heaters and coolers.

In both, normal and contaminated atmospheres, all air conditioners are designed to work with AFUs (air filtration units) all the time. From air filtration units, the air is introduced into the ship and then recirculated through the air treatment unit (ATU) throughout the ship.

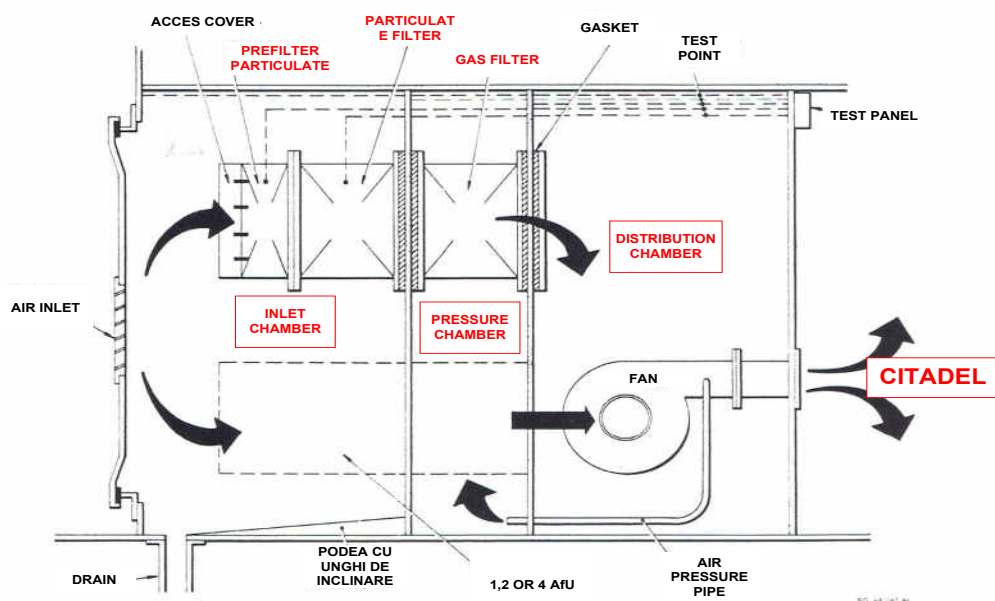


Fig. 3. System operation Air Filter Unit

For special ships, the artificial microclimate system is complex, vital and large size, impacting each compartment of the ship. The artificial microclimate system is divided into zones and is integrated with the chilled water system of the ship.

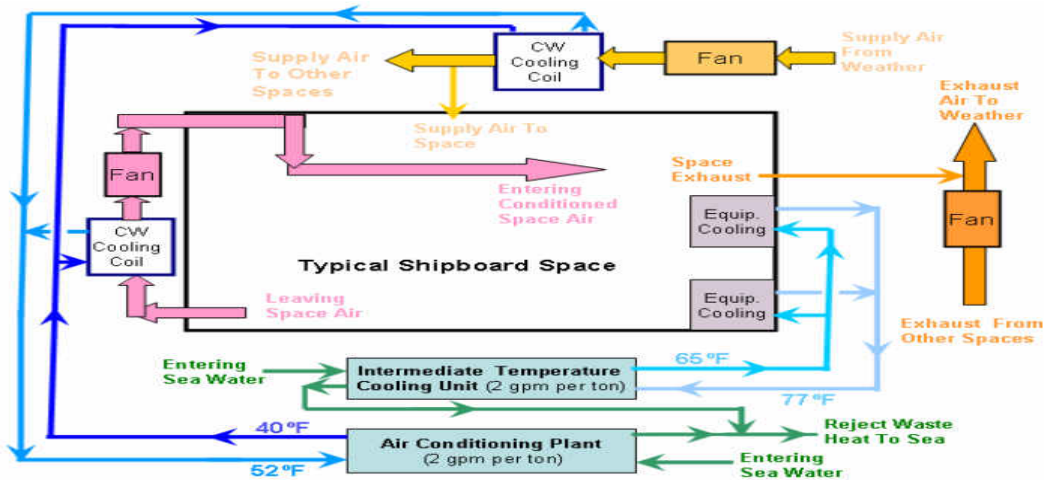


Fig. 4. HVAC operation

5. Machinery spaces ventilation

5.1. Machinery spaces configuration

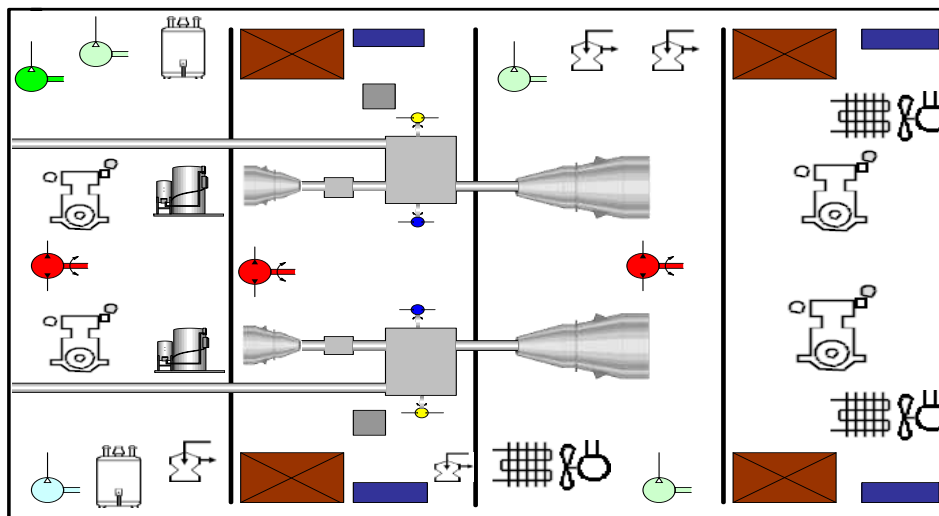


Fig. 5. Machinery spaces configuration with gas turbines for special ships

Each of the engine compartments (Forward Diesel Generator Space, Aft Diesel Generator Space, Forward Gas Turbine Space, Aft Gas Turbine Space) are ventilated with 2 supply fans and 2 exhaust fans. When the special ship is watertight against the contaminated atmosphere, the air in the engine compartments is recirculated by means of chilled water coolers for air-induction fans. The extraction capacity is greater than the air intake capacity in the machine compartments in order to ensure smoke and gas extraction in the compartments and to cool off the gas discharge routes (inlet capacity:  $11530 \left[ \frac{m^3}{\square} \right]$ , exhaust capacity:  $13250 \left[ \frac{m^3}{\square} \right]$ ).

Coolers of machinery spaces should be insulated and drained as needed. The system must be ventilated during coolers recharging.

The machinery spaces ventilation must be reduced sufficiently in order to maintain the ambient temperature above 2 [°C].

In the CBRN atmosphere, the machinery spaces will be contaminated with gas and the area will

become a contaminated one. Before starting the intake fans, the intake galleries must be drained by the water that has accumulated during spraying of the ship with the sprinkler.

Machine room exhausts are also used to cool out gas routes for engines and turbines.

The turbine modules are ventilated by a separate natural ventilation system that uses the depression in the turbine suction galleries to maintain a cooling air flow for the mode when the turbines are in operation [9, 10].

All fans mounted in machinery spaces are of the axial type with constant flow and vertical position. The upper end of the fan is provided with a screen to protect foreign objects that may enter.

The rainwater infiltration shutters are fitted to all the openings in the deck for ventilation. At the top of the vessel, the ventilation openings are provided with hinged caps, except for openings for ventilation of turbine modules.

In a contaminated atmosphere, the air of the machinery is evacuated by means of air valves that open when the internal pressure is more than half the atmospheric pressure.

## 5.2. Air flow calculation for cruising gas turbines compartment

We will consider a machine compartment for a special ship equipped with two Rolls Royce Tyne RM1C turbines.

The characteristics of the reference engine are as follows:

- effective power:  $2 \times 4500 = 9000$  [kW];
- specific fuel consumption:  $0.260 \left[ \frac{Kg}{kW \square} \right]$ ;



Fig. 6. Rolls Royce Tyne RM1C gas turbine [11]

Specific air flow for gas exchange:

$$d_{asg} = m_{tsg} \cdot \alpha_{sg} \cdot C_e \left[ \frac{Kgair}{kW \square} \right] \quad (2)$$

where:

- $m_{tsg} = 14.2 \left[ \frac{Kgair}{Kgcomb} \right]$  - theoretical air mass needed for burn of one fuel kilogram;
- $\alpha_{sg} = 1.8$  - excess air coefficient for gas exchange;
- $C_e = 0.260 \left[ \frac{Kgcomb}{kW \square} \right]$  - specific fuel consumption;

$$d_{asg} = 14.2 \cdot 1.8 \cdot 0.260 = 6.64 \left[ \frac{Kgair}{kW \square} \right] \quad (3)$$

Specific air flow needed for ventilation:

$$d_{av} = 2 \cdot d_{asg} = 13.29 \left[ \frac{Kgair}{kW \square} \right] \quad (4)$$

Mass Air Flow for Ventilation:

$$\dot{D}_{av} = 2 \cdot d_{asg} \cdot P_e = 119620.8 \left[ \frac{Kg_{air}}{\square} \right] \quad (5)$$

Volumetric Air Flow for Ventilation:

$$\dot{V}_{av} = 2 \cdot \frac{d_{asg}}{\rho_a} \cdot P_e = 108845.1 \left[ \frac{m^3_{air}}{\square} \right] \quad (6)$$

## 6. Ventilation flow simulation in machinery spaces

Ansys offers a complete range of simulation solutions [12,13,14], engineering kits offer almost any field of simulation engineering, and a pre-rendering machine is required.

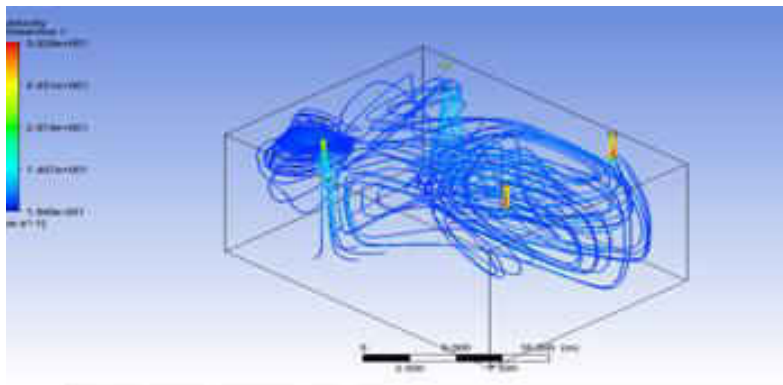


Fig. 7. Air velocity – Ansys CFX – 25 points [4]

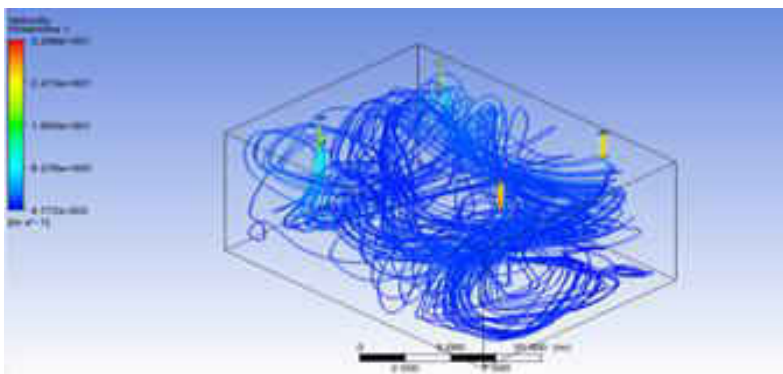


Fig. 8. Air velocity – Ansys CFX – 40 points [4]

## 7. Conclusions

For special ships, the artificial microclimate system is complex, vital and of large size, impacting each compartment of the ship. The artificial microclimate system is divided into zones and is integrated with the chilled water system of the ship.

The NATO functional objectives for the ventilation system are as follows:

- ambient conditions must be controlled in accordance with the requirements of on-board aggregates;
- ambient conditions must be controlled in accordance with the requirements of on-board personnel;
- ventilation must be provided in hazardous areas.

In order to eliminate thermal flows in the compartments of the ship, it is necessary to calculate the following sizes:

- calculation of the air flow introduced into air-conditioned compartments;
- calculation of the air flow extracted from the crew compartments;

- the calculation of the airflow required to evacuate the heat flow from the engine compartments

To optimize the energy utilization required for air entrainment fans must consider the weight of warm drive machine works, to be specific the quantity of motors to run all the while, the quantity of steam boilers burners in operation at the same time.

Ambient conditions require adjusting the air flow which ventilates the engine room and supplies the necessary air for engines, and engine room air temperature control.

## References

- [1] American Bureau of Shipping, “Crew habitability on ships”, February 2016;
- [2] ANSI/ASHRAE Standing Standard Project Committee, “Ventilation for Acceptable Indoor Air Quality”, 2007;
- [3] I. Serbanescu, “Consideration Regarding Maritime Ship Engine Room Ventilation System”, January 2016;
- [4] ISO 7547, “Ships and marine technology — Air-conditioning and ventilation of accommodation spaces — Design conditions and basis of calculations”, 01.09.2002;
- [5] ISO 8861, “Engine room ventilation in diesel-engine ships”, January 2001;
- [6] Lloyd’s Register – “Military Design and Special Features”, January 2015;
- [7] NATO Standard – *Naval Ship code* – April 2017 – NATO Standardisation office;
- [8] Naval Surface Warfare Center Carderock Division, *21 Century HVAC System for Future Naval Surface Combatants – Concept Development Report*, USA, September 2007;
- [9] <http://www.seaforces.org/marint/Royal-Navy/Frigate/Broadsword-Type-22-class.htm>;
- [10] <https://commons.wikimedia.org/wiki/File:SMS-Bayern-protection-scheme-EN.svg>;
- [11] <http://www.directindustry.fr/prod/rolls-royce/product-22649-1096587.html>;
- [12] [www.ansys.com](http://www.ansys.com);
- [13] I. Călimănescu, L.C. Stan, “Computer fluid dynamics (CFD) study of a micro annular gear pump”, *Atom 2016*, Conference Paper - Proceedings Volume 10010, Advanced Topics in Optoelectronics, Microelectronics, and Nanotechnologies VIII; 1001020 (2016); doi: 10.1117/12.2241674 Event: Advanced Topics in Optoelectronics, Microelectronics, and Nanotechnologies 2016, 2016, Constanta, Romania;
- [14] L.C. Stan, I. Călimănescu, “A New innovative turbocharger concept numerically tested and optimised with CFD”, 2016, Conference Paper - 10th International Conference on Turbochargers and Turbocharging.

## Researches regarding the Behavior of CuAl10.5Ni5Fe4.8Mn1.5 at Erosion Generated by Vibratory Cavitation

PhD. Student eng. **Iosif LAZAR**<sup>1</sup>, Prof. PhD.eng. **Ilare BORDEASU**<sup>2</sup>,  
Prof. PhD.eng. **Mircea O. POPOVICIU**<sup>3</sup>, Lect. PhD.eng. **Lavinia Madalina MICU**<sup>4</sup>

<sup>1</sup> Politehnica University of Timisoara, Mihai Viteazul St. No.1, 300222, Timisoara, Romania, E-mail: office@ducodan.ro,

<sup>2</sup> Politehnica University of Timisoara, Mihai Viteazul St. No.1, 300222, Timisoara, Romania, E-mail: ilarica59@gmail.com,

<sup>3</sup> Academy of Romanian Scientists, Mihai Viteazul St. No. 1, 300222, Timisoara, Romania, E-mail: mpopoviciu@gmail.com

<sup>4</sup> “Mihai I King of Romania” University of Agricultural Sciences and Veterinary Medicine of Banat in Timisoara, Route of Arad no.119, 300645 Timisoara, Romania, E-mail: lavimicu@yahoo.com

**Abstract:** The paper presents research results regarding the behavior at cavitation erosion of the CuAl10.5Ni5Fe4.8Mn1.5 bronze used in manufacturing ship propellers. For the experimental research it was used the Standard Vibratory Apparatus with piezoelectric crystals, of the Timisoara Polytechnic University Cavitation Laboratory. The analyze is realized by using the curves and parameters recommended in the ASTM G32-2010 Standard, the photographic images and the profiles of the surface subjected to cavitation. The resistance evaluation was obtained by comparisons with the behavior of the stainless steel OH12NDL for which we have numerous laboratory researches as well as detailed informations about the behavior in field running. The final conclusion is that the researched bronze has a very good cavitation erosion and can be used for manufacturing ship propellers.

**Keywords:** Bronze, cavitation resistance, roughness, characteristic curves, microstructure

### 1. Introduction

The cavitation effect upon ship propellers has been notified in the year 1848, when the first modern metallic passenger ship with mechanical propulsion constructed in Great Britain, was subjected to technical verification. The ship was designed by Isambard Kingdom Brunel and launched to the water in 1843 [12]. The negative effects such as important erosion and the reduction of the propulsion velocity were identified only in 1893 by Parsons [4, 7], after studies effected in a hydrodynamic tunnel. The aspect of the cavitation phenomenon and the effects upon the blades, both presented in Fig. 1, show that the most affected zones are blades tips [12].

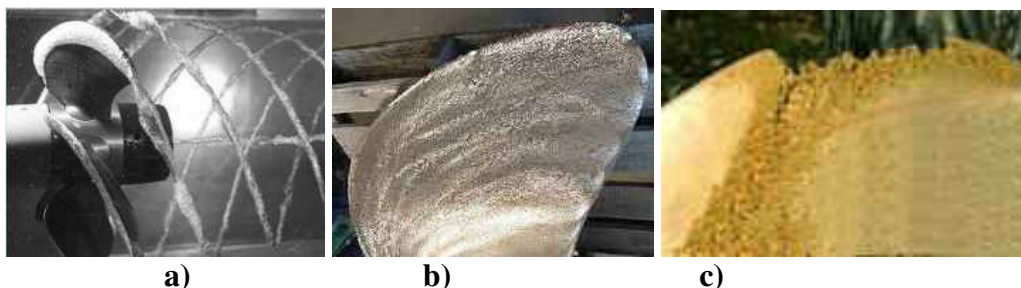


**Fig. 1.** Ship propellers running in cavitation and a blade eroded by cavitation [11]  
a) cavitation vortex at the propeller blade peak; b) blade with cavitation erosion;  
c) detail of the eroded zone

As a result of those inconveniences, from them on until now, there are effected multiple researches to find materials having increased resistance both to cavitation and corrosion. Simultaneously are made studies regarding various procedures for increasing the cavitation erosion resistance of the

areas subjected to cavitation [1, 2, 3, 6]. The results of the present researches are in line with those trends [5, 7, 8].

## 2. Researched material

For researches was used the bronze CuAl10.5Ni5Fe4.8Mn1.5 [11]. The chemical composition and the mechanical characteristics with relevance to cavitation erosion, determined in the Timisoara Polytechnic University Laboratory for the Material Sciences and Engineering are: 10.46 % Al, 4.85% Ni, 4.72 %Fe, 1.41 % Mn, the rest being Cu; fracture strength  $R_m = 980$  MPa, yield strength  $R_{p0.5} = 789$  MPa, Brinell hardness = 283 HB30, elongation  $A_5 = 8$  %, resilience KCU= 7 J.

## 3. Cavitation tests

The cavitation erosion tests were realized in the vibratory device T2, with piezoelectric crystals, in conformity with the rules of the Timisoara Polytechnic University Cavitation Laboratory [9], [2], [6], [7] in the same time respecting all the requirements of the ASTM G32-2010 Standard [11].

All tests were realized in double distilled water. The liquid temperature during the researches was maintained at  $22 \pm 1^\circ\text{C}$ . In conformity with the requirements, there were subjected to the tests 3 identical samples.

Before beginning the tests the active surface of the samples were polished with abrasive paper and with the paste PROFILINE SONAX FS 05-04. The mean roughness of the active surface, before the beginning of tests (Fig. 2 present one of the three tested samples) was obtained with the portable roughness measuring device TR 110. The measuring was done in 6 points. The values for  $R_a$  are:

- for sample 1:  $R_a = 0.167 \mu\text{m}$ ,
- for sample 2:  $R_a = 0.171 \mu\text{m}$ ,
- for sample 3:  $R_a = 0.179 \mu\text{m}$

Surface exposed  
to cavitation



Fig. 2. The sample surface before cavitation exposure

The exposure time for each sample, in conformity with the Laboratory rules [1], [2], [3], [8], [6] was 165 minutes, at the beginning with two short periods of 5 and 10 minutes, afterwards with 15 minutes periods. At the end of each individual period it was measured the mass  $\Delta m_i$  lost as the result of the cavitation exposure. With these results there were computed:

- The cumulative mass losses  $M$ :

$$M_i = \sum_{i=1}^{12} \Delta m_i \quad (1)$$

- The mean erosion rate:

$$v_i = \Delta m_i / \Delta t_i \quad (2)$$

The meaning of the notations used above i :

i – testing period (i = 1, 2, ..., 12)

$\Delta m_i$  – the lost mass in the period i, measured in grammes,

$\Delta t_i$  – the time of the exposure in period "i", (5, 10 or 15 minutes).

The mediation of the experimental values was realized through analytical curves obtained with the following relations [7]:

- for the mass losses:

$$M(t) = A \cdot t \cdot (1 - e^{-Bt}) \quad (4)$$

- for the erosion velocity:

$$v(t) = A \cdot (1 - e^{-Bt}) + A \cdot B \cdot t \cdot e^{-Bt} \quad (5)$$

where:

**A** – is the scale parameter, statistically established, from the condition of minimum scatter of the experimentally obtained points, with regard to the obtained curve.

**B** – is the form parameter of the curve.

The approximation curves were used for analyzing the erosion evolution during the exposure time, taking into account both the shape and the scatter of experimental points. In order to evaluate the mass losses, were used the mean mass losses obtained on the three samples, for each intermediary testing period, the cumulative mass loss as well as the loss velocity. In order to assess the cavitation erosion resistance, the obtained curves were compared with those obtained for the OH12NDL stainless steel, material with good behavior both in laboratory tests and in the field in the operation of hydraulic turbines. Supplementary, there were made comparisons between the stable velocities for final erosion exposure times. In Fig. 3 are presented the experimental obtained values together with the cavitation erosion characteristic curves.

The dispersion of the experimental points with regard to the mediation curves show that cavitation erosion is a statistic event. Thousands of tiny and patchy bubbles impacts very tiny sample areas, each with his one resistance. That is why three samples obtained from the same rod presents cavitation erosion resistance with small differences. The evolution of curve  $M(t)$  in Fig. 3a show that, beginning approximately with the minute 45, its shape is almost linear, it means that from this moment the behavior of the bronze remain approximately the same till the final exposure time. The curve  $v(t)$  gives more exactly values for the beginning of the stabilization curve, namely the minute 90 but the difference between the maximum velocity and the final value is very small (0.126 mg/min).

The differences between the experimental values of the three tested samples, whether we mean the cumulative mass loss  $M_i$  or the erosion velocity  $v_i$  are very small. It prove that the structure and the mechanical characteristics are very uniform distributed on the exposed area.

From the experience of 70 year [1], [7], such a dispersion mode is specific for the materials with very good cavitation erosion resistance, Also the evolution of the curves  $v(t)$  from the maximum value towards the stabilization one show that the researched bronzes are materials with very good cavitation erosion resistance and can be used for manufacturing details subjected to a very strong cavitation erosion and can be used for manufacturing navy propellers.

The differences between the experimental values and the approximation curves, till the minute 15 (see Fig. 3b) are given by the metallic dust and the sharp roughness expelled in this period. Normal this beginning period is not taken into account in the material behavior analyze, because it depends in great measure on the sample polishing and cleaning before the beginning of tests [1], [7].

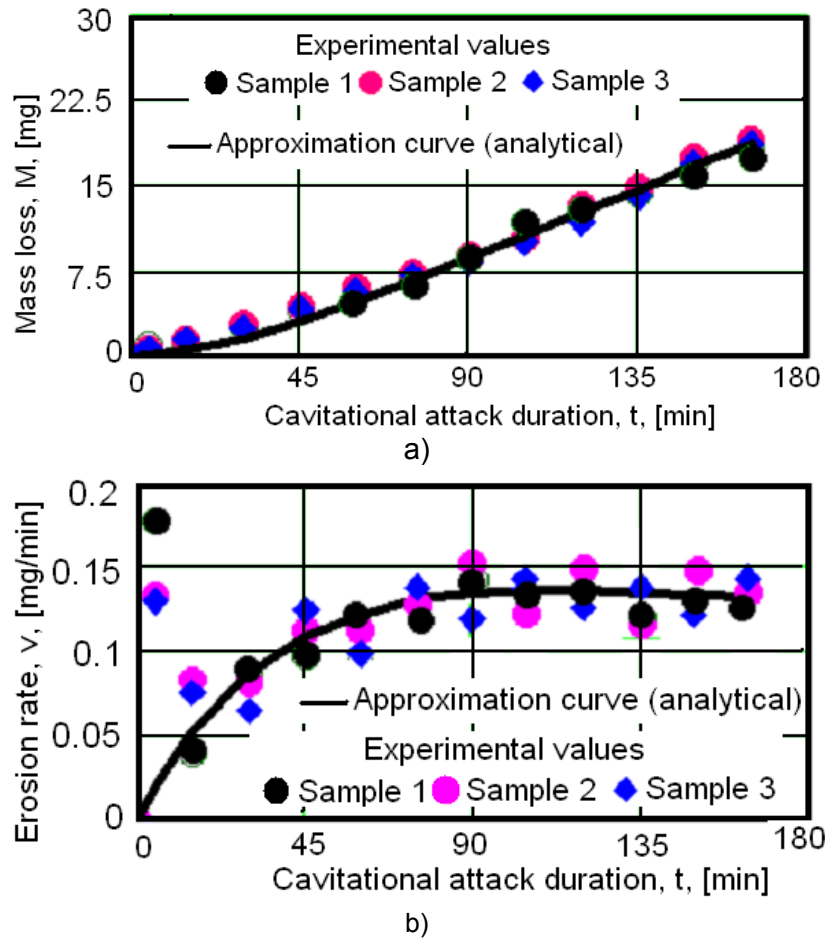


**Fig. 3.** Specific curves of behavior evolution and cavitation resistance  
 a) mass loss against the exposure to cavitation attack  
 b) erosion rate against exposure to cavitation attack

The evolution of the sample surface erosion is presented in the images of Table 1, realized for two specific intervals. The photographic images show clearly the increase of the cavitation erosion intensity upon the whole area and the penetration in the depth of sample.

**Table 1:** Erosion evolution of the exposed area

Attack duration	Sample		
	1	2	3
75 minutes			
165 minutes			

To put into evidence the cavitation erosion behavior, as well as the resistance to the mechanical fatigue stresses generated by the impacts of the surface with the microjets and the shock waves generated by the implosion of the cavitation bubbles, in Fig. 4 there are made comparisons between the obtained experimental curves and values and those for the martensitic stainless steel OH12NDL for which we have both laboratory experimental results and field results in hydraulic turbines. In the same time there were made discussions regarding the comparisons between specific parameters ( $M_{tot}$  and  $v_s$ ).

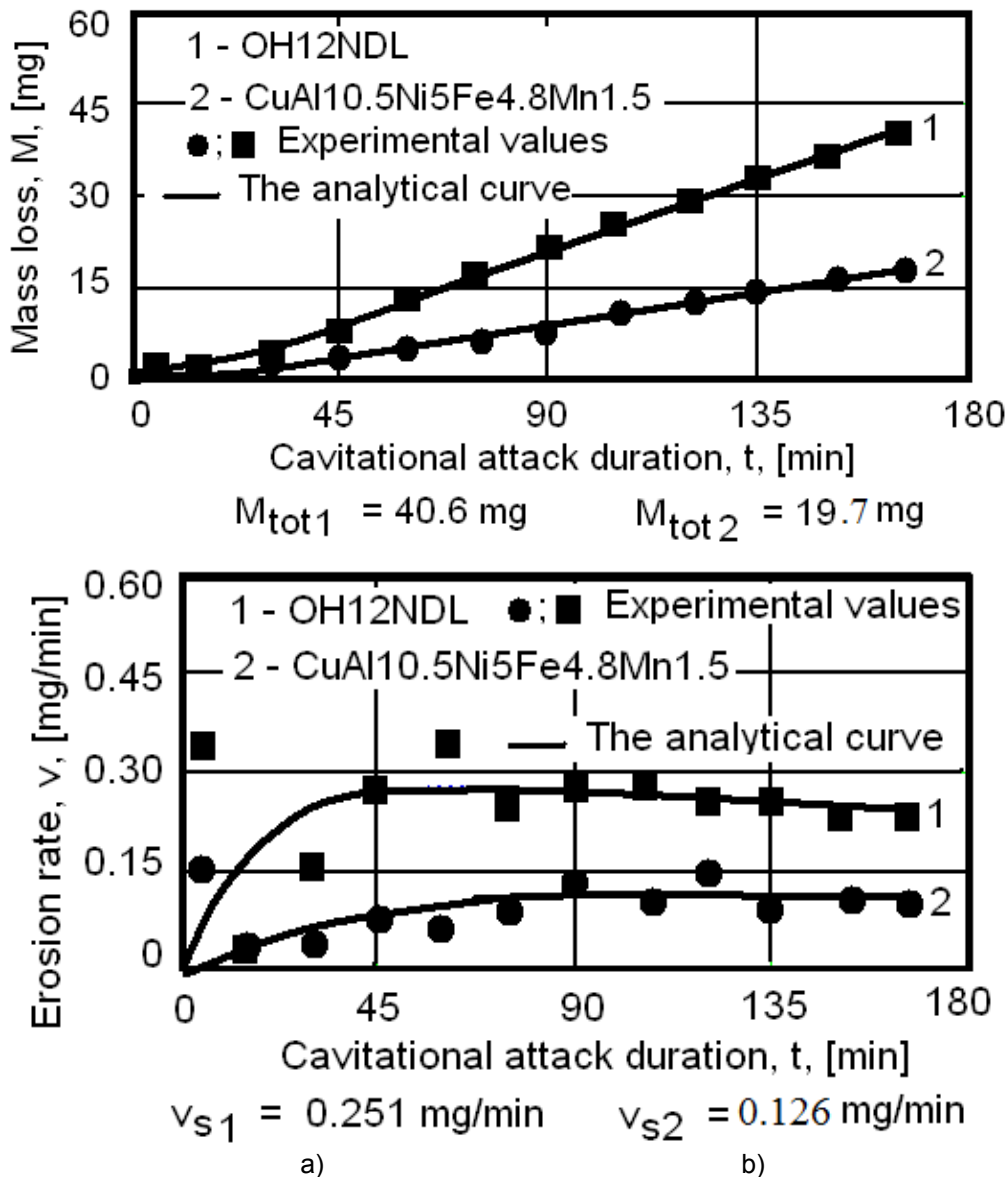


Fig. 4. Comparison with OH12NDL etalon steel:  
a) mass loss comparison; b) erosion rate comparison

Taking into account the values of both parameters the resistance of the researched bronze is about two times greater than the resistance of the martensitic stainless steel OH12NDL. In conclusion the bronze CuAl10.5Ni5Fe4.8Mn1.5 has excellent behavior to cavitation erosion.

#### 4. Phenomenological investigation of the eroded microstructure

The investigation of the eroded structure was done on the scanning electronic microscope Philips XL 30 ESEM in the Laboratories for Materials Science and Engineering.

The images presented in Fig. 5 (before the cavitation exposure, on separate specimens designed only for this purpose) and in Fig 6 (specimens subjected to the maximum exposure time) show that the microstructure of the material is constituted in principal from a solid solution  $\alpha$  and a small proportion of the eutectoid  $\alpha + \gamma'$ .

The images of figures 5...7 reveal the peculiarities of the eroded surface degraded by cracks at the grain boundaries but also by realizing caverns and pitting as the result of the expelled grains. Because the solid solution  $\alpha$  gives a good plasticity and the eutectoid enhances the mechanical characteristics, the initiation of the cavitation erosion take place at the interface of these two structural constituents and only afterwards continues with expelling of the whole grain. This behavior results from the images presented in Fig. 6. Supplementary, the electronic scanning microscopy put into evidence the formation of annealing mackles and the priority expelling of the solid solution grains.

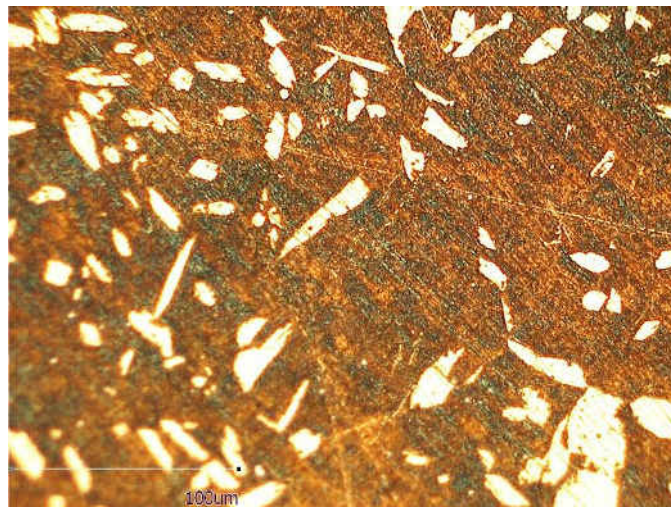


Fig. 5. Microstructure of the bronze CuAl10.5Ni5Fe4.8Mn1.5 (1750 x)

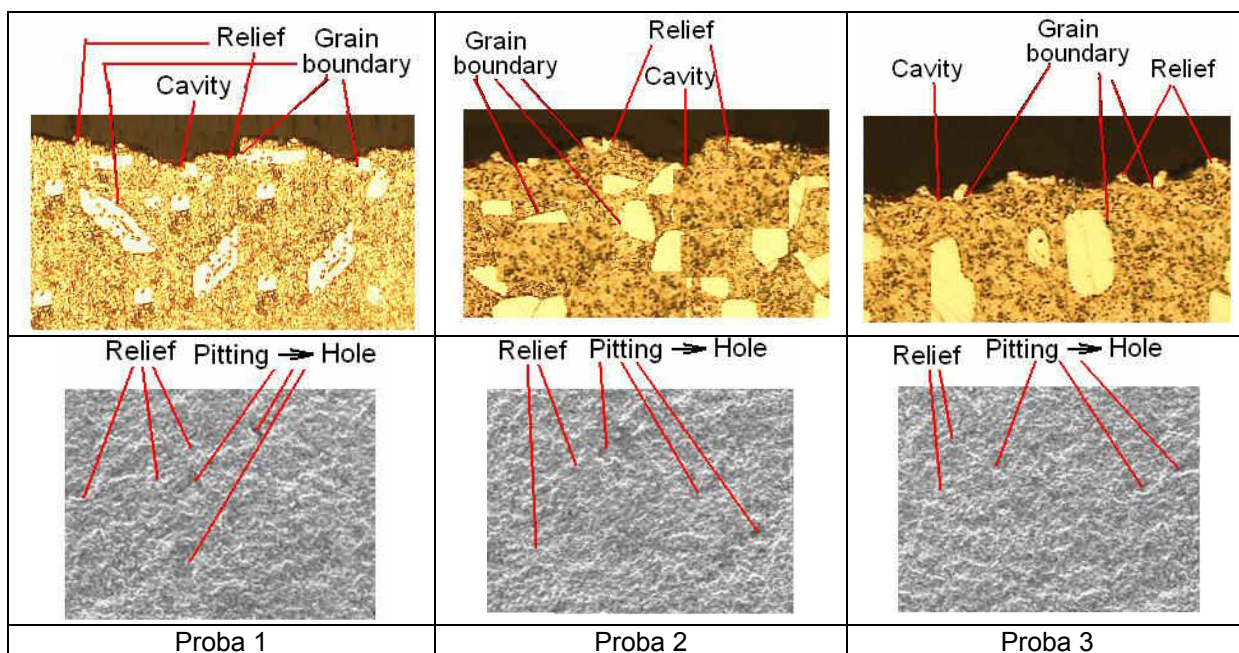


Fig. 6. Images of structure degradation (pitting, hole, deformations) Final exposure time, 165 minutes (1750x)

The images in Fig. 8 presents the profiles of the eroded surface, obtained in the central zone, in conformity with Fig 7, on a 4 mm length, using the roughness device Mitutoyo.

Recording area with Mitutoyo roughness apparatus



Fig. 7. Recording zone of cavitated area roughness, with the Mitutoyo apparatus

In comparison with the images in Fig. 6 it can be seen a very good concordance between the profiles and the erosion mechanism. Taking into account the bronze density, computed upon the chemical composition (7.45 grams/mm<sup>3</sup>) it results that the maxim penetration depth computed with the relation:

$$MDE_i = \sum_{i=1}^{12} \Delta MDE_i = \sum_{i=1}^{12} \frac{4 \cdot \Delta m_i}{\rho \cdot \pi \cdot d_p^2} \tag{6}$$

are:

- for the sample 1: MDE ≅ 13.584 μm
- for the sample 2: MDE ≅ 12.997 μm
- for the sample 3: MDE ≅ 13.871 μm

This observation confirm the idea that cavitation resistance evaluation can be done, with a good approximation, also using the parameters of roughness, especially R<sub>z</sub>.

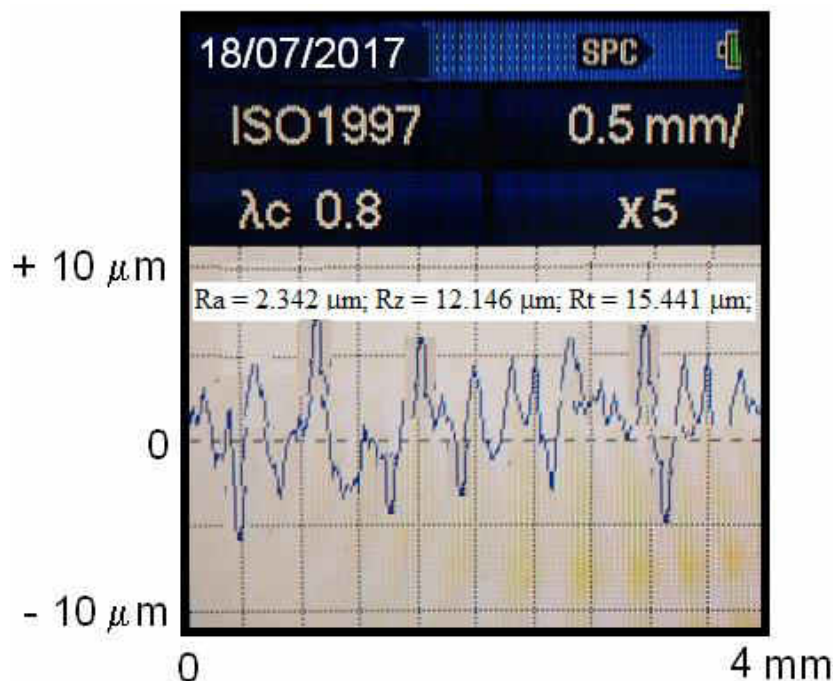


Fig. 8. - Sample 1

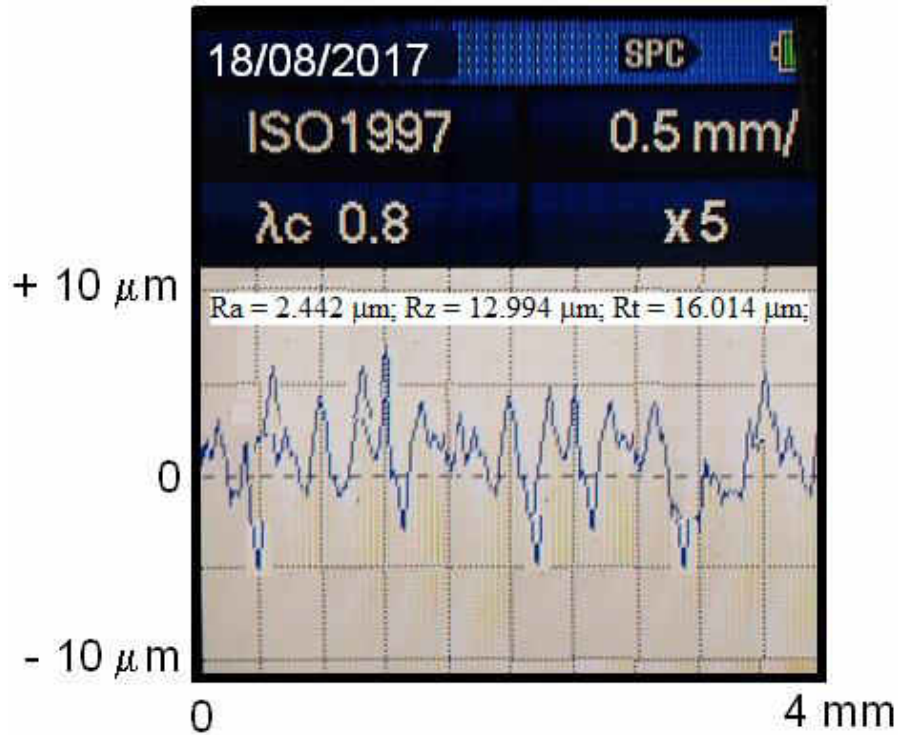


Fig. 8. - Sample 2

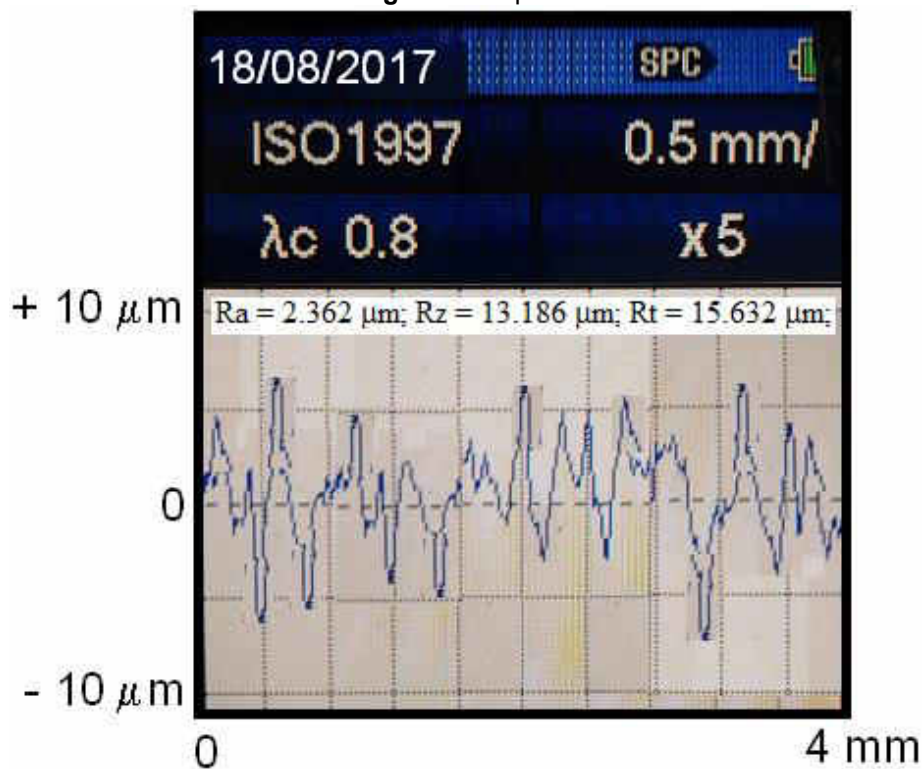


Fig. 8.- Sample 3

Fig. 8. Profile of the eroded surface, recorded in the center of the cavitated area

## 5. Conclusions

The evolution of cavitation characteristic curves and reduced scatter for experimental results, of the three tested samples, suggest that the bronze CuAl10.5Ni5Fe4.8Mn1.5 has a homogenous structure giving a very good resistance to cavitation erosion.

Because the solid solution  $\alpha$  is responsible for a good plasticity and the eutectoid enhance the mechanical resistance, the cavitation erosion begin on the interface of the two constituents and only afterwards continues towards the inner part of the grains.

The roughness profile, obtained with a Mitutoyo device, confirm the uniform degradation of the cavitation exposed surface, the behavior being specific for materials with very good cavitation erosion behavior, as well as with fine structures, great homogeneity which give uniform mechanical properties.

The comparison with the stainless steel OH12NDL, with which we obtained good cavitation erosion behavior both in laboratory and in running hydraulic turbines show that the tested bronze satisfy the requested demands also for ship propellers.

## References

- [1] I. Bordeasu, „Eroziunea cavitațională a materialelor”, Editura Politehnica, Timișoara, 2006;
- [2] I. Bordeasu, M.O. Popoviciu, „Contributions Regarding Cavitation Erosion Hierarchy For Stainless Steels”, *Machine Design*, Vol.5 (2013) No.4, ISSN 1821-1259, pp. 157-162;
- [3] I. Bordeasu, M.O. Popoviciu, T.S. Duma, „Consideration concerning the Steels Cavitation Erosion Resistance Modification with Specific Heat Treatments”, *KOD 2012, Proceedings The 7-th international symposium about forming and design in mechanical engineering*, 24-26 mai.2012, Balatonfured, Ungaria, ISBN 978-86-7892-399-9, pp.519-522;
- [4] J.P. Breslin, P. Andersen, „Hydrodynamics of ship propellers”, 3, Editor Cambridge University Press: United Kingdom, 2003;
- [5] J.P. Franc, et al, „La Cavitation”, *Mecanismes physiques et aspects industriels*, Press Universitaires de Grenoble, 1995;
- [6] L. M. Micu, I. Bordeasu, M. Popoviciu, „Cavitation erosion of HVOF metal-ceramic composite coatings deposited onto Duplex stainless steel substrate”, *Revista de Materiale Plastice*, vol.53, no.4, 2016, ISSN 0025-5289, pp.781-786;
- [7] O. Oanca, „Tehnici de optimizare a rezistenței la eroziunea prin cavitație a unor aliaje CuAlNiFeMn destinate execuției elicelor navale”, Teza de doctorat, Timișoara, 2014;
- [8] M.O. Popoviciu, I. Bordeasu, „Proposed Model for Cavitation Erosion Test Results Presentation”, *Machine Design*, Vol.5(2013) No.1, ISSN 1821-1259, pp. 11-16;
- [9] \*\*\* (2010). Standard method of vibratory cavitation erosion test, ASTM, Standard G32-10;
- [10] \*\*\* Registrul Naval Roman, „Reguli pentru clasificarea și construcția navelor maritime”, Vol. V, București, 1986;
- [11] \*\*\* [http://www.ampcometal.com/common/datasheets/en/AM4\\_EX\\_E.pdf](http://www.ampcometal.com/common/datasheets/en/AM4_EX_E.pdf);
- [12] \*\*\* [https://www.google.ro/search?q=image+of+ship+propeller+cavitation+damage&oq=image+of++ship+propeller+cavitation&gs\\_l](https://www.google.ro/search?q=image+of+ship+propeller+cavitation+damage&oq=image+of++ship+propeller+cavitation&gs_l)

## The Influence of Deviation from Circularity on the Stress of a Pressurized Fuel Cylindrical Tank

Assoc. Prof. PhD. Eng. Ștefan ȚĂLU<sup>1</sup>, Assoc. Prof. PhD. Eng. Mihai ȚĂLU<sup>2,\*</sup>

<sup>1</sup> Technical University of Cluj-Napoca, The Directorate of Research, Development and Innovation Management (DMCDI), Constantin Daicoviciu Street, no. 15, Cluj-Napoca, 400020, Cluj county, Romania. E-mail: stefan\_ta@yahoo.com

<sup>2</sup> University of Craiova, Faculty of Mechanics, Department of Applied Mechanics and Civil Engineering, Calea București Street, no. 107, 200512 Craiova, Dolj county, Romania. Corresponding author\* e-mail: mihai\_talu@yahoo.com

§: Both authors contributed equally to this work.

**Abstract:** *The objective of this study is to determine the state of stress that occurs in the shape deformation of the lateral shell of a pressurized fuel cylindrical tank made of AISI 4340 steel, by modification of the cylindrical shape to an elliptical shape. The study of the state of efforts is carried out in the context of the overlapping of the influence of the deviations of the form over the influences caused by the temperature and corrosion variation. The CAD analysis is done on a parameterized model, finalizing with the determination of the laws of variation of the stress by polynomial interpolation and graphical representation. In this study it is also defined the graphic domain characterized by parameters such as: temperature  $T$ , pressure  $p$ , duration of exploitation and coefficient of ellipticity  $k$ , for which the lateral is oved from use as a result of exceeding the admissible effort values.*

**Keywords:** *Automotive industry, coefficient of ellipticity, corrosion, elliptical cover, industrial engineering design, optimization methods, pressurized fuel tank*

### 1. Introduction

The fuel tanks market in the automotive industry has a dynamic development, sustained by the continuous research of trained specialists with direct applicability and utilization of high technologies [1-4]. These challenges help to increase safety in exploitation and competitiveness in production [5-9].

The construction geometry of pressurized fuel tanks (made especially of steel or aluminum) in the automotive industry is a complex process based on an appropriate documentation [10-13].

Pressurized cylindrical fuel tanks are used to store liquefied petroleum gas (LPG) or compressed natural gas (CNG) fuel. For these tanks the state of stress in the lateral cover has significant changes if there are circular deviations from the cylindrical shape [6]. On the other hand, other factors that influence the state of effort are: pressure, temperature and corrosion [7-10, 14, 15].

The hydraulic testing pressure of the pressurized fuel tank are relatively high and can attain up to a  $p = 300$  bar in the case of CNG tanks [5, 6, 16]. The optimal engineering design of the fuel tanks, with more and less components, involves engineering level tools [17-28], both computational and experimental, which includes modeling [29-37] and testing to a better solution at less cost [38-44].

In practice, the transformation of the lateral cover of a cylindrical fuel tank into an elliptical shape can be found either by the inappropriate application of some technological processes in the realization of the covering or as a result of an impact resulting from a road accident.

### 2. The parameterized model of the elliptical lateral cover of the pressurized fuel tank

This study was performed on an optimally designed lateral cover of a pressurized cylindrical fuel tank, which was deformed into an elliptical shape. The cylindrical initial shape of the lateral cover and its state of stress constitute the basis of comparison of the effect introduced on the state of stress by deforming it in elliptical form. The parametric modeling of the pressurized cylindrical fuel tank was made with AutoCAD Autodesk 2017 software [45].

The initial data of design process for the cylindrical lateral cover are:

- maximum hydraulic test pressure  $p_{\max} = 30$  N/mm<sup>2</sup>; on the interior surface  $S_5$ , (Figure 1);

- working temperature with variation between the limits  $T = -30\text{ }^{\circ}\text{C}$  up to  $T = +60\text{ }^{\circ}\text{C}$ , on the exterior surface  $S_6$ , (Figure 1);
  - the corrosion velocity of the material:  $v_c = 0.12\text{ mm/year}$ ;
  - the lateral cover material, AISI 4340 steel; - the exploitation period:  $n_a = 20\text{ years}$ ;
  - the outer diameter and length of the lateral cover are:  $\phi = 250\text{ mm}$  and  $L = 700\text{ mm}$ , (Figure 1).
- Noting with:  $a$  and  $b$ , the semi-major and semi-minor axes of the ellipse, the coefficient of ellipticity  $k_e$  is given by the following formula:

$$k_e = \frac{a}{b} > 1 \quad (1)$$

It is assumed the medium perimeter of the initial ring section passing in the elliptical form is equal to the medium perimeter of the elliptical ring section after deformation, according next formula:

$$2\pi R = \frac{3\pi}{2}(a+b) - \pi\sqrt{a \cdot b} \quad (2)$$

If we take into account the calculation formula of the coefficient of ellipticity  $k_e$ , then the median annular ellipse semi-axes have the graphic variation given in Figure 2 and can be calculated with the following formulas:

$$b = \frac{4R}{3(k_e + 1) - 2\sqrt{k_e}} ; a = b \cdot k_e \quad (3)$$

Based on the symmetry of the lateral cover with respect to the planes containing the semi-major and semi-minor axes of ellipse and of the longitudinal axis of the lateral cover our study was carried out on a model divided into  $\frac{1}{2}$  of the initial shape of the lateral cover (Figure 1).

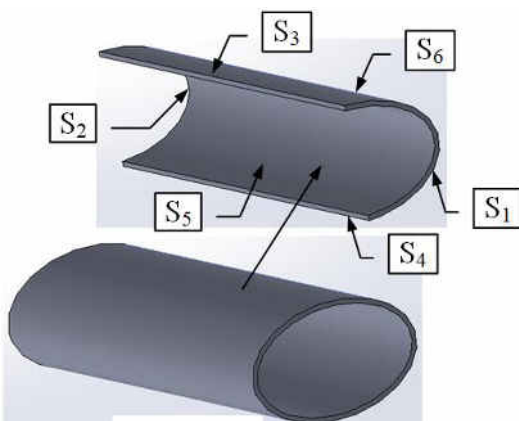


Fig. 1. The outer surfaces of elliptical cover

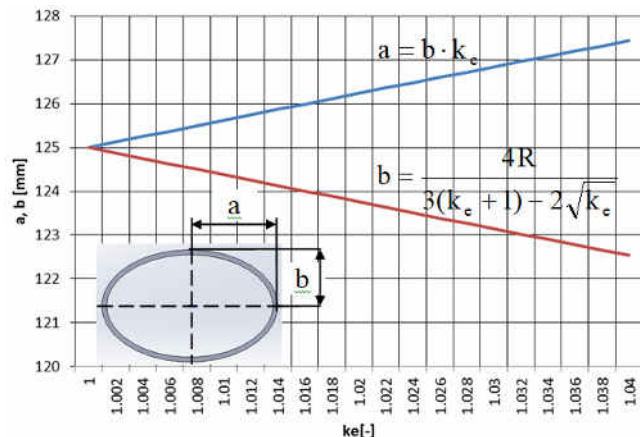


Fig. 2. The graphical variations of the ellipse semi-axes

### 3. The CAD study of the Von Mises stress state in the elliptical lateral cover

The existence of the two head cover with the pressure  $p_{\max} = 30\text{ N/mm}^2$  on the inner surfaces  $S_5$ , causes the apparition of two traction forces on the end surfaces:  $S_1$  and  $S_2$ , Figure 1, which have the following value:

$$F = \pi a b p_{\max} = \pi b^2 k_e p_{\max} = \frac{16\pi R^2 k_e}{[3(k_e + 1) - 2\sqrt{k_e}]^2} \cdot p_{\max} = 1471875\text{ N} \quad (4)$$

This model was imported to SolidWorks 2017 software [46] for analysis with the: Static, Thermal and Design Study modules. In this mode the variance of the Von Mises resultant stress on the lateral cover was calculated as a result of the requirements specified in the design data and the effect of the shape change in the cross-section through the coefficient of ellipticity.

The calculation was made for discrete values of: the coefficient of ellipticity, the thickness of the elliptical cover, the number of years of exploitation and the temperature variation.

The results are given in Tables 1 to 5. It is necessary to correctly evaluate the influence of ellipticity, take as base the Von Mises stress corresponding to the undeformed initial state of the lateral cover for  $k_e = 1$ , Table 1.

For each case of ellipticity, were calculated the laws of variation and plotted graphically [47, 48].

- the variation of the stress  $\sigma(n_a, T = \text{constant})$  and the laws of variation determined by polynomial interpolation, (as shown in Figure 3a to Figure 7a); the graph of the 3D variation of the stress dependence  $\sigma(n_a, T)$ , (as shown in Figure 3b to Figure 7b);
- the top view of the surface associated with the dependence  $\sigma(n_a, T)$  on which the area delimited by temperature and years of exploitation can be identified, in which the cover loses its working capacity, being put out of use because the Von Mises stress exceeds the admitted effort of the material traction,  $\sigma_a = 710 \text{ N/mm}^2$ ; (as shown in Figure 3c to Figure 7c);
- the graph of the percentage increase of the stress  $\Delta\sigma(n_a, T = \text{constant})$  for the elliptical shape, computed in relation to the undeformed initial state, on which identifies the maximum interval time from the beginning  $n_{a \text{ maximum}}$  of the maximum exploitation to which the covering is functional, specifying in the same time and the law of variation determined by an polynomial interpolation, (as shown in Figure 3d to Figure 7d);

For the initial cylindrical undeformed state of lateral cover the results are given in Table 1.

Table 1: The Von Mises stress in cylindrical lateral cover

$n_a$ [years]	$s$ [mm]	$\sigma \text{ [N/mm}^2\text{]}$									
		-30°C	-20°C	-10°C	0°C	10°C	20°C	30°C	40°C	50°C	60°C
0	9.2	531.36	504.46	478.19	453.75	431.69	410.54	395.55	398.56	406.94	417.27
1	9.08	533.07	506.18	480.48	455.45	434.48	414.31	400.03	404.09	413.49	424.81
2	8.96	535.17	508.31	483.13	459.47	437.6	418.34	404.76	409.77	420.13	432.35
3	8.84	537.67	510.85	486.15	462.83	441.05	422.65	409.74	415.6	426.85	439.91
4	8.72	540.57	513.81	489.54	466.53	444.84	427.21	414.95	421.57	433.64	447.48
5	8.6	543.87	517.17	493.3	470.55	448.96	432.05	420.41	427.7	440.52	455.06
6	8.48	547.54	520.95	497.42	474.91	453.41	437.15	426.12	433.98	447.48	462.64
7	8.36	551.66	525.15	501.91	479.6	458.19	442.52	432.06	440.41	454.53	470.24
8	8.24	556.15	529.75	506.77	484.63	463.31	448.15	438.26	446.98	461.65	477.84
9	8.12	561.05	534.77	512	489.99	468.76	454.05	444.69	453.71	468.85	485.46
10	8	566.33	540.2	517.59	495.68	474.55	460.22	451.37	460.58	476.13	493.09
11	7.88	572.02	546.04	523.56	501.7	480.66	466.65	458.29	467.61	483.5	500.72
12	7.76	578.11	552.29	529.89	508.06	487.11	473.35	465.46	474.79	490.94	508.37
13	7.64	584.59	558.96	536.58	514.75	493.9	480.31	472.87	482.11	498.47	516.02
14	7.52	591.47	566.04	543.65	521.78	501.01	487.54	480.53	489.54	506.08	523.68
15	7.4	598.75	573.53	551.08	529.13	508.46	495.04	488.42	497.21	513.77	531.36
16	7.28	606.42	581.44	558.88	536.82	516.24	502.81	496.57	504.98	521.54	539.04
17	7.16	614.5	589.75	567.05	544.85	524.36	510.84	504.95	512.91	529.39	546.73
18	7.04	622.97	598.48	575.58	553.21	532.81	519.14	513.58	520.98	537.32	554.44
19	6.92	631.85	607.62	584.49	561.9	541.59	527.7	522.45	529.21	545.33	562.15
20	6.8	641.11	617.18	593.76	570.92	550.7	536.53	531.57	537.58	553.42	569.87

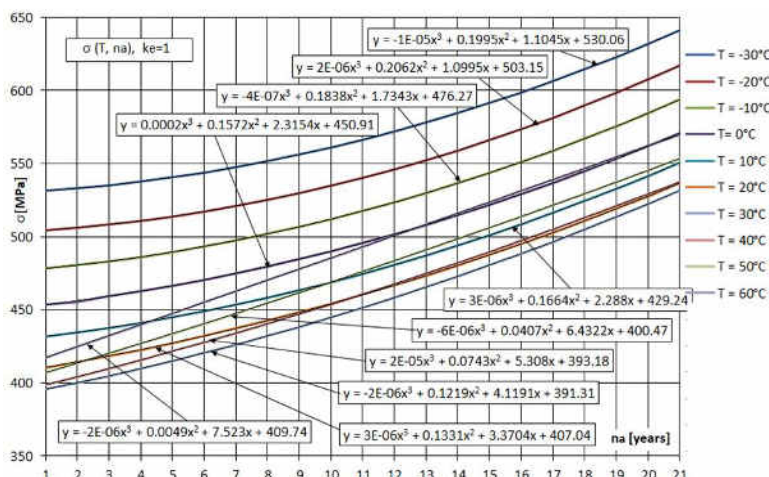


Fig. 3a. The graphs of Von Mises stress  $\sigma(n_a, T = \text{ct.})$  for  $k_e = 1$

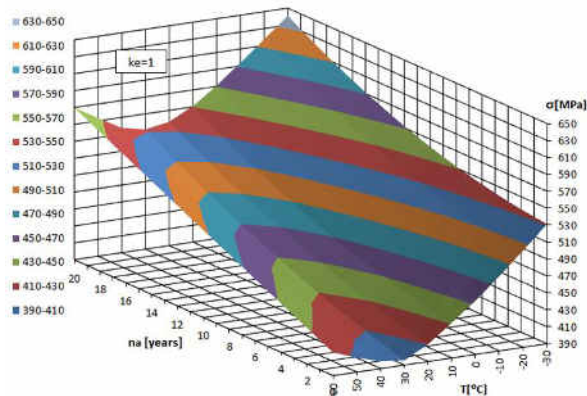


Fig. 3b. The graph of Von Mises stress  $\sigma (n_a, T)$  for  $k_e = 1$

For lateral cover with ellipticity  $k_e = 1.01$ , the results are given in Table 2.

Table 2: The Von Mises stress in elliptical lateral cover with  $k_e = 1.01$

		$T [^{\circ}C]$										
		$-30^{\circ}C$	$-20^{\circ}C$	$-10^{\circ}C$	$0^{\circ}C$	$10^{\circ}C$	$20^{\circ}C$	$30^{\circ}C$	$40^{\circ}C$	$50^{\circ}C$	$60^{\circ}C$	
$n_a$	$s$	$\sigma [N/mm^2]$										
[years]	[mm]											
0	9.2	592.96	565.46	540.59	517.38	494.84	474.26	459.46	445.65	443.25	450.76	
1	9.08	600.32	572.31	546.50	522.74	499.90	478.77	464.03	450.84	448.48	456.04	
2	8.96	607.34	579.06	552.48	528.22	505.11	483.54	468.87	456.27	453.89	461.46	
3	8.84	614.64	585.75	558.50	533.81	510.50	488.56	473.96	461.90	459.47	467.03	
4	8.72	621.6	592.4	564.58	539.52	516.06	493.82	479.30	467.74	465.22	472.74	
5	8.6	628.44	598.99	570.70	545.35	521.80	499.34	484.89	473.79	471.14	478.59	
6	8.48	635.14	605.53	576.88	551.3	527.71	505.11	490.73	480.04	477.23	484.59	
7	8.36	641.71	612.02	583.11	557.37	533.79	511.12	496.82	486.50	483.5	490.73	
8	8.24	648.16	618.45	589.39	563.56	540.05	517.39	503.16	493.16	489.94	497.01	
9	8.12	654.47	624.84	595.71	569.86	546.48	523.91	509.75	500.03	496.55	503.44	
10	8	660.63	631.16	602.1	576.3	553.05	530.75	516.16	507.12	503.33	509.97	
11	7.88	666.7	637.45	608.53	582.83	559.86	537.69	523.67	514.39	510.28	516.73	
12	7.76	672.62	643.67	615.01	589.49	566.82	544.95	531.00	521.89	517.41	523.59	
13	7.64	678.41	649.85	621.54	596.27	573.94	552.46	538.59	529.58	524.71	530.59	
14	7.52	684.07	655.97	628.13	603.17	581.24	560.23	546.42	537.49	532.18	537.74	
15	7.4	689.6	662.04	634.76	610.19	588.71	568.24	554.51	545.60	539.82	545.04	
16	7.28	695	668.06	641.45	617.33	596.36	576.5	562.84	553.92	547.63	552.47	
17	7.16	700.27	674.02	648.18	624.58	604.18	585.01	571.42	562.44	555.62	560.05	
18	7.04	705.41	679.94	654.97	631.95	612.17	593.77	580.25	571.17	563.77	567.78	
19	6.92	0	685.8	661.81	639.45	620.34	602.79	589.33	580.11	572.10	575.65	
20	6.8	0	691.57	668.70	647.06	628.68	612.04	598.65	589.23	580.58	583.61	

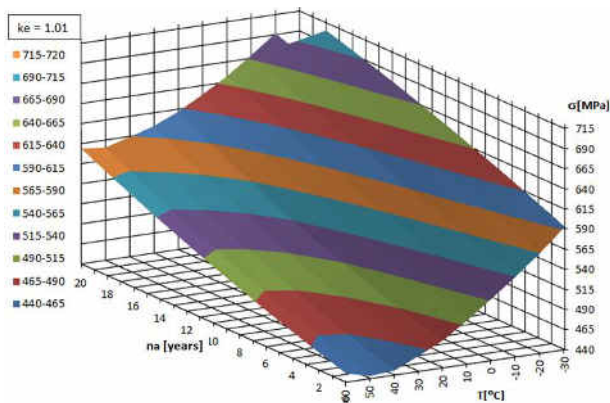


Fig. 4a. The graph of Von Mises stress  $\sigma (n_a, T)$  for  $k_e = 1.01$

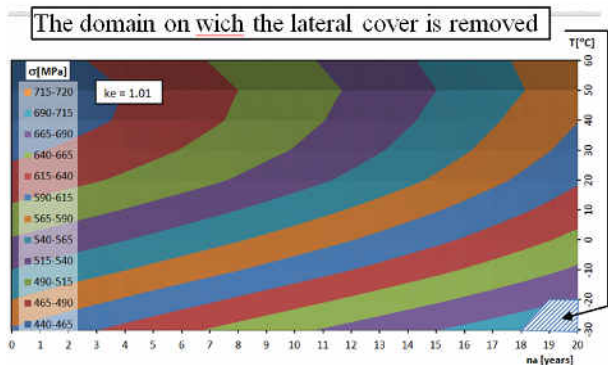


Fig. 4b. The graph in top view of Von Mises stress  $\sigma (n_a, T)$  for  $k_e = 1.01$

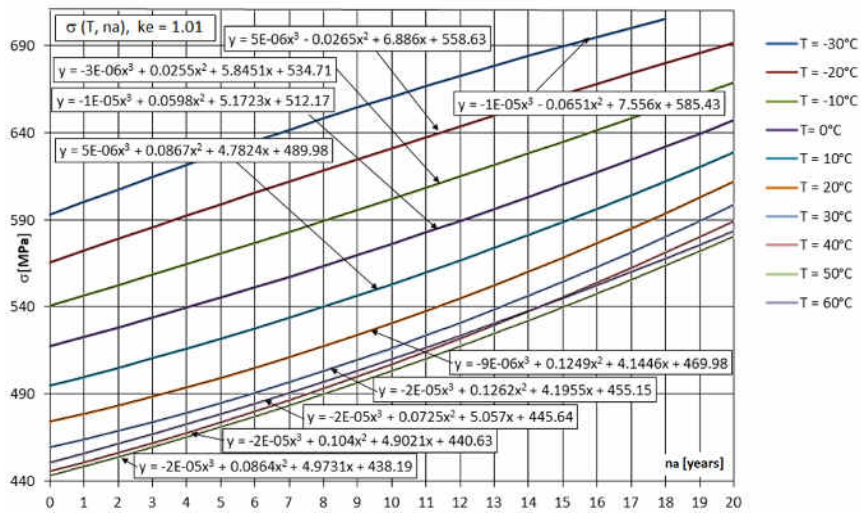


Fig. 4c. The graphs of Von Mises stress  $\sigma$  ( $n_a, T = \text{ct.}$ ) for  $k_e = 1.01$

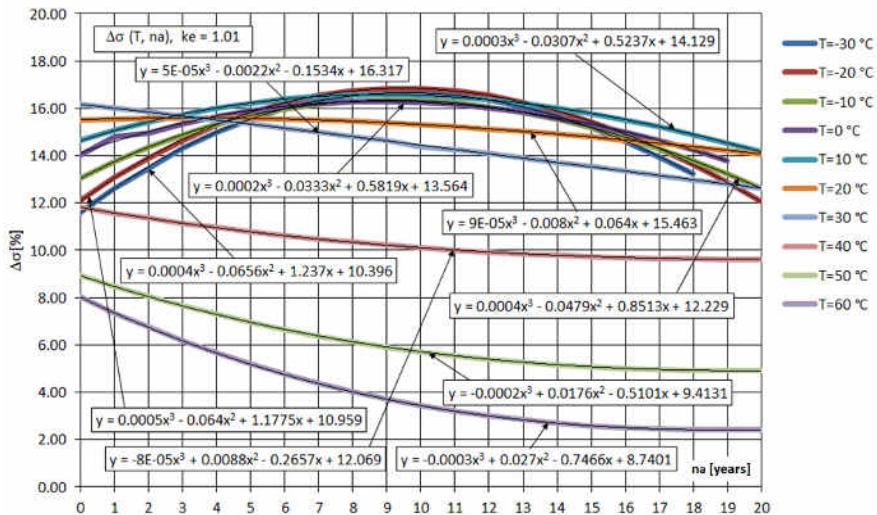


Fig. 4d. The graphs of Von Mises stress variation  $\Delta\sigma$  ( $n_a, T = \text{ct.}$ ) for  $k_e = 1.01$

For the lateral cover with ellipticity  $k_e = 1.02$ , the results are given in Table 3.

Table 3: The Von Mises stress in elliptical lateral cover with  $k_e = 1.02$

$n_a$ [years]	$T$ [ $^\circ\text{C}$ ]	$-30^\circ\text{C}$	$-20^\circ\text{C}$	$-10^\circ\text{C}$	$0^\circ\text{C}$	$10^\circ\text{C}$	$20^\circ\text{C}$	$30^\circ\text{C}$	$40^\circ\text{C}$	$50^\circ\text{C}$	$60^\circ\text{C}$
		$\sigma$ [ $\text{N}/\text{mm}^2$ ]									
0	9.2	668.23	642.07	616.33	591.39	568.08	547.18	532.25	520.56	509.2	516.17
1	9.08	681.00	648.51	622.83	597.85	574.07	552.53	537.56	526.02	514.61	520.7
2	8.96	672.19	655.01	629.37	604.39	580.19	558.07	542.9	531.66	520.21	525.42
3	8.84	682.03	661.54	635.93	610.95	586.42	563.82	548.47	537.5	526	530.33
4	8.72	689.20	668.1	642.53	617.54	592.76	569.78	554.25	543.52	531.98	535.43
5	8.6	697.88	674.69	649.15	624.16	599.22	575.94	560.26	549.73	538.16	540.73
6	8.48	704.22	681.31	655.8	630.81	605.79	582.31	566.5	556.13	544.53	546.12
7	8.36	709.74	687.95	662.48	637.49	612.48	588.88	572.96	562.72	551.09	551.89
8	8.24	0	694.63	669.19	644.2	619.28	595.66	579.64	569.49	557.85	557.75
9	8.12	0	701.34	675.92	650.94	626.2	602.65	586.55	576.45	564.8	563.81
10	8	0	708.07	682.68	657.72	633.23	609.82	593.7	581.52	571.87	570.09
11	7.88	0	0	689.47	664.51	640.38	617.23	601.03	590.93	579.28	576.5
12	7.76	0	0	696.29	671.34	647.64	624.84	608.61	598.45	586.81	583.14
13	7.64	0	0	703.14	678.19	655.02	632.65	616.41	606.16	594.53	589.96
14	7.52	0	0	0	685.08	662.51	640.66	624.43	614.06	602.45	596.98

15	7.4	0	0	0	692.00	670.12	648.88	632.68	622.14	610.56	604.18
16	7.28	0	0	0	698.95	677.84	657.31	641.15	630.41	618.86	611.58
17	7.16	0	0	0	705.93	685.67	665.94	649.85	638.87	627.36	619.17
18	7.04	0	0	0	0	693.62	674.78	658.77	647.52	636.05	626.95
19	6.92	0	0	0	0	701.69	683.83	667.91	656.35	644.93	634.93
20	6.8	0	0	0	0	709.9	693.17	677.24	665.36	653.95	642.57

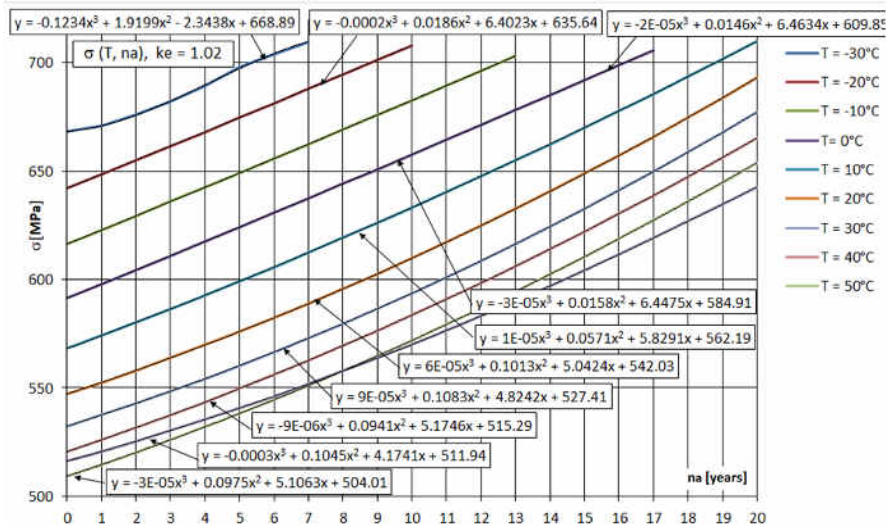


Fig. 5a. The graphs of Von Mises stress  $\sigma$  ( $n_a, T = ct.$ ) for  $k_e = 1.02$

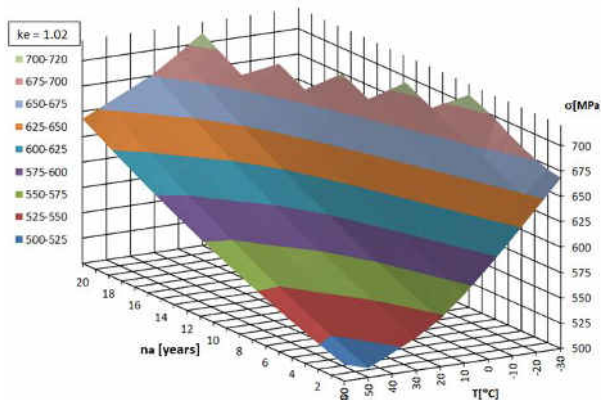


Fig. 5b. The graph of Von Mises stress  $\sigma$  ( $n_a, T$ ) for  $k_e = 1.02$

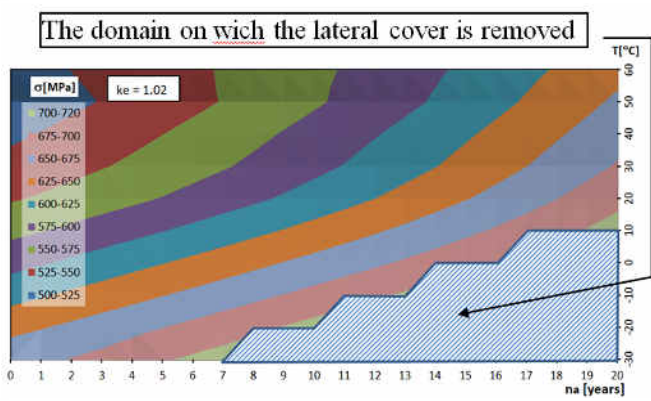


Fig. 5c. The graph in top view of Von Mises stress  $\sigma$  ( $n_a, T$ ) for  $k_e = 1.02$

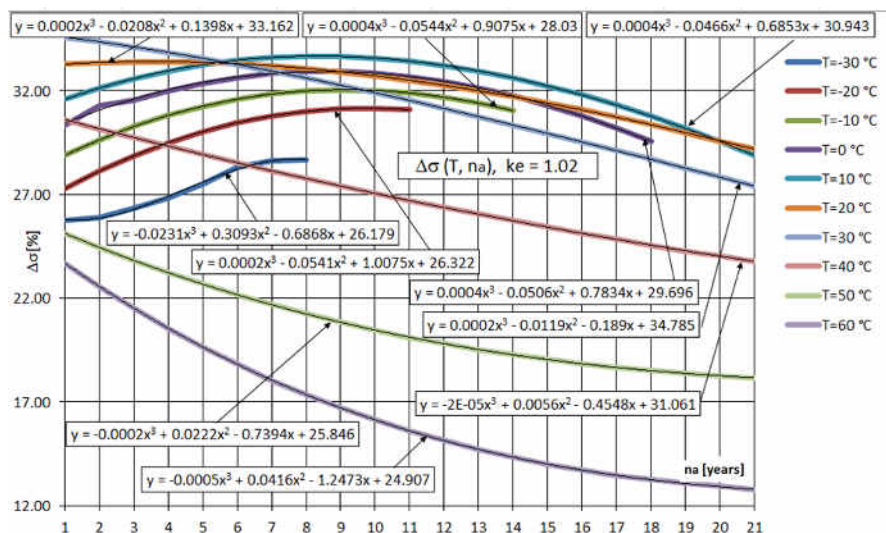
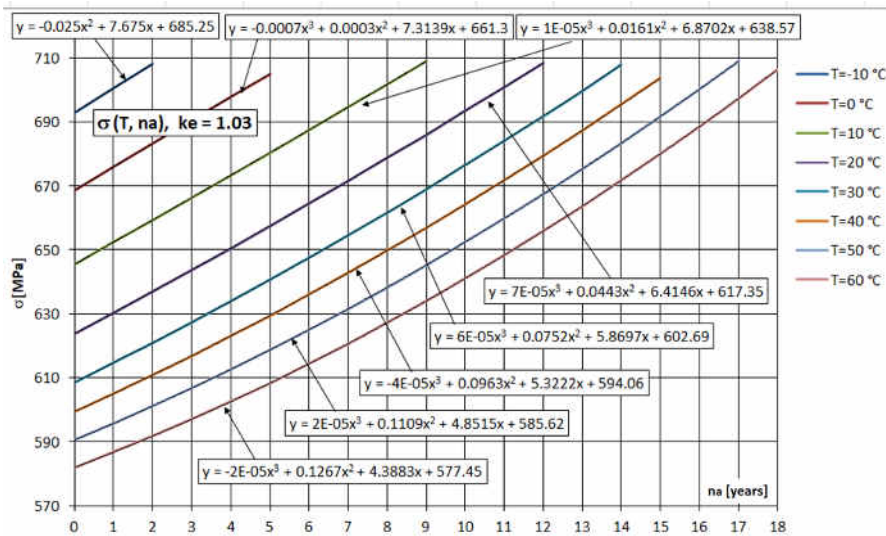


Fig. 5d. The graphs of Von Mises stress variation  $\Delta\sigma$  ( $n_a, T = ct.$ ) for  $k_e = 1.02$

For the lateral cover with ellipticity  $k_e = 1.03$ , the results are given in Table 4.

**Table 4:** The Von Mises stress in elliptical lateral cover with  $k_e = 1.03$

$n_a$ [years]	$s$ [mm]	$\sigma$ [N/mm <sup>2</sup> ]										
		-30°C	-20°C	-10°C	0°C	10°C	20°C	30°C	40°C	50°C	60°C	
0	9.2	0	0	692.9	668.61	645.46	623.8	608.63	599.48	590.57	581.97	
1	9.08	0	0	700.5	675.92	652.38	630.36	614.74	605.08	595.77	586.73	
2	8.96	0	0	708.05	683.22	659.33	636.99	620.98	610.89	601.17	591.75	
3	8.84	0	0	0	690.51	666.31	643.72	627.38	616.88	606.8	597.03	
4	8.72	0	0	0	697.78	673.33	650.53	633.93	623.07	612.65	602.56	
5	8.6	0	0	0	705.03	680.38	657.44	640.63	629.45	618.72	608.34	
6	8.48	0	0	0	0	687.46	664.44	647.48	636.02	625.01	614.37	
7	8.36	0	0	0	0	694.57	671.54	654.49	642.78	631.53	620.66	
8	8.24	0	0	0	0	701.72	678.72	661.66	649.73	638.27	627.2	
9	8.12	0	0	0	0	708.9	686	668.97	656.87	645.23	633.99	
10	8	0	0	0	0	0	693.35	676.43	664.2	652.42	641.02	
11	7.88	0	0	0	0	0	700.83	684.07	671.72	659.83	648.33	
12	7.76	0	0	0	0	0	708.38	691.85	679.43	667.46	655.87	
13	7.64	0	0	0	0	0	0	699.78	687.33	675.32	663.67	
14	7.52	0	0	0	0	0	0	707.86	695.42	683.39	671.73	
15	7.4	0	0	0	0	0	0	0	703.7	691.69	680.03	
16	7.28	0	0	0	0	0	0	0	0	700.22	688.59	
17	7.16	0	0	0	0	0	0	0	0	708.96	697.39	
18	7.04	0	0	0	0	0	0	0	0	0	706.45	



**Fig. 6a.** The graphs of Von Mises stress  $\sigma$  ( $n_a, T = ct.$ ) for  $k_e = 1.03$

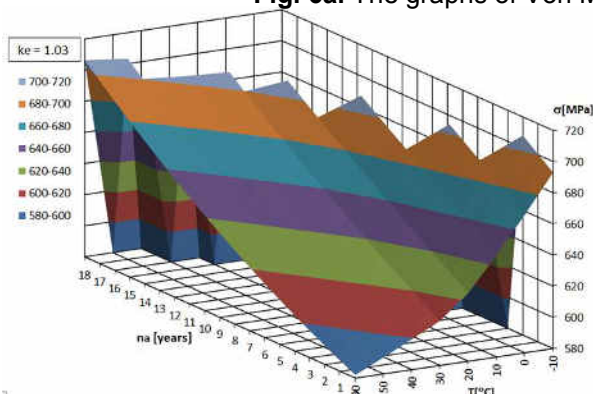


**Fig. 6b.** The graphs of Von Mises stress  $\sigma$  ( $n_a, T$ ) for  $k_e = 1.03$

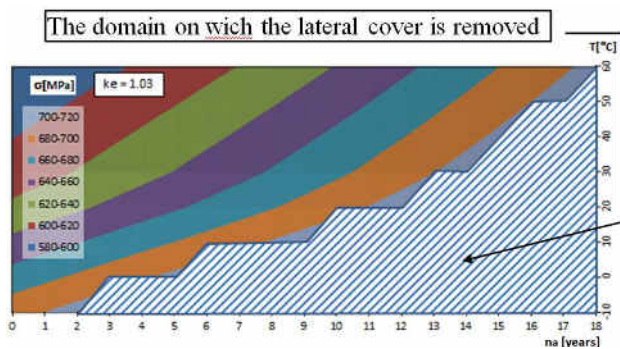


**Fig. 6c.** The graphs in top view of Von Mises stress  $\sigma$  ( $n_a, T$ ) for  $k_e = 1.03$

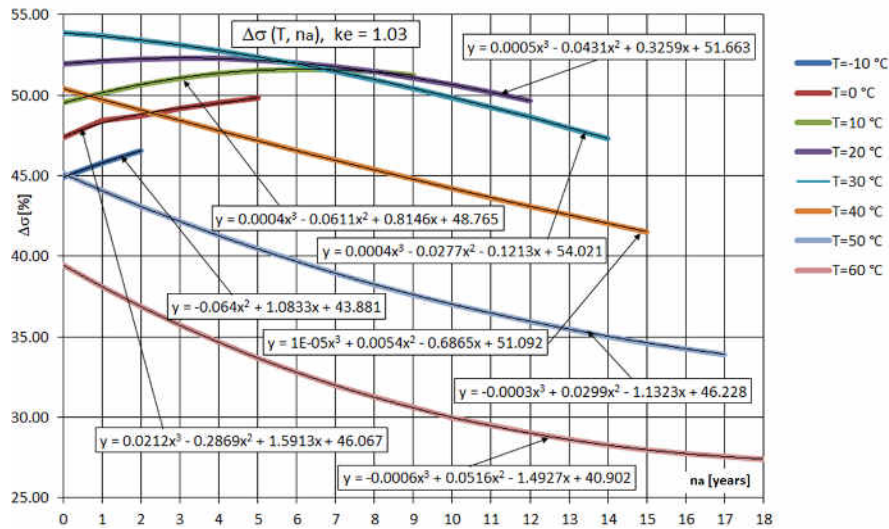


Fig. 6d. The graphs of Von Mises stress variation  $\Delta\sigma$  ( $n_a, T = ct.$ ) for  $k_e = 1.03$

For lateral cover with ellipticity  $k_e = 1.04$ , the results are given in Table 5.

Table 5: The Von Mises stress in elliptical lateral cover with  $k_e = 1.04$

	T [°C]	-30°C	-20°C	-10°C	0°C	10°C	20°C	30°C	40°C	50°C	60°C
$n_a$	s	$\sigma$ [N/mm <sup>2</sup> ]									
[years]	[mm]										
0	9.2	0	0	0	0	0	704.51	687.54	676.32	665.62	655.22
1	9.08	0	0	0	0	0	0	694.75	683.23	672.46	662.02
2	8.96	0	0	0	0	0	0	702	690.26	679.4	668.95
3	8.84	0	0	0	0	0	0	709.3	697.37	686.45	675.98
4	8.72	0	0	0	0	0	0	0	704.58	693.61	683.14
5	8.6	0	0	0	0	0	0	0	0	700.87	690.41
6	8.48	0	0	0	0	0	0	0	0	708.24	697.79
7	8.36	0	0	0	0	0	0	0	0	0	705.28

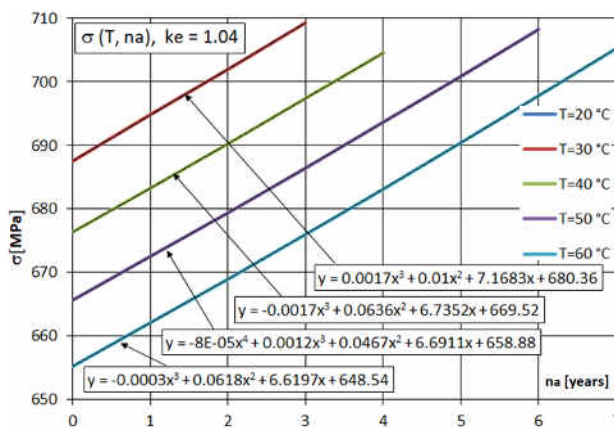


Fig. 7a. The graphs of Von Mises stress  $\sigma$  ( $n_a, T = ct.$ ) for  $k_e = 1.04$

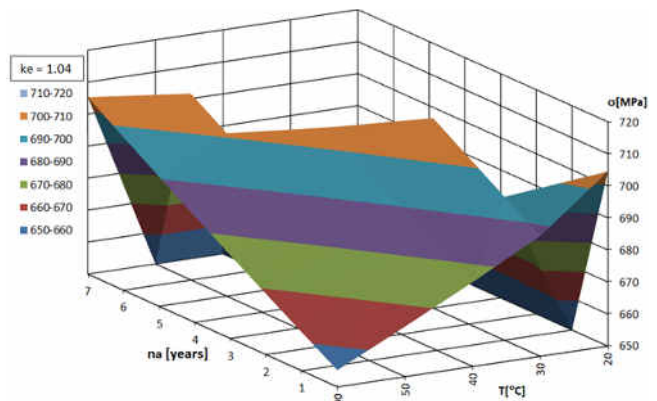


Fig. 7b. The graphs of Von Mises stress  $\sigma$  ( $n_a, T$ ) for  $k_e = 1.04$

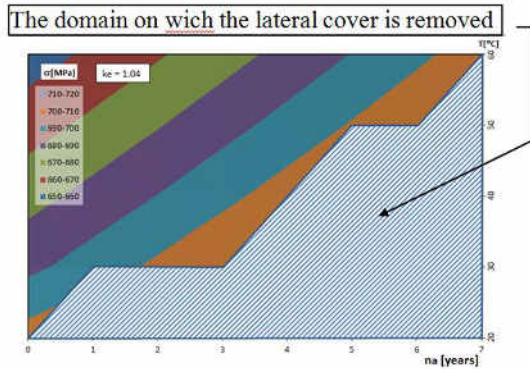


Fig. 7c. The graphs in top view of Von Mises stress for  $k_e = 1.04$

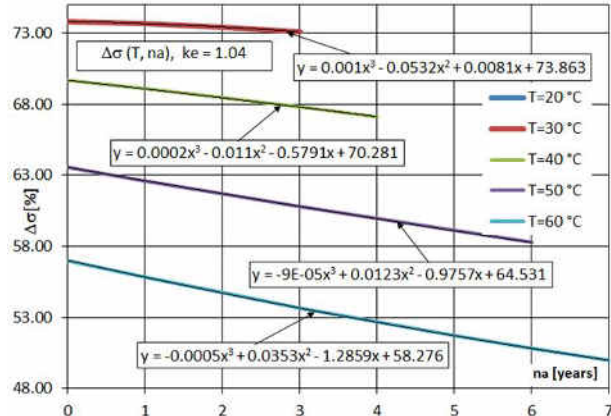


Fig. 7d. The graphs of Von Mises stress variation  $\Delta\sigma(n_a, T = ct.)$ ,  $\sigma(n_a, T)$  for  $k_e = 1.04$

#### 4. Discussion

In the elliptical deformation state for  $k_e = 1.01$ , the semi-axes of the ellipse have deviations from the radius of undeformed circular cover of:  $\Delta a, \Delta b < 0.49\%$ , producing the following overlapped effects over the corrosion effect:

- the stress state is comprised between the minimum value of  $\sigma = 443.5$  MPa at  $T = 50^\circ\text{C}$  and  $n_a = 0$  years and the maximum value of  $\sigma = 705.41$  MPa at  $T = -30^\circ\text{C}$  and  $n_a = 18$  years, (Table 1).
- at the same time in Table 1 it can be seen that for  $T = -30^\circ\text{C}$ , the cover totally loses the capacity to resist to stress coming out of use after  $n_a = 18$  years of exploitation.
- the stress state increases from  $\Delta\sigma = 2.41\%$  at  $T = 60^\circ\text{C}$ , for  $n_a = 20$  years, to  $\Delta\sigma = 16.84\%$  for  $T = -20^\circ\text{C}$ , for  $n_a = 10$  years, (as shown in Figure 4d) they touch maximum growth values over  $\Delta\sigma > 16\%$ , for  $n_a = 4$  years up to  $n_a = 14$  years and temperatures between  $T = -30^\circ\text{C}$  up to  $T = 10^\circ\text{C}$ , (as shown in Table 2 and Figure 4d).
- overall exploitation time is reduced by 1 % of imposed design time.

At the elliptic deformation state for  $k_e = 1.02$ , the semi-axes have the deviation:  $\Delta a, \Delta b < 0.99\%$ .

- the exploitation time is reduced by 16.5% over the total exploitation time, especially at the negative temperatures where we have for  $T = -30^\circ\text{C} / -20^\circ\text{C} / -10^\circ\text{C}$  and  $0^\circ\text{C}$ , large diminutions of: 65 % / 50 % / 35 % and 15 %, respectively.
- the minimum stress is  $\sigma = 509.2$  MPa at  $T = 50^\circ\text{C}$  and  $n_a = 0$  years and maximum of  $\sigma = 709.74$  MPa at  $T = -30^\circ\text{C}$  and  $n_a = 7$  years, (as shown in Table 3 and Figure 5a).
- the stress state increases between  $\Delta\sigma = 12.76\%$  at  $T = 60^\circ\text{C}$ , for  $n_a = 20$  years, up to  $\Delta\sigma = 34.56\%$  at  $T = 30^\circ\text{C}$ , for  $n_a = 0$  years, (as shown in Fig. 5d) growing maximum  $\Delta\sigma > 34\%$ , for  $n_a = 0$  year up to  $n_a = 2$  years and  $T = 30^\circ\text{C}$ , (as shown in Table 3 and Figure 5d).

At the elliptic deflection state for  $k_e = 1.03$ , the semi-axes have deviations of:  $\Delta a, \Delta b < 1.48\%$ .

- overall exploitation time is greatly diminished throughout the operating temperature range, becoming 54.5 % of the total time; at negative temperatures of:  $T = -30^\circ\text{C}$  and  $T = -20^\circ\text{C}$ , the reduction is complete and then continued at:  $T / -10^\circ\text{C} / 0^\circ\text{C} / 10^\circ\text{C} / 20^\circ\text{C} / 30^\circ\text{C} / 40^\circ\text{C} / 50^\circ\text{C} / 60^\circ\text{C}$  with decreased values by: 75 % / 55 % / 40 % / 30 % / 25 % / 15 % and 10 %.
- the minimum effort is  $\sigma = 581.97.2$  MPa at  $T = 60^\circ\text{C}$  and  $n_a = 0$  years and maximum  $\sigma = 708.96$  MPa at  $T = 50^\circ\text{C}$  and  $n_a = 17$  years, (as shown in Table 4 and Figure 6a).
- the state of stress increases between  $\Delta\sigma = 27.42\%$  at  $T = 60^\circ\text{C}$ , for  $n_a = 18$  years, to  $\Delta\sigma = 53.87\%$  at  $T = 30^\circ\text{C}$ , for  $n_a = 0$  years, (as shown in Figure 6d) growing maximum  $\Delta\sigma > 53\%$ , for  $n_a = 0$  years up to  $n_a = 3$  years and  $T = 30^\circ\text{C}$ , (as shown in Table 4 and Figure 6d).

At the elliptic deflection state for  $k_e = 1.04$ , the semi-axes of the ellipse have deviations of:  $\Delta a, \Delta b < 1.97\%$ .

- the overall exploitation time is drastically reduced over the entire temperature range to 87.5 % of the total exploitation time, especially at temperatures between  $T = -30^\circ\text{C}$  to  $T = 10^\circ\text{C}$  for:  $T = 20^\circ\text{C}$ ,  $60^\circ\text{C}$  and regressive, at the temperatures of:  $T / 20^\circ\text{C} / 30^\circ\text{C} / 40^\circ\text{C} / 50^\circ\text{C} /$  and  $60^\circ\text{C}$ , we have diminutions of: 95 % / 85 % / 80 % and 70 %.

- the minimum stress is  $\sigma = 655.22$  MPa at  $T = 60$  °C and  $n_a = 0$  years and maximum  $\sigma = 709.30$  MPa at  $T = 30$  °C and  $n_a = 3$  years, (as shown in Table 5).
- the stress state increases from  $\Delta\sigma = 27.42$  % to  $T = 60$  °C, for  $n_a = 18$  years, to  $\Delta\sigma = 73.82$  % at  $T = 30$  °C, for  $n_a = 0$  years, (as shown in Fig. 6d) maximum growth values  $\Delta\sigma > 73$  %, for  $n_a = 0$  years up to  $n_a = 2$  years and  $T = 30$  °C, (as shown in Table 5 and Figure 7d).

The final conclusion is that ellipticity has a major influence on the state of stress and the exploitation period (which corresponds to the time of premature elimination from use of the cover) for ellipticity with  $k_e = 1.01$  the stress state increases to  $\Delta\sigma = 16.84$  % with a modest decrease in exploitation time  $< 1\%$ , but increasing this ellipticity to:  $k_e = 1.02 / k_e = 1.03$  and  $k_e = 1.04$ , the state of stress increases greatly with:  $\Delta\sigma = 34.56$  % /  $\Delta\sigma = 53.87$  %, respectively  $\Delta\sigma = 73.82$  %, decreasing the total or partial exploitation time by: 16.5 %, 54.5 % and 87.5 %; for the ellipticity  $k_e = 1.03$ , the exploitation time is reduced to  $n_a = 18$  years, while for  $k_e = 1.04$  the exploitation time is reduced at  $n_a = 7$  years.

## 5. Conclusions

This study shows the influence on the Von Mises effort state by modification of the cylindrical shape to an elliptical shape of a lateral pressurized cylindrical fuel tank.

It can be concluded that at low values of coefficient of ellipticity  $k_e$  the increase in elliptical cover efforts is very important.

At negative temperatures with increasing the ellipticity coefficient, Von Mises stresses are much higher than in the case of positive temperature stresses produced by the same deformation state.

The influence of the shape deviation of the lateral shell of the tank generates efforts that overlap with the efforts of the variation of temperature, corrosion and loading pressure.

The limitation of the exploitation period by removal from use to exceed the permissible effort is strongly influenced by the deviation of the shape from the circularity through the elliptical form compared to the initial cylindrical cover at which the pressurized fuel tank was designed.

**Financial disclosure:** Neither author has a financial or proprietary interest in any material or method mentioned.

**Competing interests:** The authors declare that they have no significant competing financial, professional or personal interests that might have influenced the performance or presentation of the work described in this manuscript.

## References

- [1] A.C. Nedelcu, “Romanian automotive industry – analysis made from the intellectual capital perspective“, *Revista Economica*, vol. 67, no. 5, pp. 80-89, 2015;
- [2] A. Hagiu, M. Platis, “The evolution of the Romanian car industry and its position on European market“, *STUDIA UBB NEGOTIA*, vol. 57 (LVII), 2, pp. 65 - 91, 2012;
- [3] A. Misztal, N. Belu, N. Rachieru, “Comparative Analysis of Awareness and Knowledge of APQP Requirements in Polish and Romanian Automotive Industry“, *Applied Mechanics and Materials*, vol. 657, pp. 981-985, 2014;
- [4] G. Matache, C. Cristescu, C. Dumitrescu, V. Miroiu, “Pregătirea specialiștilor în vederea adaptabilității și creșterii competitivității“, *Magazine of Hydraulics, Pneumatics, Tribology, Ecology, Sensorics, Mechatronics (HIDRAULICA)*, no. 3-4, pp. 7-14, 2012. ISSN 1453-7303;
- [5] E. Lisowski, W. Czyzycki, “Transport and storage of LNG in container tanks“, *Journal of KONES Powertrain and Transport*, vol. 18, no. 3, pp. 193-201, 2011;
- [6] Chen Shr-Hung, “Novel design and optimization of vehicle’s natural gas fuel tank“. Master’s Thesis presented to the Faculty of the College of the Engineering and Technology, Ohio University, March 1997;
- [7] M.C. Ghiță, A.C. Micu, M. Țălu, Ș. Țălu, E. Adam, “Computer-Aided Design of a classical cylinder gas tank for the automotive industry“, *Annals of Faculty of Engineering Hunedoara - International Journal of Engineering*, Hunedoara, Tome XI, Fascicule 4, pp. 59-64, 2013;
- [8] M.C. Ghiță, A.C. Micu, M. Țălu, Ș. Țălu, “Shape optimization of vehicle’s methane gas tank“, *Annals of Faculty of Engineering Hunedoara - International Journal of Engineering*, Hunedoara, Tome X, Fascicule 3, pp. 259-266, 2012;

- [9] M.C. Ghiță, A.C. Micu, M. Țălu, Ș. Țălu, “3D modelling of a shrink fitted concave ended cylindrical tank for automotive industry”. *Acta Technica Corviniensis – Bulletin of Engineering, Hunedoara, Romania, Tome VI, Fascicule 4*, pp. 87-92, 2013;
- [10] M.C. Ghiță, A.C. Micu, M. Țălu, Ș. Țălu, “3D modelling of a gas tank with reversed end up covers for automotive industry”, *Annals of Faculty of Engineering Hunedoara - International Journal of Engineering, Hunedoara, Tome XI, Fascicule 3*, 2013, pp. 195-200, 2013;
- [11] M.C. Ghiță, C.Ș. Ghiță, Ș. Țălu, S. Rotaru, “Optimal design of cylindrical rings used for the shrinkage of vehicle tanks for compressed natural gas”, *Annals of Faculty of Engineering Hunedoara - International Journal of Engineering, Hunedoara, Tome XII, Fascicule 3*, pp. 243-250, 2014;
- [12] M.C. Ghiță, A.C. Micu, M. Țălu, Ș. Țălu, “Shape optimization of a thoroidal methane gas tank for automotive industry”, *Annals of Faculty of Engineering Hunedoara - International Journal of Engineering, Hunedoara, Tome X, Fascicule 3*, pp. 295-297, 2012;
- [13] M.V.J. Bhavana, Rao S. Janardhana, B A.N. Murthy, "Design and analysis of horizontal LPG storage pressure vessel for variable dimensional constraints under given physical parameters", *International Journal & Magazine of Engineering, Technology, Management and Research*, vol. 4, issue 5, pp. 342 - 351, 2017;
- [14] M. Ziólkowska, D. Wardzińska, "Corrosiveness of fuels during storage processes", published by IntechOpen. <http://dx.doi.org/10.5772/59803>;
- [15] P. Mould, T. Burton, R. Daley, S. Itonaga, T. Kikuchi, S. Jokela, M. Luciani, M. McCosby, D. Paul, T. Sakiyama, G. Schwerzel, R. Sheffield, G. Tarrance, W. Warnecke, "Evaluation of the corrosion durability of steel systems for automobile fuel tanks," *SAE Technical Paper 2005-01-0540*, 2005, <https://doi.org/10.4271/2005-01-0540>;
- [16] P.P. Deshpande, “Structural analysis of integration of a non-cylindrical CNG fuel tank”, Master's report, Michigan Technological University, 2015. <https://digitalcommons.mtu.edu/etds/988>;
- [17] Ș. Țălu, “Geometrie descriptivă” (Descriptive geometry), Cluj-Napoca, Risoprint Publishing house, 2010;
- [18] A. Florescu-Gligore, Ș. Țălu, D. Noveanu, “Reprezentarea și vizualizarea formelor geometrice în desenul industrial” (Representation and visualization of geometric shapes in industrial drawing), Cluj-Napoca, U. T. Pres Publishing house, 2006;
- [19] A. Florescu-Gligore, M. Orban, Ș. Țălu, “Cotarea în proiectarea constructivă și tehnologică” (Dimensioning in technological and constructive engineering graphics), Cluj-Napoca, Lithography of The Technical University of Cluj-Napoca, 1998;
- [20] C. Racocea, Ș. Țălu, “Reprezentarea formelor geometrice tehnice în axonometrie” (The axonometric representation of technical geometric shapes), Cluj-Napoca, Napoca Star Publishing house, 2011;
- [21] Ș. Țălu, C. Racocea, “Reprezentări axonometrice cu aplicații în tehnică” (Axonometric representations with applications in technique), Cluj-Napoca, MEGA Publishing house, 2007;
- [22] Carlos Martines Ortiz, “2D and 3D shape descriptors”. Thesis for the degree of Doctor of Philosophy in Computer Science, University of Exeter, GBR, 2010;
- [23] Ș. Țălu, M. Țălu, “CAD generating of 3D supershapes in different coordinate systems”, *Annals of Faculty of Engineering Hunedoara - International Journal of Engineering, Hunedoara, Tome VIII, Fascicule 3*, pp. 215-219, 2010;
- [24] Ș. Țălu, M. Țălu, “A CAD study on generating of 2D supershapes in different coordinate systems”, *Annals of Faculty of Engineering Hunedoara - International Journal of Engineering, Hunedoara, Tome VIII, Fascicule 3*, pp. 201-203, 2010;
- [25] Ș. Țălu, “CAD representations of 3D shapes with superellipsoids and convex polyhedrons”, *Annals of Faculty of Engineering Hunedoara - International Journal of Engineering, Hunedoara, Tome IX, Fascicule 3*, 2011, pp. 349-352, 2011;
- [26] Ș. Țălu, “Study on the construction of complex 3D shapes with superellipsoids and supertoroids”, *Annals of Faculty of Engineering Hunedoara - International Journal of Engineering, Hunedoara, Tome IX, Fascicule 3*, pp. 299-302, 2011;
- [27] Ș. Țălu, “Complex 3D shapes with superellipsoids, supertoroids and convex polyhedrons”, *Journal of Engineering Studies and Research, Bacău*, vol. 17, no. 4, pp. 96-100, 2011;
- [28] Ș. Țălu, “Generation of 3D shapes with superellipsoids, supertoroids, super cylinders and super cones”, *Journal of Engineering Studies and Research, Bacău*, vol. 18, no. 2, pp. 135-139, 2012;
- [29] Ș. Țălu, “Grafică tehnică asistată de calculator” (Computer assisted technical graphics), Cluj-Napoca, Victor Melenti Publishing house, 2001;
- [30] Ș. Țălu, “Reprezentări grafice asistate de calculator” (Computer assisted graphical representations), Cluj-Napoca, Osama Publishing house, 2001;
- [31] Ș. Țălu, “Limbajul de programare AutoLISP. Teorie și aplicații”, (AutoLISP programming language. Theory and applications), Cluj-Napoca, Risoprint Publishing house, 2001;
- [32] Ș. Țălu, “AutoCAD 2005”, Cluj-Napoca, Risoprint Publishing house, 2005;

- [33] Ș. Țălu, M. Țălu, “AutoCAD 2006. Proiectare tridimensională” (AutoCAD 2006. Three-dimensional designing), Cluj-Napoca, MEGA Publishing house, 2007;
- [34] Ș. Țălu, “AutoCAD 2017”, Cluj-Napoca, Napoca Star Publishing house, 2017;
- [35] C. Birleanu, Ș. Țălu, “Organe de mașini. Proiectare și reprezentare grafică asistată de calculator” (Machine elements. Designing and computer assisted graphical representations), Cluj-Napoca, Victor Melenti Publishing house, 2001;
- [36] T. Nițulescu, Ș. Țălu, “Aplicații ale geometriei descriptive și graficii asistate de calculator în desenul industrial” (Applications of descriptive geometry and computer aided design in engineering graphics), Cluj-Napoca, Risoprint Publishing house, 2001;
- [37] Ș. Țălu, “Micro and nanoscale characterization of three dimensional surfaces. Basics and applications”, Napoca Star Publishing House, Cluj-Napoca, Romania, 2015;
- [38] M. Rusănescu, “Material requirements planning, inventory control system in industry”, Magazine of Hydraulics, Pneumatics, Tribology, Ecology, Sensorics, Mechatronics (HIDRAULICA), no. 1, pp. 21-25, 2014. ISSN 1453-7303;
- [39] M. Țălu, “Calculul pierderilor de presiune distribuite în conducte hidraulice” (Calculation of distributed pressure loss in hydraulic pipelines), Craiova, Universitaria Publishing house, 2016;
- [40] M. Țălu, “Pierderi de presiune hidraulică în conducte tehnice cu secțiune inelară. Calcul numeric și analiză C.F.D.” (Hydraulic pressure loss in technical piping with annular section. Numerical calculation and C.F.D.), Craiova, Universitaria Publishing house, 2016;
- [41] M. Țălu, “Mecanica fluidelor. Curgeri laminare monodimensionale” (Fluid mechanics. The monodimensional laminar flow), Craiova, Universitaria Publishing house, 2016;
- [42] M. Țălu, “The influence of the corrosion and temperature on the Von Mises stress in the lateral cover of a pressurized fuel tank”, Magazine of Hydraulics, Pneumatics, Tribology, Ecology, Sensorics, Mechatronics (HIDRAULICA), no. 4, pp. 89-97, 2017, ISSN 1453-7303;
- [43] D. Vintilă, M. Țălu, Ș. Țălu, “The CAD analyses of a torospheric head cover of a pressurized cylindrical fuel tank after the crash test”, Magazine of Hydraulics, Pneumatics, Tribology, Ecology, Sensorics, Mechatronics (HIDRAULICA), no. 4, pp. 57-66, 2017, ISSN 1453-7303;
- [44] M. Bică, M. Țălu, Ș. Țălu, “Optimal shapes of the cylindrical pressurized fuel tanks”, Magazine of Hydraulics, Pneumatics, Tribology, Ecology, Sensorics, Mechatronics (HIDRAULICA), no. 4, pp. 6-17, 2017. ISSN 1453-7303;
- [45] \*\*\* Autodesk AutoCAD 2017 software;
- [46] \*\*\* SolidWorks 2017 software;
- [47] \*\*\* Microsoft Excel 2017 software;
- [48] \*\*\* Maple 2016 software.

## Distributed Hardware and Software Architecture for Monitoring and Control of Hydraulic Drives

PhD.std. Eng. **Ioana ILIE**<sup>1</sup>, PhD. Eng. **Marian BLEJAN**<sup>2</sup>

<sup>1</sup> Hydraulics and Pneumatics Research Institute – INOE 2000-IHP Bucharest, ilie.ihp@fluidas.ro

<sup>2</sup> blejan.ihp@fluidas.ro

**Abstract:** *The paper presents a short-overview of a distributed monitoring and control system designed for hydraulic drives that allows immediate access to system performance measurements, behaviour analysis over time, and maintaining the hydraulic systems in the most efficient working manner. The monitoring and control system was implemented on various applications in industry (metallurgic field), in training equipment for aircraft crew and in laboratory equipment.*

**Keywords:** *Monitoring, control, process data, programmable controller*

### 1. Introduction

Monitoring and control hydraulic equipment, respective components, can be achieved in two different ways: a simple approach that means simple measures for component monitoring, and an advanced way based on the methods of signal acquisition and conditioning.

Conceptually, the monitoring and control system was designed as a distributed system which allows users and other applications outside it to interact with it in a uniform and coherent manner. The system components are placed on interconnected processing units, in both hydraulic and informatics levels, and their actions are communicated and coordinated by messaging. The convenient and secure online access to system condition allows taking the best decisions regarding system operation.

The monitoring and control system functionality is implemented on a programmable controller at hydraulic level, on computers network at information system level and the software application created is based on event-driven approach.

### 2. The monitoring and control system architecture

The monitoring and control system is designed for electro-hydraulic drives so the main support for it is a processing unit placed on hydraulics, that means electronics, microprocessors, PLCs or process computers. These process units have implemented both control and monitoring application for hydraulic drives using.

At the information system level there is a one or more PCs running a software application - Operator Console and standard DBMS. The operator console provides data reception from the hydraulic drive, stores the data in the database, and displays the process data locally in numeric or graphic form.

#### 2.1 Hardware architecture

The system concept was implemented on various applications and for each one on the hydraulic level the hardware support chosen was a common PLC (figure no. 1). For the informatics system it was used a PC running the operator console and one or more PCs running the DBMS. The process data transmission at the PLC level was ensured by a serial data line: Ethernet, RS485, and Wi-Fi.

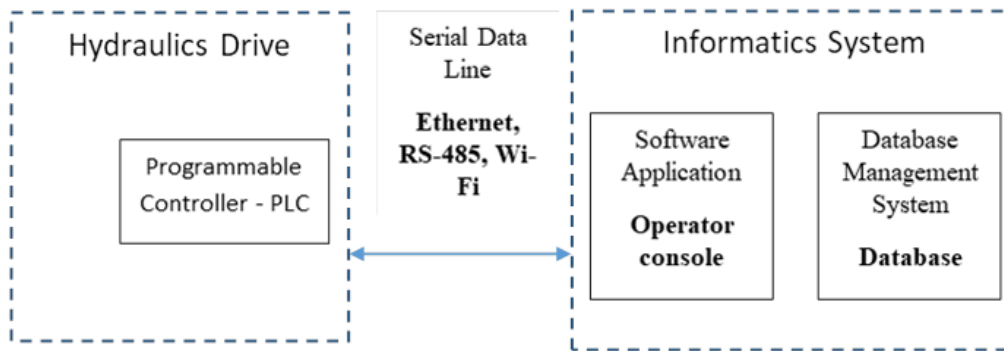


Fig. 1. Hardware architecture

**2.2 Software architecture**

The functionality of the monitoring and control software is provided by three components: first is the monitoring level running on Programmable Controller, the second component is Operator Console that’s running on the PC System and the third component is the DBMS. It have to say that this paper refers only to the first two components mentioned below (figure no. 2).

The monitoring and control software running at the programmable controller level consists of a program loop that runs at within 20ms. This allows a monitoring and control rate of 50 samples/s for each monitored and controlled process quantity. Within these loops are packed the process data that will be transmitted to the operator console application.

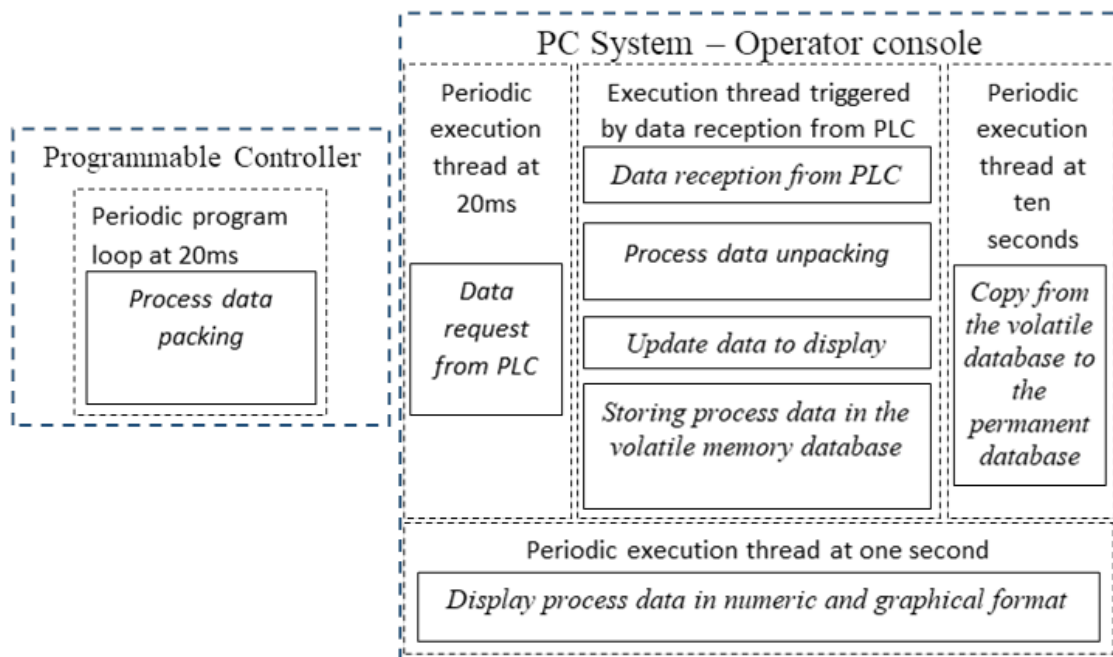


Fig. 2. Software architecture

The operator console software application has a 4-thread parallel execution structure. A thread executes periodically at 20ms to make a data request to the PLC through the data line. The second thread is triggered by PLC data reception and its functions is to unpacks the received process data, prepares data for display (PLC formats in real units), and stores data in a local database in volatile memory and PC. The third thread executes periodically at a time of 1 second, displays the process data in numeric or graphical format in the application panel. The fourth thread is executed periodically at a time interval of 10 seconds copies the data from the temporary database to the permanent one.

### 3. Practical implementation of the monitoring and control system

#### 3.1 Electrohydraulic system for winding rolled wire

The concept of distributed monitoring and control system was implemented on various applications in industry, in training equipment for aircraft crew and in laboratory equipment.

In the metallurgy field the monitoring and control concept was used on the electrohydraulic system for winding rolled wire (figure no. 3). This ensures wire stringing on spool coil by coil, by controlling movements of the debugger head, adapting itself to changes in spool rotational speed; spool rotational speed is dictated by the rolling process parameters and also the wire load of the spool that is diameter of the coil being wound[1].

This electrohydraulic system contains a linear axis consisting of a bilateral rod hydraulic cylinder, on its liner being located the debugger head, controlled with a proportional flow distributor. *Hardware components* of the monitoring and control system contains *sensors* for monitoring spool rotational speed and the speed of the debugger head, *electronics* necessary for interfacing the execution elements and transducers with the *programmable controller* ( figure no. 4)

Software components consist of *software* application that running on PLC and the operator console and the DBMS. The PLC software implements both the control of the mechatronic system and the monitoring features. This application has two data communication lines, a serial RS485 line with MODBUS protocol implemented to connect the PLC with the operator console, and an Ethernet line, that allows TCP / IP networks connection between the operator console and the company server where the DBMS was implemented [1].



Fig. 3. Winding roller



Fig. 4. Electric cabinet

The operator console (figure no.5) displays the process data locally in numeric or graphic form and allows connection with the DBMS to stores the process data in the database. The graphic shown in figure no. 6 is obtained with DBMS stored data.

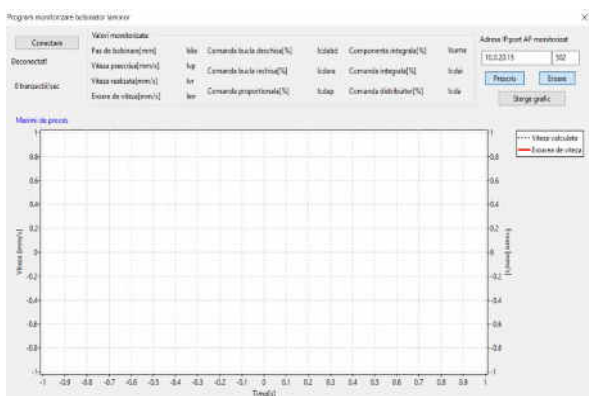


Fig. 5. Operator console

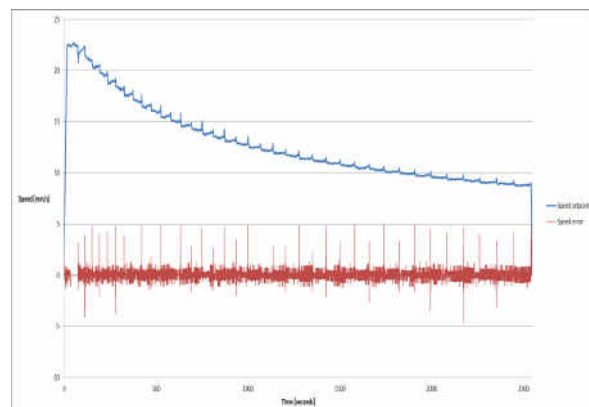


Fig. 6. Data process for one coil

### 3.2 Electrohydraulic actuation system for Cabin Emergency and Escape Trainer CEET B732

The electro-hydraulic actuation system is used on the Cabin Emergency and Escape Trainer CEET B732 for the Sea Survival School Tuzla (figure no 7) [3], and also implements the concept of distributed monitoring and control system. The monitoring and control system hardware contains sensors and PLC (figure no 8) at the and a single PC that contains the operator console and DBMS. Interfaces with data communication networks, namely the master-slave network implemented on RS485 communication line and the TCP/IP network implemented on Ethernet line. The PLC software application allows parameterization of the control system and updates both pseudo-analog (Pulse Width Modulation) and discrete outputs. The arithmetic on PLC is based on 16 and 32 bits words; for this application the calculus is made only with 16 bits signed words. Taking into account that the PLC arithmetic operation has only two operands, for the calculus of the error value (one of the monitored parameter) was used the PLC feature that could execute the program loop in fixed program execution time (for this application it was used 50ms scan time)[2].



Fig. 7. The Cabin Emergency and Escape Trainer



Fig. 8. Electric cabinet

The electro-hydraulic system has been tested for two command inputs types: for a ramp type and for a step type and the monitored value was positioning error. In figure no 9 is shown the experimental results obtained for a ramp type excitation signal (the dashed line) with a 17mm/s speed value. The positioning error (the continuous line) is 4 mm for a positioning range of 500mm; this error can be minimized by introducing in program a derivative component of error. In the figure no 10 is shown the results obtained for a step type input signal. The settling time for a 250mm step value is 2.5s. In this case introducing in command a derivative component of error would worsen the system response; respectively the settling time and the overshooting value would increase [2].

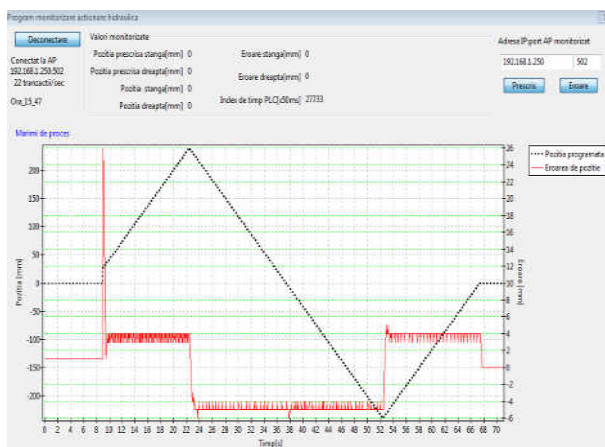


Fig. 9. The operator console – ramp type input signal

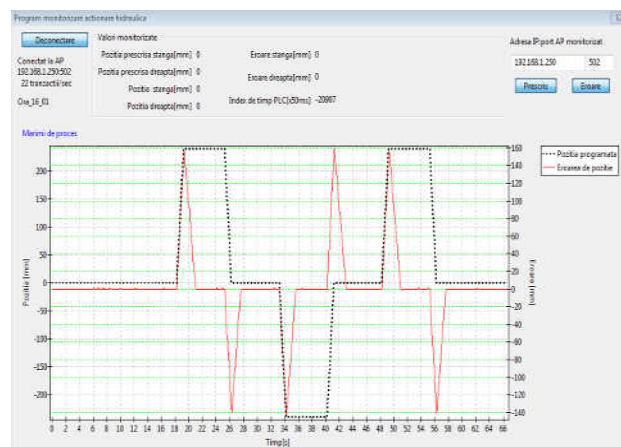


Fig. 10. The operator console – step type input signal

#### 4. Conclusions

The distributed system for monitoring and control electrohydraulic drives is designed to be used in various application in different field from heavy industry to laboratory equipment, and its main advantages are:

- Changing and adjusting the operating algorithm, for each kind of application, only requires rewriting software in the PLC, operator console and updating DBMS;
- Due its communication capabilities via Ethernet it can be integrated in a tracking IT system;
- Using new devices coupled to the serial bus, additional functions can be implemented on the process units, namely new parameters monitoring or control;
- The PLC that implements the monitoring and control program may be equipped with HMI console (human machine interface).
- Continuous monitoring allows early detection of potential issues and prevents unnecessary downtime for unneeded maintenance.

#### Acknowledgments

This paper has been developed in INOE 2000-IHP, with the financial support of the Executive Agency for Higher Education, Research, Development and Innovation Funding (UEFISCDI), under PN III, Programme 2- Increasing the competitiveness of the Romanian economy through research, development and innovation, Subprogramme 2.1- Competitiveness through Research, Development and Innovation - Innovation Cheques, project title: *Computerizing the technological process of heat treatment of metallic materials*, Financial Agreement no. 126CI/2017.

#### References

- [1] T. C. Popescu, M. Blejan, D. Vasiliu, “Innovative solution of energy efficiency and management for the production of aluminum wires”, *14th International Multidisciplinary Scientific GeoConference SGEM 2014*, www.sgem.org, SGEM2014 Conference Proceedings, ISBN 978-619-7105-15-5 / ISSN 1314-2704, June 19-25, 2014, Book 4, Vol. 1, 315-322 pp. - DOI: 10.5593/SGEM2014/B41/S17.041;
- [2] M. Blejan, I. Ilie, C. Cristescu, “Electronics for Electro-Hydraulic Actuation System” („Acționări hidraulice și pneumatice”), *2015 IEEE 21st International Symposium for Design and Technology in Electronic Packaging (SIITME)*, 22-25 Oct. 2015, Brasov, Romania, 978-1-5090-0332-7/15/\$31.00 ©2015 IEEE;
- [3] <http://www.sea-survival.ro/en/news/105-simulator-improvement>.

## Specific Methods for Acquiring Controlled Atmosphere for Clean Rooms Used in Industrial and Medical Domains

Assistant professor Fănel Dorel ȘCHEAUA<sup>1</sup>

<sup>1</sup>"Dunărea de Jos" University of Galați, MECMET Research Center, fanel.scheaua@ugal.ro

**Abstract:** *There are industry branches requiring a certain degree of internal air purity where the production process takes place. Consequently, there is a need of arranging special chambers with artificially controlled atmosphere and a high level of cleanliness, named clean rooms used in industry and medicine. Within these chambers the air is introduced by the means of special air plants that realises air treatment and filtration, achieving a continuous filtration and circulation so that the air foreign particles that would endanger the production process are retained and removed. Such special production enclosures are used predominantly in electronics, optics, biotechnology, pharmaceuticals, medical equipment, food industries, where an internal atmosphere with a certain degree of purity is required.*

*As a first method of providing optimal parameters for the atmosphere of a protected enclosure, a continuous ventilation of the filtered external air was adopted. A method of designing the interior space and the inlet and outlet orifices that allow a continuous air circulation within a virtual enclosure model is presented in this paper. An air circulation analysis is performed inside the enclosure virtual model, and the results are presented as flow velocity values, as well as specific pressure values on the interior areas of the analyzed fluid region of the enclosure model. Thus, the possibilities of reducing the turbulences occurring during air circulation within the enclosure model are monitored so that the circulation can be close to the laminar flowing range.*

**Keywords:** *Clean rooms, fluid flow, air flow, flow regime, 3D modelling, computational fluid dynamics (CFD)*

### 1. Introduction

Modern industrial branches whose activity object is the production of goods whose manufacturing process requires a high degree of cleanliness both of the production area and of the atmosphere in which they work, have led to the emergence of clean spaces with a controlled atmosphere where the production process can be carried out in order to obtain optimum results.

Such chambers are specially designed and constructed enclosures with special materials that do not tend to retain foreign particles on the surface, be it walls, floor or ceiling. The air introduced through the air power plants must comply with the purity level of the enclosure's interior atmosphere, without causing any momentary changes affecting the degree of purity.

As a first method used to provide a clean and controlled atmosphere inside an enclosure was the continuous circulation of filtered air inside the enclosure clean room. Various air filter types were used in order to retain the foreign particles from air introduced into the enclosure by means of fans. The method belongs to Florence Nightingale (1895), but inconveniences of this method related to the effect of the temperature difference between the enclosure and the exterior, pressure differences between the enclosure air and the outside air, but also the existence of strong air currents inside the enclosure. [1]

Thus, due to air streams passing through the enclosure in certain directions, particles from the floor are entrained in motion and raised in the room atmosphere. Solutions must therefore be adopted in order to overcome this disadvantage involving the air turbulent flow inside the premises with clean and controlled atmosphere. One of these solutions is to provide the unidirectional air circulation inside the enclosure between the inlet orifices area and the outlet orifices area of the enclosure, with a certain value of the air circulation velocity, thus avoiding unwanted strong turbulent flow.

### 2. Clean rooms constructive types

Depending on the activity object to be carried out inside the clean room enclosure, there are several types of enclosures classified according to the degree of cleanliness of the indoor atmosphere.

Table 1 summarizes some of the industry branches that require the existence of clean rooms with controlled atmosphere in order to achieve the proposed activity. [1]

**Table 1:** The industry branches where clean rooms are in use

Current number	Industry Branch	Manufactured products
1.	Electronics	Computers and components
2.	Micro-electronics	Integrated circuits
3.	Optics	Lenses, laser equipment
4.	Pharmaceutical	Pharmaceutical sterile products
5.	Medical equipment industry	Medical equipments
6.	Food industry	Sterile foods
7.	Medicine	Operating rooms, sterile salons

According to international standards ISO 14044/01 a clean room is an enclosure within which the particle concentration contained within the indoor atmosphere is controlled and which is constructed so as to minimize the introduction, formation and storage of foreign particles inside. It is also possible to control other parameters related to the temperature, humidity, pressure inside the enclosure.

Depending on the cleanliness degree of the enclosure indoor atmosphere, clean rooms can be classified. The cleaning degree is given by the number of particles contained in the volume unit of the inner atmosphere. Classification according to ISO standards is based on the following relationship:

$$C_{\max} = 10^N + \left( \frac{0.1}{D_p} \right)^{2.08} \quad (1)$$

where:

$C_{\max}$  - maximum allowed concentration;

$N$  - ISO classification number;

$D_p$  - particle diameter in microns;

The ISO, N classification is in the range of 0-9, and each integer within this range represents a cleanliness class for the enclosure internal atmosphere.

The enclosures with controlled atmosphere can be classified according to the type of indoor air circulation introduced by the means of the air plants as follows:

Type 1 - a clean room enclosure inside which there is a turbulent airflow introduced in several directions;

Type 2 - clean room enclosures inside which the air circulation is laminar unidirectional, using high-efficiency filters;

Type 3 - clean room enclosures inside which there is a mixed air circulation;

Type 4 - laminar and unidirectional air circulation within enclosures having insulating walls.

Both in the industry and also in the medical field, clean room standards must be strictly respected. These spaces are clean rooms with a controlled atmosphere, which can be arranged according to the requirements of the proposed activity object. Such enclosures are made of special materials of the walls, floor, or ceiling, to which the particles in the atmosphere can not adhere and with the air intake devices a permanent air circulation is maintained inside the enclosure. Air circulation is achieved between the inlet orifices positioned on the ceilings or the walls and outlet openings positioned at the base walls or even in the floor inside the enclosure.

By means of filters the foreign particles from external air is retained from the outdoor air introduced into the enclosure.

Depending on the cleaning class requirements for enclosure atmosphere where the production process takes place the work rooms types with different configurations in terms of working space and air circulation may be arranged as shown in the models presented in Figure 1.

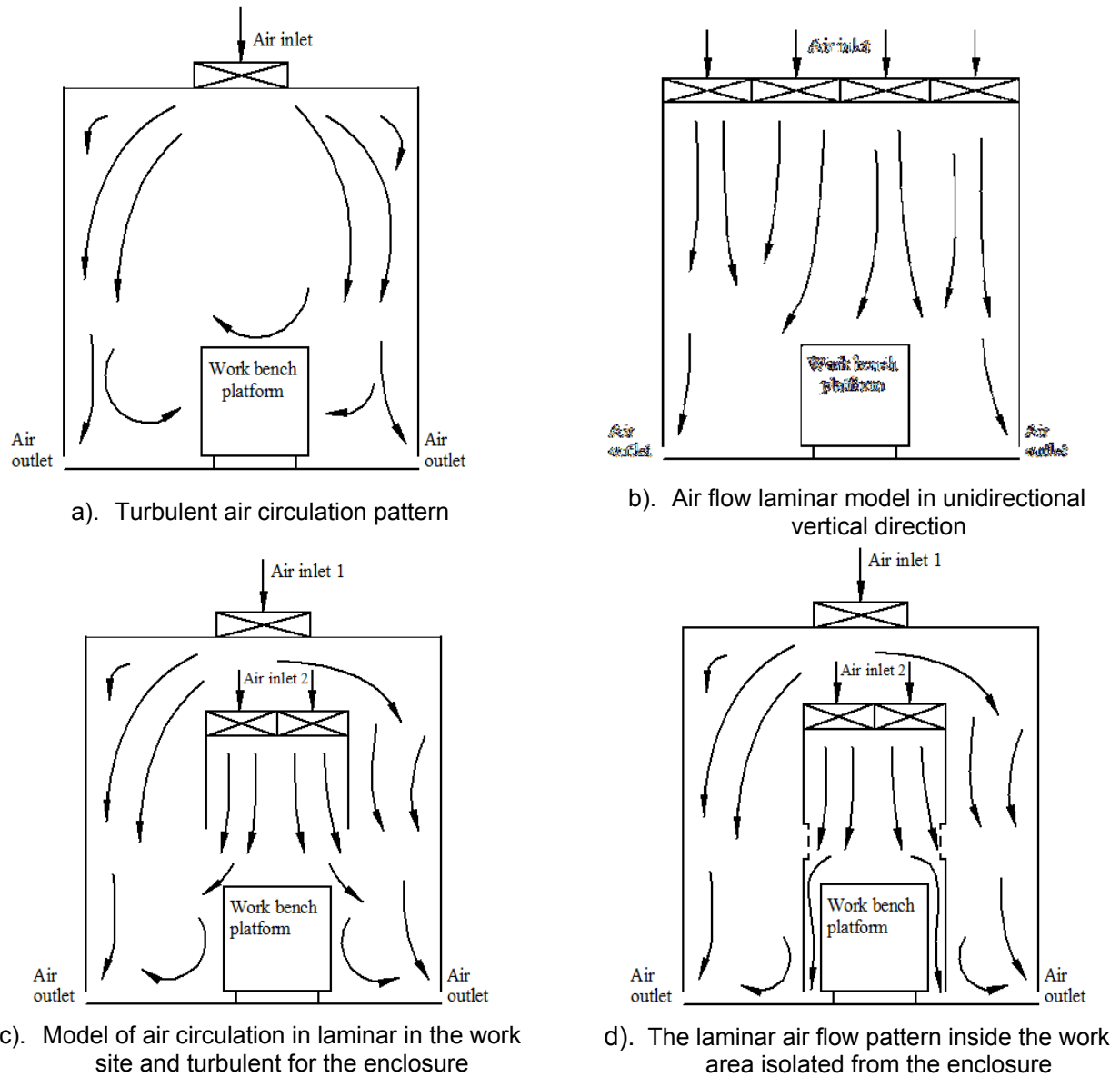


**Fig. 1.** Schematically representation of air flow within clean room enclosure types

Depending on the enclosure clean atmosphere class, different configurations are provided with respect to the positioning of the work space, which can be placed both in the enclosure and inside a protected area with unidirectional overflow circulation of the air streams within the enclosure where the operator has access by the means of special access slots.

**3. The air flow analysis for the clean room enclosure model**

A three-dimensional model for a virtual clean room was built with a length of 7 meters, 5 meters width and 3 meters height. The openings that represent the air inlet and outlet orifices areas are also initially designed on the enclosure model. For the air inlet were made 4 rectangular orifices (60x70 cm), placed on the enclosure ceiling and for the outlet a number of 12 rectangular orifices (70x10 cm), placed at the bottom of the chamber walls, were adopted. The model was introduced into the ANSYS CFX flow analysis and for the working fluid was selected air at 20 degrees Celsius.

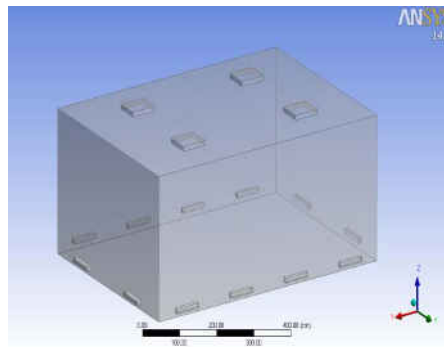
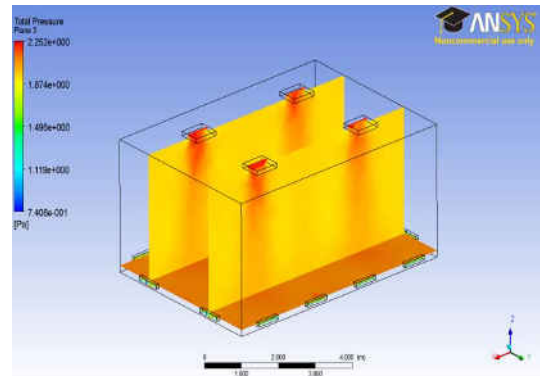
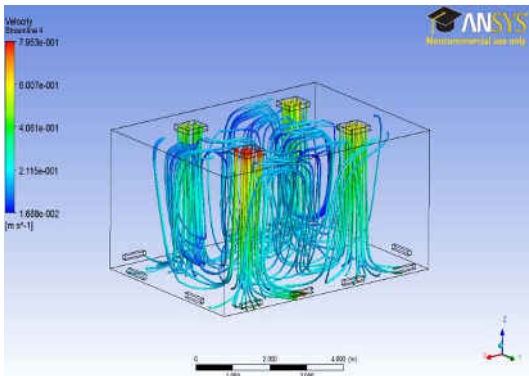


Fig. 2. Enclosure model fluid region

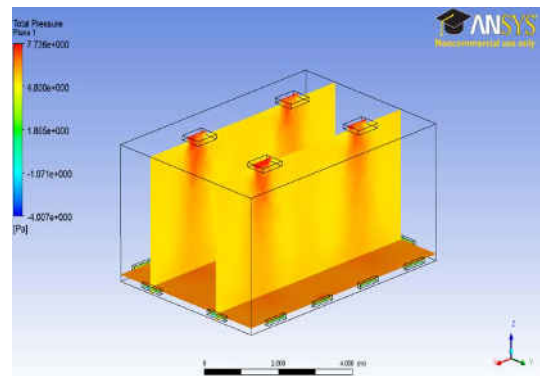
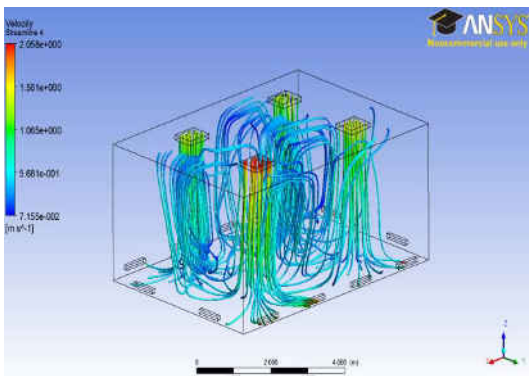
Four distinct cases were analyzed with different air flow rates values declared at the inlet orifices. The obtained results highlight the air circulation model inside the enclosure by the described pathlines having different velocity and pressure values at the analyzed fluid regions. It can be noticed that the flow model is generally turbulent but with different values for the air movement velocity. Table 2 describes the initial values regarding air flow rate declared for each analyzed case.

Table 2: The initial values for air flow rates

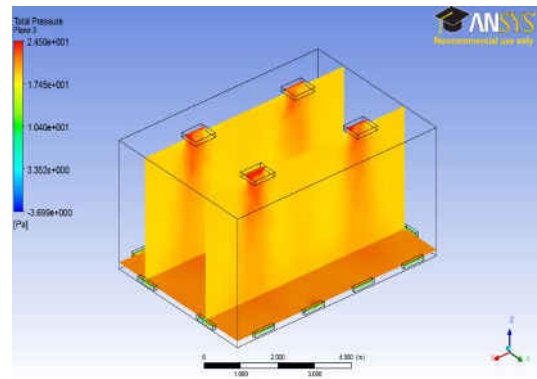
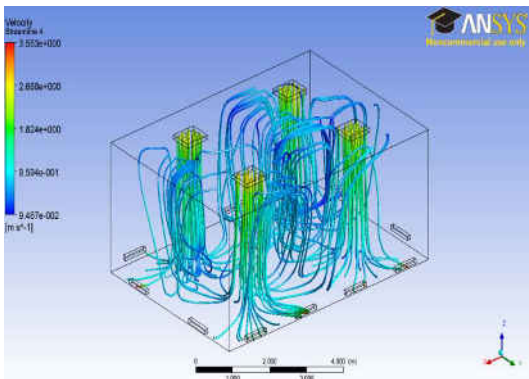
Case number	Air flow rates [kg/s]	Air flow rates [m3/h]
Case 1	0.3	896.2656
Case 2	0.7	2091.286
Case 3	1.3	3883.817
Case 4	2	5975.104



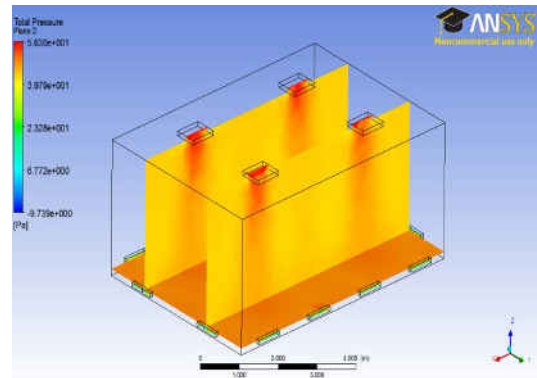
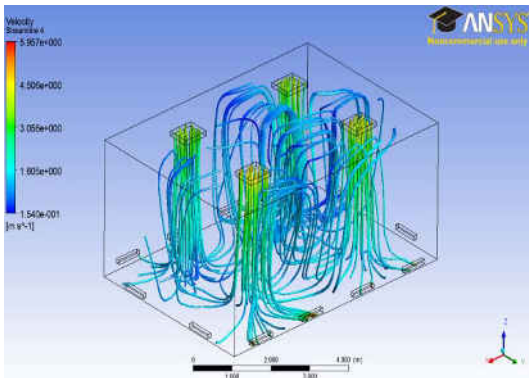
a). The obtained values for Case 1



b). The obtained values for Case 2



c). The obtained values for Case 3

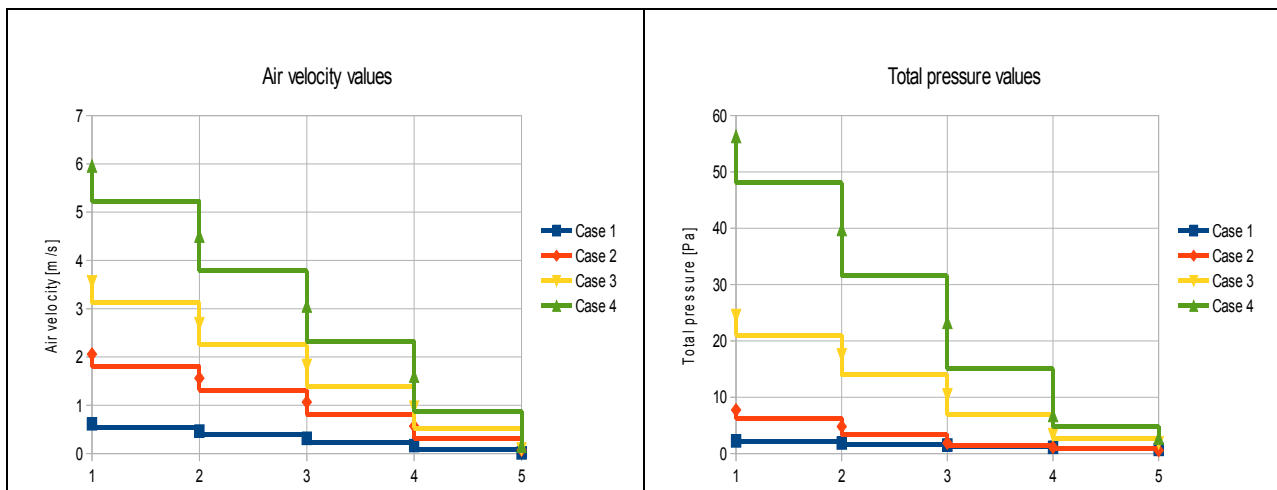


d). The obtained values for Case 4

Fig. 3. Fluid velocity and total pressure values for the analyzed cases

Using the obtained result values from the analyzed cases, the diagrams corresponding to the air velocity and total pressure values were plotted, presented in Table 3.

Table 3: Air velocity and total pressure diagrams



The diagrams show the minimum and maximum values in which the velocity and total pressure ranges inside the analyzed fluid region for all 4 analyzed cases.

Generally, for a clean room with a controlled atmosphere with a certain class of cleanliness, the circulated air velocity values are limited at values ranging between 0.2 - 0.5 m/s, for the turbulent air flow model inside the enclosure and the optimal values for pressure ranges from 7 to 20 Pa. [2]

Air circulation velocity values are limited in order to prevent particles entrainment in circulating air, while a reduced air circulation velocity can create the deposition of these particles on the clean room surfaces.

The pressure values must be higher than the external environment pressure in order to prevent particle infiltration from the enclosure outside environment.

Thus, basing on the requirements for air velocity and pressure values correlated with the values obtained from air flow analysis within the virtual model of the analyzed enclosure model, the case 2 (air flow of 0.7 kg/s) values presents the closest terms for air velocity and pressure values.

#### 4. Conclusions

Clean rooms with controlled atmosphere have arisen due to the existing needs in both the industry and the medical field, regarding the cleanliness of both the enclosure and the air present on the premises. Specific cleaning classes have been developed that describe the premises used in various branches of industry and medicine.

The presence of foreign particles in the clean rooms atmosphere can not be avoided but can be reduced by number based on the specific construction procedures and the introduction, circulation and filtration of indoor air.

A virtual enclosure model was built and analyzed regarding the air circulation mode in this paper.

Four distinct cases were considered for which different air flow rates were declared at the inlet orifices. The results show the air circulation mode within the analyzed fluid region, with the specific recorded values for the velocity and total pressure.

The flow model is of turbulent type as the air stream pathlines for all analyzed cases are presented.

Based on the recommended values for clean room enclosures, Case 2 was chosen as the optimal case, as the values obtained for the air circulation velocity and the pressure values inside the enclosure model are the closest to the recommended values.

Values for airflow velocity inside the enclosure must be limited for practical reasons in order to reduce the turbulences created and to ensure an optimal degree of comfort for human operators working in such premises.

Regarding the pressure values, the highest pressure value must be ensured for the higher cleanliness class from clean room standards in order to avoid external contamination of this enclosure.

In addition to the air circulation velocity, an optimal level of temperature and humidity values inside the clean rooms premises with controlled atmosphere are also provided, depending on the technological process that takes place in the enclosure.

Further conditions of sterility of the clean room enclosures must be provided that describe the level of microbial contamination directly related to the microorganisms and particles from the enclosure indoor air atmosphere which are added to the total particle number that provides the specific cleaning class for the clean room enclosure. [2]

#### References

- [1] V.L. Cartaș, “Elemente de proiectare a incintelor cu atmosferă controlată”, Impuls Publishing House, Bucharest, 2001;
- [2] <http://camerrecurate.ro/camera-curata/32-parametrii-generalii-ai-camelor-curate>;
- [3] <http://www.cleanairtechnology.com/cleanroom-classifications-class.php>;
- [4] <http://www.cleanroom-system.com/index.asp>;
- [5] <http://www.lufttec.ro/cc-clasificare.html>.

## The CAD Analyses of a Torospheric Head Cover of a Pressurized Cylindrical Fuel Tank after the Crash Test

Prof. PhD. Eng. **Daniela VINTILĂ**<sup>1</sup>, Assoc. Prof. PhD. Eng. **Mihai ȚĂLU**<sup>2\*</sup>,  
Assoc. Prof. PhD. Eng. **Ștefan ȚĂLU**<sup>3</sup>

<sup>1</sup> University of Craiova, Faculty of Mechanics, Department of Applied Mechanics and Civil Engineering, Calea București Street, no. 107, 200512 Craiova, Dolj county, Romania. E-mail: vintila\_dnl@yahoo.com

<sup>2</sup> University of Craiova, Faculty of Mechanics, Department of Applied Mechanics and Civil Engineering, Calea București Street, no. 107, 200512 Craiova, Dolj county, Romania. Corresponding author\* e-mail: mihai\_talu@yahoo.com

<sup>3</sup> Technical University of Cluj-Napoca, The Directorate of Research, Development and Innovation Management (DMCDI), Constantin Daicoviciu Street, no. 15, Cluj-Napoca, 400020, Cluj county, Romania. E-mail: stefan\_ta@yahoo.com

§: All authors contributed equally to this work.

**Abstract:** *The purpose of the study described in this paper was to assess the effect of impact during the crash test on the Von Mises effort state that appear in the end cover on a pressurized cylindrical fuel tank. An optimal CAD design of the torospheric head cover was first determined. The state of stress was determined by the thermal stress and computed by polynomial interpolation. The effectiveness of the method is evaluated by Von Mises stress variance laws during the impact were assessed as well as the influence of the corrosion phenomenon on the state of effort. The obtained results can be applied to experimental modeling of vehicle collision phenomena.*

**Keywords:** *Automotive industry, corrosion, crash test, industrial engineering design, optimization, pressurized fuel tank, state of effort, torospheric head cover*

### 1. Introduction

The automotive fuel tank market dynamics offers a vision on the automotive industry trends and help plan effective business strategies based on a rigorous research and analysis of the key data especially over the medium to long term [1-4].

Automotive fuel tank is an important safety and functional part of vehicle used to store liquefied petroleum gas (LPG) or compressed natural gas (CNG) fuel with a complex geometry, made especially of steel or aluminum [5-11].

In computer aided engineering of the fuel tanks structure for representing geometry and material details, various shape design variables [12, 13], structural design variables [14] and software tools [15-20] are used to find an optimal geometrical solution [21-27] at less cost [28-33].

When is installed a pressurized fuel tank for LPG or CNG on a car, it is planned by the automotive constructor to be placed in a special location reinforced and padded with materials capable of amortizing impact shocks resulting from a road accident [5].

The crash test, due to the higher mathematical complexity of a crash event representation, is a special stress test performed on pressurized tanks during the homologation process in which a metal bar is projected in the tank at a speed of  $v = 15$  m/s [31-34].

The selected collision phenomenon is provided by a set of complicated experiments on the sidewalls of the pressurized fuel tank and in particular on the lateral cover or the head cover in case of a cylindrical fuel tank.

In order to generate new dataset which will be used to evaluate the proposed crash modeling methodology, it was decided to create a virtual crash test by numerical simulations to reproduce the test conditions in a realistic manner to be as close as possible to the actual conditions encountered in service. On the other hand, the obtained models and mathematical algorithms are valid only for one given set of collision conditions and increase the cost and time of such simulation [34-37].

There have been numerous examples of applications of fractal and multifractal theory to find patterns in large and complex datasets as in crash data to identify high-crash locations and in traffic management strategies, such as crash analysis, spatial distribution of road traffic accidents and travel time reliability [38-41].

## 2. The optimal design of the torospheric head cover of the pressurized fuel tank

The torospheric head cover of pressurized fuel tank is calculated by a series of dimensional constructive relations according to the recommendations given by DIN 28011 (Figures 1 and 2).

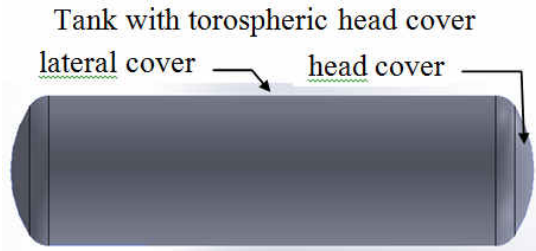


Fig. 1. The components of pressurized fuel tank

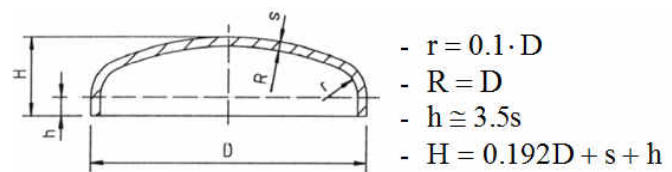


Fig. 2. The sketch of the torospheric lateral cover

### 2.1. The CAD design of optimal sizing of the head cover

The parameterized modeling of the torospheric head cover (as shown in Figures 3 and 4) was done in the AutoCAD Autodesk 2017 software [42], which was imported to SolidWorks 2017 software [43] for analysis with the: Static, Thermal and Design Study modules.



Fig. 3. The model of torospheric head cover

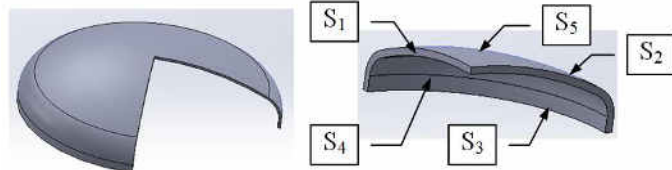


Fig. 4. The  $\frac{3}{4}$  and  $\frac{1}{4}$  sections of torospheric head cover model with indications of the exterior surfaces

The optimization parameters are: thickness  $s$  and height  $h$  of the torospheric head cover, which have a continuous variation between the limits:  $s = 2.5 \dots 6$  mm and  $h = 10 \dots 16$  mm.

To evaluate the objective and constraint functions next conditions were imposed:

- obtaining of a maximum resultant Von Mises stress equal to or less than the admissible stress of material AISI 4340,  $\sigma_{rez} \leq \sigma_a = 710$  N/mm<sup>2</sup>;
- to respect the minimum cover mass condition.

For CAD analysis of the head cover constructive shape a quarter of the model was chosen (due to the model symmetry), (as shown in Figure 4).

The design data used for optimized sizing of cover are:

- non-penetrative torospheric cover with diameter  $D = 250$  mm;
- construction material of the sheet metal: steel AISI 4340;
- geometrical symmetry of  $S_1$  and  $S_2$  surfaces and zero axial displacement of the cover;
- Loads:
  - with maximum pressure of  $p_{max} = 30$  bar on surface  $S_4$ ;
  - with thermal load between the limits  $T = -30$  °C up to  $T = 60$  °C on the surfaces:  $S_4$  and  $S_5$ ;
  - with a normal impact on the surface  $S_5$  produced with a bar having an initial velocity of  $v = 15$  m/s while impacting the obstacle;
- the duration of the cover exploitation is:  $n_a = 15$  years;
- the corrosion rate of the material is equal to:  $v_c = 0.06$  mm / year.

The optimal values obtained by computation are:  $s_{opt} = 2.8$  mm, and height  $h = 10$  mm. In the same time, the Von Mises maximum stress response occurs at a temperature of  $T = -30$  °C.

The optimized thickness has been corrected taking into account next factors: the corrosion phenomenon, the negative tolerance of the sheet metal and the thinning phenomenon (by 10 % of the thickness of the laminate to the embossing process).

The formula for calculating the thickness is the following:

$$s_{\text{real}} = s_{\text{opt}} + v_c \cdot n_a + \text{abs}(A_i) + \Delta s_a \quad (1)$$

where:

- $v_c$ , corrosion rate of the cover,  $v_c = 0.06$  mm / year;
- $n_a$ , number of years of exploitation,  $n_a = 15$  years;
- $A_i$ , the lower deviation of the laminate sheet,  $A_i = -0.6$  mm, for  $s = 3 \dots 5$  mm;
- $\Delta s_a = 0.1$  s = 0.5 mm, thinning of the sheet caused by the head cover embossing.

Finally, the minimum thickness of the sheet laminate is determined as:

$$s_{\text{real min}} = 2.8 + 0.06 \cdot 15 + \text{abs}(-0.6) + 0.1 \cdot 5 = 4.8 \text{ mm} \quad (2)$$

A laminate sheet of AISI 4340 steel with a thickness of  $s = 5^{+0.25}_{-0.6}$  mm is chosen for analysis.

The calculation at impact through numerical simulation was made for  $n_a = 15$  years which corresponds to the end of exploitation time, when the thickness of the head cover is minimal  $s = 3$  mm as a result of corrosion and the Von Mises stress become maximal.

### 3. The CAD analysis of Von Mises stress in the head cover at the crash test

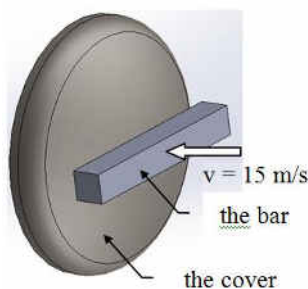
The impact simulation was considered as a non-linear contact problem. In order to have a basis of comparison at the time of the initial impact, the state of stress due to pressure loading and thermal load was calculated.

Table 1 shows the numerical results of the Von Mises stress as a function of time (for the same interval of time  $\Delta t = 5 \mu\text{s}$  and the same interval of temperature at  $\Delta T = 10$  °C). The total impact time was chosen at  $t = 40 \mu\text{s}$ .

**Table 1:** The Von Mises stress during the impact of torospheric head cover

	Temperature T [°C]									
	-30 °C	-20 °C	-10 °C	0 °C	10 °C	20 °C	30 °C	40 °C	50 °C	60 °C
t [μs]	Effort state at the time of the initial impact test, $\sigma_i$ [N/mm <sup>2</sup> ]									
0	428.750	426.48	424.31	422.24	420.27	418.4	416.84	416.63	417.71	418.85
5	431.773	429.504	427.335	425.266	423.297	421.428	419.869	419.66	420.743	421.886
10	443.321	441.052	438.883	436.745	434.848	432.981	431.425	431.218	432.30	433.451
15	467.049	464.781	462.614	460.302	458.579	456.712	455.154	454.947	456.029	457.172
20	530.741	537.488	535.335	531.688	531.329	529.475	527.932	527.738	528.834	529.989
25	618.060	615.835	613.709	607.534	609.755	607.927	606.409	606.240	607.360	608.540
30	638.855	636.643	634.531	627.050	630.603	628.789	627.283	627.127	628.260	629.452
35	638.820	636.609	634.496	627.026	630.568	628.753	627.247	627.091	628.224	629.416
	Effort state after t = 40 [μs] from the impact initiation, $\sigma_i$ [N/mm <sup>2</sup> ]									
40	638.786	636.574	634.461	627.001	630.533	628.718	627.212	627.055	628.187	629.379

The parameterized model consisting of the head cover and the impact metal bar (with a square section having the side  $B = 40$  mm and the length  $L = 250$  mm), as shown in Figures 5 to 7.



**Fig. 5.** The isometric view of impact model



**Fig. 6.** The left view of impact model

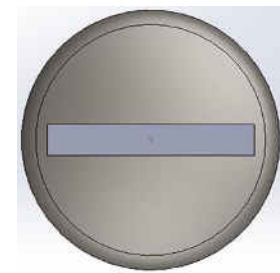


**Fig. 7.** The front view of impact model

The impact study is carried out in the most unfavorable situation, with the normal incidence of the bar applied on the outer surface of the head cover. At the same time, the bar is in translation along the symmetry axis of the head cover.

Starting from the data in Table 1, the Von Mises maximum stress variation graphs were computed throughout the impact of  $t = 40 \mu\text{s}$  for the temperature in range of limits  $T = -30^\circ\text{C}$  up to  $T = 60^\circ\text{C}$ . The laws of variation of stress obtained by polynomial interpolation are represented for each graph (as shown in Figures 7 to 17).

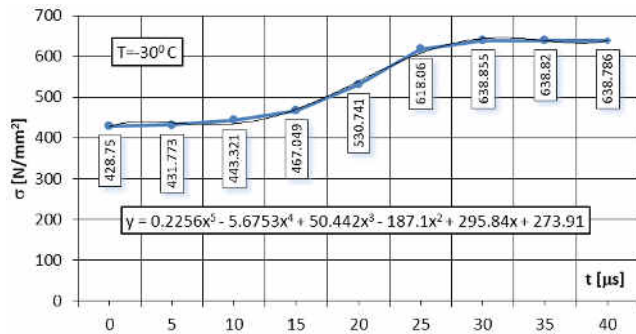


Fig. 8. The Von Mises stress at impact for  $T = -30^\circ\text{C}$

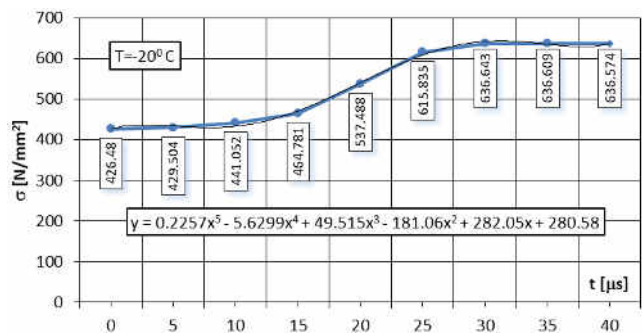


Fig. 9. The Von Mises stress at impact for  $T = -20^\circ\text{C}$

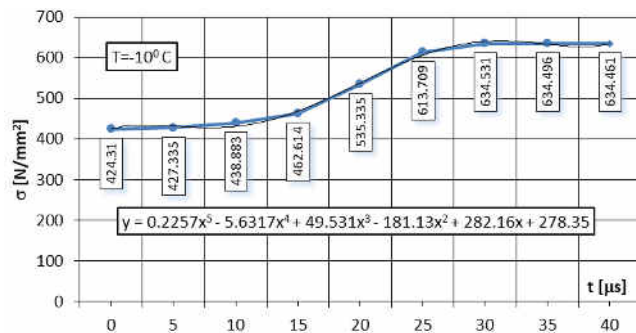


Fig. 10. The Von Mises stress at impact for  $T = -10^\circ\text{C}$

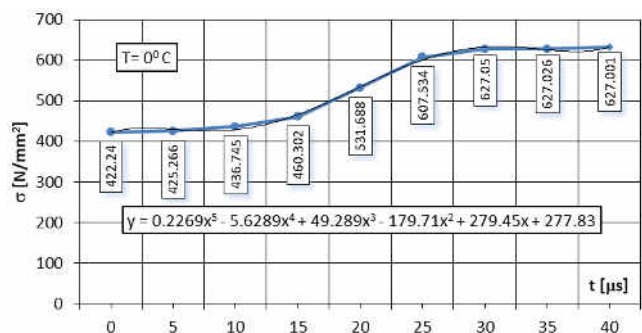


Fig. 11. The Von Mises stress at impact for  $T = 0^\circ\text{C}$

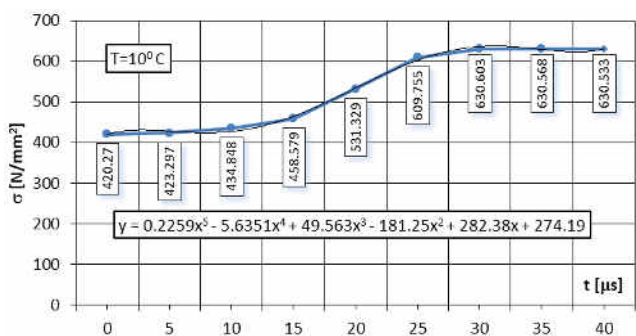


Fig. 12. The Von Mises stress at impact for  $T = 10^\circ\text{C}$

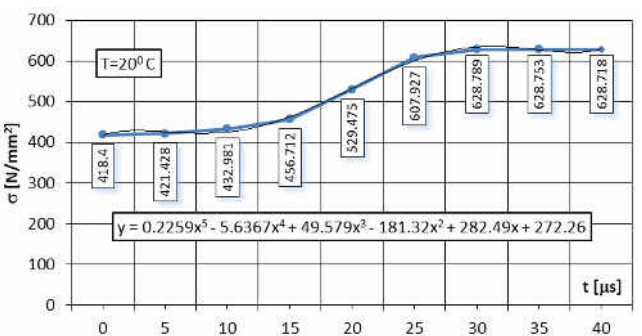


Fig. 13. The Von Mises stress at impact for  $T = 20^\circ\text{C}$

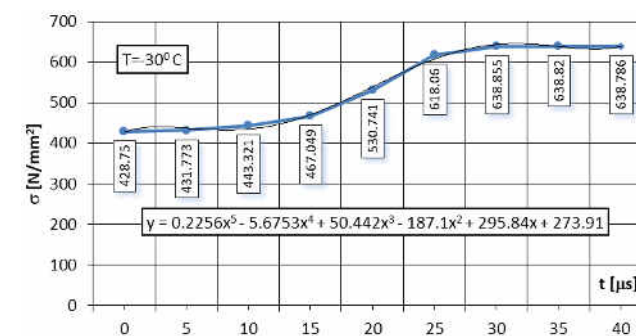


Fig. 14. The Von Mises stress at impact for  $T = 30^\circ\text{C}$

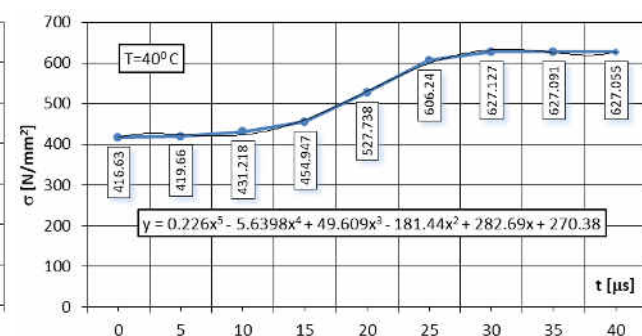
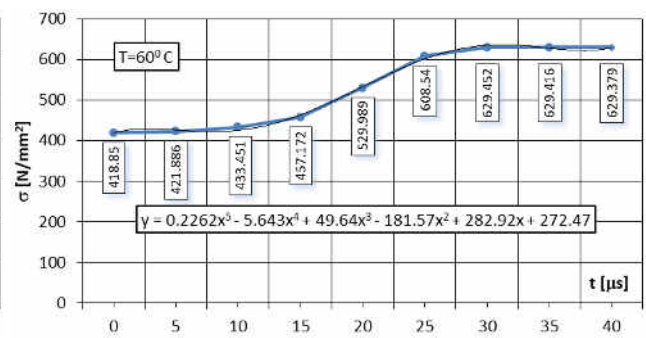
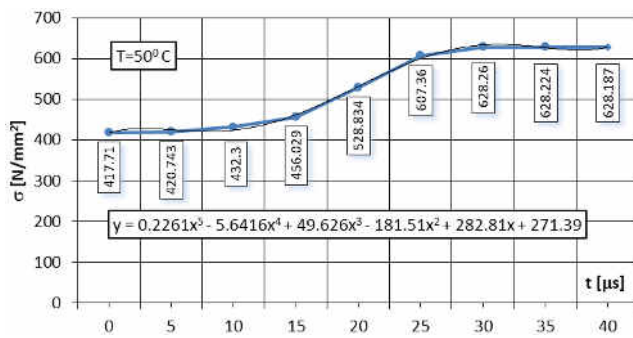
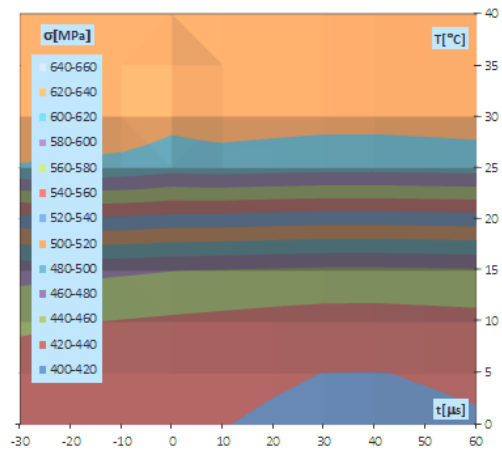
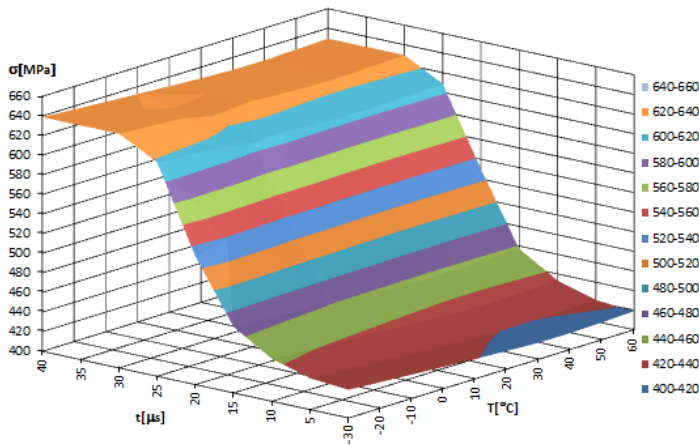


Fig. 15. The Von Mises stress at impact for  $T = 40^\circ\text{C}$



**Fig. 16.** The Von Mises stress at impact for T = 50 °C **Fig. 17.** The Von Mises stress at impact for T = 60 °C

Graphical representation in axonometric projection of the 3D variation of Von Mises stress state  $\sigma(t, T)$  as a result of the cumulative impact-temperature effect produced on the study interval of  $t = 40 \mu s$  is shown in Figure 18. Figure 19 shows a graphical representation of the dependency graph for surface  $\sigma(t, T)$  in the top view representation.



**Fig. 18.** The graph of Von Mises stress  $\sigma(t, T)$  in torospheric cover

**Fig. 19.** The superior view of  $\sigma(t, T)$  on the torospheric cover

The variance of Von Mises stress generated only by the impact action, based on the numerical values given in Table 2, was computed and represented in axonometric projection in Figure 20. Figure 21 shows a graphical representation of the dependency graph  $\sigma(t, T)$  in the upper view.

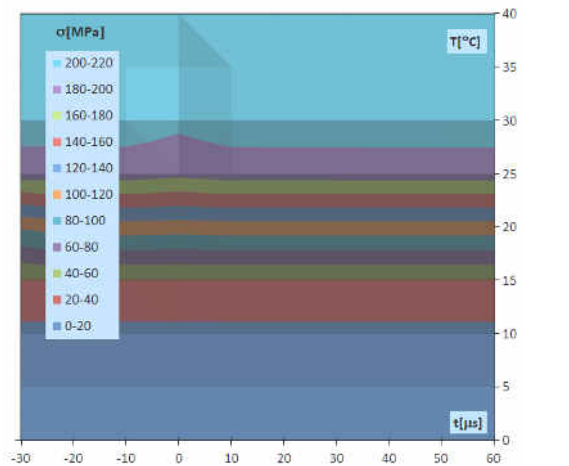
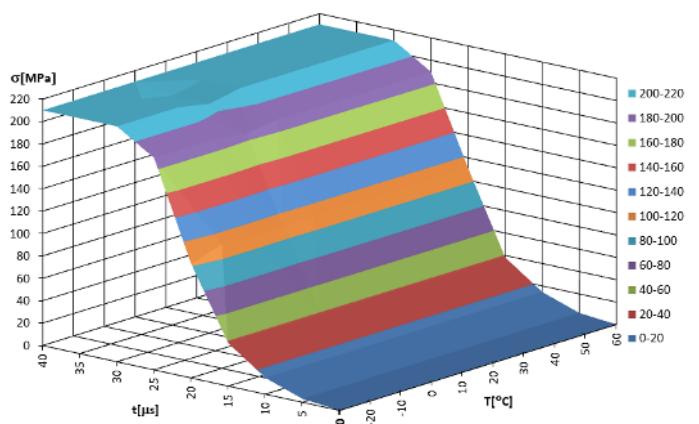


**Fig. 20.** The graph of Von Mises stress given by the impact in torospheric head cover

**Fig. 21.** The superior view of  $\sigma(t, T)$  given by impact on the torospheric head cover

**Table 2:** The Von Mises stress given only by impact in torospheric head cover

		Temperature T [°C]									
		-30 °C	-20 °C	-10 °C	0 °C	10 °C	20 °C	30 °C	40 °C	50 °C	60 °C
T[μs]	Effort state at the time of the initial impact test, $\sigma_i$ [N/mm <sup>2</sup> ]										
0	0	0	0	0	0	0	0	0	0	0	
5	3.023	3.024	3.025	3.026	3.027	3.028	3.029	3.03	3.033	3.036	
10	14.571	14.572	14.573	14.505	14.578	14.581	14.585	14.588	14.59	14.601	
15	38.299	38.301	38.304	38.062	38.309	38.312	38.314	38.317	38.319	38.322	
20	101.991	111.008	111.025	109.448	111.059	111.075	111.092	111.108	111.124	111.139	
25	189.310	189.355	189.399	185.294	189.485	189.527	189.569	189.61	189.65	189.69	
30	210.105	210.163	210.221	204.81	210.333	210.389	210.443	210.497	210.55	210.602	
35	210.070	210.129	210.186	204.786	210.298	210.353	210.407	210.461	210.514	210.566	
		Effort state after t= 40 [μs] from the impact initiation, $\sigma_i$ [N/mm <sup>2</sup> ]									
40	210.036	210.094	210.151	204.761	210.263	210.318	210.372	210.425	210.477	210.529	

The envelope stress state computed before the initial impact moment due to variation in temperature and the maximum load pressure on the interior surfaces of toroidal head cover is shown in Figures 22 to 27.

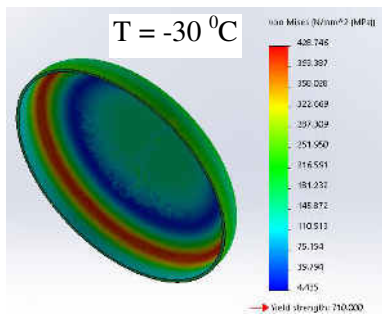


**Fig. 22.** The Von Mises stress before impact at T = -30 °C

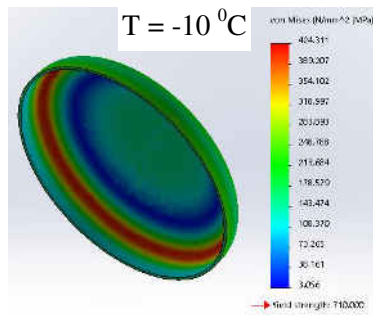


**Fig. 23.** The Von Mises stress before impact at T = -10 °C

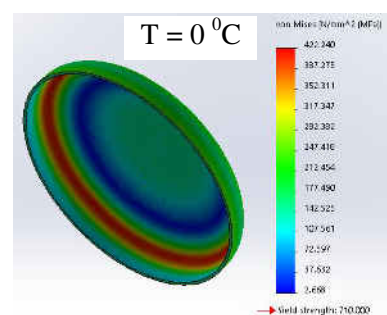


**Fig. 24.** The Von Mises stress before impact at T = 0 °C

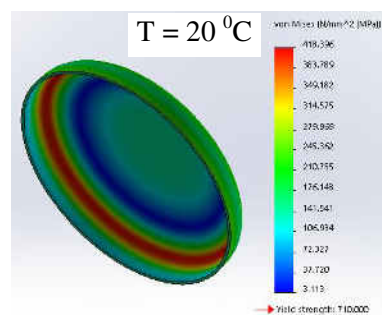


**Fig. 25.** The Von Mises stress before impact at T = 20 °C

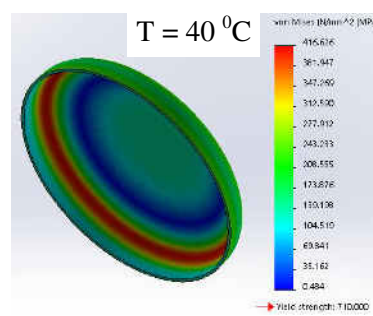


**Fig. 26.** The Von Mises stress before impact at T = 40 °C

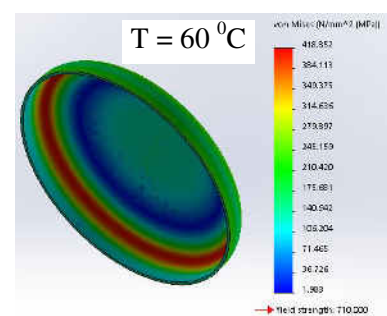


**Fig. 27.** The Von Mises stress before impact at T = 60 °C

The numerical summary of influence of the temperature on the stress at the moment of the initial impact (considering that the calculation stress is computed at the temperature T = 0 °C) is shown in Table 3 and the corresponding variation graph is shown in Figure 28.

**Table 3:** The Von Mises stress variation given by the influence of temperature in torospheric head cover

T [°C]	-30	-20	-10	0	10	20	30	40	50	60
$\Delta\sigma$ [N/mm <sup>2</sup> ]	6.51	4.24	2.07	0	-1.97	-3.84	-5.4	-5.61	-4.53	-3.39
$\Delta\sigma$ [%]	1.52	0.99	0.49	0.00	-0.47	-0.92	-1.30	-1.35	-1.08	-0.81

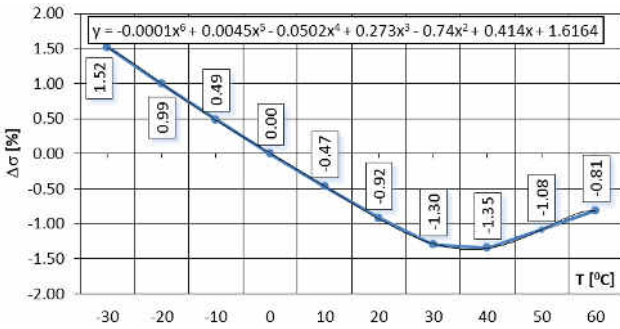


Fig. 28. The procentual deviation of stress given by the temperature at t = 0 μs of impact in head cover

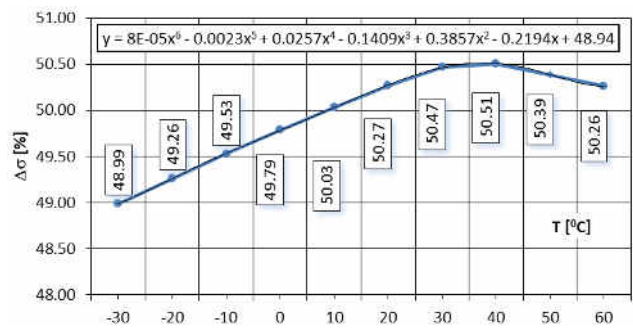


Fig. 29. The procentual variation of Von Mises stress given by impact at t = 40 μs in head cover

The increase in the effort due only to the impact action during the t = 40 μs is shown in Table 4 and the corresponding graph is shown in Figure 29.

Table 4: The Von Mises stress variation given by impact after t = 40 μs in torospheric head cover

T [°C]	-30	-20	-10	0	10	20	30	40	50	60
$\sigma_{\text{impact}}$ [N/mm <sup>2</sup> ]	210.036	210.094	210.151	204.761	210.263	210.318	210.372	210.425	210.477	210.529
$\sigma_{\text{initial}}$ [N/mm <sup>2</sup> ]	428.75	426.48	424.31	422.24	420.27	418.4	416.84	416.63	417.71	418.85
$\Delta\sigma$ [%]	48.99	49.26	49.53	48.49	50.03	50.27	50.47	50.51	50.39	50.26

The percentage variation in the ratio of the Von Mises stress generated by the temperature and impact is shown in Table 5 and the corresponding graph is given in Figure 30.

Table 5: The procentual variation of Von Mises stress given by ratio of temperature per impact in the torospheric head cover

T [°C]	-30	-20	-10	0	10	20	30	40	50	60
$\Delta\sigma_{\text{initial}}$ [N/mm <sup>2</sup> ]	6.51	4.24	2.07	0.00	-1.97	-3.84	-5.40	-5.61	-4.53	-3.39
$\Delta\sigma_{\text{impact}}$ [N/mm <sup>2</sup> ]	210.036	210.094	210.151	204.761	210.263	210.318	210.372	210.425	210.477	210.529
$\Delta\sigma_{\text{initial}} / \Delta\sigma_{\text{impact}} \times 100$ [%]	3.10	2.01	0.99	0.00	-0.94	-1.83	-2.57	-2.67	-2.15	-1.61

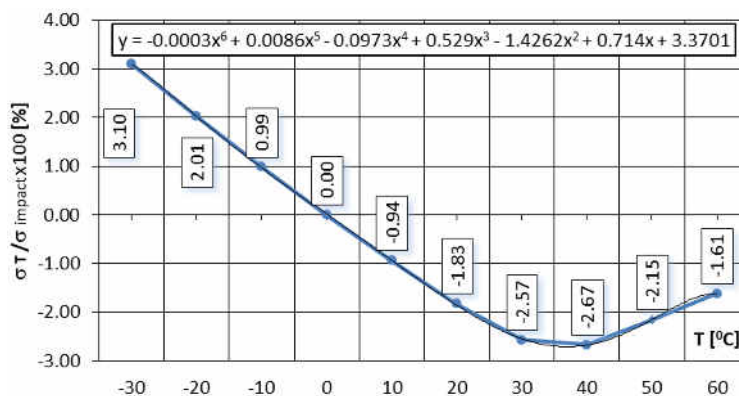
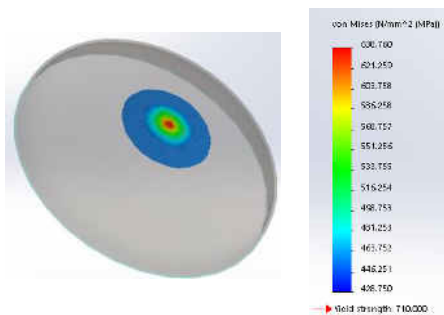


Fig. 30. The graph of Von Mises stress variation ratio  $\Delta\sigma_{\text{initial}} / \Delta\sigma_{\text{impact}} \times 100$  [%]  $\sigma(t, T)$  in torospheric head cover

In the point of contact between the bar and the head cover the state of tension increases sharply in the impact time span of t = 40 μs.

The stress state is graphically shown for: a) t = 40 μs and T = -30 °C in Figure 31 and Figure 32; b) for T = 60 °C in Figure 33 and Figure 34.



**Fig. 31.** The Von Mises stress on the superior view of head cover at  $t = 40 \mu\text{s}$  and  $T = -30 \text{ }^\circ\text{C}$

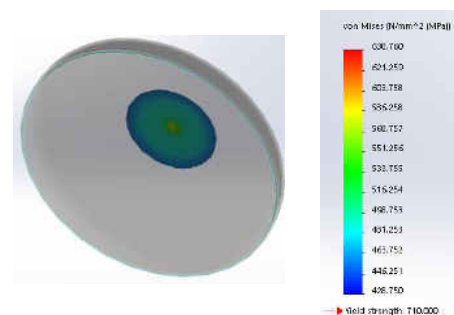


**Fig. 32.** The Von Mises stress on the inferior view of head cover at  $t = 40 \mu\text{s}$  and  $T = -30 \text{ }^\circ\text{C}$

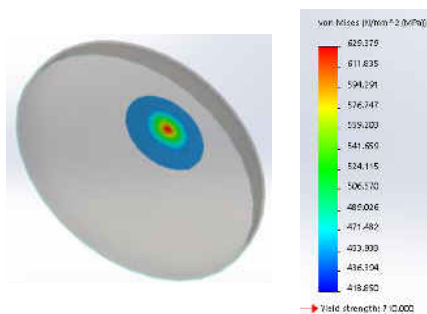


**Fig. 33.** The Von Mises stress on the superior view of head cover at  $t = 40 \mu\text{s}$  and  $T = 60 \text{ }^\circ\text{C}$

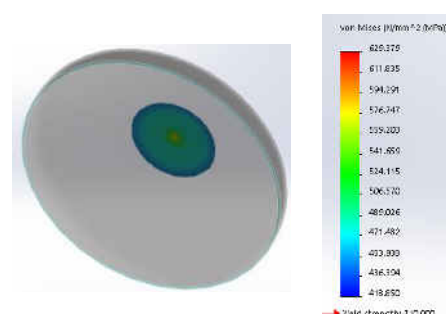


**Fig. 34.** The Von Mises stress on the inferior view of head cover at  $t = 40 \mu\text{s}$  and  $T = 60 \text{ }^\circ\text{C}$

#### 4. Discussion

From these analyses we can say that:

- for any temperature value, the Von Mises stress increases during impact with the highest value at the negative temperature of  $T = -30 \text{ }^\circ\text{C}$ , as shown in Figures 8 to 17.
- at the beginning of about 20 % of the total impact time there is a moderate increase of the Von Mises stress, after which the highest increase of the effort is made in the next 60 % of the total time, while the remaining 20 % make a small increase until reaching the final value. This is illustrated in the 3D stress-strain graph  $\sigma(T, t)$  from Figure 18.
- the increase of Von Mises stress due to the temperature variation considering that the stress state generated at the temperature  $T = 0 \text{ }^\circ\text{C}$ , (as shown in Table 3), is comprised between the limits  $\Delta\sigma_T = [-0.81 \text{ } \dots 1.52 \text{ } \%]$  (as shown in Figure 28).
- While the percentage increase in stress due to impact force action is comprised between limits  $\Delta\sigma_{\text{impact}} = [48.49 \text{ } \dots 50.51 \text{ } \%]$ , (as shown in Table 4 and Figure 29).
- the ratio between the percentage increase of the stress caused by the temperature and the stress caused by the impact is comprised between limits  $\Delta\sigma_T / \Delta\sigma_{\text{impact}} = [-2.67 \text{ } \dots 3.10 \text{ } \%]$ , according the results from Table 5 and Figure 30.
- The front / back views of the cover for the surfaces centered around the impact point show that the effort is higher on the outer contact surface and more attenuated on the inner surface of the cover, as shown in Figures 31 to 34.

#### 5. Conclusions

The following conclusions are drawn from the present study:

- a) The highest stresses occurring in the crash test are focused around the point of impact at the contact between the bar and the tank;
- b) Increasing effort is done within a very small time interval of order of microseconds;
- c) From the onset of impact, there is a short time  $\cong 1/5$  of the total impact time, which increases slowly, after which they increase very much for  $\cong 3/5$  of the total impact time, reaching the final effort state;

- d) The impact effort overlaps the initial effort of the shell, representing a high percentage of it;
- e) The effort made by other causes of stress-generating impact during the impact is very low compared to impact-generated stress;
- f) The state of effort is greater on the outer surface around the impact point than the state of effort that occurs on the homologous inner surface around this point;
- g) The final conclusion of the simulation results is that the Von Mises stress increase due to impact on the crash test is very important and can not be neglected, representing in this case about 50 % of the Von Mises stress caused by other causes before the impact test.

**Financial disclosure:** Neither author has a financial or proprietary interest in any material or method mentioned.

**Competing interests:** The authors declare that they have no significant competing financial, professional or personal interests that might have influenced the performance or presentation of the work described in this manuscript.

## References

- [1] A.C. Nedelcu, “Romanian automotive industry – analysis made from the intellectual capital perspective“, Revista Economica, vol. 67, no. 5, pp. 80-89, 2015;
- [2] A. Misztal, N. Belu, N. Rachieru, “Comparative Analysis of Awareness and Knowledge of APQP Requirements in Polish and Romanian Automotive Industry“, Applied Mechanics and Materials, vol. 657, pp. 981-985, 2014;
- [3] G. Matache, C. Cristescu, u C. Dumitresc, V. Miroiu, “Pregătirea specialiștilor în vederea adaptabilității și creșterii competitivității”, Magazine of Hydraulics, Pneumatics, Tribology, Ecology, Sensorics, Mechatronics (HIDRAULICA), no. 3-4, pp. 7-14, 2012. ISSN 1453-7303;
- [4] M. Rusănescu, “Material requirements planning, inventory control system in industry”, Magazine of Hydraulics, Pneumatics, Tribology, Ecology, Sensorics, Mechatronics (HIDRAULICA), no. 1, pp. 21-25, 2014. ISSN 1453-7303;
- [5] Chen Shr-Hung, “Novel design and optimization of vehicle’s natural gas fuel tank“. Master’s Thesis presented to the Faculty of the College of the Engineering and Technology, Ohio University, March 1997;
- [6] M.C. Ghiță, A.C. Micu, M. Țălu, Ș. Țălu, E. Adam, “Computer-Aided Design of a classical cylinder gas tank for the automotive industry“, Annals of Faculty of Engineering Hunedoara - International Journal of Engineering, Hunedoara, Tome XI, Fascicule 4, pp. 59-64, 2013;
- [7] M.C. Ghiță, A.C. Micu, M. Țălu, Ș. Țălu, “Shape optimization of vehicle’s methane gas tank“, Annals of Faculty of Engineering Hunedoara - International Journal of Engineering, Hunedoara, Tome X, Fascicule 3, pp. 259-266, 2012;
- [8] M.C. Ghiță, A.C. Micu, M. Țălu, Ș. Țălu, “3D modelling of a shrink fitted concave ended cylindrical tank for automotive industry“. Acta Technica Corviniensis – Bulletin of Engineering, Hunedoara, Romania, Tome VI, Fascicule 4, pp. 87-92, 2013;
- [9] M.C. Ghiță, A.C. Micu, M. Țălu, Ș. Țălu, “3D modelling of a gas tank with reversed end up covers for automotive industry“, Annals of Faculty of Engineering Hunedoara - International Journal of Engineering, Hunedoara, Tome XI, Fascicule 3, 2013, pp. 195-200, 2013;
- [10] M.C. Ghiță, C.Ș. Ghiță, Ș. Țălu, S. Rotaru, “Optimal design of cylindrical rings used for the shrinkage of vehicle tanks for compressed natural gas“, Annals of Faculty of Engineering Hunedoara - International Journal of Engineering, Hunedoara, Tome XII, Fascicule 3, pp. 243-250, 2014;
- [11] M.C. Ghiță, A.C. Micu, M. Țălu, Ș. Țălu, “Shape optimization of a thoroidal methane gas tank for automotive industry“, Annals of Faculty of Engineering Hunedoara - International Journal of Engineering, Hunedoara, Tome X, Fascicule 3, pp. 295-297, 2012;
- [12] Ș. Țălu, M. Țălu, “CAD generating of 3D supershapes in different coordinate systems“, Annals of Faculty of Engineering Hunedoara - International Journal of Engineering, Hunedoara, Tome VIII, Fascicule 3, pp. 215-219, 2010;
- [13] Ș. Țălu, M. Țălu, “A CAD study on generating of 2D supershapes in different coordinate systems“, Annals of Faculty of Engineering Hunedoara - International Journal of Engineering, Hunedoara, Tome VIII, Fascicule 3, pp. 201-203, 2010;
- [14] C. Bîrleanu, Ș. Țălu, “Organe de mașini. Proiectare și reprezentare grafică asistată de calculator“ (Machine elements. Designing and computer assisted graphical representations), Cluj-Napoca, Victor Melenti Publishing house, 2001;
- [15] Ș. Țălu, “Limbajul de programare AutoLISP. Teorie și aplicații“, (AutoLISP programming language. Theory and applications), Cluj-Napoca, Risoprint Publishing house, 2001;

- [16] Ș. Țălu, “Grafică tehnică asistată de calculator” (Computer assisted technical graphics), Cluj-Napoca, Victor Melenti Publishing house, 2001;
- [17] Ș. Țălu, “Reprezentări grafice asistate de calculator” (Computer assisted graphical representations), Cluj-Napoca, Osama Publishing House, 2001;
- [18] Ș. Țălu, “AutoCAD 2005”, Cluj-Napoca, Risoprint Publishing house, 2005;
- [19] Ș. Țălu, M. Țălu, “AutoCAD 2006. Proiectare tridimensională” (AutoCAD 2006. Three-dimensional designing), Cluj-Napoca, MEGA Publishing house, 2007;
- [20] Ș. Țălu, “AutoCAD 2017”, Cluj-Napoca, Napoca Star Publishing house, 2017;
- [21] Ș. Țălu, “Geometrie descriptivă” (Descriptive geometry), Cluj-Napoca, Risoprint Publishing house, 2010;
- [22] A. Florescu-Gligore, Ș. Țălu, D. Noveanu, “Reprezentarea și vizualizarea formelor geometrice în desenul industrial” (Representation and visualization of geometric shapes in industrial drawing), Cluj-Napoca, U. T. Pres Publishing house, 2006;
- [23] A. Florescu-Gligore, M. Orban, Ș. Țălu, “Cotarea în proiectarea constructivă și tehnologică” (Dimensioning in technological and constructive engineering graphics), Cluj-Napoca, Lithography of The Technical University of Cluj-Napoca, 1998;
- [24] C. Racocea, Ș. Țălu, “Reprezentarea formelor geometrice tehnice în axonometrie” (The axonometric representation of technical geometric shapes), Cluj-Napoca, Napoca Star Publishing house, 2011;
- [25] Ș. Țălu, C. Racocea, “Reprezentări axonometrice cu aplicații în tehnică” (Axonometric representations with applications in technique), Cluj-Napoca, MEGA Publishing house, 2007;
- [26] T. Nițulescu, Ș. Țălu, “Aplicații ale geometriei descriptive și graficii asistate de calculator în desenul industrial” (Applications of descriptive geometry and computer aided design in engineering graphics), Cluj-Napoca, Risoprint Publishing house, 2001;
- [27] Ș. Țălu, “Micro and nanoscale characterization of three dimensional surfaces. Basics and applications”, Napoca Star Publishing House, Cluj-Napoca, Romania, 2015;
- [28] M. Țălu, “Calculul pierderilor de presiune distribuite în conducte hidraulice” (Calculation of distributed pressure loss in hydraulic pipelines), Craiova, Universitaria Publishing house, 2016;
- [29] M. Țălu, “Pierderi de presiune hidraulică în conducte tehnice cu secțiune inelară. Calcul numeric și analiză C.F.D.” (Hydraulic pressure loss in technical piping with annular section. Numerical calculation and C.F.D.), Craiova, Universitaria Publishing house, 2016;
- [30] M. Țălu, “Mecanica fluidelor. Curgeri laminare monodimensionale” (Fluid mechanics. The monodimensional laminar flow), Craiova, Universitaria Publishing house, 2016;
- [31] M. Țălu, “The influence of the corrosion and temperature on the Von Mises stress in the lateral cover of a pressurized fuel tank”, Magazine of Hydraulics, Pneumatics, Tribology, Ecology, Sensorics, Mechatronics (HIDRAULICA), no. 4, pp. 89-97, 2017, ISSN 1453-7303;
- [32] Ș. Țălu, M. Țălu, “The influence of deviation from circularity on the stress of a pressurized fuel cylindrical tank”, Magazine of Hydraulics, Pneumatics, Tribology, Ecology, Sensorics, Mechatronics (HIDRAULICA), no. 4, pp. 34-45, 2017, ISSN 1453-7303;
- [33] M. Bică, M. Țălu, Ș. Țălu, “Optimal shapes of the cylindrical pressurized fuel tanks”, Magazine of Hydraulics, Pneumatics, Tribology, Ecology, Sensorics, Mechatronics (HIDRAULICA), no. 4, pp. 6-17, 2017, ISSN 1453-7303;
- [34] T. Ambati, K.V.N.S. Srikanth, P. Veeraraju, “Simulation of vehicular frontal crash-test”, International Journal of Applied Research in Mechanical Engineering (IJARME), vol. 2, issue 1, pp. 37-42, 2012.
- [35] W. Pawlus, H.R. Karimi, K.G. Robbersmyr, “Mathematical modeling of a vehicle crash test based on elasto-plastic unloading scenarios of spring-mass models”, The International Journal of Advanced Manufacturing Technology, vol. 55, pp. 369-378, 2011;
- [36] W. Pawlus, H.R. Karimi, K.G. Robbersmyr, “Investigation of vehicle crash modeling techniques: theory and application”, The International Journal of Advanced Manufacturing Technology, vol. 70, issue 5-8, pp. 965-993, 2014;
- [37] G. Šušteršič, I. Grabec, I. Prebil, “Statistical model of a vehicle-to-barrier collision”, International Journal of Impact Engineering, vol. 34, Issue 10, pp. 1585-1593, 2007;
- [38] K. Haleem, P. Alluri, A. Gan, “Investigating fractal characteristics in crash trends for potential traffic safety prediction”, Proceedings of the 95th Annual Meeting of the Transportation Research Board, Washington DC, United States, 2016;
- [39] Yu Rende, Shen Juan, “Analysis on road traffic accidents spatial distribution based on the multi-fractal theory”, Computer Modelling & New Technologies, vol. 18, no. 7, pp. 283-289, 2014;
- [40] Chen Peng, Li Xu-hong, Sun Hua-can, “Analysis of Traffic Accident Based on Fractal Theory”, Journal of Highway and Transportation Research and Development, vol. 25, no. 3, pp. 130-3, 2008;
- [41] Zhang Xiao-hong, Yu Ren-de, Zhang Qiang, “Traffic accidents analysis based on multi-fractal spectrum”, Journal of Shandong University of Technology (Natural Science Edition), vol. 27, no. 2, pp. 62-64, 2013;
- [42] \*\*\* Autodesk AutoCAD 2017 software;
- [43] \*\*\* SolidWorks 2017 software.

## Testing Means of Piston –Type Seals

PhD. Eng. **Gabriela MATACHE**<sup>1</sup>, PhD Eng. **Gheorghe ȘOVĂIALĂ**,  
Dipl. Eng. **Alina Iolanda POPESCU**, Res. Assist. **Ana-Maria POPESCU**

<sup>1</sup> INOE 2000-IHP, fluidas@fluidas.ro

**Abstract:** *To improve energy efficiency of hydraulic drive systems, an important direction of action was the increase in energy efficiency of each component, in the direction of decreasing hydraulic flow and pressure losses, energy losses in general, and respectively increasing outputs and their lifespan.*

*One of the most important components of hydraulic applications is the hydraulic drive motors, which convert hydrostatic energy into mechanical energy.*

*Tribological research on linear hydraulic motors, also known as "hydraulic cylinders", aims at assessing total energy losses during operation and increasing their lifespan.*

*These total energy losses include viscous friction losses occurring at fluid flow, frictional losses occurring in rod seals (between the rod and bush), frictional losses occurring between the piston seals and the liner, as well as energy losses through dry friction inside the guides of the rod and piston. An important role in increasing the life of hydraulic cylinders is played by the durability of sealing systems, which are the first to remove hydraulic cylinders from operation.*

*In order to optimize the total energy losses in the operation of the hydraulic cylinders and to increase their lifetime (by increasing the sealing lifetime), two innovative sealing elements for the piston and rod were developed at IHP Bucharest, tested by using the means presented in this article.*

**Keywords:** *Piston-type seals, hydraulic cylinders, testing stand*

### 1. Introduction

The methodology and the device developed during the stage *Developing new sealing elements by tribological research on the sealing systems in the hydraulic equipment* serve the economic agents specialized in the manufacture of sealing elements for hydraulic equipment, hydraulic cylinder manufacturers and companies that have reconditioning in their activity profile, enabling them to test performance and lifetime of sealing elements in an accelerated mode.

This methodology establishes the way of performing hydrostatic sealing tests, tests of endurance and measurement of internal fluid losses for piston seals in the structure of linear hydraulic motors (cylinders) used in the field of hydraulic drives.

### 2. Testing methods applied in laboratory

At present, the tests are carried out on a hydraulic cylinder, with piston-mounted test sealing elements actuated by an antagonist force cylinder. This method has major drawbacks: very high energy consumption, excessive oil heating, large stand size. The device developed removes the mentioned disadvantages by the fact that:

- it uses a small volume of oil;
- the (constant) test pressure is only exerted on the active surfaces of the sealing elements [1];
- testing of seals is done at pulsating pressure generated by an electric pump - directional control valve system, which has low power consumption, according to the test diagram shown below.

The two sleeve-type sealing elements for the piston will work in dynamic mode (alternative linear movement) at a maximum pressure of 160 bar.

Benefits:

- energy savings;
- small oil volume being used;
- the (constant) test pressure is only exerted on the active surfaces of the sealing elements;
- testing of seals is done at pulsating pressure;
- the possibility to simulate the tests in conditions similar to the operational ones [2].

Technical specifications:

- Type of sealing element ..... sleeve;
- Working pressure on the sleeve ..... 160 bar;
- Linear displacement velocity of the sleeve ..... 0.1 m / s;
- The outer diameter of the sleeve with its own test box ..... from 25 to 125 mm;
- Working environment ..... H46 A hydraulic oil;
- Stroke..... 145 mm.

## 2. 1 Hydraulic schematic diagram

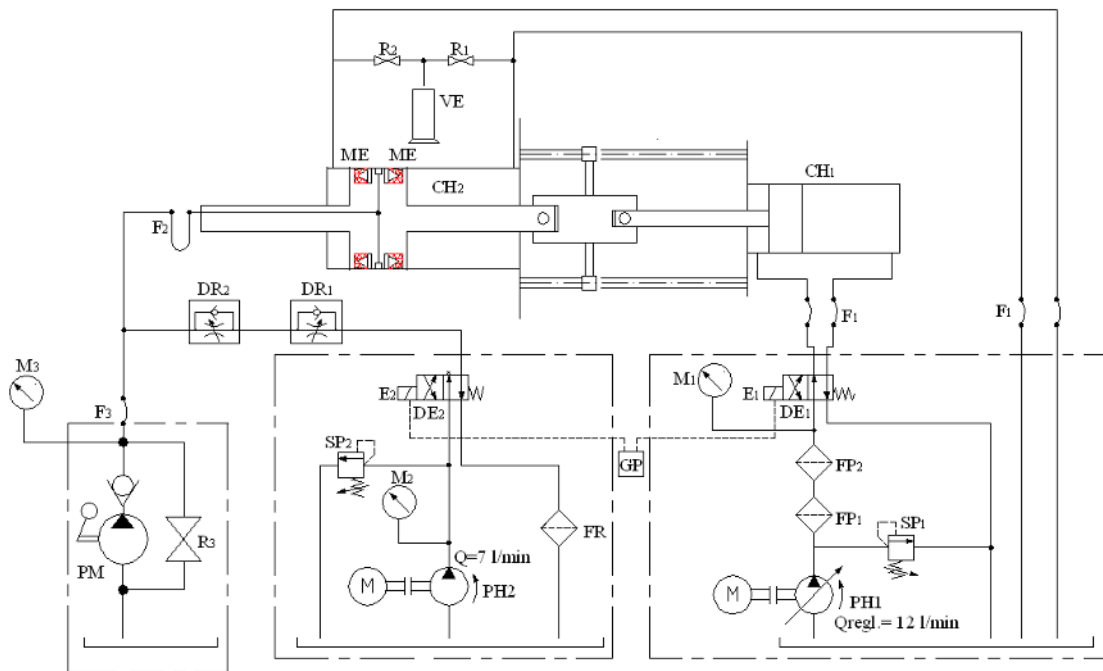


Fig. 1. Hydraulic schematic diagram of the test stand designed for piston-type seals

The device for testing hydraulic piston seals [3], Figure 2, is composed of a frame made as a welded structure (1), on which a special design hydraulic cylinder is mounted, consisting of the caps (2) and (6), which together with the liner (5) form the chamber in which the piston (3) and a standard brake drive cylinder (8) move. The rods of the two hydraulic cylinders are coupled by a translation coupler (7) which slides on two horizontal columns (9) by means of the guides (10).

The hydraulic cylinder mounted on the right wall of the frame is purchased from the series production of Wipro Infrastructure Engineering SA - Râmnicu.Vâlcea. Fixing is done by using a front flange, and there occurs piston brake at the end of the stroke. This cylinder is designed to overcome friction forces that occur when moving the rods, pistons and guides.

The hydrostatic test on the two identical seals mounted on the piston is carried out by using the PM hand pump, which sends the pressurized oil in the circular duct of the seals through the longitudinal slot in the testing box rod; oil loss behind the seals is collected in graduated vessels, from the fittings of the testing box caps (2) and (6).

For the endurance (lifetime) test the piston 3 is alternately displaced in the liner (5), by means of the two rods, by the cylinder 8.

During a stroke, the annular chamber pressure has a maximum value of 160 bar, and on the reverse stroke pressure has a minimum value of about 6-8 bar, which is generated by the hydraulic resistors on the return circuit of the hydraulic test unit. In this way, the sealing element functioning is reproduced in the actual working conditions of the hydraulic cylinders. Following a couple of stroke mileages, the piston on which the gaskets are mounted is stopped and the fluid losses at the holes in the caps are measured. The amount of lost fluid, correlated with the number of kilometres of stroke, define the degree of wear of the gasket.

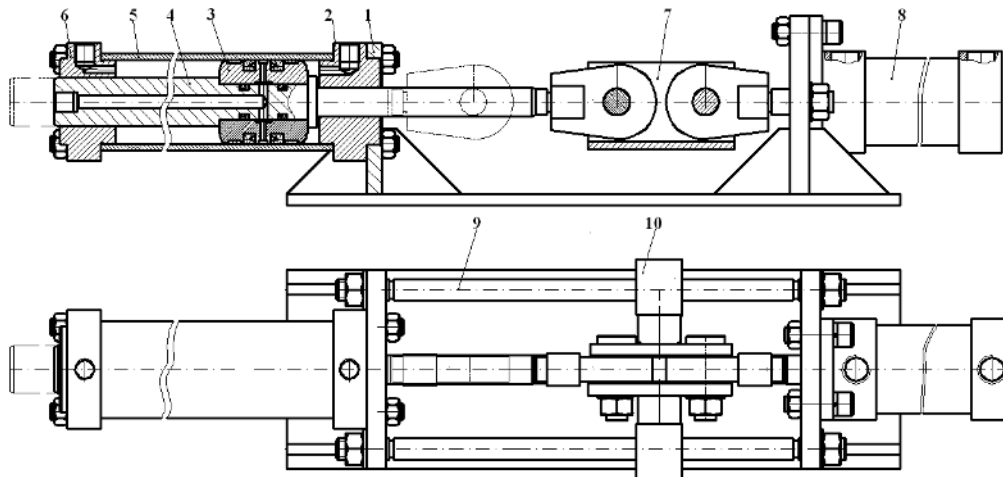


**Fig. 2.** The main parts of the device  
 1-frame, 2,6-caps, 3-piston, 4-rod, 5-liner, 7-coupling,  
 8-standard hydraulic cylinder, 9- guide columns, 10-guide

The piston of the special cylinder, fig. 3, is equipped with the sealing elements to be tested, in this case, sleeves for  $\phi$  63 -code PA-63 x 48 x 9.5 hydraulic cylinders.

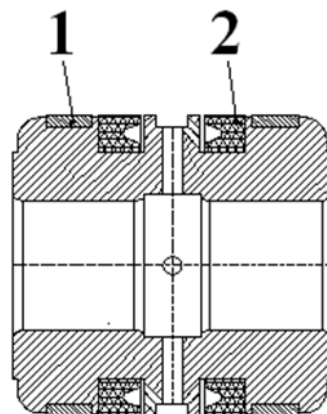


**Fig. 3.** Special construction of the piston  
 1-guide ring, 2-piston sleeve



a



b

**Fig. 4.** Component of the cylinder for testing piston-type sealing elements



a



b

**Fig. 5.** Special construction piston on which the piston- type seals are mounted



**Fig. 6.** Frame of the testing device for piston- type sealing elements



**Fig. 7.** Standard hydraulic cylinder D<sub>p</sub> 50-code CH 16U050/22-145.4.HM3.0



**Fig. 8.** Coupling for connecting the rods of the cylinders in the structure of the device



**Fig. 9.** Components of the device for testing of piston-type sealing elements, before assembly



**Fig. 10.** Device for testing piston-type seals, assembled



Testing of the sealing elements has been conducted on a stand from the Laboratory of servo-technique at IHP – Bucharest; the test stand has been adjusted in order to meet the requirements of the diagram in fig. 1.

## 2.2 Stand for testing piston seals of hydraulic cylinders

The stand, fig. 11, generates and distributes the working fluid at the parameters mentioned in the technical sheet to the drive cylinder, respectively to the seal testing box in the structure of the testing device.



**Fig. 11.** Stand for testing piston seals of hydraulic cylinders

The pressure at which the piston-type seal elements are tested by using the device is the working pressure at which they operate in the linear hydraulic motors for which they have been designed, that is 160 bar.

The speed of movement of the sealing element is adjusted according to its construction and the materials used. The travel speed of the sleeve under tests is in the range from 0.01 to 0.5 m / s.

The PH1 pump provides the hydraulic parameters (flow rate, set at 5 ... 6 l / min, and pressure, set to 100 bar through the SP1 valve) which are required for CH1 hydraulic cylinder to operate. The PH2 pump provides the hydraulic parameters required to test the two sealing sleeves of the device (fixed flow rate of 7 l/min, pressure set at 160 bar through the SP2 valve).

To ensure the displacement of the pistons of the hydraulic cylinders in the structure of the device, the electromagnets E1 and E2 are simultaneously operated by engaging them to perform the active stroke, when in the areas of the test sleeves the pressure of 160 bar is created, or by disengaging them to perform the retraction stroke of the pistons, when the pressure in the areas of the sleeves decreases to 6 ... 8 bar. The R1, R2, R3 tap valves are closed, and the DR1 and DR2 throttles are completely open. The operation is repeated 8 ... 10 times.

Checking of safety and external sealing - The hydrostatic pressure of 240 ... 245 bar is generated by the PM manual pump. Displaying its value is done on the M3 pressure gauge. The pressure maintenance time is 3 minutes, while the R3 valve and the DR1 throttle are closed, and the PH1 and PH2 pumps stopped.

The test piston displacement speed is achieved by adjusting the flow rate of the PH1 pump and timing the stroke duration, so that to obtain a speed of 0.1 m / s.

The fluid loss check  $[\Delta q]$  is done according to the diagram. The PH1 pump is adjusted so that the CH2 cylinder moves at a speed of 0.1 m / s. The PH2 fixed flow pump achieves the pressure of 160 bar required to test the two sleeves, adjusted by the SP2 valve. The E1 and E2 electromagnets are simultaneously engaged, and then disengaged. Duration of engagement and disengagement times are equal, with a value of 2s. The operation is carried out by the GP program

generator, which performs operation of electromagnets and adjusts the 2-second engagement duration. During the alternate displacement of the CH1 drive cylinder, the rod of the CH2 cylinder also moves; in the two chambers adjacent to the piston on which the sleeves are mounted mineral oil is sucked in and discharged. During this period, a pulsating pressure of 6 ... 160 bar is installed in the annular chamber of the piston; its impulse has a slope of increase and decrease adjustable by means of the DR1 and DR2 throttles. Following approx. 35,000 double strokes (5 km) - duration 2h 30sec, the program generator and the PH1 pump are stopped. The E2 is actuated from button; the R1 and R2 tap valves open and close successively, and after the oil on the pipes drains, the flow losses corresponding to each sleeve are collected. The collecting time is 10 minutes.

### 3. Conclusions

- Methodology and testing device are used for an accelerated testing of piston-type seals;
- Currently, tests on these seals are carried out on a hydraulic cylinder driven by an antagonist force cylinder, with piston-mounted sealing elements to be tested; in this case, energy consumption is very high, excessive oil heating occurs, and the test stand has a large gauge;
- The benefits of the present methodology and test device result from the following considerations:
  - use of a small oil volume;
  - the (constant) test pressure is exerted only on the active surfaces of the sealing elements;
  - testing of the seals is done at pulsating pressure, achieved by a low flow rate and low power consumption electro-pump – directional control valve system, according to the test scheme presented;
  - the sleeve-type sealing elements for the piston will work in dynamic mode (alternative linear motion) at the actual working pressure of the hydraulic cylinder that they will fit.

### Acknowledgments

This paper has been developed in INOE 2000-IHP, with financial support of Ministry of Research and Innovation (MCI), under the national research *Programme NUCLEU-2016*, project title: *Physics of processes for reducing energy losses and developing renewable energy resources by use of high-performance equipment*, project code PN 16 40.03.01, financial agreement no. 5N/2016, Additional act no. 1/2017.

### References

- [1] C. Cristescu, P. Drumea, S. Anghel, P. Krevey, M. Neacșu, C. Cristescu, "Experimental device and test stand for determination of friction forces in hydraulic cylinders pistons seals" ("Dispozitiv experimental și stand de testare pentru determinarea forțelor de frecare din etanșările pistoanelor cilindrilor hidraulici"), *The 13th National Multidisciplinary Conference - with international participation, Prof. Dorin Pavel-founder of Romanian hydropower*, Sebes 2013, pp. 121-126;
- [2] C-tin Călinoiu, "Sensors and transducers" ("Senzori și traductoare"), vol. I, Technical Publishing House, Bucharest, 2009;
- [3] Șt. Alexandrescu, S. Anghel, Gh. Șovăială, "Device for testing the piston sealing in hydraulic cylinders" ("Dispozitiv pentru probarea etansarilor pistoanelor cilindrilor hidraulici"), patent no. RO126790 (B1) / 2010, Classification: - international: G01M3/02.

## Operational Management with Application on Streamline Sewage Treatment Stations

Prof. Dr. Eng. Mariana PANAITESCU<sup>1</sup>, Prof. Dr. Eng. Fanel-Viorel PANAITESCU<sup>2</sup>

<sup>1</sup> Constanta Maritime University, marianapan@yahoo.com

<sup>2</sup> Constanta Maritime University, viopanaitescu@yahoo.ro

**Abstract:** *The main objective of this paper is to propose technical solutions to streamline processes of purification and treatment of municipal and industrial wastewater by introducing mathematical models and simulations made for processes from a wastewater treatment plant, to identify the optimal values of operating parameters which lead to energy efficiency and reducing costs.*

*This paper proposes to develop the concept of optimizing the processes of wastewater treatment plant as part of a wastewater purification stations, through simulation with STOAT. As a case study, the Sewage Treatment station from Mangalia city has been chosen. Simulations of wastewater treatment processes are performed with STOAT software. The simulation results and the training of personnel help with optimizing the operating times.*

**Keywords:** *Operational management, sewage treatment station, simulation, software, optimization, consumption, costs*

### 1. Introduction

Waste water treatment is a complex process-based physical, chemical and biological materials through which dissolved and dispersed in an aqueous environment are retained and neutralized so that spill into the environment not to harm population, flora and fauna. Wastewater treatment technology represents a sequence of unit processes each of which is designed to hold a specific category of watery environment bodies dissolved, dispersed or fine granular.

Wastewater treatment efficiency refers to the entire facility-overall efficiency of purification or judging process unit: restraint, sedimentation, separation, remove organic material, etc. [1].

For each unit process determine the effectiveness of restraint that can have values in the range 50...98% depending on the facility and appropriate equipment technology. It is evident that in the present circumstances to find that restraint and neutralization efficiency is raised in order to properly protect the environment.

The stations of the wastewater treatment plant (SEAU) in Romania have been designed and equipped with the appropriate mechanical equipment of the Decade of the 7th century of the last century [2]. In the past two decades, with the support of EU funds have been running several municipal wastewater treatment plants, but the overall situation remains far behind the requirements imposed by the environment and legislation. As a result the researchers' efforts have focused on the study of the processes that can rapidly restore the situation.

Processes used in treatment plants have a special character in that it addresses the processing of some waters loaded with different concentrations of these substances have the global economic exploitable. As such, the installations and equipment must be effective, safe in operation-high reliability to manage separation/destruction of polluting materials. At the same time it should be noted that in a wastewater treatment plant wastewater flow is continuous, without interruption; the wastewater treatment plant sewage waters from entering the network on an ongoing basis with inherent variations of flow and diurnal and seasonal loads.

Municipal treatment plants are major consumers of energy in the national energy system [2]. Costs of these energy consumption accounts for a significant share of the costs of operating a wastewater treatment plant [3].

For the stations of the wastewater treatment plant it is very difficult to make energy savings because the process is continuous.

On the one hand, the WWTP wastewater enters continuously water sewer network, and, on the other hand, the technology of wastewater treatment is based on uniform (physical, chemical, biological) processes that cannot be turned off or disconnected from the network [3].

The electricity consumption of a wastewater treatment plant wastewater is very high and in the context of the increase in the price it will be increasingly more difficult to cover these costs. At present the share of energy costs in total operating costs is of the order of 35 ... 45% which is very much [2, 3].

Considering the weight of the biological step in energy consumption of the entire wastewater treatment plant-more than 50% of the staff in research efforts have focused on increasing the efficiency of sewage treatment plants in this area. The complexity of the processes in this step requires knowledge of physical, chemical and biochemical which are on the border between the different areas of existing sciences.

The main objective of this paper is to propose technical solutions to streamline processes [3] of purification and treatment of municipal wastewater and industrial by introducing mathematical models and simulations, made for processes from a wastewater treatment plant, to identify the optimal values of operating parameters which lead to energy efficiency and reducing costs.

The methods used at present are exceeded and the consideration of the actual items is now available to engineers and specialists in the field.

## 2. Materials and Researches

This paper proposes to develop the concept of optimizing the processes of wastewater treatment plant as part of a wastewater purification stations, through simulation with STOAT software [4]. Urban wastewater contains a number of pollutants and contaminants. Prior to discharge water into the mouth, should be made for a reduction of the quantity of harmful substances in accordance with local standards for wastewater.

With regard to the prevention of water pollution, the main agents of pollution from wastewater are compounds of carbon, nitrogen and phosphorus.

Thus these contaminants must be eliminated to a large extent. In most stations municipal sewage treatment, this will be achieved through a biological process. A number of micro-organisms play the role of a biological purifier in the process.

As a case study, we have chosen Sewage Treatment Station from Mangalia city (photo 1), which has three stages of purification: mechanical treatment, biological-physical treatment and sludge treatment.



Photo 1. Mangalia WWTP

Simulation of wastewater treatment processes are performed with the STOAT and software aims to streamline costs and operating times. Software help and the training of personnel are useful in order to optimize operating times.

To make a simulation of the process of active sludge treatment is the general layout of the WWTP (waste water treatment plant) (Fig. 1) [3]:

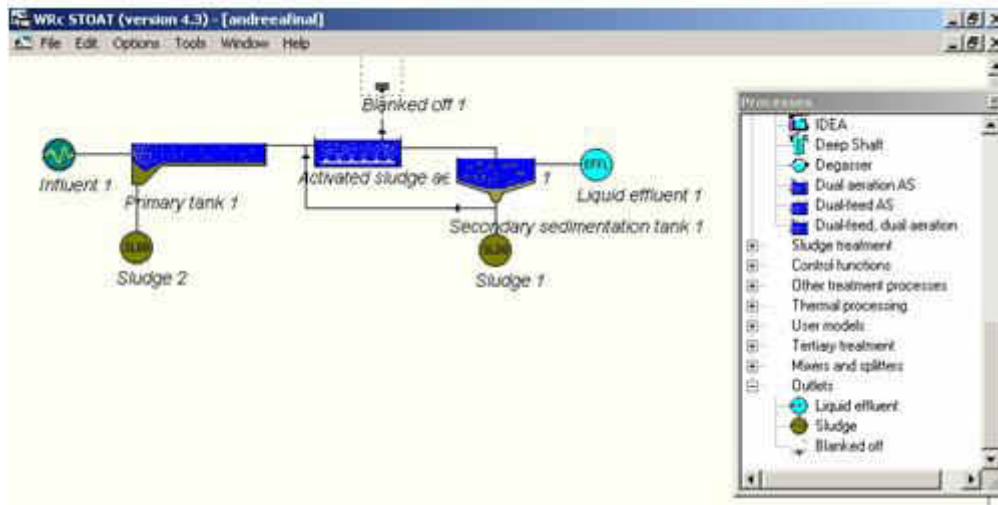


Fig. 1. General layout of the WWTP Mangalia

After it have defined the physical schema of the data have been entered and appropriate for each process in hand, follows the effective running of the simulation process of active sludge treatment (Fig. 2).

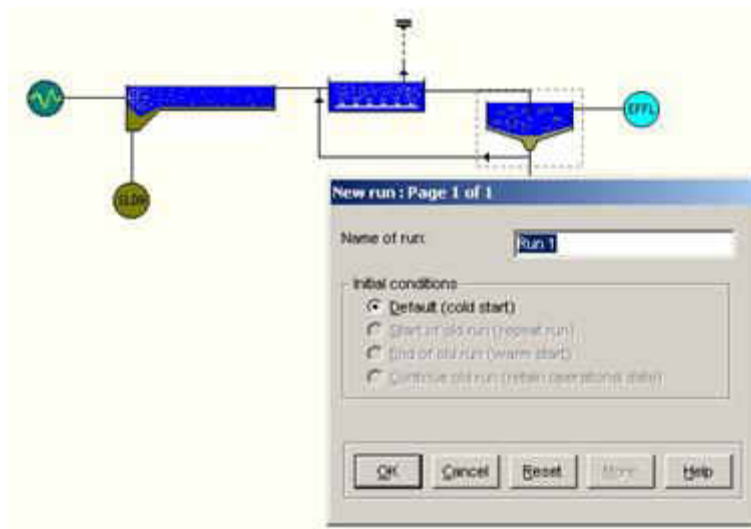


Fig. 2. The first step of simulation

Specify an appropriate set of values, but when using the STOAT, the first simulation program should be established for 20-40 days and should be treated primarily, as a rolling sighting, to evaluate a set of reasonable values for initial conditions.

(For activated sludge systems, normally this is sludge age, and would need to recompile three ages of sludge to be sure that we are looking for a state of dynamic equilibrium, rather than the effect of initial conditions. There will be other occasions when there is a good starting point and there are interested in steady state dynamic, but the effect of short-term changes in initial conditions defined). The simulation will last for two days at 15 ° C.

## 2.1 Input data for simulation

Data of influence are:

Average Flow-100 m<sup>3</sup>/h

Average speeds for settling tanks-0.25 m/h

Retention time for Aeration Basin-8 hours

Work time-48 hours.

After this step, must edited data sets for each process (Fig. 3, Fig. 4, fig. 5).

		Stage1	Stage2	Stage3
1	Soluble BOD (mg/l)	150.00	150.00	150.00
2	Soluble inert COD (mg/l)	0.00	0.00	0.00
3	Ammonia (mg/l)	40.00	40.00	40.00
4	Nitrate (mg/l)	0.00	0.00	0.00
5	Soluble organic nitrogen (mg/l)	0.00	0.00	0.00
6	Soluble phosphate (mg/l)	0.00	0.00	0.00
7	Dissolved oxygen (mg/l)	0.00	0.00	0.00
8	BOD of volatile fatty acids (mg/l)	0.00	0.00	0.00
9	Settl. particulate BOD (mg/l)	70.00	70.00	70.00
10	Non-settl. partic. BOD (mg/l)	30.00	30.00	30.00
11	Settleable particulate inert COD (mg/l)	0.00	0.00	0.00
12	Nonsettleable particulate inert COD (mg/l)	0.00	0.00	0.00
13	Settl. volatile solids (mg/l)	140.00	140.00	140.00
14	Non-settl. volatile solids (mg/l)	40.00	40.00	40.00
15	Settl. non-volatile solids (mg/l)	40.00	40.00	40.00
16	Non-settl. non-volatile solids (mg/l)	20.00	20.00	20.00
17	Settl. partic. organic N (mg/l)	0.00	0.00	0.00
18	Non-settl. partic. organic N (mg/l)	0.00	0.00	0.00
19	Temperature [°C]	15.00	15.00	15.00

Fig. 3. Edit the original data for the primary settler tank

		Stage1
1	Soluble BOD (mg/l)	5.00
2	Ammonia (mg/l)	40.00
3	Nitrate (mg/l)	0.00
4	Soluble phosphate (mg/l)	0.00
5	Dissolved oxygen (mg/l)	2.00
6	MLSS (mg/l)	3000.00
7	Viable autotrophs (mg/l)	100.00
8	Non-viable autotrophs (mg/l)	0.00
9	Viable heterotrophs (mg/l)	1000.00
10	Non-viable heterotrophs (mg/l)	0.00
11	Particulate BOD (mg/l)	0.00
12	Excess P (mg/l)	0.00

Fig. 4. Edit the original data for the sedimentation basin

		Stage5	Stage6	Stage7	Stage8
1	Soluble BOD (mg/l)	5.00	5.00	5.00	5.00
2	Ammonia (mg/l)	40.00	40.00	40.00	40.00
3	Nitrate (mg/l)	0.00	0.00	0.00	0.00
4	Soluble phosphate (mg/l)	0.00	0.00	0.00	0.00
5	Dissolved oxygen (mg/l)	2.00	2.00	2.00	2.00
6	Particulate BOD (mg/l)	0.00	0.00	0.00	0.00
7	Particulate phosphate (mg/l)	0.00	0.00	0.00	0.00
8	Mixed liquor suspended solids (mg/l)	300.00	300.00	300.00	6000.00
9	Non-settleable (volatile) solids (mg/l)	0.00	0.00	0.00	0.00
10	Viable heterotrophs (mg/l)	100.00	100.00	100.00	2000.00
11	Non-viable heterotrophs (mg/l)	0.00	0.00	0.00	0.00
12	Viable autotrophs (mg/l)	10.00	10.00	10.00	200.00
13	Non-viable autotrophs (mg/l)	0.00	0.00	0.00	0.00

Fig. 5. Edit the original data for the secondary settler tank

After editing data for each of the processes, simulation is running for 48 hours.

### 3. Results and interpretations

For the first selected items characteristic of wastewater received in the wastewater treatment plant, the graphical result is shown in Figure 6.

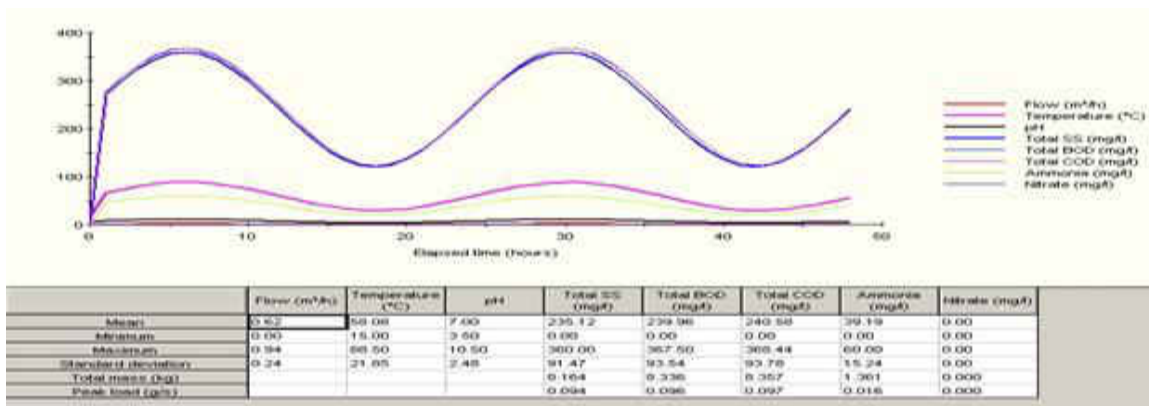


Fig. 6. The results of first page selection of characteristics

One can notice the variations for the following elements: flow, temperature, pH, ammonia concentration, nitrate concentration, biochemical consumption of oxygen, total COD and particulate matter.

The results of next selection are shown in the Fig. 7.

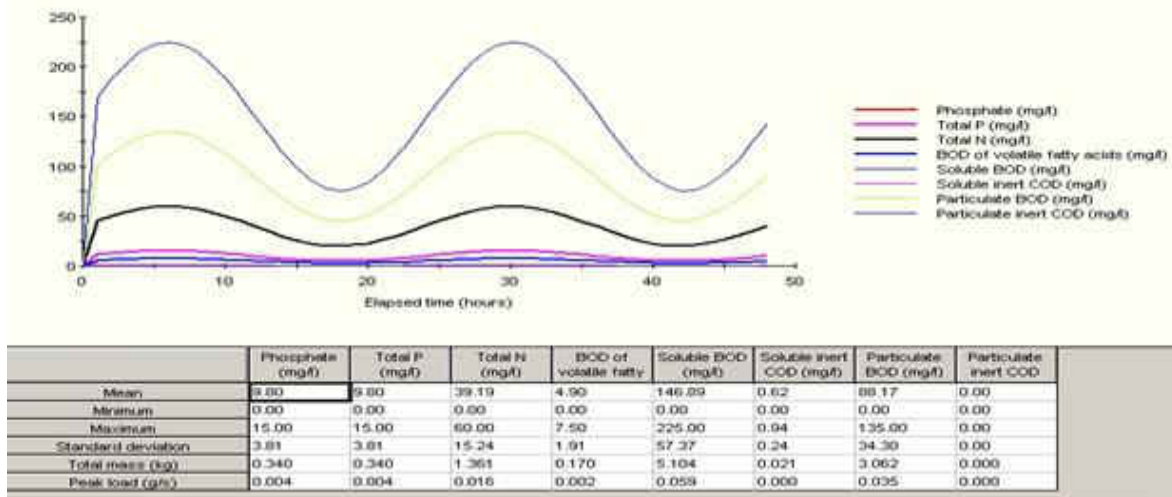


Fig. 7. The results of second page selection of characteristics

Graph 7 shows the variation in time of the following elements: phosphorus, total phosphate, total nitrogen, BOD from volatile fatty acids, soluble BOD, soluble inert COD, BOD particles, inert particle COD.

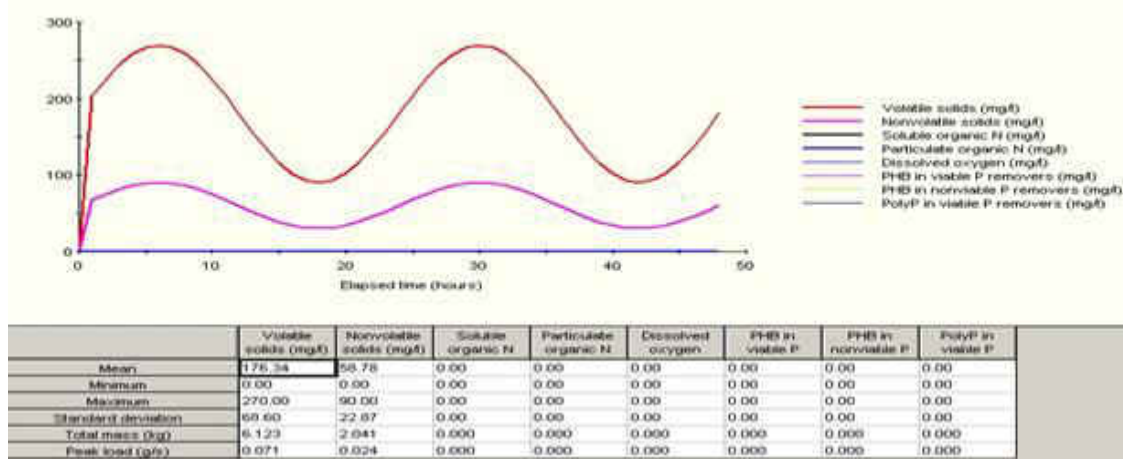


Fig. 8. The results of third page selection of characteristics

Graph 8 contains the following selected elements: volatile solids, uncoated solids, soluble organic nitrogen, organic nitrogen particles, dissolved oxygen, PHB in the viable elimination of phosphorus, PHB in the elimination of non-viable phosphorus, poly-phosphorus in eliminating Viable phosphorus (where PHB – polyhydroxybutyrate).

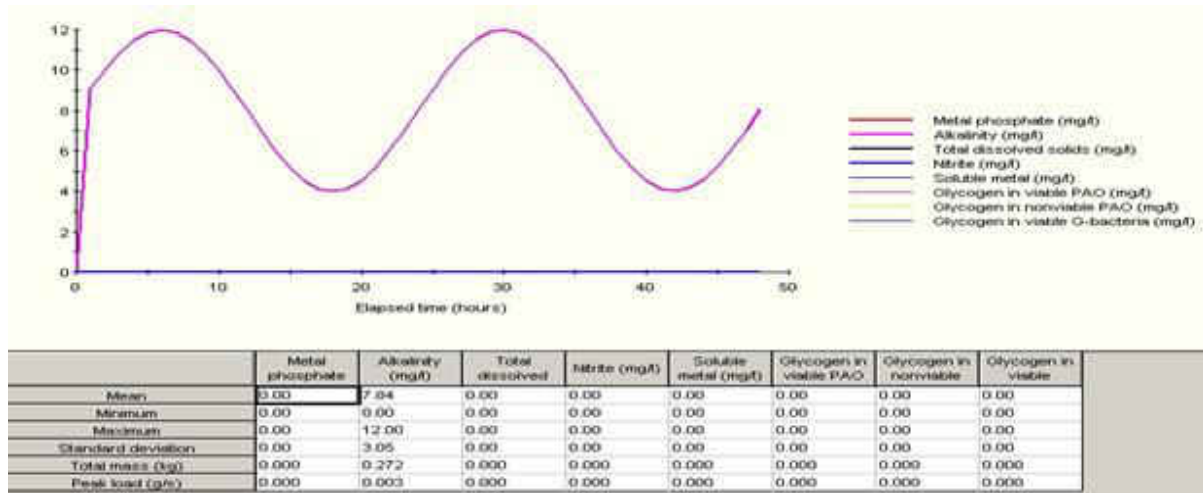


Fig. 9. The results of fourth page selection of characteristics

Graph 9 contains the following selected elements: poly-phosphorus in the unviable elimination of phosphorus, viable autotrophic, non-viable autotrophic, viable heterotrophic, non-viable heterotrophic, elimination of viable phosphorus, elimination of non-viable phosphorus, Metal hydroxide.

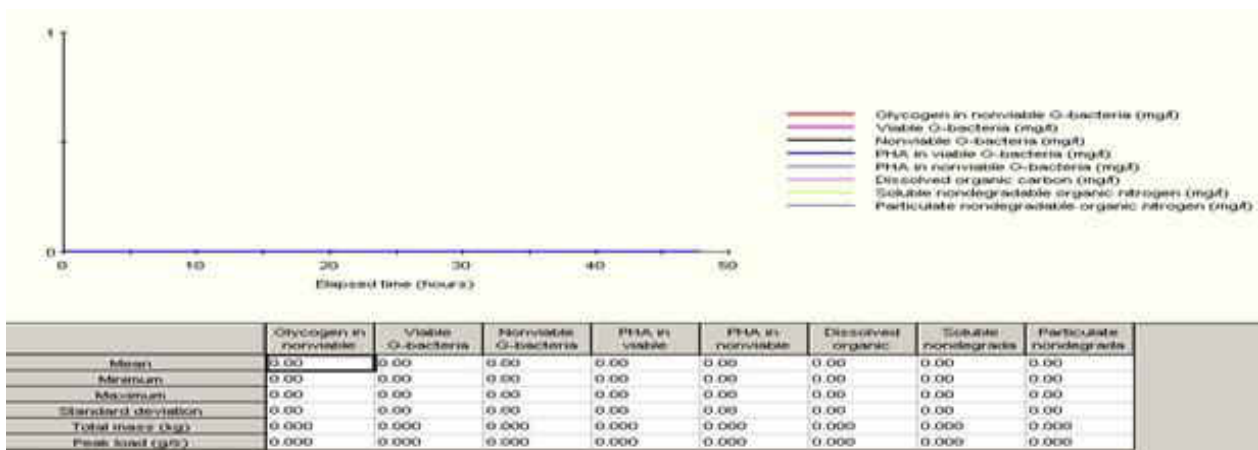


Fig. 10. The results of five page selection of characteristics

Graph 10 for the fifth page of selected items contains: Metal phosphate, alkalinity, total dissolved solids, nitrates, soluble metal, glycogen in PAO viable, glycogen in PAO unviable, glycogen in the viable bacteria-G.

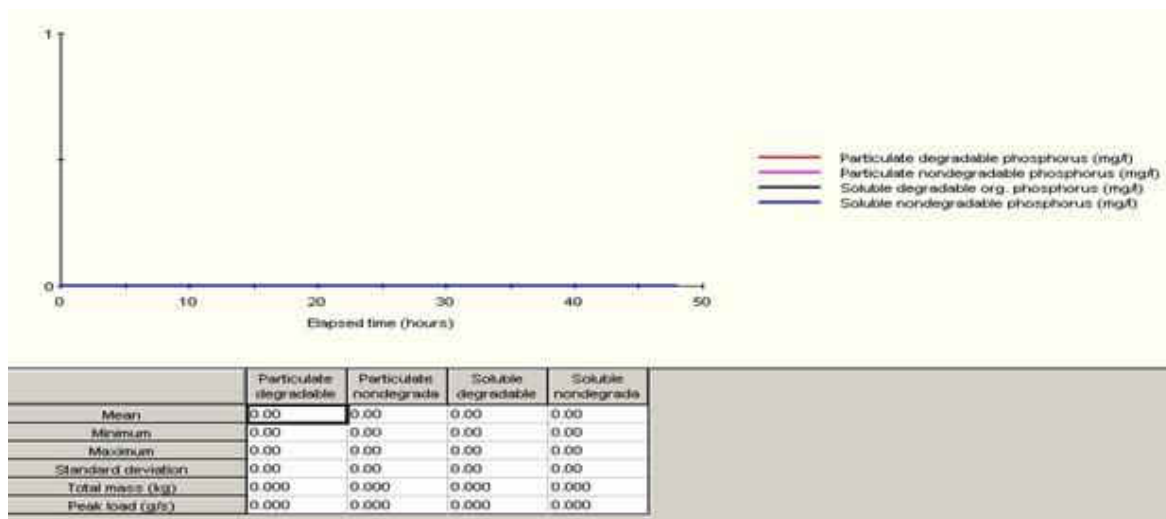


Fig. 11. The results of 6 page selection of characteristics

Graph 11 contains the following selected elements: degradable phosphorus particles, non-degradable phosphorus particles, degraded organic soluble phosphate, non-degradable soluble phosphate.

The 6 -11 graphs show the variation of the various elements along the 48 h during the course of the wastewater flow from the point of entry of the flow into the station to the primary settler tank. After identifying the various characteristics of the influential fluid, the program goes further to the next element, the primary deckhead, where it analyses in time of 48h (time set for the duration of the simulation) variation of the characteristics of the fluid content in the settler tank.

Thus, the programme is primarily oriented after the initial conditions set before to determine the variation in time of soluble BOD, soluble inert code, ammonia content, nitrate content, phosphate content, etc., and the graphical results are playable in graphs 12 and 13.

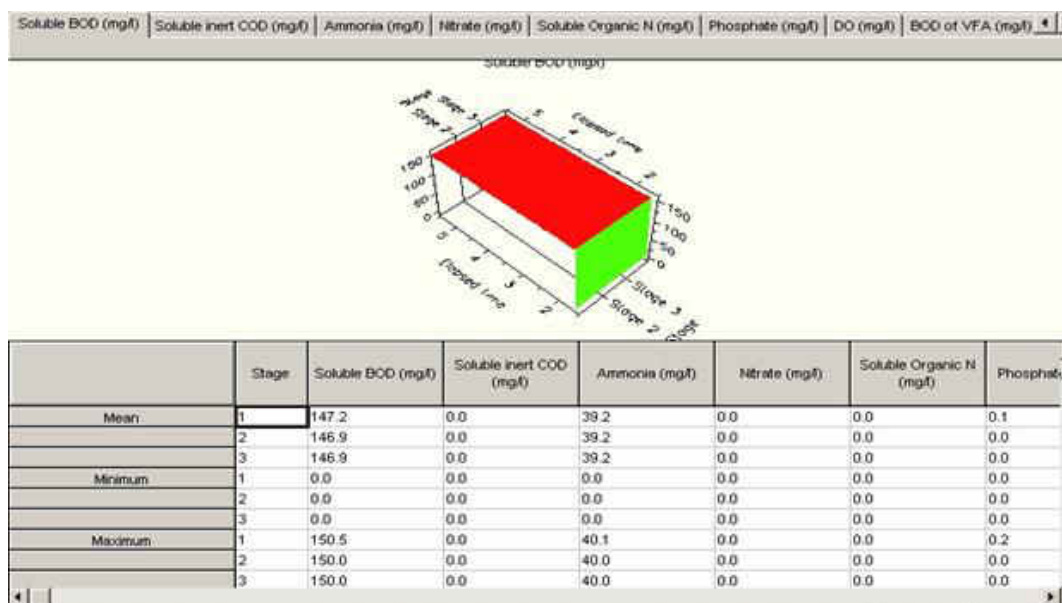


Fig. 12. The variation in time of effluent for primary tank

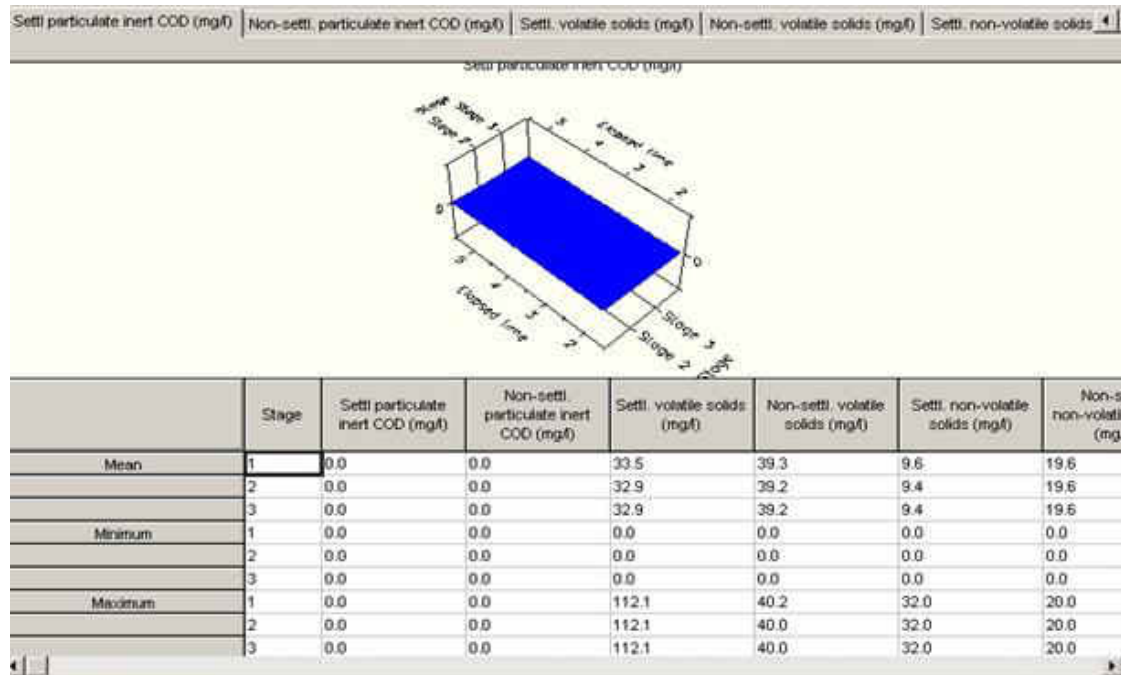


Fig. 13. Other characteristics of effluent for primary tank

After the program has run and determined the variation of the 3-stage characteristics of the fluid contained in the primary decanter, move on, when displaying the graphs of the various characteristics for the fluid between the primary settling tank and the first treatment pool of the active sludge.

In the first hours we have a sudden increase in temperature and soluble substances from a minimum value of 0 to a maximum of 129559, 20mg/L and at a short interval of time a sudden decrease in value and maintaining it to a constant value throughout the remaining time. The pH is constant, and nitrates do not exist (Fig. 14).

Results from the analysis of the fluid flow between the primary decanter and the first active sludge treatment basin are presented in the following figures (Fig. 14, Fig. 15, Fig. 16, Fig. 17):

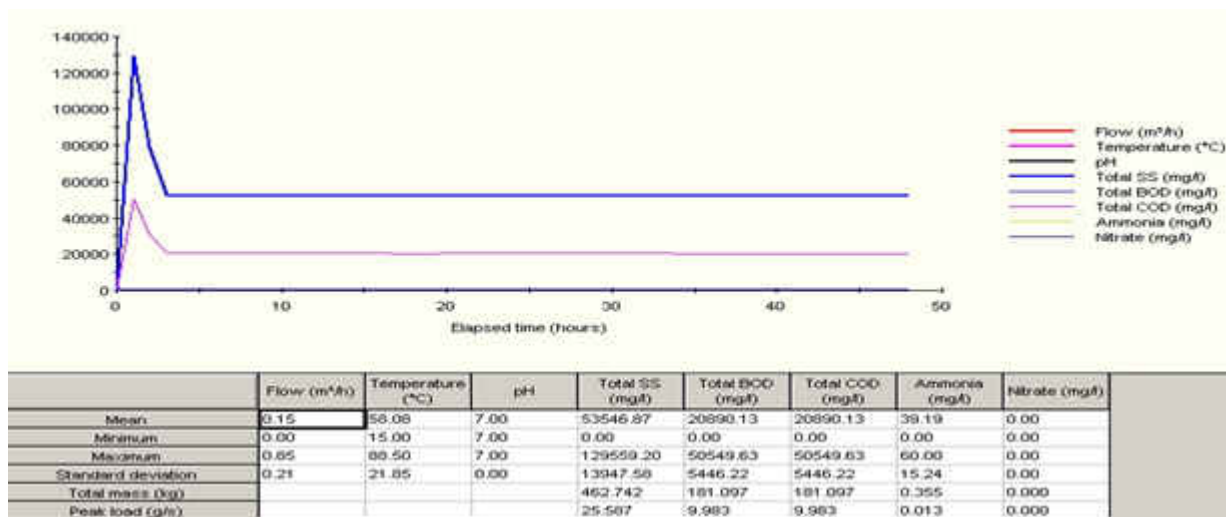


Fig. 14. The variation of Total SS, Total BOD, Total COD, Ammonia and Nitrate

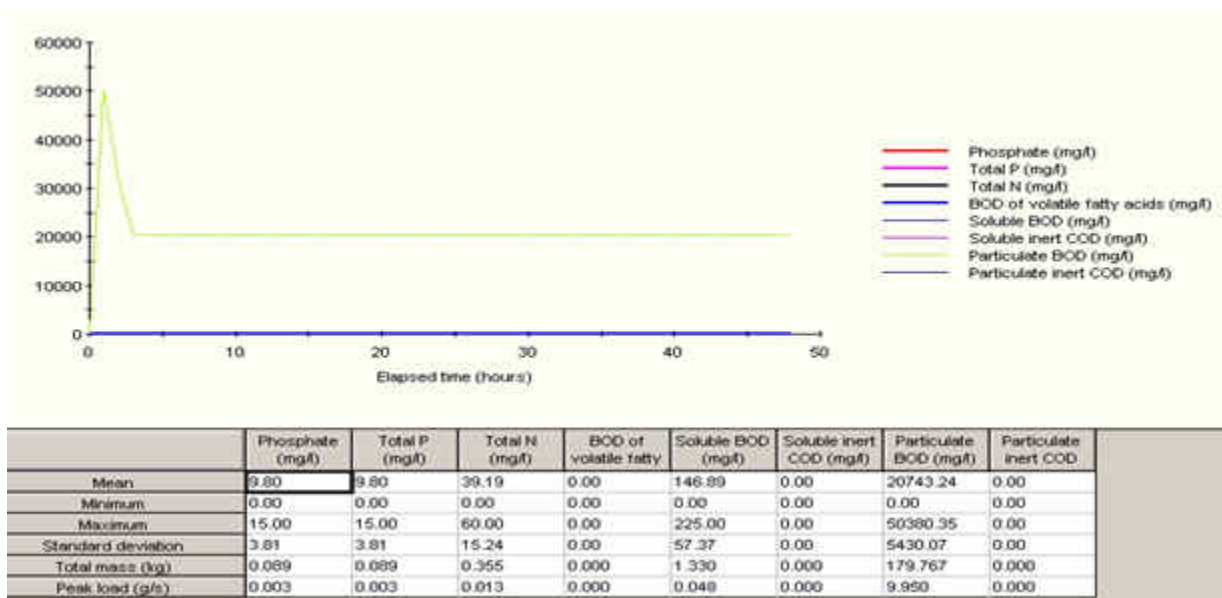


Fig. 15. The variation of phosphate, phosphorus total, nitrogen total, BOD of volatile fatty acids, soluble BOD, soluble inert code, BOD particles, inert cod particles

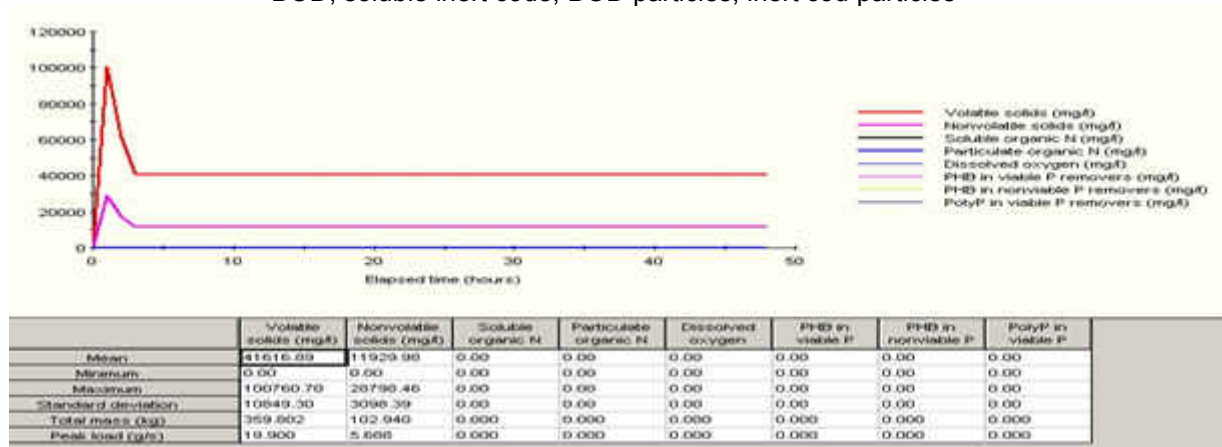


Fig. 16. The variation of volatile solids, nonvolatile solids, soluble organic N, particulate organic N, DO, PHB in viable P removers, PHB in nonviable P removers, polyP in viable P removers

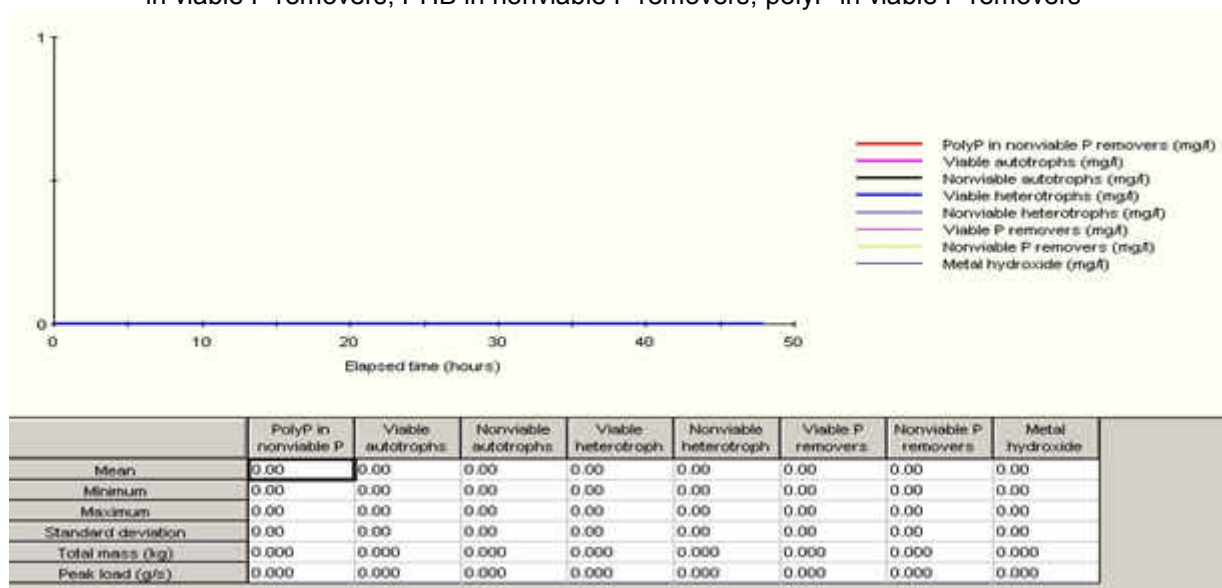


Fig. 17. The variation of polyP in nonviable P removers, viable autotrophs, nonviable autotrophs, viable heterotrophs, nonviable heterotrophs, viable P removers, nonviable P removers, metal hydroxide

For the secondary settling tank the results are shown in Fig. 18 and Fig. 19:

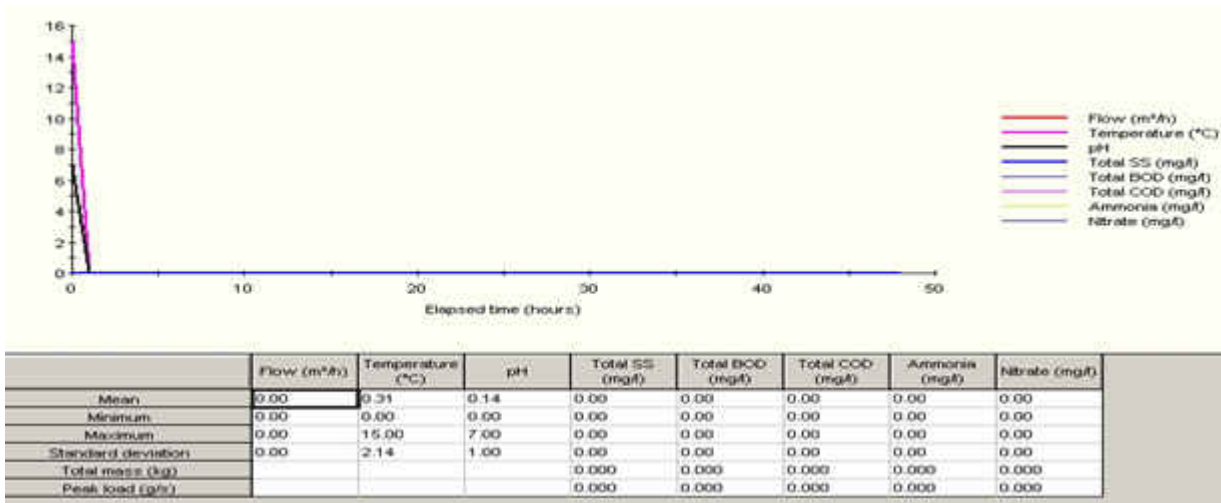


Fig. 18. The variation of flow for secondary settling tank

As we can see, the analysis is done on 7 stages, where it is set for each element, a minimum value, a maximum value and the average of all values (Fig. 19).

	Stage	Soluble BOD (mg/l)	Ammonia (mg/l)	Nitrate (mg/l)	Soluble phosphate (mg/l)	DO (mg/l)	Particulate BOD (mg/l)	Particulate phosphate (mg/l)	MLSS (mg/l)
Mean	1	4.9	39.2	0.0	0.0	2.0	0.0	0.0	
	2	4.9	39.2	0.0	0.0	2.0	0.0	0.0	
	3	4.9	39.2	0.0	0.0	2.0	0.0	0.0	
	4	4.9	39.2	0.0	0.0	2.0	0.0	0.0	
	5	4.9	39.2	0.0	0.0	2.0	0.0	0.0	
	6	4.9	39.1	0.1	0.0	2.0	0.0	0.0	
	7	4.9	39.2	0.0	0.0	2.0	0.0	0.0	
	8	4.9	39.2	0.0	0.0	2.0	0.0	0.0	
Minimum	1	0.0	0.0	0.0	0.0	0.0	0.0	0.0	
	2	0.0	0.0	0.0	0.0	0.0	0.0	0.0	
	3	0.0	0.0	0.0	0.0	0.0	0.0	0.0	
	4	0.0	0.0	0.0	0.0	0.0	0.0	0.0	
	5	0.0	0.0	0.0	0.0	0.0	0.0	0.0	
	6	0.0	0.0	0.0	0.0	0.0	0.0	0.0	
	7	0.0	0.0	0.0	0.0	0.0	0.0	0.0	
	8	0.0	0.0	0.0	0.0	0.0	0.0	0.0	
Maximum	1	5.0	40.0	0.0	0.0	2.0	0.0	0.0	
	2	5.0	40.0	0.0	0.0	2.0	0.0	0.0	
	3	5.0	40.0	0.0	0.0	2.0	0.0	0.0	
	4	5.0	40.0	0.0	0.0	2.0	0.0	0.0	
	5	5.0	40.0	0.0	0.0	2.0	0.0	0.0	
	6	5.0	40.0	0.1	0.0	2.0	0.0	0.0	
	7	5.0	40.0	0.0	0.0	2.0	0.0	0.0	
	8	5.0	40.0	0.0	0.0	2.0	0.0	0.0	

Fig. 19. The values for secondary settling tank

It is observed that soluble CBO resulted in an average value of 4.9 mg/l, an average value of 39.2 mg/L of Nitrates, and there was also a lack of nitrates and soluble phosphonates.

The program also analyzes for the aeration basin and the non-viable heterotrophic content, viable autotrophic and non-viable autotrophic (Fig. 20).

Non-viable heterotrophs (mg/l)		Viable autotrophs (mg/l)		Non-viable autotrophs (mg/l)	
	Stage	Non-viable heterotrophs (mg/l)	Viable autotrophs (mg/l)	Non-viable autotrophs (mg/l)	
Mean	1	0.0	0.0	0.0	
	2	0.0	0.0	0.0	
	3	0.0	0.0	0.0	
	4	0.0	0.1	0.0	
	5	0.0	0.2	0.0	
	6	0.0	0.3	0.0	
	7	0.0	0.8	0.0	
	8	0.0	233.8	0.0	
Minimum	1	0.0	0.0	0.0	
	2	0.0	0.0	0.0	
	3	0.0	0.0	0.0	
	4	0.0	0.0	0.0	
	5	0.0	0.0	0.0	
	6	0.0	0.0	0.0	
	7	0.0	0.0	0.0	
	8	0.0	0.0	0.0	
Maximum	1	0.0	0.0	0.0	
	2	0.0	0.0	0.0	
	3	0.0	0.0	0.0	
	4	0.0	1.7	0.0	
	5	0.0	4.5	0.0	
	6	0.0	7.4	0.0	
	7	0.0	14.4	0.0	
	8	0.0	240.2	0.0	

**Fig. 20.** The non-viable heterotrophic content, viable autotrophic and non-viable autotrophic for aeration basin

It is noticed the total reduction of nitrogen content, soluble substances and COD code which leads to the conclusion that the wastewater is purged when it is discharged into the Emisar.

#### 4. Conclusions

There is a high increase in the early hours of the simulation preceded by a sudden drop in short time after reaching the maximum, and then maintaining a constant value of the various elements.

The use of a specialized program for the follow-up of each process is beneficial both for the personnel who are in administration and use a clean wastewater treatment plant and for the emissary receiving the daily intake of treated water.

It is recommended to use the Stoat plant for the treatment station SEAU Mangalia because the simulation performed in this paper was clearly observed the difference between the values of each characteristics at the entrance to the treatment plant and the values of the characteristics in the final stages.

The same reasoning applies when dealing with treatment processes. The use of integrated models as a planning tool in the operational phases can be much more important to develop a more efficient complex use of the existing resources in the sewage system and the wastewater treatment station.

#### References

- [1] A. Jack, R.M. Ashley, "The impact of the controlled emptying of in-sewer storage on wastewater treatment plant performance"; *Proc. The Municipality Conference of Halmstad, Västra Strandens reningsverk, Halmstad, Sweden, 2001*, pp. 124-128;
- [2] <http://www.greenagenda.org/eco-aqua/epurare.htm>;
- [3] I.-I. Panaitescu, M. Panaitescu, F.-V. Panaitescu, I.-A. Enache, "Using PC simulation for flow sensitivity analysis with application to a wastewater treatment plant", *Global Journal on Advances Pure and Applied Sciences*, Vol. 1 (2013), ISSN: 2301-2706, 2013;
- [4] <http://sites.wrcplc.co.uk/freeware/STOAT/downloadform.aspx>.

## Mobile Equipment for Testing the Power Steering of Cars

Dipl. eng. **Alexandru HRISTEA**<sup>1</sup>, PhD. eng. **Radu RADOI**<sup>1</sup>,  
Dipl. eng. **Bogdan TUDOR**<sup>1</sup>, Eng. **Ion BALAN**<sup>1</sup>

<sup>1</sup> INOE 2000-IHP, hristea.ihp@fluidas.ro

**Abstract:** The steering system is one of the components that ensure safe movement of vehicles; besides this, keeping it in optimum condition leads to a minimum fuel consumption but also the lack of pollution associated with the loss of hydraulic fluid. Power steering is one of the most requested options in a car of small and medium size, for the vehicles weighing over 1200 kg entirely common. In figure 1 is represented the percent's according to the type of assistance steering boxes; from this graph, in conjunction with the average age of the fleet in Romania (13 years in the year 2017), it is deduced that most power-steering's mounted on cars have hydraulic power steering or electro-hydraulic, so the need for a portable test equipment is needed to discover and resolve the problem regarding faults of the system without disassembling the vehicle. Advantage of the device lies in its capability to transmit data that is collected by flow and pressure transducers and sent to a mobile (smartphone or tablet) or fixed device (PC) using wireless technology. Also data can be transmitted to an operator who is specializes in repairing hydraulic steering boxes to confirm their state of function.

This article presents the state of the art portable test equipment with data transmission for hydraulic power boxes and pumps from cars, this test device will have reduced dimensions and will be formed of a flow transducer and pressure transducer and a 2 way distributor with and a wireless module, all of which are connected to an electronic unit with an display located on the device panel.

This data is then transmitted to a device that has software installed on it, capable of play back information that receives from the transducers.

**Keywords:** Fault test, power steering, public safety, automotive

### 1. Introduction

The basic functionality of the hydraulic power box and components are represented in figure 2. Hydraulic power steering main purpose is that it can provide the driver less effort to steer the wheels of the car when driving at typical speeds, and reduce considerably the physical effort necessary to turn the wheels when a vehicle is stopped or moving slowly, is achieved by applying pressure to the sides of a piston rod mounted on a bilateral body (Fig.2); fluid access is made thru an opening after rotary valve mounted on the steering column, receives a response from the pinion always engaging the steering rack rigidly connected to the piston. The fluid flows through ducts and position represent the body of hydraulic cylinder.

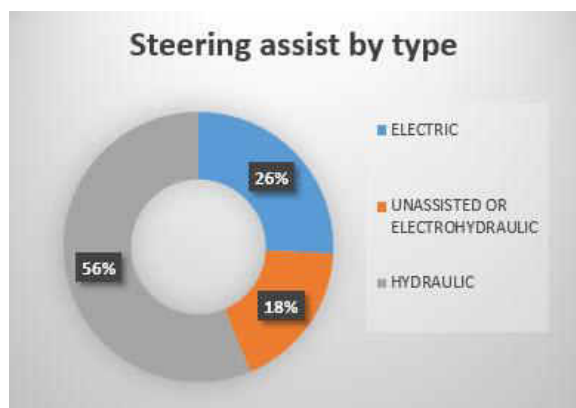


**Fig. 1.** Steering assist by type of the vehicles manufactured today in the world

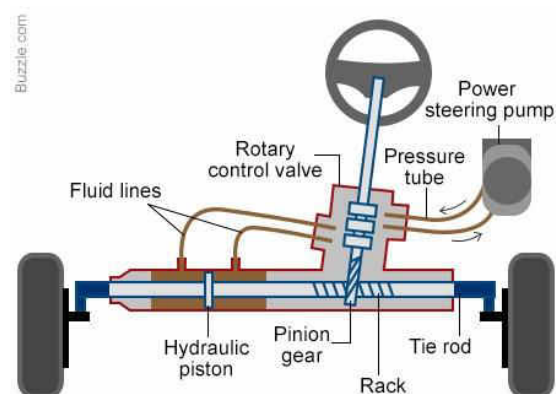


**Fig. 2.** Main components of the hydraulic steering box

Hydraulic power steering (pump directly driven by the vehicle engine with its rpm) is responsible for fuel consumption of approx. 0.3 l / 100 km; For drive pump by a separate electric motor (electro-hydraulic power steering), that consumption is reduced by half.

However, regardless of version, malfunction is accompanied by an increase in consumption and the loss of power steering fluid, both with negative effects on the environment and road safety [1].

## 2. Product description

The portable test equipment provided with data transmission, fig. 3, is a new product which allows testing of the hydraulic power steering system of vehicles without having to dismantle the subassemblies, thus reducing the immobilization time of the vehicle and possible hydraulic fluid drainage on the road, endangering the safety of the others involved in traffic. The device is also capable of transmitting data from pressure and flow sensors to a smartphone, tablet, or to desktop PC via a wireless module. It can also be produced with an integrated display for rendering the measured values as well as with the possibility of storing this information.

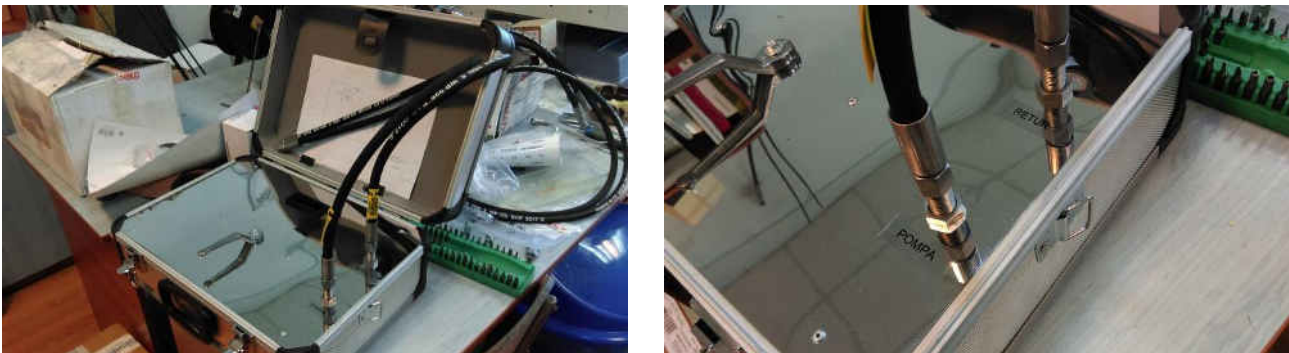


Fig. 3. The portable equipment

The usefulness of this equipment is due to the poor quality of roads in some areas that puts the power steering's under a lot of wear and tear, when over the operating limit designed by the manufacturer. This new device, very much needed in the field of repair and maintenance, it also reduces the time with the defects repair due to the flexibility offered by the data transmission system, with which information can be sent to a repair specialist of the hydraulic power steering boxes. The device is also capable of generating a test report, which it can then be passed on to a specialist who can accurately determine the cause of the fault and the solution needed to repair the servo-hydraulic system. This portable test device is been produced in Romania being only one with sensors and data transmission. In fig.4 it can be seen a block diagram with the components of the portable test equipment and the informatics data transmission system and local display.

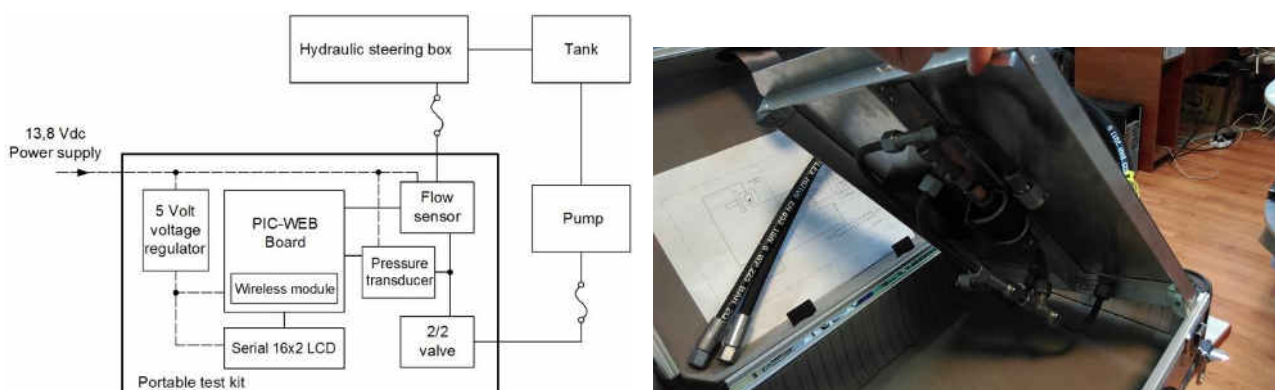
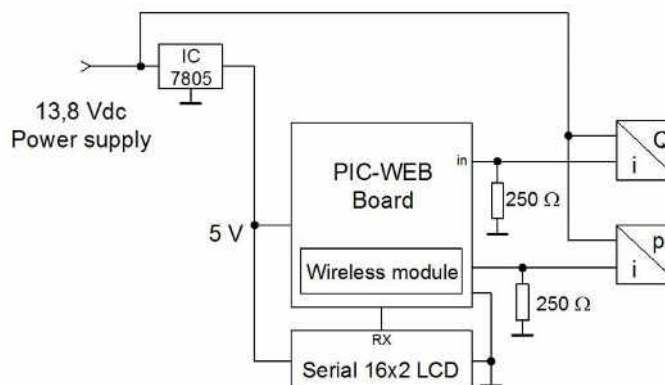


Fig. 4. Block diagram and the physical circuit of portable test equipment with data transmission

The portable test equipment is composed of several sensors needed to record the parameters which are critical to determine the condition of the steering box. The sensors used in the hydraulic scheme are: pressure sensor with a domain of 0-160 bar, flow sensor 0.1-12 l/min [2]. All the sensors are connected to the input ports from Pic Web Board. The equipment is supplied with electricity from the cigarette lighter socket on the vehicle. The electrical connection of the electronic components can be seen in figure 5. The pressure and flow transducer are powered by a voltage of 13.8 V, and the PIC-Web and the liquid-crystal electronic module are powered by 5 V via a voltage regulator integrated circuit. The pic-web module is provided with an optional wireless transmission module connected via the UEXT connector. The display receives the data to be displayed through the serial port from the pic-web module to the RX pin.



**Fig. 5.** The electric connection of electronic components of portable equipment



**Fig. 6.** The Pic-Web electronic development board from Olimex

Figure 6 shows the Pic-Web electronic development board from Olimex [3]. The Pic-Web board is designed to have Web page of no more than 128 kB. If necessary a lot of images in the application they can be stored on other server visible on the network where you have the PIC-WEB connected. The potential of the board is to generate a fluid communication between some specific sensors or actuators across a TCP/IP net including the controls of it.

Pic-Web board features:

- PIC18F67J60 microcontroller
- 1Mbit on board serial flash for web pages storage
- ICSP/ICD mini connector for programming and debugging with PIC-ICD2, PIC-ICD2-POCKET and PIC-ICD2-TINY.
- Reset button
- User event button
- Analogue trimmer potentiometer
- Thermistor for temperature monitoring
- RS232 driver and connector
- Complete web server and TCP-IP stack support as per Microchip's open source TCP-IP stack
- Power plug-in jack for DC power supply
- Voltage regulator +3.3V and filtering capacitors
- Status LED

- UEXT connector
- Extension header to connect to other boards
- Dimensions 60×65 mm (2.36×2.55")

### 3. Operation of the equipment

The test kit connects to the car's hydraulic assisted steering system with two hoses. Unscrew the hose that comes from the pump to the hydraulically assisted steering box and insert the equipment between the pump and the steering box. The built-in transducers will read the system pressure and flow. By closing the valve for a short time, the maximum pressure delivered by the steering pump can be determined. At the end of the stroke hydraulic cylinder piston, the steering box leakage can be determined.

All the tests are performed with the help of the software developed by Hydraulics and pneumatics research Institute with the aid of an internet protocol Web page program. Test data is displayed locally on the device panel and transmitted wirelessly by the web application stored in the Pic-Web module. Viewing test data and recording data is done by accessing the application through a web browser on any mobile device (phone or tablet). Connection of the mobile device to the web application is done wirelessly by accessing the IP address of the web application. Connecting to the web application can also be done with a desktop PC via an Ethernet cable, the Pic-Web module being equipped with an RJ45 Ethernet connector.

All the data recorded it will be compared with those in the database and the system will decide whether the data recorded for the hydraulic steering box comply with the standards accepted by its manufacturer. In the software application page, the parameters obtained from the test can be seen and it is possible to record the data such as: name of the operator that perform testing, beneficiary of the test report, date and registration number of the test report. With this portable test device can be determined the rate of oil leakages at the stroke ends of steering box or in the middle of the stroke of hydraulic cylinder (the car wheels in the center position). The leakage rate is determined by the wear of the piston and rotary valve seals. The panel of the software application displays data obtained from testing. If the flow of loss at the end of stroke is above 1.5 l / min is recommended to replace or repair the steering box. A steering box worn, with large internal losses, will lead to disturbance in handling the power steering [4].

In order to issue the test report, in the software application the information for the beneficiary, the test operator and the test date must be noted. Once the data has been filled in, it will be possible to save a file containing the test parameters and identification data (report number, date, beneficiary, etc.). This report is stored and can be printed or sent by e-mail [5].

### 4. Conclusions

The test portable equipment with data transmission allows quick testing of the hydraulically assisted steering system without the need to dismantle the parts from the car.

Advantage of the device lies in its capability to transmit data that is collected by flow and pressure transducers and sent to a mobile (smartphone or tablet) or fixed device (PC) using wireless technology.

Through the web application can issue test reports with data transmitted wirelessly from the test equipment, which can then be archived.

The amount of sensors and the domain of them determine how accurate is the report for increase the road safety and human loses due to malfunction of hydraulic power steering.

### Acknowledgements

This work has been funded by Executive Unit for Financing Higher Education, Research, Development and Innovation - UEFISCDI, under PNCDI III - Programme 2, Subprogram 2.1 – Cheques of Innovation (CI-2017), Submission code PN-III-P2-2.1-CI-2017-0229, Financial agreement no. 3CI/2017, project title: Portable test equipment for the power steering of vehicles with data transmission, project acronym ETSAD,

Project main domain: 2. Information of technology and communications space and security, Subdomain: 2.3. Security.

### References

- [1] P.A. Adegbuyi, I.L. Marcu, “Hydraulic and pneumatic cylinder failures, the effect of fluid cleanliness on component life”, *Hidraulica Magazine*, ISSN 1453-7303, Romania, no.1, pp. 27-30, 2013;
- [2] I. Dutu, G. Matache, “Computer assisted electro-hydraulic stand for testing servovalves”, *Hidraulica Magazine*, ISSN 1453-7303, Romania, no.3-4, pp. 73-77, 2012;
- [3] <https://www.olimex.com/Products/PIC/Development/PIC-WEB/resources/PIC-WEB-manual.pdf>;
- [4] G. Matache, St. Alexandrescu, Gh. Sovaiala, I. Pavel, I.C. Girleanu, “Testing of linear pneumatic actuators with hydraulic load”, *Hidraulica Magazine*, ISSN 1453-7303, Romania, no.3, pp. 53-56, 2013;
- [5] G. Matache, St. Alexandrescu, A. Pantiru, Gh. Sovaiala, M. Petrache, “The analysis of flow losses through dynamic seals of hydraulic cylinders”, *Hidraulica Magazine*, ISSN 1453-7303, Romania, no.1, pp. 52-60, 2013.

## The Influence of the Corrosion and Temperature on the Von Mises Stress in the Lateral Cover of a Pressurized Fuel Tank

Assoc. Prof. PhD. Eng. **Mihai ȚĂLU**

University of Craiova, Faculty of Mechanics, Department of Applied Mechanics and Civil Engineering, Calea București Street, no. 107, 200512 Craiova, Dolj county, Romania. E-mail: mihai\_talu@yahoo.com

**Abstract:** The objective of this study was to evaluate the effect of the corrosion and temperature on the state of stress in the lateral cover of a pressurized fuel tank of AISI 4340 steel used in automotive industry. This analysis of the Von Mises stress laws variation in the lateral cylindrical cover with the corresponding CAD solutions and results of simulations will improve the design and performances of the pressurized fuel tank during the exploitation period. Furthermore, it offers design guidance for pressurized fuel tank durability in the early stages of product development to reduce overall new product development costs significantly.

**Keywords:** Automotive industry, corrosion, cylindrical cover, industrial engineering design, optimization methods, pressurized fuel tank, state of effort

### 1. Introduction

One of the most dynamic sectors of the economy is that of automotive construction [1-4]. A pressurized fuel tank has the role of safely storing and supplying fuel to the engine [5-9]. Optimum tank design with reduced production costs and start-up time in manufacturing is key to competition in the automotive market [10-13]. Pressurized fuel tanks have complex geometries and are especially made of steel or aluminum [5, 6, 8-13]. For tanks of storing compressed natural gas (CNG) fuel, the maximum pressure test is at  $p = 300$  bar, while pressures for liquefied petroleum gas (LPG) storage are 10 times lower [5, 6, 9]. Currently, various design methods [14-20] and data analysis techniques for both quantitative and qualitative research [21-34] as well as recommendations from renowned researchers are used in the computer engineering design and manufacturing process of pressurized fuel tanks [35-37]. The use of these pressurized fuel tanks in the automotive mass production was made after some new modifications in the design of the machines, which led to increased safety and reliability in operation [5, 6], using a computer-based information system [38]. The CAD study allows for the establishment of high stress states, after which the pressurized fuel tanks are redesigned to admissible values to meet the optimization criteria imposed [39-41].

### 2. The optimal design of lateral cover of the cylindrical pressurized fuel tank

The main structural elements which make up a pressurized cylindrical tank are shown in Figure 1. In this study it is considered that the corrosion action is uniform and takes place only on the interior surfaces of the pressurized fuel tank where the CNG or LPG fuel is in contact with them, being considered as an aggressive chemical environment.

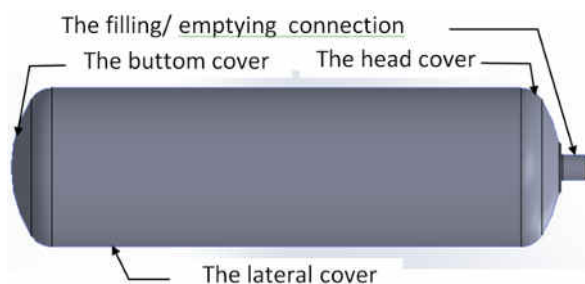


Fig. 1. Pressurized cylindrical fuel tank

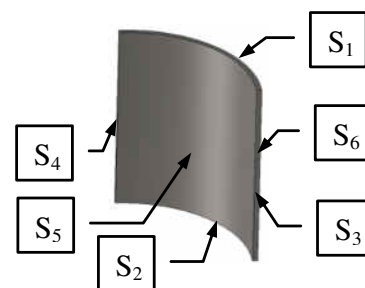


Fig. 2. The outer surface of the pressurized fuel tank

On the outer surface of the tank (Figure 2), the corrosion is attenuated by the paint protective layers which are applied against the aggression of the agents from the external environment.

The CAD optimal design of the lateral cover of the pressurized fuel tank permits to determine the thickness of the lateral cover to resist to the required demands, starting from the following initial data:

- the lateral cover has: the external diameter of  $D = 250$  mm and the length of  $L = 700$  mm;
- the maximum hydraulic pressure test is:  $p_{\max} = 30$  N/mm<sup>2</sup>;
- the ambient environment temperature varies between the limits:  $T = -30$  °C,...,+60 °C;
- the material of tank is made from AISI 4340 steel.

From the analysis of the constructive form it was found that the cover has an axial symmetry (according to Figure 1), which allows us to use in the calculations of a parameterized model with section at  $\frac{1}{4}$  of the initial model (according to Figure 2).

Initially parameterized modeling of the pressurized cylindrical tank was done in the AutoCAD Autodesk 2017 software [42], which was imported to SolidWorks 2017 software [43] for analysis with the: Static, Thermal and Design Study modules.

The parameterized model was applied to the surfaces specified in Figure 2 (load forces, link restrictions) and symmetry conditions (as shown in Figures 3 to 6):

- maximum loading pressure on the inner surface,  $S_5$ :  $p_{\max} = 30$  N/mm<sup>2</sup>, (according to Figure 3);
- thermal loading on the outer surface  $S_6$ , with variation between the limits:  $T = -30$  °C,..., +60 °C, (as shown in Figure 4);
- opposing and equal traction forces on the surfaces:  $S_1$  and  $S_2$  given by the pressure action on the inner surfaces of the end covers with the value of:  $F = p_{\max} (\pi R^2)/4 = 367969$  N, (Figure 5);
- symmetry conditions on the surfaces:  $S_1$  and  $S_2$ ;
- the null displacement of the cover in the direction of the symmetry axis.

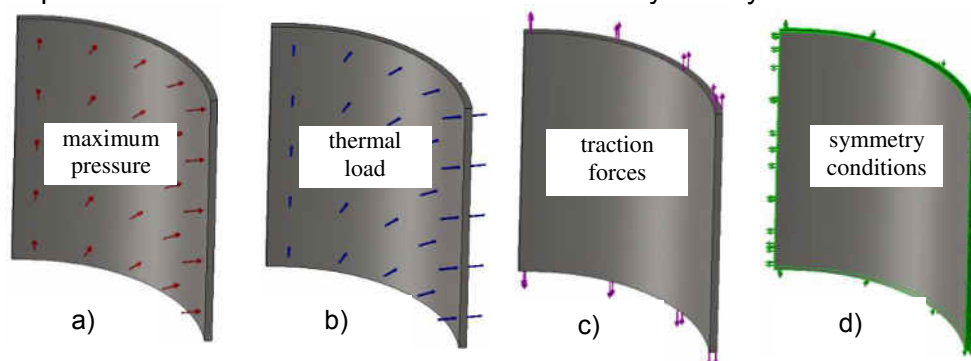


**Fig. 3.** a) The loading pressure on the inner surface  $S_5$ ; b) The thermal load on the outer surface  $S_6$ ; c) The traction forces on the surfaces  $S_1$  and  $S_2$ ; d) The symmetry conditions on surface  $S_1$  and  $S_2$

In the calculation the parameter under optimization is defined as the thickness of the cover with continuous variation between the limits:  $s = 4 \dots 7$  mm. Namely, the temperature is considered to be continuously variable between the limits of the exploitation range:  $T = -30$  °C, ..., +60 °C.

The goal optimization function is defined as a target to achieving a minimum mass.

As a calculation restriction it was imposed that the Von Mises resulting stress must be less than or equal to the permissible traction value of the material cover AISI 4340 steel, equal to  $\sigma_a = 710$  N/mm<sup>2</sup>.

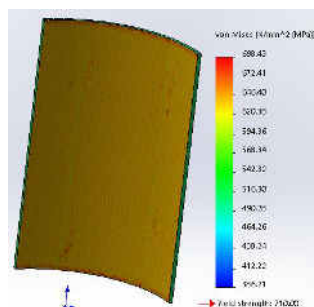


**Fig. 4.** The Von Mises stress at  $T = -30$  °C

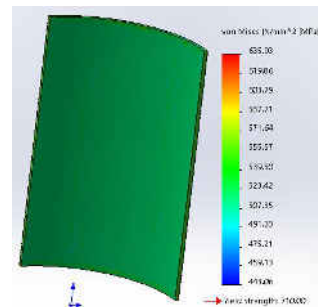


**Fig. 5.** The Von Mises stress at  $T = 60$  °C

After the optimization calculation, the program gives a minimum thickness of  $s = 6.05$  mm, for which we have a uniform Von Mises stress of  $\sigma_{\max} = 698.43$  N/mm<sup>2</sup> value at the temperature of  $T = -30$  °C, (as shown in Figure 4).

In the addition, for this thickness has been calculated the Von Mises stress at  $T = 60$  °C, which has the  $\sigma_{\text{rez}} = 635.93$  N/mm<sup>2</sup> value, and his distribution is shown in Figure 5.

Now, in order to resist to the entire exploitation interval by  $n_a = 20$  years imposed from the design theme, the optimal thickness is corrected considering the influence of the corrosion and the negative tolerance of the metal sheet, using the following formula [5, 6]:

$$S_{\text{real}} = S_{\text{opt}} + \Delta S_C + \Delta S_T = S_{\text{opt}} + v_c \cdot n_a + \text{abs}(A_i) \quad (1)$$

where:

- $\Delta S_C$ , the addition of thickness due to the corrosion of the laminate sheet;
- $\Delta S_T$ , the addition of thickness due to the negative tolerance of the execution of laminate metal sheet;
- $v_c$ , the corrosion rate of the cover with values between the limits:  $v_c = 0.1, \dots, 0.15$  mm/year, where we adopt the  $v_c = 0.12$  mm/year;
- $n_a$ , the number of years of exploitation;  $n_a = 20$  years;
- $A_i$ , the lower negative deviation of the laminate metal sheet;  $A_i = -0.8$  mm, for thicknesses between the limits:  $s = 8 \dots 12$  mm.

By substituting the minimum thickness of the laminate sheet it is obtained has the following value:

$$S_{\text{real min}} = 6.05 + 0.12 \cdot 20 + \text{abs}(-0.8) = 9.25 \text{ mm} \quad (2)$$

For the execution, we choose a laminate sheet of AISI 4340 steel that has a thickness of  $s = 10^{+0.3}_{-0.8}$  mm.

## 2.1. The CAD analysis of Von Mises stress in lateral cover

Knowing the complete geometry of the cover, the Von Mises stress calculation was further performed and it was found to have a maximum value at the temperature of  $T = -30$  °C.

At the initial moment of exploitation, when  $n_a = 0$  years, the thickness to be taken into account in the calculation has the value of  $s = 9.2$  mm, where from the covering has subtract the negative deviation from the maximum thickness of the laminate sheet.

The maximum working pressure at which the cover can resist before the resultant Von Mises stress becomes equal with the admissible traction value of material,  $\sigma_a = 710$  N/mm<sup>2</sup>, has the value of  $p = 45.5$  N/mm<sup>2</sup>, showing the graph distribution from the Figure 6a.

The explosion pressure at this moment that occurs when touched the breaking stress of material  $\sigma_r = 1100$  N/mm<sup>2</sup>, has the value of  $p_r = 74.8$  N/mm<sup>2</sup>, (according to Figure 6b).

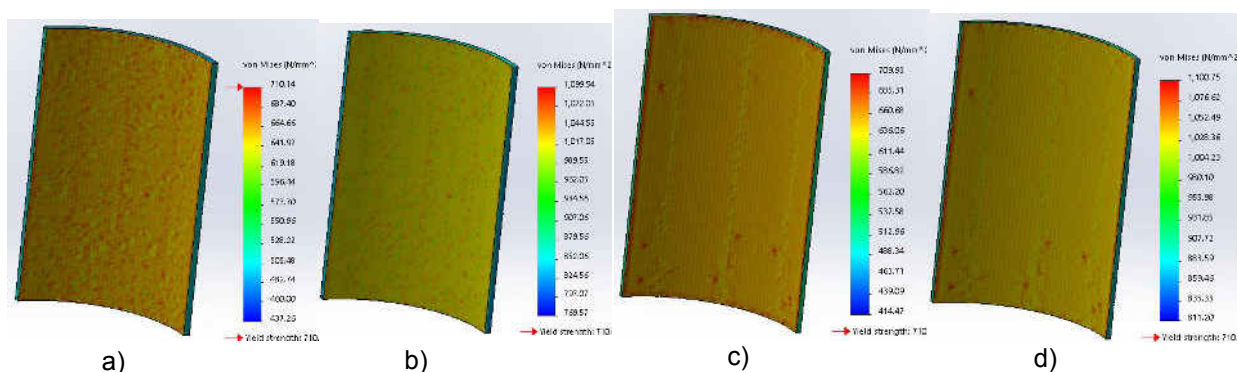


**Fig. 6.** a) The stress at maximum pressure,  $n_a = 0$  year; b) The stress at explosion pressure,  $n_a = 0$  year; c) The stress at maximum pressure,  $n_a = 20$  years; d) The stress at explosion pressure,  $n_a = 20$  years

By calculating the pressure value at the beginning and the end of the exploitation period when  $n_a = 20$  years, after what the corrosion has reduced the thickness of the cover to  $s = 6.8$  mm, the maximum working pressure is obtained for  $p = 34.5$  N/mm<sup>2</sup>, which has the stress distribution from

Figure 6c and for the value of the explosion pressure  $p_r = 57.75 \text{ N/mm}^2$ , has the stress distribution shown in Figure 6d.

From the analysis of the results of corrosion influence at the end of the exploitation period when the thickness of the cover decreases by  $\Delta s = 26.09 \%$ , the maximum working pressure decreased by  $\Delta p_{\max} = 24.17 \%$  and the explosion pressure decreased by  $\Delta p_r = 23.1 \%$ .

The calculation made for determining the combined influence of the corrosion with temperature on the resulting stress Von Mises state, when loading the cover with the maximum hydraulic test pressure  $p_{\max} = 30 \text{ N/mm}^2$ , is given in Table 1.

**Table 1:** The influence of the corrosion with temperature on the resulting stress Von Mises state

no. year	s [mm]	T [°C]									
		-30 °C	-20 °C	-10 °C	0 °C	10 °C	20 °C	30 °C	40 °C	50 °C	60 °C
		$\sigma \text{ [N/mm}^2\text{]}$									
0	9.2	531.36	504.46	478.19	453.75	431.69	410.54	395.55	398.56	406.94	417.27
1	9.08	533.07	506.18	480.48	456.45	434.48	414.31	400.03	404.09	413.49	424.81
2	8.96	535.17	508.31	483.13	459.47	437.6	418.34	404.76	409.77	420.13	432.35
3	8.84	537.67	510.85	486.15	462.83	441.05	422.65	409.74	415.6	426.85	439.91
4	8.72	540.57	513.81	489.54	466.53	444.84	427.21	414.95	421.57	433.64	447.48
5	8.6	543.87	517.17	493.3	470.55	448.96	432.05	420.41	427.7	440.52	455.06
6	8.48	547.54	520.95	497.42	474.91	453.41	437.15	426.12	433.98	447.48	462.64
7	8.36	551.66	525.15	501.91	479.6	458.19	442.52	432.06	440.41	454.53	470.24
8	8.24	556.15	529.75	506.77	484.63	463.31	448.15	438.26	446.98	461.65	477.84
9	8.12	561.05	534.77	512.00	489.99	468.76	454.05	444.69	453.71	468.85	485.46
10	8	566.33	540.20	517.59	495.68	474.55	460.22	451.37	460.58	476.13	493.09
11	7.88	572.02	546.04	523.56	501.7	480.66	466.65	458.29	467.61	483.5	500.72
12	7.76	578.11	552.29	529.89	508.06	487.11	473.35	465.46	474.79	490.94	508.37
13	7.64	584.59	558.96	536.58	514.75	493.9	480.31	472.87	482.11	498.47	516.02
14	7.52	591.47	566.04	543.65	521.78	501.01	487.54	480.53	489.54	506.08	523.68
15	7.4	598.75	573.53	551.08	529.13	508.46	495.04	488.42	497.21	513.77	531.36
16	7.28	606.42	581.44	558.88	536.82	516.24	502.81	496.57	504.98	521.54	539.04
17	7.16	614.5	589.75	567.05	544.85	524.36	510.84	504.95	512.91	529.39	546.73
18	7.04	622.97	598.48	575.58	553.21	532.81	519.14	513.58	520.98	537.32	554.44
19	6.92	631.85	607.62	584.49	561.9	541.59	527.7	522.45	529.21	545.33	562.15
20	6.8	641.11	617.18	593.76	570.92	550.7	536.53	531.57	537.58	553.42	569.87

Starting from these results, the graphical representation of the 3D variation of the Von Mises  $\sigma(n_a, T)$  stress is given in the Figure 7, computed using Microsoft Excel 2017 software [44].

For the constant working temperatures, with a interval of  $\Delta T = 10 \text{ }^\circ\text{C}$  from the temperature range, the variation of the Von Mises stress  $\sigma(T = ct, n_a)$  is shown in Figure 8 and for  $n_a = \text{constant}$ , with the variable temperature, the variation of stress  $\sigma(T, n_a = ct)$  is given in Figure 9.

The superior view of the dependence surfaces  $\sigma(n_a, T)$  is shown in Figure 10.

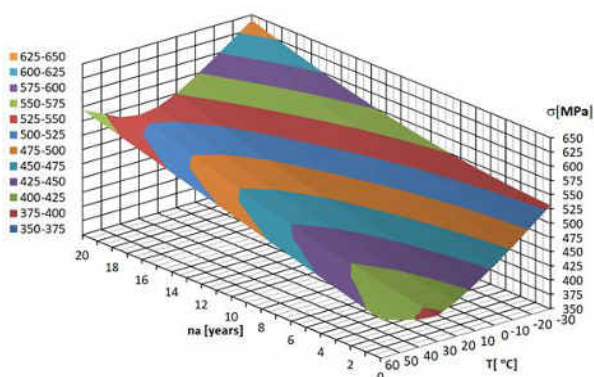


**Fig. 7.** The Von Mises stress  $\sigma(n_a, T)$

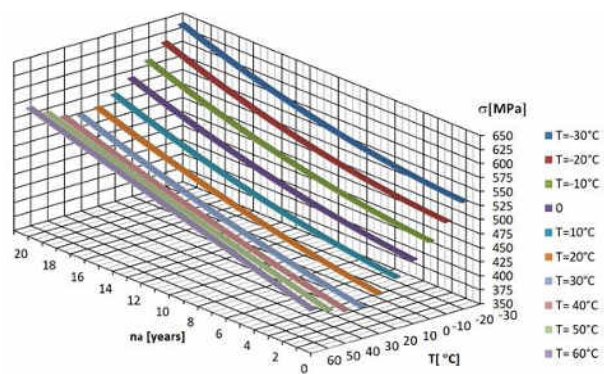


**Fig. 8.** The Von Mises stress  $\sigma(n_a, T=ct.)$

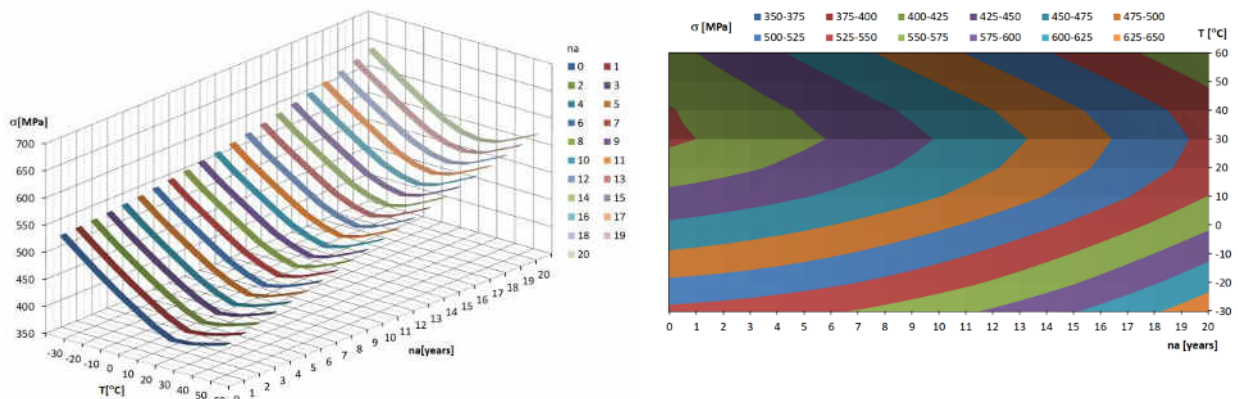


Fig. 9. The Von Mises stress  $\sigma(n_a=ct., T)$  Fig. 10. The superior view of Von Mises stress  $\sigma(n_a, T)$

Further study directions of the variation of the stress starting from the results given in Table 1, are the following:

- a) the influence of the corrosion variation on the stress, with  $s = \text{variable}$  and  $T = \text{constant}$ , which is shown in Figure 11;
- b) the influence of the temperature variation on the stress, with  $T = \text{variable}$  and  $s = \text{constant}$ , which is shown in Figure 13;
- c) the combined corrosion-temperature influence on the stress,  $\sigma(T, n_a)$  which are shown in Figures 7 to 10.

**2.2. Study of corrosion influence on the resulting stress Von Mises**

The corrosion for a given time, establishes through  $n_a$  a value of the cover thickness. In the Figure 11 for different temperature values with  $T = \text{constant}$ , it is shown the graphs and laws of the variance of resulting Von Mises stress  $\sigma(T = ct, n_a)$ , calculated through an polynomial interpolation using Microsoft Excel 2017 [44] and Maple 2016 software applications [45].

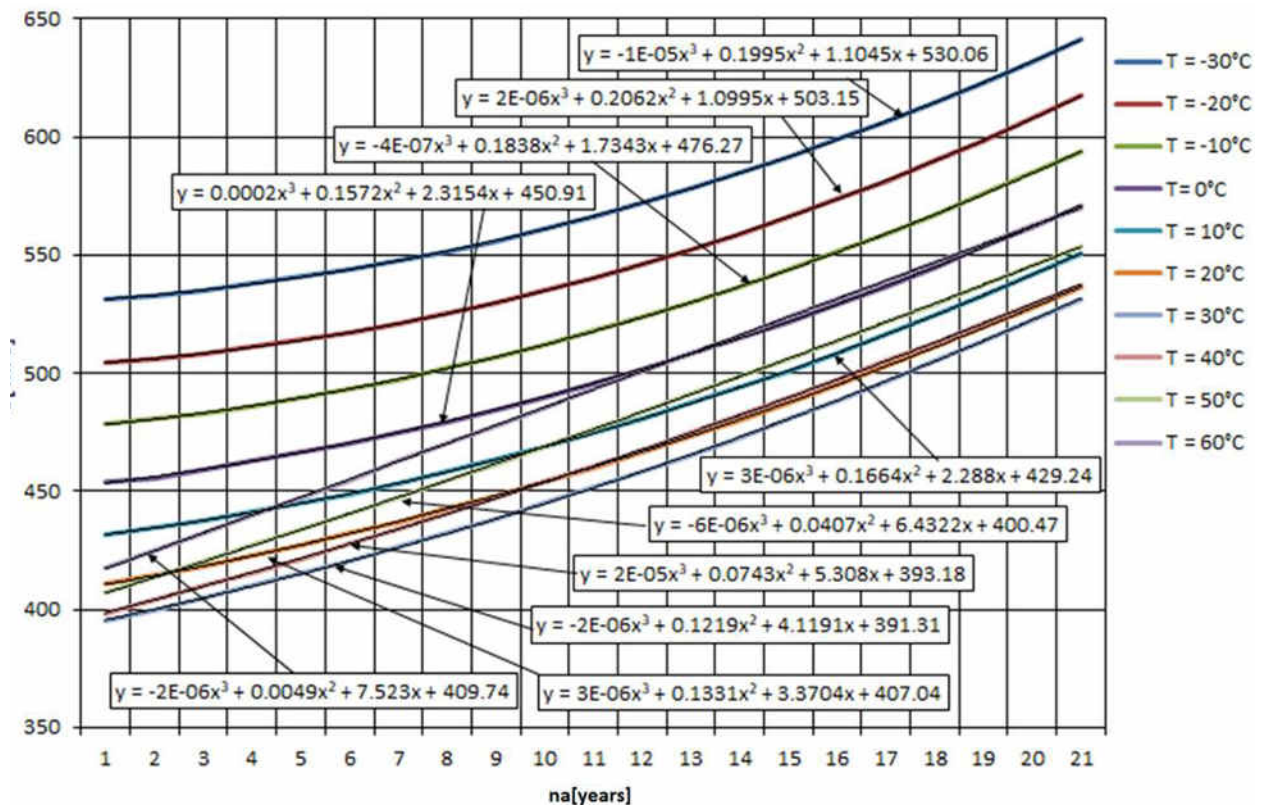


Fig. 11. The 2D graphs of Von Mises stress  $\sigma(n_a, T=ct)$

In practice, this operating case occurs in controlled temperature environments, such as in the case of thermostated halls or warehouses.

The percentage decrease of Von Mises stress for ( $T_K = ct$ ), with  $n_a = \text{variable}$ ,  $\Delta\sigma(n_a)$ , taking the maximum stress from  $T = 60\text{ }^\circ\text{C}$  as the basis of calculation, and the graph of these curves is given in Figure 12, computed using Microsoft Excel 2017 software [44].

The percentage decrease of the Von Mises stress, for ( $n_{aK} = ct$ ), with  $T = \text{variable}$ , taking as the basis for calculation the maximum stress  $\Delta\sigma(T)$ , that exists at  $T = -30\text{ }^\circ\text{C}$ , is shown in Figure 13.

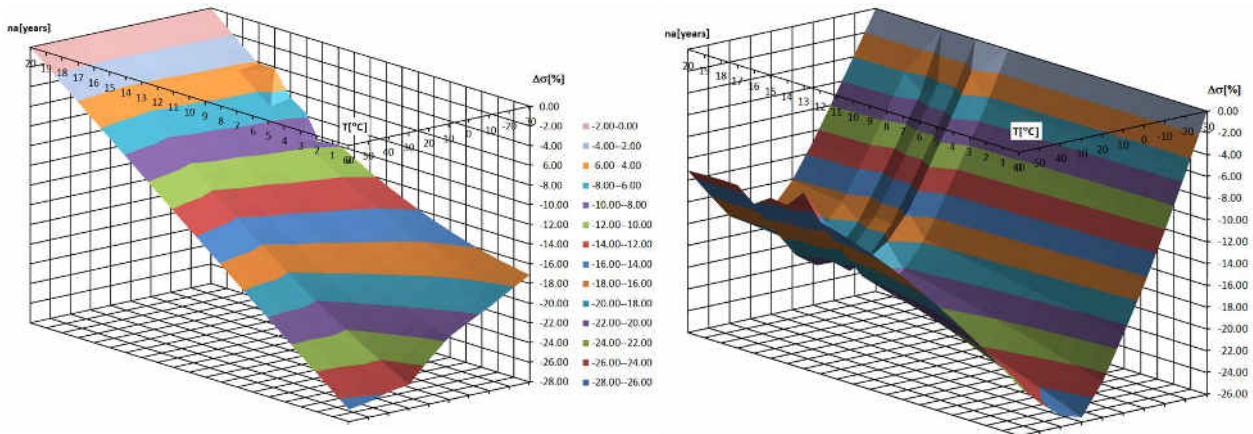


Fig. 12. The Von Mises stress variation  $\Delta\sigma(n_a, T=ct.)$  Fig. 13. The Von Mises stress variation  $\Delta\sigma(n_a=ct., T)$

### 2.3. The study of the influence of temperature on the resulting stress Von Mises

Knowing the temperature variation between the operating limits  $T = -30\text{ }^\circ\text{C} \dots 60\text{ }^\circ\text{C}$  and for constant thicknesses between in the limits:  $s = 7.6 \dots 10\text{ mm}$ , according to Table 1, the laws of variation of stress were determined by polynomial interpolation, computed using Microsoft Excel 2017 software. The graphs of these curves are shown in Figure 14.

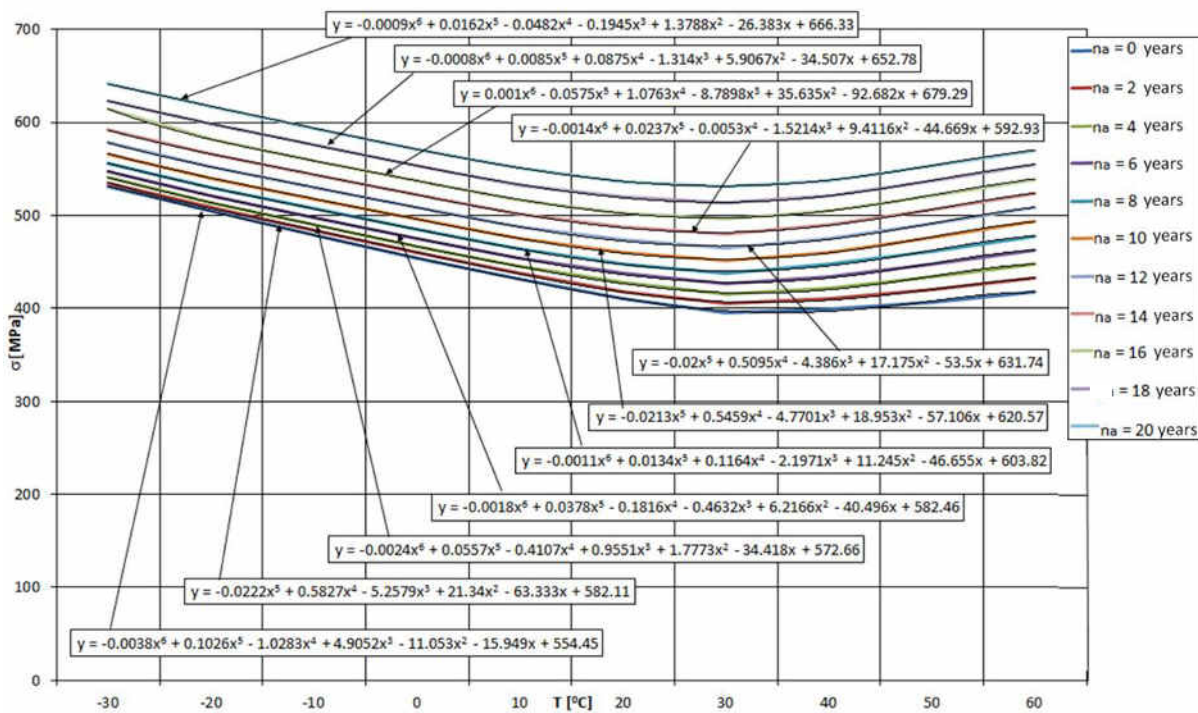


Fig. 14. The 2D graphs of Von Mises stress  $\sigma(n_a = ct, T)$

As the cover has to provide the stress resistance over the entire exploitation range, the stress variation graphs from the beginning of  $n = 0$  years to the end of the exploitation period  $n_a = 20$  years are shown in Figure 15.

The effort difference  $\Delta\sigma = \sigma_{n_a = 20 \text{ years}} - \sigma_{n_a = 0 \text{ years}}$ , which appears between the beginning and the end of the exploitation period is represented graphically in Figure 16, and the law of variation is calculated by polynomial interpolation.

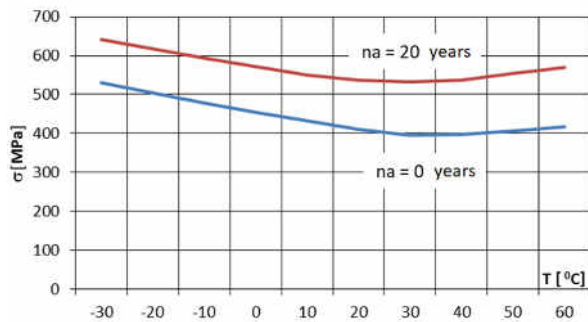


Fig. 15. The Von Mises stress at  $n_a = 0$  years and  $n_a = 20$  years

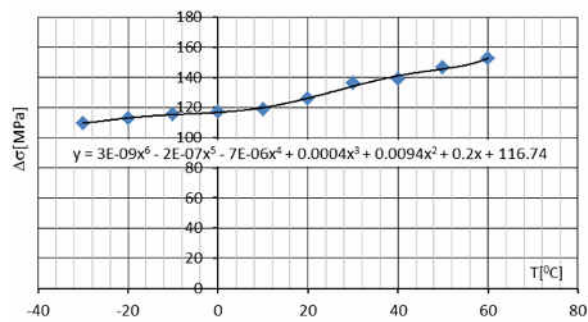


Fig. 16. The variation of Von Mises stress difference  $\Delta\sigma = \sigma_{n_a = 20 \text{ years}} - \sigma_{n_a = 0 \text{ years}}$

### 3. Discussion

The increase of corrosion during the exploitation period, causes the thickness cover to decrease with the  $\Delta s = 26.09$  %, which results in increased unitary Von Mises stress, (according to Table 1). Following the correction of the optimized thickness and the choice of the sheet metal with an immediate superior thickness, the cover receives a thickness supplement equal to  $\Delta s = 0.75$  mm, which makes the maximum effective Von Mises stress to be less than the calculated maximum stress to optimization.

The maximum unitary Von Mises stress occur at the negative temperature of  $T = -30$  °C irrespective of the moment of exploitation  $n_a$ , (as shown in Figures 7 to 11).

At  $n_a = \text{ct.}$ , the graph of the dependence of stress variation  $\sigma(T)$  from the Figure 14 has a minimum for the temperature  $T = 30$  °C; the stress decreases with the temperature rise from the maximum value of  $T = -30$  °C to the minimum value of  $T = 30$  °C, then rises again to the temperature  $T = 60$  °C, but below the maximum stress reached at the temperature of  $T = -30$  °C.

For  $T = \text{ct.}$ , with  $n_a = \text{variable}$  (as shown in Figure 11), shows that the evolution of corrosion determines the increase of the stress from the positive temperatures to the negative temperatures; the minimum stress being at  $T = 60$  °C and the maximum stress it is at  $T = -30$  °C.

The variance of the stress difference between the end and the beginning of the exploitation period, is comprised between the limits  $\Delta\sigma = 115$  up to  $152$  MPa, having an increasing character over the entire interval of temperature variation, (according to Figure 10).

In case of the variation stress  $\Delta\sigma(n_a)$ , at  $T = \text{ct.}$ , it has the maximum value of  $\Delta\sigma(n_a) = -26.78$  % for  $n_a = 0$  years and at the temperature of  $T = 60$  °C, (according to Figure 12).

For  $\Delta\sigma(T)$ , at  $n_a = \text{ct.}$ , (according Fig. 14), it has the maximum value of  $\Delta\sigma(T) = -25.65$  %, at  $n_a = 0$  years and  $T = 30$  °C.

Concerning to the state of stress that can be reached up to the admissible limits of the material cover ( $\sigma_a = 710$  N/mm<sup>2</sup> and  $\sigma_r = 1100$  N/mm<sup>2</sup>), due to the maximum working pressure and the explosion pressure, influenced by the growth of corrosion and temperature variation, it is found that both pressures decrease.

At the beginning of the operating period, when  $n_a = 0$  years, the pressure of the cover, which is initially higher by  $\Delta p = 151.66$  % than the hydraulic pressure test, decreases with  $\Delta p = 249.33$  %, until the end of the exploitation period,  $n_a = 20$  years, and the explosion pressure which is also initially greater than  $\Delta p = 249.33$  %, also decreases with  $\Delta p_{\text{max}} = 22.68$  %.

### 4. Conclusions

This paper presents a study concerning the simultaneous influence of temperature and corrosion on Von Mises efforts in the lateral cylindrical cover of a pressurized fuel tank. In the calculation a parameterized model sectioned into  $\frac{1}{4}$  of the initial model was used. The lateral cover was optimally dimensioned at mechanical stresses, with the additional minimum mass condition.

The CAD simulation on the Von Mises effort state was done and the 3D variation of the stress  $\sigma(n_a, T)$  was studied together with the particular cases of variation for  $\sigma(n_a = ct, T)$  and  $\sigma(n_a, T = ct)$ , at the same time determining the polynomials of variation through interpolation.

The final conclusion is that the influence of corrosion and temperature on the Von Mises efforts in the side cover is important and cannot be neglected in design process.

**Financial disclosure:** The author has no financial or proprietary interest in any material or method mentioned.

**Competing interests:** The author declare that he has no significant competing financial, professional or personal interests that might have influenced the performance or presentation of the study.

## References

- [1] A.C. Nedelcu, “Romanian automotive industry – analysis made from the intellectual capital perspective”, *Revista Economica*, vol. 67, no. 5, pp. 80-89, 2015;
- [2] A. Misztal, N. Belu, N. Rachieru, “Comparative Analysis of Awareness and Knowledge of APQP Requirements in Polish and Romanian Automotive Industry”, *Applied Mechanics and Materials*, vol. 657, pp. 981-985, 2014;
- [3] A. Hagi, M. Platis, “The evolution of the Romanian car industry and its position on European market”, *STUDIA UBB NEGOTIA*, vol. 57 (LVII), 2, pp. 65 - 91, 2012;
- [4] G. Matache, C. Cristescu, C. Dumitrescu, V. Miroiu, “Pregătirea specialiștilor în vederea adaptabilității și creșterii competitivității”, *Magazine of Hydraulics, Pneumatics, Tribology, Ecology, Sensorics, Mechatronics (HIDRAULICA)*, no. 3-4, pp. 7-14, 2012. ISSN 1453-7303;
- [5] Chen Shr-Hung, “Novel design and optimization of vehicle’s natural gas fuel tank”. Master’s Thesis presented to the Faculty of the College of the Engineering and Technology, Ohio University, March 1997;
- [6] E. Lisowski, W. Czyzycki, “Transport and storage of LNG in container tanks”, *Journal of KONES Powertrain and Transport*, vol. 18, no. 3, pp. 193-201, 2011;
- [7] M.C. Ghiță, A.C. Micu, M. Țălu, Ș. Țălu, “Shape optimization of vehicle's methane gas tank”, *Annals of Faculty of Engineering Hunedoara - International Journal of Engineering, Hunedoara, Tome X, Fascicule 3*, pp. 259-266, 2012;
- [8] M.C. Ghiță, A.C. Micu, M. Țălu, Ș. Țălu, E. Adam, “Computer-Aided Design of a classical cylinder gas tank for the automotive industry”, *Annals of Faculty of Engineering Hunedoara - International Journal of Engineering, Hunedoara, Tome XI, Fascicule 4*, pp. 59-64, 2013;
- [9] M.C. Ghiță, A.C. Micu, M. Țălu, Ș. Țălu, “3D modelling of a gas tank with reversed end up covers for automotive industry”, *Annals of Faculty of Engineering Hunedoara - International Journal of Engineering, Hunedoara, Tome XI, Fascicule 3*, 2013, pp. 195-200, 2013;
- [10] M.C. Ghiță, A.C. Micu, M. Țălu, Ș. Țălu, “3D modelling of a shrink fitted concave ended cylindrical tank for automotive industry”. *Acta Technica Corviniensis – Bulletin of Engineering, Hunedoara, Romania, Tome VI, Fascicule 4*, pp. 87-92, 2013;
- [11] M.C. Ghiță, C.Ș. Ghiță, Ș. Țălu, S. Rotaru, “Optimal design of cylindrical rings used for the shrinkage of vehicle tanks for compressed natural gas”, *Annals of Faculty of Engineering Hunedoara - International Journal of Engineering, Hunedoara, Tome XII, Fascicule 3*, pp. 243-250, 2014;
- [12] M.C. Ghiță, A.C. Micu, M. Țălu, Ș. Țălu, “Shape optimization of a thoroidal methane gas tank for automotive industry”, *Annals of Faculty of Engineering Hunedoara - International Journal of Engineering, Hunedoara, Tome X, Fascicule 3*, pp. 295-297, 2012;
- [13] M.V.J. Bhavana, Rao S. Janardhana, B A.N. Murthy, “Design and analysis of horizontal LPG storage pressure vessel for variable dimensional constraints under given physical parameters”, *International Journal & Magazine of Engineering, Technology, Management and Research*, vol. 4, issue 5, pp. 342 - 351, 2017;
- [14] Ș. Țălu, “Limbajul de programare AutoLISP. Teorie și aplicații”, (AutoLISP programming language. Theory and applications), Cluj-Napoca, Risoprint Publishing house, 2001;
- [15] Ș. Țălu, “AutoCAD 2005”, Cluj-Napoca, Risoprint Publishing house, 2005;
- [16] Ș. Țălu, “Geometrie descriptivă” (Descriptive geometry), Cluj-Napoca, Risoprint Publishing house, 2010;
- [17] A. Florescu-Gligore, M. Orban Ș. Țălu, “Cotarea în proiectarea constructivă și tehnologică” (Dimensioning in technological and constructive engineering graphics), Cluj-Napoca, Lithography of The Technical University of Cluj-Napoca, 1998;
- [18] A. Florescu-Gligore, Ș. Țălu, D. Noveanu, “Reprezentarea și vizualizarea formelor geometrice în desenul industrial” (Representation and visualization of geometric shapes in industrial drawing), Cluj-Napoca, U. T. Pres Publishing house, 2006;
- [19] Ș. Țălu, C. Racocea, “Reprezentări axonometrice cu aplicații în tehnică” (Axonometric representations with applications in technique), Cluj-Napoca, MEGA Publishing house, 2007;

- [20] C. Racocea, Ș. Țălu, “Reprezentarea formelor geometrice tehnice în axonometrie” (The axonometric representation of technical geometric shapes), Cluj-Napoca, Napoca Star Publishing house, 2011;
- [21] Carlos Martines Ortiz, “2D and 3D shape descriptors”. Thesis for the degree of Doctor of Philosophy in Computer Science, University of Exeter, GBR, 2010;
- [22] Ș. Țălu, M. Țălu, “A CAD study on generating of 2D supershapes in different coordinate systems”, Annals of Faculty of Engineering Hunedoara - International Journal of Engineering, Hunedoara, Tome VIII, Fascicule 3, pp. 201-203, 2010;
- [23] Ș. Țălu, M. Țălu, “CAD generating of 3D supershapes in different coordinate systems”, Annals of Faculty of Engineering Hunedoara - International Journal of Engineering, Hunedoara, Tome VIII, Fascicule 3, pp. 215-219, 2010;
- [24] Ș. Țălu, “CAD representations of 3D shapes with superellipsoids and convex polyhedrons”, Annals of Faculty of Engineering Hunedoara - International Journal of Engineering, Hunedoara, Tome IX, Fascicule 3, 2011, pp. 349-352, 2011;
- [25] Ș. Țălu, “Study on the construction of complex 3D shapes with superellipsoids and supertoroids”, Annals of Faculty of Engineering Hunedoara - International Journal of Engineering, Hunedoara, Tome IX, Fascicule 3, pp. 299-302, 2011;
- [26] Ș. Țălu, “Complex 3D shapes with superellipsoids, supertoroids and convex polyhedrons”, Journal of Engineering Studies and Research, Bacău, vol. 17, no. 4, pp. 96-100, 2011;
- [27] Ș. Țălu, “Generation of 3D shapes with superellipsoids, supertoroids, super cylinders and super cones”, Journal of Engineering Studies and Research, Bacău, vol. 18, no. 2, pp. 135-139, 2012;
- [28] Ș. Țălu, M. Țălu, “AutoCAD 2006. Proiectare tridimensională” (AutoCAD 2006. Three-dimensional designing), Cluj-Napoca, MEGA Publishing house, 2007;
- [29] Ș. Țălu, “Reprezentări grafice asistate de calculator” (Computer assisted graphical representations), Cluj-Napoca, Osama Publishing house, 2001;
- [30] Ș. Țălu, “Grafică tehnică asistată de calculator” (Computer assisted technical graphics), Cluj-Napoca, Victor Melenti Publishing house, 2001;
- [31] Ș. Țălu, “AutoCAD 2017”, Cluj-Napoca, Napoca Star Publishing house, 2017;
- [32] T. Nițulescu, Ș. Țălu, “Aplicații ale geometriei descriptive și graficii asistate de calculator în desenul industrial” (Applications of descriptive geometry and computer aided design in engineering graphics), Cluj-Napoca, Risoprint Publishing house, 2001;
- [33] C. Bîrleanu, Ș. Țălu, “Organe de mașini. Proiectare și reprezentare grafică asistată de calculator” (Machine elements. Designing and computer assisted graphical representations), Cluj-Napoca, Victor Melenti Publishing house, 2001;
- [34] Ș. Țălu, “Micro and nanoscale characterization of three dimensional surfaces. Basics and applications”, Napoca Star Publishing House, Cluj-Napoca, Romania, 2015;
- [35] M. Țălu, “Calculul pierderilor de presiune distribuite în conducte hidraulice” (Calculation of distributed pressure loss in hydraulic pipelines), Craiova, Universitaria Publishing house, 2016;
- [36] M. Țălu, “Pierderi de presiune hidraulică în conducte tehnice cu secțiuni inelară. Calcul numeric și analiză C.F.D.” (Hydraulic pressure loss in technical piping with annular section. Numerical calculation and C.F.D.), Craiova, Universitaria Publishing house, 2016;
- [37] M. Țălu, “Mecanica fluidelor. Curgeri laminare monodimensionale” (Fluid mechanics. The monodimensional laminar flow), Craiova, Universitaria Publishing house, 2016;
- [38] M. Rusănescu, "Material requirements planning, inventory control system in industry", Magazine of Hydraulics, Pneumatics, Tribology, Ecology, Sensorics, Mechatronics (HIDRAULICA), no. 1, pp. 21-25, 2014. ISSN 1453-7303;
- [39] Ș. Țălu, M. Țălu, "The influence of deviation from circularity on the stress of a pressurized fuel cylindrical tank", Magazine of Hydraulics, Pneumatics, Tribology, Ecology, Sensorics, Mechatronics (HIDRAULICA), no. 4, pp. 34-45, 2017, ISSN 1453-7303;
- [40] D. Vintilă, M. Țălu, Ș. Țălu, “The CAD analyses of a torospheric head cover of a pressurized cylindrical fuel tank after the crash test”, Magazine of Hydraulics, Pneumatics, Tribology, Ecology, Sensorics, Mechatronics (HIDRAULICA), no. 4, pp. 57-66, 2017, ISSN 1453-7303;
- [41] M. Bică, M. Țălu, Ș. Țălu, “Optimal shapes of the cylindrical pressurized fuel tanks”, Magazine of Hydraulics, Pneumatics, Tribology, Ecology, Sensorics, Mechatronics (HIDRAULICA), no. 4, pp. 6-17, 2017, ISSN 1453-7303;
- [42] \*\*\* Autodesk AutoCAD 2017 software;
- [43] \*\*\* SolidWorks 2017 software;
- [44] \*\*\* Microsoft Excel 2017 software;
- [45] \*\*\* Maple 2016 software.

## Examining Fire Pump Metz FP 24/8 on Cavitation

Assist. Prof. PhD. Stud. Eng. **Nikolett FECSER**<sup>1</sup>, Assist. Prof. PhD. **Rajmund KUTI**<sup>2</sup>

<sup>1</sup> Széchenyi István University, Department of Mechatronics and Machine Design H-9026 1 Egyetem tér, Győr, fecser.nikolett@sze.hu

<sup>2</sup> Széchenyi István University, Department of Mechatronics and Machine Design, H-9026 1 Egyetem tér, Győr, kuti.rajmund@sze.hu

**Abstract:** *For the safe operation of pumps, it is essential to examine the operation parameters, in particular regarding fire pumps, which are occasionally used under extreme conditions. Operation deviating from the operational parameters defined by the manufacturers would damage the pumps. The majority of specialists who are experts at pump technology and fluid mechanics are familiar with cavitation and aware of its detrimental effects. Our goal is to call the attention to the proper way of the operation of centrifugal pumps, the cavitation generated during operation as a harmful phenomenon and its development examined in practice by us. Firstly, in our study we will briefly present the cavitation as a phenomenon taking place during operation and its counting method. Then we state the results of our measurements carried out during the operation of a pump built in a fire engine type Metz FP 24/8.*

**Keywords:** *Operation of a pump, centrifugal pump, operational parameters, cavitation, NPSH*

### 1. Introduction

In order to maintain an uninterrupted water supply and to achieve effective firefighting, it is vital to ensure the safe operation of fire pumps. Factors like terrain, the conditions of the places to obtain water from and the quality of water highly influence the performance of the pumps, which can change significantly and alter from the expected values. Operation not in conformity with the standards recommended by the manufacturer can result in a decline in performance or a failure of the pump. Cavitation is one of the phenomena which causes pump failure and whose development we monitored in our practical tests. Before presenting our measurements, we find it important to give a short introduction to cavitation and the mathematical basis of its calculation to help a better understanding of the topic. We believe that publishing our experience contributes to the safe operation of fire pumps.

### 2. Defining cavitation

The available scientific literature provides several definitions for cavitation. István Józsa claims that the physical process of cavitation is linked to the phenomenon of the boiling point, because if saturated steam pressure corresponding to the temperature develops at a given location in the flowing fluid, there the fluid turns into vapour and a bubble filled with steam evolves. The head space of the bubble is condensed of the flow travels the vapour cavity (i.e. bubble) into a location of higher pressure and the bubble implodes as a result of the thus created vacuum. This bubble implosion is called cavitation [1]. According to another definition, cavitation takes place when the gas bubbles developed in the fluid suddenly collapse. This process takes place at those locations in the pump where the pressure is subjected to the vapour-pressure of the pumped medium. Vapour-pressure of a fluid is a kind of pressure at which the fluid starts boiling or vaporising. Cavitation, which may cause even serious damage to the pump, occurs when the Net Positive Suction Head (NPSH) needed for the pump is not available [2]. Intense shock waves, various sound effects (cracking, flapping and sometimes howling sounds), changed fluid mechanics characteristics, significant decline of performance and mechanical errors belong to the detrimental effects of cavitation. Cavitation has a decisive effect on the pump's ability to suck as well. During the operation of the pump, the fluid entering from the suction pipe to the impeller has the lowest pressure here.

When cavitation occurs at this location, the flow pattern of rotating pump wheel changes along with the pump characteristic curves. [3].

Cavitation is divided into two classes:

- Physical cavitation: a smaller type of cavitation occurs under normal operational conditions in holes or due to detachments caused by collision. Its effects can be tracked down by noise and smaller erosive dissolutions. The effects are undetectable in the pump characteristic curves and do not cause reduction in transfer or a decline in efficiency.
- Mechanical cavitation: causes “detachments” in the pump characteristic curves and the operation of the pump becomes chaotic.

Cavitation can occur in the course of operating pumps used by firefighters. In the initial phase well-detectable noises develop, then continuously stronger and stronger shockwaves and vibrations are forming in the fluid and the travelling systems. Since the fluid has a minimum pressure at the leading edge of the impeller from the direction of the suction pipe, this is the location where cavitation may occur the earliest. The decrease of suction depth, applying suction pipes with a narrow diameter, resistance emerged in the suction pipe or an increase in the temperature of the fluid all contribute to the emergence of the phenomenon. [4].

## 2. 1. The mathematical basis of cavitation

Manometric suction head value

$$H_{sm} = \frac{p_0 - p_1}{\rho \times g} = A_0 - h_1 = H_{sg} + h'_s + h_c \quad (1)$$

Table 1: Labels

Name	Signal	Unit of Measure
Manometric suction head	$H_{sm}$	m
Atmosphere	$p_0$	bar
Pressure measured in suction pipe in front of the impeller	$p_1$	bar
Saturated steam pressure	$p_g$	bar
Amount of pressure drop	$\Delta p$	bar
Water density at 20°C 998.23 kg/m <sup>3</sup>	$\rho$	kg/m <sup>3</sup>
Gravitational acceleration 9.81 m/s <sup>2</sup>	$g$	m/s <sup>2</sup>
Height of atmospheric pressure	$A_0$	m
Pressure at blades entering	$h_1$	m
Geodetic suction depth	$H_{sg}$	m
Frictional and hydraulic resistance of suction pipe	$h'_s$	m
Geodetic suction height	$h_c$	m
Blade depression value	$\Delta h$	m

$$A_0 = \frac{p_0}{\rho \times g} \quad (2)$$

$$h_1 = \frac{p_1}{\rho \times g} \quad (3)$$

$$h_g = \frac{p_g}{\rho \times g} \quad (4)$$

$$h_c = \frac{c_1^2}{2g} \quad (5)$$

$$H_{sm} = \frac{p_0 - p_1}{\rho \times g} = A_0 - h_1 = H_{sg} + h'_s + NPSH_{pump} = \Delta h + h_c \quad (6)$$

$$NPSH_{pump} = \Delta h + h_c \quad (7)$$

$$\Delta h = \frac{\Delta p}{\rho \times g} \quad (8)$$

$$NPSH_{system} = A_0 - H_{sg} - h'_s - h_g \quad (9)$$

The condition of a cavitation-free operation:

$$NPSH_{system} \gg \gg \gg NPSH_{pump} \quad (10)$$

### 3. Introduction to Measurement

Our measurements were carried out on field and we used the Csepel-Metz TLF 24/50 type heavy-duty truck fire hose illustrated in Figure 1 into which a Metz FP 24/8 centrifugal pump was inbuilt whose drive is ensured by the engine through the driving mechanism mounted on the gear box. In our measurement we gradually increased the performance of the pump under the conditions determined by us, then we provoked cavitation and measured the change in the performance of the pump.



Fig. 1. Csepel-Metz TLF 24/50 heavy-duty truck fire hose and the inbuilt FP 24/8 type pump (Sources: Authors' photos)

#### 3.1. The tools applied for the measurement

In accordance with the regulations applied by fire departments, standard fire-fighting equipment and pressure hoses were used during the measurement. 1 piece of suction hose “A” of  $d=110$  mm internal diameter, 4 pcs of pressure hoses “B” of  $d=75$  mm internal diameter, 8 pcs of pressure hoses “C” of  $d = 52$  mm inner diameter and 4 pcs of 75/52 quadruple stands were applied during the installation. The amount of water carrying through the hoses was measured by a MOM 4233 type certified flow meter (fire hydrant pitot tube) and the amount of water exiting the nozzle was measured by CSSZ C52 type flow meter. In the case of the rest of the water streams we applied 7 pcs of standard curved hoses fitted with a manual shut-off valve and the diameters of its nozzle equals to the diameter of the nozzle of the measuring hose.

#### 3.2. Measuring nominal fluid flow and cavitation

Regarding fire pumps, the manufacturing companies measure the flow performance of the pumps under laboratory conditions creating an optimal operational environment. The nominal fluid flow of the Metz FP 24/8 type fire pump examined by us is  $Q = 2400$  l/p, at  $H_{sg} = 1.5$  m suction depth. In the course of firefighter interventions the operational conditions of the pumps are not optimal in most cases, thus flow performance alters. So we found it crucial to measure the nominal fluid flow of the pump under the conditions we provided. The pump measured by us has 1 pc of intake

manifold “A” of  $d = 110$  mm inner diameter, 4 pcs discharge manifolds “B” of  $d=75$  mm inner diameter and 1 pc of water cannon with carrying  $Q=1600$  l/p fluid. During the measurement we used 4 pcs of fire hose “B” and 8 pcs of fire hose “C”, 4 pcs of stands, 7 pcs of standard, 1 pc of fire hydrant pitot tube and 1 pc of flow meter. We stood the fire engine by a pool used for storing firefighter-water and the intake manifold of the pump got connected to the connection point built for suction by 1 piece of suction hose “A”. The water level was set 1.5 m above the centre line of the pump shaft. All the four discharge manifolds of the vehicle were assembled with multiple streams, 1 pc with hose B and 2 pcs with hose, C each of  $d=52$  mm inner diameter. A flow meter type MOM 4233 was built into one of the main hoses. A flow meter type CSSZ C52 with a  $d = 16$  mm inner diameter nozzle was connected to the first stream. The flow meter is fitted with a certified pressure gauge, which comes with a factory catalogue. The catalogue makes the mating of discharge pressure and the belonging water amount easy, which simplifies the process of our measurement and calculating with losses generated in the hoses is unnecessary. Since the fire hose nozzle jet we applied is identical with the jet mounted on the flow gauge, the amount of water discharged at each stream can be taken as equal. Figure 2 shows the arrangement we set and made the firefighting system operate, and the tools were marked by the conventional signs of the fire-station.

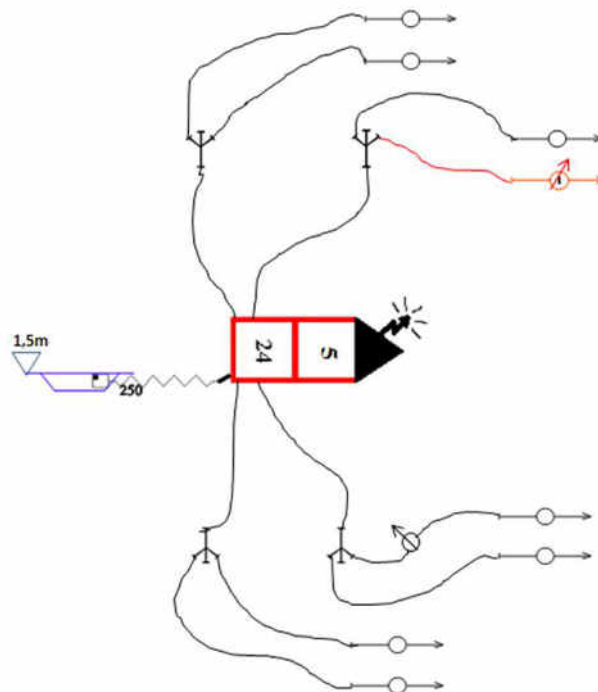


**Fig. 2.** The design of the firefighting system operated by the authors (Source: Illustration by the Authors)

The streams were operated at the height of the pump as shown in Figure 3.

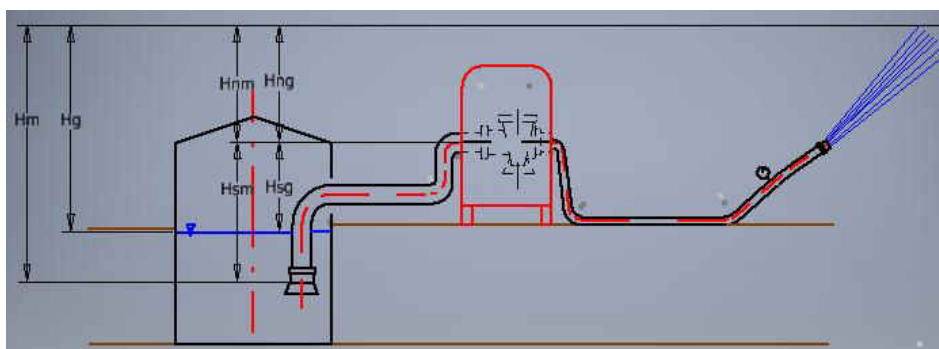


**Fig. 3.** Process of measurement (Source: Illustrated by the Authors)

We determined a 5 bar outlet pressure of the pump i.e. in the course of the actual firefighting the firefighters work with such pressure. First we put the stream mounted on the flow gauge into operation and gradually increased the pump performance up to 5 bar. Table 2 and Figure 4 illustrate the changes of the flow rate in the case of the first stream.

**Table 2:** The flow rate changes of the first stream

Pressure [bar]	Flow rate [l/min]
0	92
0.5	131
1	164
1.5	198
2	231
2.5	257
3	283
3.5	306
4	328
4.5	347
5	366

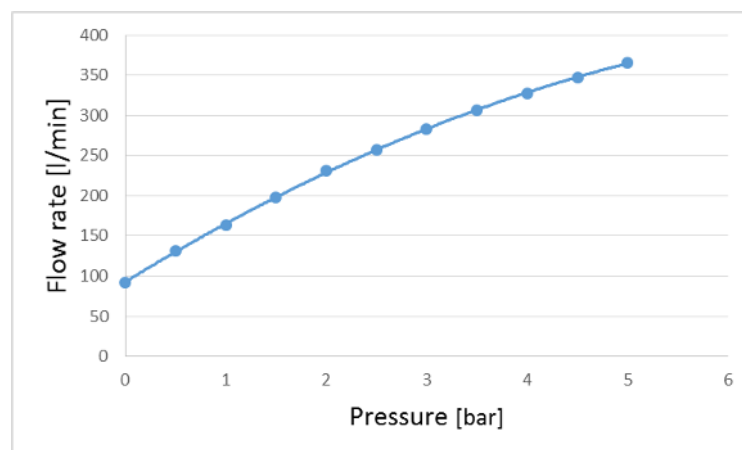


**Fig. 4.** The flow rate changes of the first stream (Source: Illustrated by the Authors)

Reaching the 5 bar outlet pressure, we also measured an approximately 5 bar pressure at the nozzle. Next, opening the closing devices slowly, we put the streams into operation one by one. The outlet pressure of the pump and the streams started to decrease continuously. After putting the 8<sup>th</sup> stream into operation, the pressure of the discharged water at the nozzle was 3 bar with 283 l/p water output set in the catalogue, which meant 2264 l/p water output totally calculated with the 8 operating streams.

Our next task was to increase water flow up to reaching 5 bar pressure, then the appearance of cavitation. Finishing the measurement, the pump was kept operating 8 streams. The refilling of the water storage tank was continuous in order to keep the 1.5 m suction depth. First, we decreased the revolution of the pump until it reached 1 bar discharge pressure to be able to draw a precise operational diagram, then we started to increase the revolution. Water flow was measured continuously and its measurements are recorded in the following table. Before reaching 4 bar pressure, the pump started to produce a rattling noise and suction pressure dropped below 0.06 bar. We continued to increase the revolution and the discharge pressure reached 4 bar. The pump grew louder and louder emitting crackling sounds and the discharge pressure dropped below 2 bar, then after a short period of time it started to decrease, then dropped back again. By that time cavitation had appeared. Discharge pressure reached 4 bar at the water flow meter for a short

period of time and the water quantity belonging to this value was 328 l/p in the catalogue and operating with 8 streams, the performance of the pump was 2624 l/p. To avoid damages, we started to decrease pump rev and finally stopped it. Figure 5 shows the values measured at the pump and the nozzle at the time of cavitation [6].



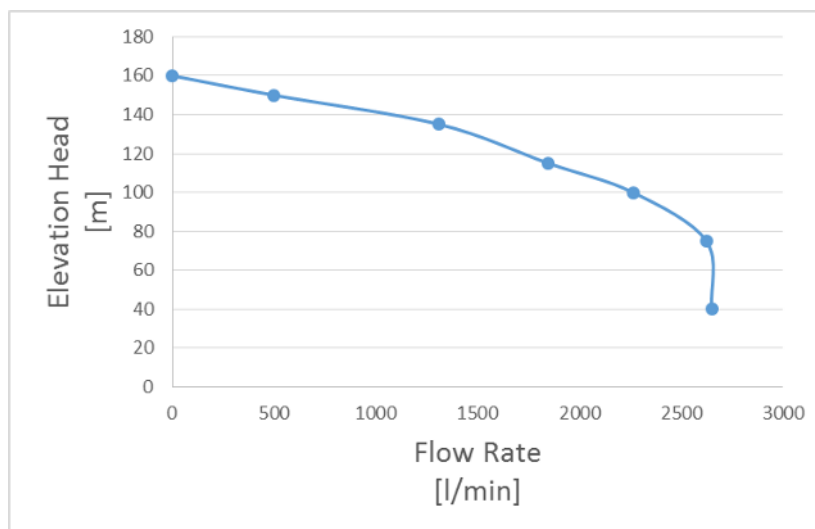
**Fig. 5.** The measured values on the Metz FP 24/8 type fire pump and the pitot tube at the moment of the cavitation (Source: Authors’ captures)

Table 3 is a demonstration of measurement results of operating 8 hose streams.

**Table 3:** Measurement results

Pressure [bar]	Elevation head [m]	Flow rate [l/min]
0	160	0
1	150	500
1.5	135	1312
2	115	1848
3	100	2264
4	75	2624
1.6	40	2650

Based on the measured values the characteristic curve of the operational process can be drawn. The following diagram illustrates the characteristic curve of a pump type FP 24/8. The appearance of cavitation in the pump was by a loud noise, there was a sudden drop in the pressure, due to which the characteristic curve broke down.



**Fig. 6.** Characteristic curve of a FP 24/8 type pump (source: Authors’ design)

In order to justify cavitation we made calculations as can be seen below.

$$NPSH_{pump} = \Delta h + h_c = 15.252 \text{ m} \quad (11)$$

$$NPSH_{system} = A_0 - H_{sg} - h'_s - h_g = 5.857 \text{ m} \quad (12)$$

$$NPSH_{system} \lll NPSH_{pump} \quad (13)$$

Our calculation shows that cavitation was generated in the system. We concluded that due to the appearance of cavitation it is not possible to achieve 5 bar pressure with operating 8 streams and applying feeding with suction. If the usage of 8 streams is inevitable during the firefighting activity, along with the pump type Metz FP 24/8 another pump is needed to be inserted into the system and connected in series to reach the required pressure and water quantity regarding all the streams [7].

#### 4. Conclusion

During the course of our research, in order to examine cavitation, we used a Csepel-Metz TLF 24/50 heavy-duty truck fire hose, into which a Metz FP 24/8 type centrifugal pump is built. We conducted measurements in field creating a realistic firefighting environment. The scientific examination of cavitation assists manufacturers and users to avoid this undesirable phenomenon, which can lead to the failure of the pump. Its possible solution is to determine the NPSH parameter and to take it into account when you are choosing and installing the pump and during its operation. We find on field measurements essential, the results of which improve the practical usage of pumps in general. Moreover, these measurements are of high importance in the case of the pumps used for firefighting purposes, where cavitation occurs suddenly and can even negatively influence the success of the fire extinguishing activity and an incidental failure of the pump can result in unexpected costs.

#### References

- [1] Cs. Fáy, Á. Trokolanski, J. Varga, “Szivattyúüzemi kézikönyv”, Műszaki Könyvkiadó, Budapest, 1966, pp.11-45;
- [2] I. Józsa, “Örvényszivattyúk a gyakorlatban”, Invest-Marketing Bt., Budapest, 2013, pp. 108-196;
- [3] M. Pázmándy, “A tűzoltás vízellátása”, Zrínyi Nyomda, Budapest, 1974, pp. 164-176;
- [4] F. Szlivka, “Vízgazdálkodás gépei”, 2002, pp. 63-75. Downloaded from: <http://www.ontozesmuzeum.hu/1.%20VIZGAZD%20aramlastani%20alapot%20tartalomjegyzekkel.pdf>;
- [5] B. Író, “A hő- és áramlástan gépei tárgyhoz kapcsolódó szivattyúüzemi mérések lebonyolításához mérési útmutató”, Győr, Széchenyi István Egyetem, 2015, pp. 3-19;
- [6] METZ FP 24/8 Feuerlöschpumpe Catalogue;
- [7] N. Fecser, “Examining the characteristics of Pedrollo\_CP130 centrifugal pump in simulated service conditions”, *Magazine of Hydraulics, Pneumatics, Tribology, Ecology, Sensorics, Mechatronics*, 2017:(2), pp. 40-49.

## Electronic Control Module for Test Stand on the Production Line of Hydraulic Cylinders and Rotary Hydraulic Motors

PhD. Eng. Radu RĂDOI<sup>1</sup>, Dipl. Eng. Alexandru HRISTEA<sup>1</sup>,  
Dipl. Eng. Bogdan TUDOR<sup>1</sup>, PhD. Stud. Eng. Mihai ALEXE<sup>1</sup>

<sup>1</sup> INOE 2000 – IHP Bucharest, radoi.ihp@fluidas.ro

**Abstract:** *In order to ensure the quality of the products delivered at the exit from the production lines there are used functionality testing stands which are located at the exit of the line. The functionality of the products is verified with the help of specialized stands. The testing stand can be controlled with dedicated electronic modules which ensure the logic of operation, or with PLC's. This paper will present an electronic module from a hydraulic motor testing stand, also provided with an operating console, which communicates serially with the control module.*

**Keywords:** *Test stand, electronic module, microcontroller, sensors*

### 1. Introduction

The electronic command module is intended for monitoring and controlling the installation of a test stand [1] which is intended for testing hydraulic cylinders and hydraulic motors. The module is capable of data acquisition from the transducers and detectors located on the installation and the control of the hydraulic installation and electro pump based on the operating graph – finite state machine (FSM) that describes the operation of the testing installation – according to the operating mode selected by the operator. In this paper is presented the description of the module, components and the operating program written in the microcontroller, based on which the electronic module for the test stand was made.

### 2. Electronic module description

The electronic module located on the device communicates with the operator console located next to the stand. Communication is physically implemented through a serial data line that complies with RS-232C specifications standard; the communication protocol used is a master protocol developed by the designer, master/slave type which uses a 7-bit ASCII coding.

The operator console contains controls and signaling to control the hydraulic installation of the test stand. The operating mode can be selected by means of two push-button controls with operation confirmation by illuminating the buttons. This makes possible the use of the “Move right” and “Left shift” or no mode is selected, the working pressure is disconnected. Hydraulic cylinder movement and hydraulic motor rotation are displayed on the console via two groups of signaling, each group having two optical signals: hydraulic cylinder movement, left/right signaling and hydraulic motor rotating group, left/right signaling. Specialized buttons are provided on the console in order to control the movement on left/right and to turn left/right. Another signaling group is located on the operator panel which allows checking the stats of the stand that are monitored: the minimum level of oil in the tank, connected pressure, maximum oil temperature and a signaling which indicates the state of communications between the console and the control module.

The module is built around a microcontroller of general use PIC16F876A manufactured by Microchip. Some of the important features of this microcontroller are:

- RISC architecture with 35 instructions with the length of one word (14 bits);
- Maximum operating speed is 200 ns on an instruction cycle;
- The program memory is a flash memory containing 8096 instructions;
- Data memory (RAM) is 368 bytes;
- EEPROM data memory is 256 bytes;

The PIC16F876A microcontroller features a wide variety of integrated peripheral devices such as:

- An 8-bit timer and two 16-bit timers;
- Two Capture/Compare/PWM modules with resolution of 12.5 ns in Capture mode, 200 ns in Compare mode and 10 bit maximum PWM resolution;
- Synchronous serial communication port that supports SPI (Master mode) and I2C;
- USART communication port with address detection;
- 10-bit analogue-to-five-channel digital converter;
- Two analog comparators;
- Programmable voltage reference.

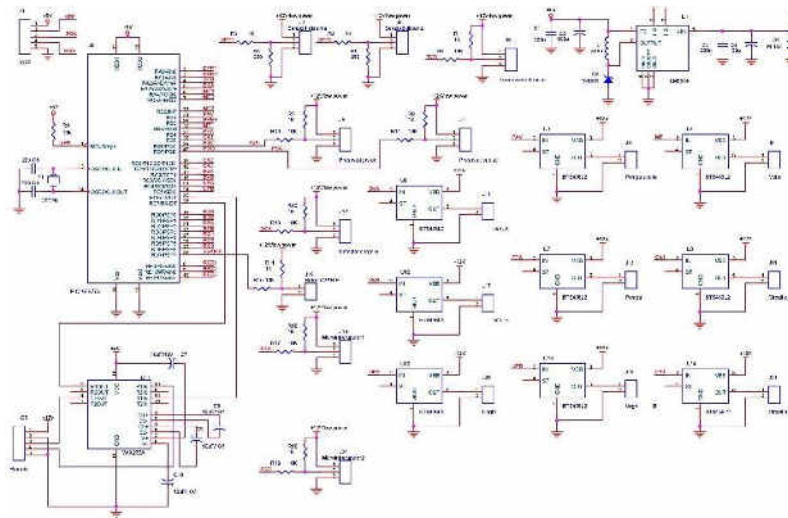


Fig. 1. Schematic of the electronic module

### 3. Elements of the electronic module

The electronic control module and operator console contain a stabilized voltage source, serial communication, analog and digital input circuits as well as digital outputs.

The stabilized voltage source receives at the input the supply voltage from the module, unstabilized continuous voltage in range of 9 to 36 V, providing a stabilized voltage at the output of 5 V with a current limitation of 0.5 A. The source is being built around the integrated circuit LM2574-05 (LM2574-05 is a step-down switch/buck converter).

The chosen solution of a switching voltage source because it has advantages in terms of high efficiency, wide range of input voltage, low wiring dimensions, reliability, etc.

The analog input circuits allow the coupling of four transducers with output of 4 to 20 mA powered by 2-3 wires. Each input has a three-pin connector: power supply (+), power supply (-) and a current input signal entering the electronic module. The circuit's input signal provides a current/voltage converter that transforms the current range from 4 to 20 mA into a voltage range of 1 to 5 V. This voltage is applied to an analog input of the analog/digital converter with successive approximations integrated into the microcontroller. The voltage input signal is available in the microcontroller as a 10-bit numeric value. The digital analog converter is configured to operate with a reference voltage of 5V, so the range is 0 ( $5 \cdot 5 / 1024 = 4.996$ ) V and it will be converted to numeric values in the 0 to 1023 range. The current signal provided by the transducer will be converted to numerical values corresponding to the range of 1 to 5 V and  $1024 / 5$  respectively = 205 to 2023. The resolution obtained on the transducer's working range is  $1023 - 205 = 818$  divisions. To improve the resolution of the signal read from the transducer, the "circular buffer" mediation technique uses the last 20 samples of the signal. In this way it is obtained a resolution of the analog input of 10,000 stable divisions on the transducer range.

The digital input circuits allow monitoring of the state of the contact type detectors such as thermocouples, limiters, and pressure switches [2]. The input circuit provides a current of 12 mA to "clean" the contact in the operating mode.

The digital output circuits allow the user to interface with the electronic module with the electromagnets of the hydraulic apparatus and the electropump. The output amplifier allows the control of an inductive DC load with a maximum of 10A being protected against overheating, voltage limits, overvoltage and reverse voltage resulting from the ON/OFF switching of the inductive load as well as from the short circuit at the load terminals.

With the right level of adaptors the serial communication enables communication with the electronic module using RS232, RS485, RS422 serial communication standards. The communication connector has a stabilized internal 5 Vcc source needed to power the communication adapter corresponding to the used standard like the TTL TX and RX level signals, transmission line(output module) and reception line(module input). For the multipoint communication lines is required a signal from the signal adapter and to switch between receive mode and the transmission mode. The signal for the operating mode selection is the TTL DIR level signal (direction).

The electronic module is provided with a ICSP header type connector (*In Circuit Serial Programming*).

The microcontroller operates with a 20 MHz quad-core oscillator clock that corresponds to an execution time of an instruction and instruction clock of 200 ns.

#### 4. The operating program in microcontroller memory

The operating program, written in the Flash memory of the microcontroller, was developed using ANSI C programming language. The program contains a sequence of initialization of microcontroller integrated circuits; the main operating loop contains a machine state that implements the electronic mode functionality and the interrupt handling routine, which performs the following: analogue acquisition, real time clock, display multiplexing, keypad reading and management of broadcast/ reception buffers for serial communication

The PIC16F877A microcontroller [3], with which the electronic module is build, treats the interruptions generated by various peripherals at the occurrence of specific events by saving the program counter's hardware stack and bypassing the execution of the instruction sequence to a fixed location in the program memory at 0x004 where the programmer inserts the interrupt handling code and as the last instruction, the instruction to return from the interrupt. The instruction restores to execution of the program from the point where it was interrupted by restoring the program counter to the stack. Note that the possibility of generating another interruption during the execution of the interrupt routine is deactivated upon entering the interrupt handling routine. Eventual interruption will be stored and treated later. A typical interrupt routine includes saving the context of the main program, identifying the source that generated the interrupt, determining the event that generated the interruption, treating the disruption, restoring the context to the existing situation at the time of the interruption, and returning from the interruption to the normal execution flow.

The discontinuity routine dealt with interrupts generated by the following peripheral devices integrated into the microcontroller:

- The 16-bit TMR1 timer is used to generate the 1ms clock. In the initialization sequence, TMR1 is configured to increment at 200 ns (instruction clock) and interrupt generation at occurrence of the overflow event (TMR1 content goes from 0xFFFF to 0x0000); in the interrupt routine, the timer content is initialized with a t1ms value which allows the occurrence of the overflow event delayed by 1 ms respectively  $(0xFFFF - t1ms) \times 200 \text{ ns} = 1 \text{ ms}$ ;
- The analog to digital converter is configured to generate an interruption when the conversion result is available; then, after taking the conversion result, the next analog input to be read is chosen;
- The USART module is configured to generate interruptions if a character has been transmitted/received; the transmission of a character activates the switch to the next character to be transmitted from the transmission buzzer, while receiving a character involves updating the receiving buzzer with the received character. The termination of the transmission is signaled to the interrupt routine by presence of a character with ASCII 0

code in the transmission buffer; signaling to the main program of the end of the transmission is achieved by positioning the TXIE bit (transmission interrupt enable) to 0. At the reception, the appearance of the 0xa or 0xd characters requires, in accordance with the MODBUS ASCII specifications, the termination of the reception; the interrupt routine detects the reception of these characters and signals the event to the main program by inserting a character with the ASCII code 0 into the receiving bucket. Note that there are two pointers, one at the broadcast buffer and one at the receiving buzzer, which marks the current character received or to be transmitted.

The 1 ms interrupt routine performs the following tasks:

- Updates real time clocks used for time synchronization of processes;
- Updating the keyboard buttons
- The launch of analog-to-digital conversion
- Initiate the 1ms interrupt by loading TMR1 with the t1ms value and deleting the T1IF interrupt flag;

The analogue to digital converter interrupt routine performs the following tasks:

- Taking over the conversion result for the current analog input;
- Numerical filtering of the analogue signal from the current analogue input
- Establishing the analog input to be treated at the next interruption as the current analog input;
- The initialization of the interrupt of the analog to digital converter by deleting the ADIF interrupt flag;

The main execution loop contains a state machine that implements the operation of the electronic module.

## 5. Conclusions

Such an electronic module equipped with high side switches no longer requires intermediate relays as for PLCs to control the solenoids of the hydraulic devices.

Dedicated electronic modules may have the disadvantage that, in the event of a failure, there must necessarily be a backup module to avoid creating long interruptions of the installation.

If there is the wish to expand the functions of an electronic automation module, you must have spare input / output pins; otherwise the module must be redesigned.

## Acknowledgments

This work has been funded by the national NUCLEU Programme, project PN16-40-03-01, 5N/2016 ad4/2017, Phase 3.1.2 - Development of electronic control blocks for hydraulic mechatronic systems.

## References

- [1] M. Blejan, A. Drumea, “Design, Implementation and Testing of an Electrohydraulic System for Automated Winding Machine for Aluminum Wire Rods”, *2013 International Conference on Electronics, Computers and Artificial Intelligence (ECAI)*, Jun. 27-29, 2013, Proceedings Paper, ISBN: 978-1-4673-4937-6, Accession Number: WOS:000343672500033;
- [2] M. Blejan, P. Drumea, A. Mirea, I. Ilie, “Mechatronic module for monitoring the hydraulic parameters of the industrial production equipments”, *ISSE 2007 - 30<sup>th</sup> International Spring Seminar on Electronics Technology*, Cluj-Napoca, 9-13 May 2007, Conference Proceedings, pp. 501 – 506, E-ISBN: 987-1-4244-1218-1, Print ISBN: 987-1-4244-1218-1, DOI: 10.1109/ISSE.2007.4432908;
- [3] <http://ww1.microchip.com/downloads/en/DeviceDoc/39582b.pdf>.

## Study on the Use of Digital Hydraulics in P.E.T. Waste Baling Presses

Lect.Ph.D.Eng. **Iulian-Claudiu DUȚU**<sup>1</sup>,

Prof.Ph.D.Eng. **Sorin-Ștefan BIRIȘ**<sup>1</sup>, Prof.Ph.D.Eng. **Edmond MAICAN**<sup>1</sup>

<sup>1</sup> University Politehnica of Bucharest, iulian\_claudiu.dutu@upb.ro

**Abstract:** *In the energy efficiency era, modern industry machinery demand now more than ever intelligent and efficient electronic control modules, in order to gradually increase their technical performances. Classic hydraulic driven machinery are complex and reliable but trying to reconfigure their schematic is a very hard to do process, in some cases impossible. Machine flexibility and energy efficiency are probably two of the most important concepts that govern the world of equipment – installation – machine design engineers. Solving this sort of demands certainly leads to a rapid increase in electronic control system complexity and designing new electro-hydraulic equipment that use modern concepts such as digital hydraulics. Nevertheless, complex electronic modules require adequate software development [1]. Referring to a narrower case, hydraulic P.E.T. waste presses, they are well acquainted for their productivity versus low cost classic hydraulics installation. Still, there remains another issue that needs to be taken into account: energy efficiency. In this paper, the authors have investigated the possibility of using the digital hydraulics concept in replacing classic electrohydraulic directional valves of a small capacity P.E.T. waste press from the energy consumption point of view. Also, there will be discussed main advantages and disadvantages of using digital hydraulics over classic hydraulics in the particular case of a P.E.T. waste press.*

**Keywords:** Digital, hydraulics, P.E.T. waste, press.

### 1. Introduction

Digital hydraulics technical concept has entered the international scientific community around 1999, as an alternative to classic hydraulic driving circuits using proportional or servo equipment. However, strong inertia of the scientific community made the concept to develop very slowly. In present, digital hydraulic valves are slightly to be found in the commercial offer of traditional hydraulic manufacturers, but there are several functional models ready to be delivered to the market. There are a few among large hydraulic manufacturers have technical knowledge and capabilities to produce custom digital hydraulics equipment. Research laboratories of universities or institutes are continuously trying to optimize existing valves, but the greatest challenge still remains the development of capable software control algorithms or proper adjustment of certain constructive parameters of valves or their electromagnets – depending on which technical solution is adopted. Digital hydraulics have two alternative solutions to classic equipment both having the benefit of reducing general energy consumption of the hydraulic driving system: high frequency PWM switching or parallel connection of several 2/2 hydraulic directional valves (very similar to valve-islands) electrically controlled independently. In the second case, the valves are smaller, having reduced installation and maintenance costs over proportional equipment. They are also robust. In P.E.T. waste presses, the main problem is energy management due to the fact that the hydraulic pumping module must always operate at almost full capacity. This means high energy consumption in normal operating mode even if there are certain functional phases that does not require so much energy. There are made some experimental studies (Finland) on a fully functional digital hydraulic equipment, mounted on an excavator boom that revealed an energy consumption reduction up to 70%, in some phases of the actuation cycle. In that case, digital hydraulics equipment was used to replace classic hydraulic LS (Load-Sensing) system of the excavator.

### 2. State of the Art in Digital Hydraulics

The investigation starts from the idea of finding a technical solution to replace hydraulic proportional directional valves with new digital valve-islands, having equivalent operation principle,

connected in parallel, with lower acquisition and maintenance costs, higher reliability and reduced overall energy consumption. It is a well-known fact that hydraulic proportional directional valves are expensive - looking, at least, from two points of view: acquisition and operation. This type of hydraulic valves is also very sensitive to the variations of some of the working environment parameters, but all of these have been somehow compensated using complex electronic modules and sensors. Furthermore, the reliability of hydraulic proportional valves is still a sensitive subject, referring mostly to the work cycle downtime, that in most cases require highly qualified personnel to diagnose and to repair – leading to increased personnel costs. Hydraulic proportional directional valves are demanding continuous operation of the pumping module in order to compensate internal losses of the directional valves. Besides these considerations, it must be taken into account that in most cases hydraulic proportional directional valves demand supplemental anti-cavitation or compensation equipment which are expensive and have complex internal structure, contributing significantly to the overall energy consumption of the hydraulic driving system.

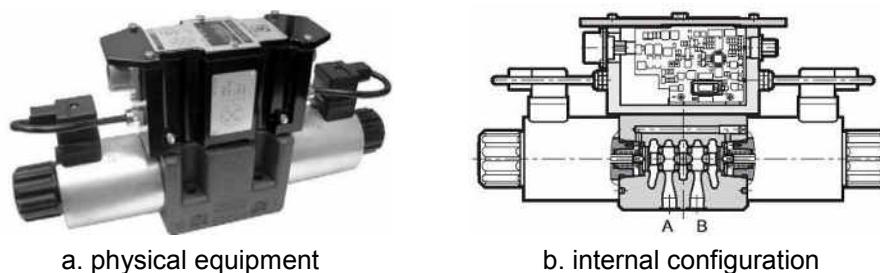
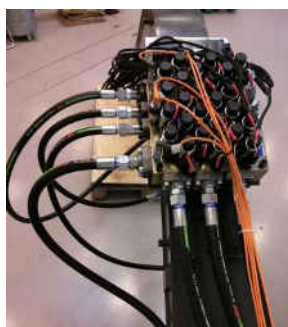
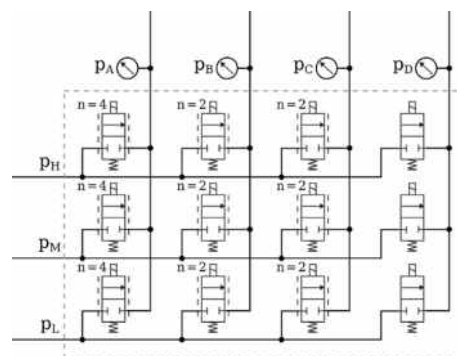


**Fig. 1.** Direct operated hydraulic proportional valve with integrated electronics proportional control [5]

As stated before, digital hydraulics valves are simpler being materialized by parallel connection of 2/2 poppet valves. In theory, these types of hydraulic directional valves have zero losses, leading to the idea that is not necessary for the pumping module to operate continuously, reducing overall energy consumption. There is not needed anymore a large, complex and low-energy efficiency pumping module, where digital hydraulics valves can properly operate with smaller pumping modules having in their structure one or more hydraulic accumulators (pressure storage reservoir). From the start we can observe an improvement of the energy efficiency of the system.



a. physical equipment



b. inner schematic

**Fig. 2.** Digital hydraulics valve [3]

Hydraulic 2/2 poppet valves, main components of the valve-islands, have small physical dimensions, they are robust and having lower acquisition, maintenance and operation costs than the proportional valves. Supposing that one of the poppet valves in the valve-island is not functional anymore, the automated electronic driving module will dynamically reconfigure the remaining operational valves of the valve-island in order to maintain process parameters near the setpoint values. Considering the case of hydraulic proportional directional valves, when one valve is defective, in most cases, the entire process will be shut down or can cause serious damages or life-threatening situations. Supplemental safety equipment is required to reduce the risks on the environment and human or animal life – adding even more costs to the initial system configuration.

Main technical challenges encountered in the discussion classic vs. digital valves will be described in the following. The size of digital hydraulic valves, as seen when comparing Fig. 1.a. and Fig. 2.a., is a delicate issue being approximated three times larger than regular hydraulic proportional directional valves. There is an obvious need for several parallel connected valves to make a valve-island in order to obtain the same operating function as in a hydraulic proportional directional valve [3]. A question arises over the reliability and cost factors of such a digital valve configuration. Being a relatively new concept, digital hydraulics equipment are highly priced and rare when referring to already existing models of hydraulic proportional valves. On long term this drawback will be overcome due to the benefits of mass production, but nowadays it is very important to take into consideration that digital hydraulics is a pioneering field of science and technology. Having a relatively large number of valves in the valve-island configuration that need to be controlled independently, it is required to develop a proper model control strategy, directly dependent to the number of poppet valves in the valve-island. Considering that  $n$  is the number of parallel poppet valves in the valve-island configuration, there will be a maximum of  $2n$  possible control values for main digital valve's output. In the first place, main problem here will not be the value of  $n$ , but the speed of the electronic controller module when computing and trying to obtain an optimum combination of control values for a certain given state of the hydraulic system.

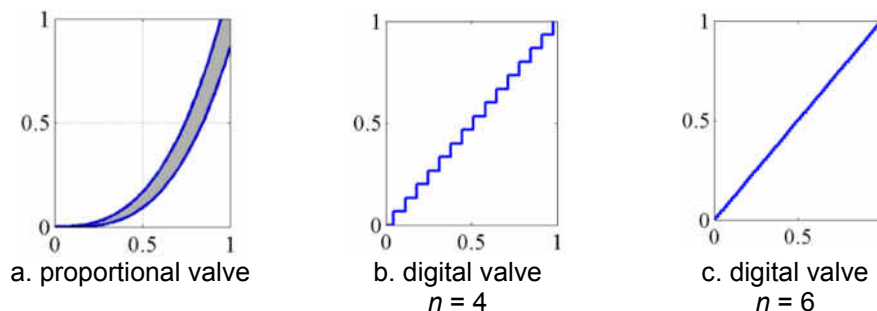


Fig. 3. Influence of  $n$  on valve's output [2]

As can be seen in Fig.3, there is a direct correlation between the value of  $n$  and valve's output, a large number of parallel valves in the construction of the digital valve result in a large range of possible output values, in the same time directly influencing the characteristic curve of the digital valve. The digital valve will always have an exact number of outputs that will always be obtained in the same conditions thus improving precision. In Fig.3.a, the valve characteristic is affected by hysteresis, while in the case of digital valves, Fig.3.b and Fig.3.c, the hysteresis does not exist. Optimal control is also a delicate issue in digital hydraulics: when defining the objective functions it can be found that these are pursuing opposite goals, such as a short transient regime of the working pressures, higher output flow resolution, higher energy efficiency, lower market costs – still an important aspect due to the novelty degree of the digital hydraulics field (implying higher costs), lower noise and vibration generated by the poppet valves themselves, being in a continuous switching working regime – where the amplitude value of the switching noise is relatively close to the value of response time. Referring to the case of classic hydraulic proportional directional valves, the switching noise is given by the constructive particularities of those.

Probably one of the most important advantages of digital valves over classic valves is their programmability, meaning that same digital valve can be used for different purposes [2], by simply reprogramming its software controller. In the case of digital valves, available number of functions that a valve can perform depends mostly on the software than its mechanical structure. Control software can be easily updated to give new functionalities to the valve. This new concept of digital hydraulics, has the benefits of working in real time and hydraulic losses reducing, depending on the application, digital valve reduces losses 30-98% [2]. In the Figure below, it is shown a very short technological progress of the hydraulics field over the years. From the 1960's where the energy losses were significantly higher than the useful work, energy efficiency was at a maximum value of 10%, the technical field of hydraulics has progressed towards LS (Load Sensing) systems and officially starting from year 2006 towards Digital Hydraulics. A load-sensing hydraulic pump will

always operate in a negative feedback control loop, establishing a new pressure drop every time the value of load pressure is changing.

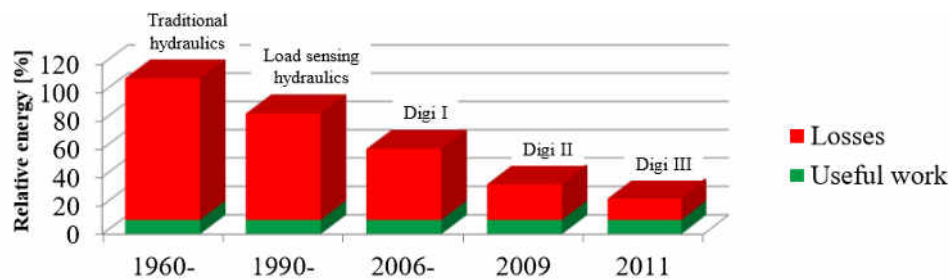


Fig. 4. Relative energy usage in hydraulics [2]

Digital hydraulics has already encountered three phases of scientific and technical development, progressively reducing the energy losses, obtained through scientific research and laboratory experiments. Limitations of current approaches in the digital hydraulics field are directly related to the novelty degree of the thematic, causing in the same time inertia in the scientific community, still adherent to classical hydraulics solutions. There are known very strong opinions that criticize the digital hydraulics field, on the difficulty to develop a highly intelligent control algorithms for digital hydraulics valves, on the limited valve resolution given by the limited number of directional valves in the valve-island, or on the still large physical dimensions vs. weight of the valve-islands or number of electrical wires and hydraulic hoses. The general trend of the industry is to miniaturize its equipment and digital hydraulics is not – nowadays – a part of that trend.

Some of the current technical approaches suggest instead of reinventing the field of hydraulics through digital hydraulics concept, to properly adjust the functional parameters of the existing hydraulic equipment available on the market, while promoting new functional models and intelligent control techniques in order to gain on the energy efficiency field. However, digital hydraulics tends to replace classic hydraulic circuits with their digital equivalent, using switching equipment and having significantly lower costs and higher efficiency. More or less, the limitations of the current approaches in digital hydraulics field are directly related to the costs of researches, still in the state of development and improvement, which implies the allocation of important funding of R&D departments of traditional hydraulic equipment manufacturers.

### 3. Digital Hydraulics and Baling Presses

Here, a question arises related to the necessity of retrofitting a hydraulic P.E.T. baling press when there are available on the market many constructive solutions with various degrees of automation and energy efficiency. In authors' opinion, baling presses are going to gain much more on the next years, knowing that every year thousands tones of used P.E.T. bottles from households of industry accumulate on waste management sites. The quantities are going to increase in the future, therefore the need of energy efficient pressing solutions will also increase, having direct impact on bales sizes, indirectly on pressed waste warehousing. Maximum working hydraulic pressure of a baling press is not always a fine measurement of its pressing efficiency, a more practical criteria is the compression degree of waste bales. Highly compressed bales can be stacked higher and safer in warehouses, also resulting in fewer bales, which reduces binding wire costs. On the logistics point of view, bales loading traffic and faster bales loading are also other benefits of energy efficient pressing.

The idea of replacing main hydraulic directional valve of one P.E.T. waste baling press, started from observing the functional cycle of an existing press in one of the laboratories of Faculty of Biotechnical Systems. The baling press construction is relatively simple, having a double metallic door design, self-latching closing technology, electro-hydraulic driving system, automated pressing cycle using sensors and microcontroller electronic board and a patented “rapid motion technology” that the manufacturer claim to reduce power consumption and to improve the cycle time by up to 40% compared to conventional drives [11]. There were made some improvements to the hydraulic power-pack, the pumping noise was reduced, with strong positive impact on both the human

operator and environment. Replacing the main hydraulic directional valve with a digital hydraulic valve (island-valve construction) it is supposed to overcome a major drawback of classic hydraulic directional valves as poor energy efficiency. Besides digital hydraulics, another solution is using load-sensing pumps, but these have high acquisition and operating costs. Of course, digital hydraulics is not probably the best cost-efficient solution (being an in-development technology), but in terms of energy it is. Another option in energy reduction is using distributed valves that are proven to reduce energy losses up to 50% in best cases.



**Fig.5.** Hydraulic baling press – studied model, available in one laboratory of Faculty of Biotechnical Systems

When thinking in terms of baling press modernization, besides energy efficiency improvements it must be taken into consideration the period of time in which the investment amortization costs will payback [12]. Looking from the economic environment point of view, this period of time must be short and bring also an increased productivity. In addition, baling press downtime, that is the retrofitting time, must also be close to a minimum – the best solution here is using distributed valves, not load-sensing. This is implying parallel connected on/off directional valves [13], having the benefits of fast switching times and redundancy. Another positive issue of using 2/2 valves is their so-called “immunity” against hydraulic oil impurities. In hydraulic systems the power supply unit is centralized having, in most of the cases, the directional valves mounted nearby and transmitting power to system’s motors, rotary or linear, through hoses or pipes that sometimes have considerable lengths. Statistics tell us that a large percent of hydraulic systems failures are related to hoses. Referring to Fig. 2.a, it can be seen that hydraulic hoses and digital hydraulics valves are very well acquainted to each other, meaning that in the digital case there will be used a significantly larger number of hydraulic hoses than the classic or proportional hydraulics case, to obtain a similar function. A larger number of hydraulic hoses implies a larger percent of failure.

Not only physical dimensions and number of hoses is the problem of a digital hydraulics system: each one of the 2/2 valves that are constructing the digital valve-island must be driven by an electromagnet. Available models of electromagnets used on commercial hydraulic equipment are not fast enough for digital hydraulics – opening and closing too slowly, far away from what it was intended to obtain. The electromagnets were redesigned in order to meet the speed demands of digital hydraulic valves. All led to an increase in control voltage. Again, referring to retrofitting the P.E.T. baling press, the electromagnets must be provided with voltage boosters and new control module. Wiring the electromagnets is another issue, both on the total electric cable length and total electrical current when all the electromagnets of the digital valve are switched on. Referring to Fig. 3 and considering a number of  $n = 6$  parallel poppet valves in the valve-island configuration and knowing that each electromagnet draws from the electrical power supply a current of almost 1A, we have a total of 6A when all electromagnets are ON. In case of a larger digital valve, for example the one shown in Fig. 2.a, a total of 27 A are needed from the electrical power supply. These values of electrical current are fair, but an electromagnet of a hydraulic proportional directional valve draws up to 800mA maximum from the electrical power supply. Considering a larger number of  $n$ , the larger the current needed when all electromagnets are switched on, in a worst case

scenario, a digital valve with a number of 100 2/2 valves will require 100 A! In that case, usual cables are not an option, so they need to be redesigned.

#### 4. Conclusions

Authors' current researches in the field of efficient P.E.T. waste pressing led to analyzing the idea of retrofitting a classic hydraulic baling press, using the digital hydraulics concept. Digital valve-islands made of 2/2 hydraulic directional valves seems to be a feasible solution over heavy and expensive load-sensing systems. The field of digital hydraulics is still in pioneering, researchers are still performing laboratory tests and formulating scientific hypotheses, their focus being on the development of optimal control strategies and valve development. Digital hydraulics can find the answer to some existing problems in hydraulics field, especially in energy efficiency and in the near future will replace available solutions. Still, digital hydraulics systems are using only one digital equipment in their configuration, such as directional valves, motors or pumps, and the others are classic or proportional equipment. When retrofitting an existing hydraulic system, fixed or mobile, it must be taken into account technical criteria such as available sensors, valves, power generators, functioning cycles, energy efficiency, control strategies, but also the economic criteria such as total cost control of the retrofitting and payback time. As a general conclusion, digital hydraulics has two strong advantages over classic hydraulics: energy efficiency and higher reliability.

#### Acknowledgments

This work has been funded by University Politehnica of Bucharest, through the “Excellence Research Grants” Program, UPB – GEX 2017. Identifier: UPB-GEX2017, contract no. 56/2017 (*DIGIPRESS*).

#### References

- [1] P. Boström, M. Linjama, L. Morel, L. Siivonen, M. Walden, “Design and Validation of Digital Controllers for Hydraulics Systems”, TUCS Technical Report, No 800, December 2006;
- [2] M. Linjama, “Digital Hydraulics”, Tampere University of Technology (TUT), Department of Intelligent Hydraulics and Automation (IHA);
- [3] M. Sethson, “The digital hydraulic challenge, to switch or not to switch”, Division of Fluid and Mechatronic Systems, Linköping University Sweden;
- [4] M. Linjama, K. Huhtala, “Digital hydraulic power management system—towards lossless hydraulics”, *Proceedings of the Third Workshop on Digital Fluid Power*, pp. 13-14, 2010;
- [5] Al. Dell’Amico, et al., “Investigation of a Digital Hydraulic Actuation System on an Excavator Arm”, *13-th Scandinavian International Conference on Fluid Power*, June 3-5, Linköping, Sweden, No. 092. Linköping University Electronic Press, 2013;
- [6] M. Jelali, A. Kroll, “Hydraulic servo-systems: modelling, identification and control”, Springer Science & Business Media, 2012;
- [7] C. Cristescu, C. Dumitrescu, G. Vrânceanu, L. Dumitrescu, “Considerations on energy losses in hydraulic drive systems”, *“Hidraulica” Magazine*, ISSN 1453-7303, Romania, No.1, pp. 36-46, 2016;
- [8] <http://www.hydraulicspneumatics.com>;
- [9] <http://www.directindustry.com>;
- [10] \*\*\*<http://www.valmet.com>, “Digital Hydraulics”, Technical Paper Series, U.S.A., March 2016, accessed in April 2017;
- [11] <https://eu.hsm.eu>;
- [12] M. Linjama, M. Paloniitty, L. Tiainen, K. Huhtala, “Mechatronic Design of Digital Hydraulic Micro Valve Package”, *Procedia Engineering*, Elsevier, vol. 106, pp. 97 – 107, 2015;
- [13] M. Linjama, M. Huova, P. Bostöm, A. Laamanen, L. Siivonen, L. Morel, M. Walden, M. Vilenius, “Design and Implementation of Energy Saving Digital Hydraulic Control System”, Vilenius, J. & Koskinen, K.T. (eds.), *The Tenth Scandinavian International Conference on Fluid Power (SICFP’07)*, May 21-23, Tampere Finland, 2 , pp. 341-359, 2007.

## Electronic Module for Data Acquisition and Transmitting for Portable Power Steering Test Equipment

Dipl. Eng. **Alexandru HRISTEA**<sup>1</sup>, PhD. Eng. **Radu RĂDOI**<sup>1</sup>,  
Dipl. Eng. **Bogdan TUDOR**<sup>1</sup>, Eng. **Ion BĂLAN**<sup>1</sup>

<sup>1</sup> INOE 2000-IHP, hristea.ihp@fluidas.ro

**Abstract:** *The electronic module allows the acquisition of data for testing the steering boxes and transmitting them to an android device through a web interface. Power steering is one of the most requested options in a car of small and medium size, for the vehicles weighing over 1200 kg entirely common. In figure 1 is represented the percent's according to the type of assistance steering boxes; from this graph, in conjunction with the average age of the fleet in Romania (13 years in the year 2017), it is deduced that most power-steering's mounted on cars have hydraulic power steering or electro-hydraulic, so the need for a portable test equipment is needed to discover and resolve the problem regarding faults of the system without disassembling the vehicle. Advantage of the device lies in its capability to transmit data that is collected by flow and pressure transducers and sent to a mobile (smartphone or tablet) or fixed device (PC) using Wireless technology. Also data can be transmitted to an operator who is specializes in repairing hydraulic steering boxes to confirm their state of function.*

*This article presents the electronic module for portable test equipment with data transmission for hydraulic power boxes and pumps from cars, this test device will have reduced dimensions and will be formed of a flow transducer and pressure transducer and a 2 way distributor with and a wireless module, all of which are connected to an electronic unit with an display located on the device panel. This data is then transmitted to a device that has a software application installed on it, capable of play back information that receives from the transducers.*

**Keywords:** *Fault test, power steering, public safety, automotive*

### 1. Introduction

The main important part of the system is the Wi-Fi data transmitter and the program, which measure the pressure and the flow of the power steering system.

Wi-Fi is a popular wireless networking technology. Wi-Fi stands for “wireless fidelity”. The Wi-Fi was invented by NCR corporation/AT&T in Netherlands in 1991. By using this technology we can exchange the information between two or more devices. Wi-Fi has been developed for mobile computing devices, such has laptops, but it is now extensively using for mobile applications and consumer electronics like televisions, DVD players and digital cameras. There should be two possibilities in communicating with the Wi-Fi connection that may be through access point to the client connection or client to client connection. Wi-Fi is a one type of wireless technology. It is commonly called as wireless LAN (local area network). Wi-Fi allows local area networks to operate without cable and wiring. It is making popular choice for home and business networks. A computer's wireless adaptor transfers the data into a radio signal and transfers the data into antenna for users.

The main advantages of wising Wi-Fi technology in industrial applications is versatility and rapid communication between devices, in our case between the mobile test equipment for power starring systems and the smart device (smartphone, tablet, PC, etc.).

#### **Advantages:**

- Wireless devices can be moved from one place to another place
- Wi-Fi network communication devices without wire can reduce the cost of wires.
- Wi-Fi setup and configuration is easy than cabling process
- It is completely safe and it will not interfere with any network
- We can also connect internet via hot spots
- We can connect wirelessly to any device

## 2. Product description

The electronic module of portable test equipment is provided with data transmission, fig. 1, is a new product which allows testing of the hydraulic power steering system of vehicles without having to dismantle the subassemblies, thus reducing the immobilization time of the vehicle and possible hydraulic fluid drainage on the road, endangering the safety of the others involved in traffic. The device is also capable of transmitting data from pressure and flow sensors to a smartphone, tablet, or to desktop PC via a wireless module. It can also be produced with an integrated display for rendering the measured values as well as with the possibility of storing this information.



Fig. 1. The portable equipment

The usefulness of this equipment is due to the poor quality of roads in some areas that puts the power steering's under a lot of wear and tear, they over the operating limit designed by the manufacturer. This new device, very much needed in the field of repair and maintenance, it also reduces the time with the defects repair due to the flexibility offered by the data transmission system, with which information's can be sent to a repair specialist of the hydraulic power steering boxes. The device is also capable of generating a test report, which it can then be passed on to a specialist who can accurately determine the cause of the fault and the solution needed to repair the servo-hydraulic system. This portable test device is been produced in Romania being only one with sensors and data transmission. In fig.2 it can be seen a block diagram with the components of the portable test equipment and the informatics data transmission system and local display.

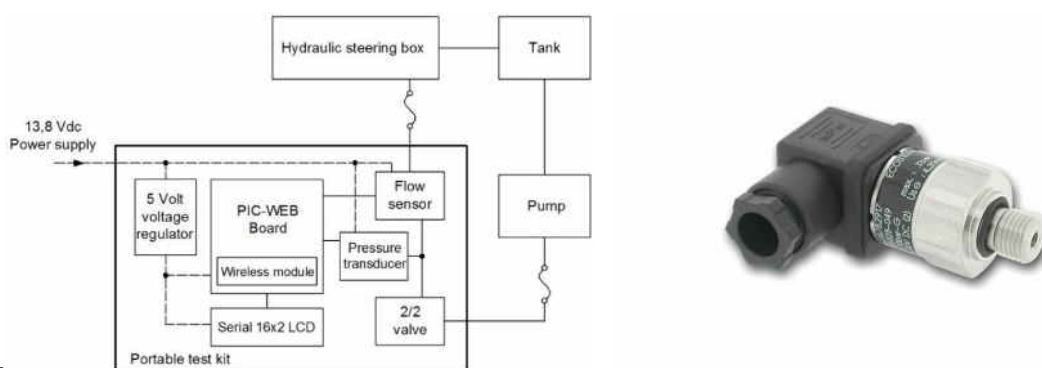


Fig. 2. Block diagram and the transducer circuit of portable test equipment with data transmission

The portable test equipment is composed of several sensors needed to record the parameters which are critical to determine the condition of the steering box. The sensors used in the hydraulic scheme are: pressure sensor with a domain of 0-160 bar, flow sensor 0,1-12 l/min [2]. All the sensors are connected to the input ports from Pic Web Board. The equipment is supplied with electricity from the cigarette lighter socket on the vehicle. Electrical connection of the microcontroller can be seen in figure 4. The pressure and flow transducer are powered by a voltage of 13.8 V, and the PIC-Web and the liquid-crystal electronic module are powered by 5 V via a voltage regulator integrated circuit. The pic-web module is provided with an optional wireless



Web module. Viewing test data and recording data is done by accessing the application through a web browser on any mobile device (phone or tablet). Connection of the mobile device to the web application is done wirelessly by accessing the IP address of the web application. Connecting to the web application can also be done with a desktop PC via an Ethernet cable, the Pic-Web module being equipped with an RJ45 Ethernet connector.

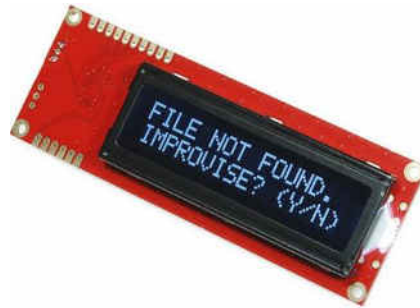


Fig. 5. Serial LCD display

All the data recorded it will be compared with those in the database and the system will decide whether the data recorded for the hydraulic steering box comply with the standards accepted by its manufacturer. In the software application page, the parameters obtained from the test can be seen and it is possible to record the data such as: name of the operator that perform testing, beneficiary of the test report, date and registration number of the test report. With this portable test device can be determined the rate of oil leakages at the stroke ends of steering box or in the middle of the stroke of hydraulic cylinder (the car wheels in the center position). The leakage rate is determined by the wear of the piston and rotary valve seals. The panel of the software application displays data obtained from testing. If the flow of loss at the end of stroke is above 1.5 l / min (fig.6) is recommended to replace or repair the steering box. A steering box worn, with large internal losses, will lead to disturbance in handling the power steering.

In order to issue the test report, in the software application the information for the beneficiary, the test operator and the test date must be noted. Once the data has been filled in, it will be possible to save a file containing the test parameters and identification data (report number, date, beneficiary, etc.).

The software it is design in a web browser that it can be modified to show the pressure and flow registered by the mobile test equipment's sensors, also the software it can make a process rapport that it can be sent by email or SMS directly to the power steering box parts supplier, ho figure the service needs of repair parts. Also the software can print the report for a documented evidence of the repair.

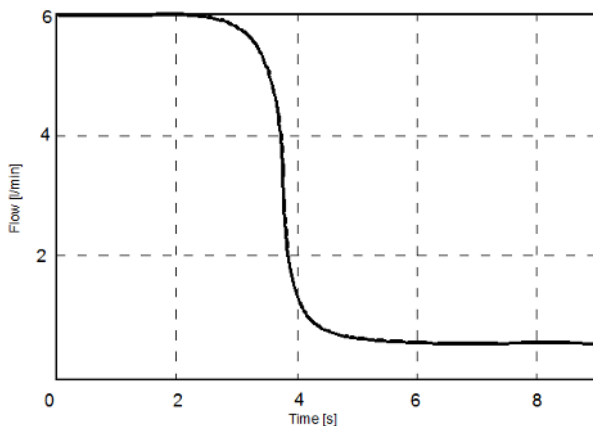


Fig. 6. Flow diagram

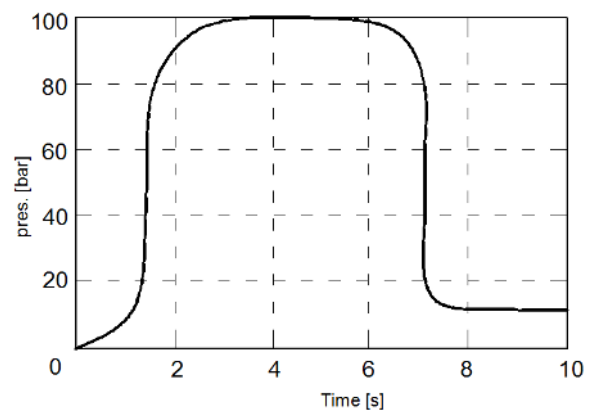


Fig. 7. Pressure diagram

#### 4. Conclusions

The test portable equipment with data transmission allows quick testing of the hydraulically assisted steering system without the need to dismantle the parts from the car.

An advantage of the device lies in its capability to transmit data that is collected by flow and pressure transducers and sent to a mobile device (smartphone or tablet) or fixed (PC) using Wireless technology.

Through the web application can issue test reports with data transmitted wirelessly from the test equipment, which can then be archived.

The amount of sensors and the domain of them, determine how accurate is the report for increase the road safety and human loses due to malfunction of hydraulic power steering.

#### Acknowledgements

This work has been funded by Executive Unit for Financing Higher Education, Research, Development and Innovation - UEFISCDI, under PNCDI III - Programme 2, Subprogram 2.1 – Cheques of Innovation (CI-2017), Submission code PN-III-P2-2.1-CI-2017-0229, Financial agreement no. 3CI/2017, project title: Portable test equipment for the power steering of vehicles with data transmission, project acronym ETSAD, Project main domain: 2. Information of technology and communications space and security, Subdomain: 2.3. Security

#### References

- [1] P.A. Adegbuyi, I.L. Marcu, “Hydraulic and pneumatic cylinder failures, the effect of fluid cleanliness on component life”, *Hidraulica Magazine*, ISSN 1453-7303, Romania, no.1, pp. 27-30, 2013;
- [2] A. Marin, P. Drumea, M. Blejan, I. Ilie, “Informatics platform for determining the dynamic performances of a two stage servo valve”, *5th International Industrial Simulation Conference*, Delft, Netherlands, June 11-13, 2007, pp. 151-154, ISBN: 978-90-77381-34-2;
- [3] <https://www.olimex.com/Products/PIC/Development/PIC-WEB/resources/PIC-WEB-manual.pdf>.

### Collaborators of our journal from abroad over recent years (2013-2017)

Name	Affiliation	Country	Journal issue
<b>Rudolf SCHEIDL</b>	Johannes Kepler University Linz	Austria	Iss. 1/2013
<b>Helmut KOGLER</b>	Johannes Kepler University Linz	Austria	Iss. 1/2013
<b>Bernd WINKLER</b>	Linz Center of Mechatronics	Austria	Iss. 1/2013
<b>Patrick Adebisi Olusegun ADEGBUYI</b>	Lagos State University	Nigeria	Iss. 1/2013
<b>Krzysztof KEDZIA</b>	Wroclaw University of Technology, Institute of Machines Design and Operation	Poland	Iss. 2/2013
<b>M. ELGADARI</b>	Université Moulay Ismail	Morocco	Iss. 2/2013
<b>Aurelian FATU</b>	L'Institut Pprime (P'), Université de Poitiers	France	Iss. 2/2013
<b>Mohamed HAJJAM</b>	L'Institut Pprime (P'), Université de Poitiers	France	Iss. 2/2013
<b>M. BELHAQ</b>	Université de Casablanca	Morocco	Iss. 2/2013
<b>Ing. Karol STRACÁR</b>	Institute of Chemical and Hydraulic Machines and Equipment, Slovak University of Technology, STU in Bratislava	Slovak Republic	Iss. 1/2014, Iss. 3/2014
doc. Ing. <b>Jozef KRCHNÁR</b> , CSc.	Institute of Chemical and Hydraulic Machines and Equipment, STU in Bratislava	Slovak Republic	Iss. 1/2014
doc. Ing. <b>Karol PRIKKEK</b> , CSc.	Institute of Chemical and Hydraulic Machines and Equipment, STU in Bratislava	Slovak Republic	Iss. 1/2014, Iss. 3/2014
<b>Andrea HARINGOVÁ</b>	Institute of Chemical and Hydraulic Machines and Equipment, STU in Bratislava	Slovak Republic	Iss. 1/2014, Iss. 3/2014
Prof. MSc. <b>Richard CASTRO</b>	School of Engineering, Criciúma	Brazil	Iss. 2/2014, Iss. 4/2014
Prof. MSc. <b>João NETO</b>	School of Engineering, Criciúma	Brazil	Iss. 2/2014, Iss. 4/2014
Prof. <b>Cleber IZIDORO</b>	School of Engineering, Criciúma	Brazil	Iss. 2/2014
Prof. MSc. <b>Anderson SPACEK</b>	School of Engineering, Criciúma	Brazil	Iss. 2/2014
Prof. MSc. <b>Oswaldo ANDO JUNIOR</b>	School of Engineering, Criciúma	Brazil	Iss. 2/2014
<b>Y.M. MORONA</b>	School of Engineering, Criciúma	Brazil	Iss. 4/2014
<b>K. MACHADO</b>	School of Engineering, Criciúma	Brazil	Iss. 4/2014
Prof. Dr. <b>A. S. ROCHA</b>	Federal University of Rio Grande do Sul - UFRGS, LdTM, Porto Alegre	Brazil	Iss. 4/2014
Prof. PhD <b>Gencho POPOV</b>	University of Ruse “Angel Kanchev”	Bulgaria	Iss. 4/2014, Iss. 1/2015, Iss. 2/2015

Name	Affiliation	Country	Journal issue
PhD <b>Boris KOSTOV</b>	University of Ruse “Angel Kanchev”	Bulgaria	Iss. 4/2014
PhD <b>Miglena HRISTOVA</b>	University of Ruse “Angel Kanchev”	Bulgaria	Iss. 4/2014
Asc. Prof. <b>Donka IVANOVA</b>	University of Ruse “Angel Kanchev”	Bulgaria	Iss. 4/2014
Asc. Prof. <b>Anka KRUSTEVA</b>	University of Ruse “Angel Kanchev”	Bulgaria	Iss. 4/2014
PhD. <b>Yuliyán ANGELOV</b>	University of Ruse “Angel Kanchev”	Bulgaria	Iss. 1/2015, Iss. 2/2015
Dr. <b>Mario PISATURO</b>	University of Salerno	Italy	Iss. 1/2015, Iss. 2/2016
Prof. Dr. <b>Adolfo SENATORE</b>	University of Salerno	Italy	Iss. 1/2015, Iss. 2/2016
Prof. PhD. <b>Ryszard DINDORF</b>	Kielce University of Technology	Poland	Iss. 2/2015
PhD. <b>Piotr WOS</b>	Kielce University of Technology	Poland	Iss. 2/2015
PhD. eng. <b>Sasko DIMITROV</b>	“Goce Delcev” University, Stip	Macedonia	Iss. 2/2015
PhD. eng. <b>Simeon SIMEONOV</b>	“Goce Delcev” University, Stip	Macedonia	Iss. 2/2015
PhD. eng. <b>Slavco CVETKOV</b>	“Goce Delcev” University, Stip	Macedonia	Iss. 2/2015
Assist. Prof. <b>Sunny NARAYAN</b>	Indus International University, Himachal Pradesh	India	Iss. 2/2015, Iss. 3/2015, Iss. 4/2015, Iss. 1/2016, Iss. 3/2016, Iss. 4/2016, Iss. 1/2017
PhD. stud. Eng. <b>Amir ROSTAMI</b>	Georgia Institute of Technology	USA	Iss. 3/2015
Prof. PhD. Eng. <b>Jeffrey L. STREATOR</b>	Georgia Institute of Technology	USA	Iss. 3/2015
Prof. <b>Basavaraj V.HUBBALLI</b>	Jain College of Engineering, Belagavi Karnataka	India	Iss. 3/2015, Iss. 1/2016
Dr. <b>Vilas B.SONDUR</b>	Sondur Academy, Belagavi Karnataka	India	Iss. 3/2015, Iss. 1/2016
Assist. Prof. M.Tech <b>M. HANIEF</b>	National Institute of Technology, Srinagar	India	Iss. 3/2015
Professor PhD. <b>M. F. WANI</b>	National Institute of Technology, Srinagar	India	Iss. 3/2015
<b>Aman GUPTA</b>	Indus International University, Himachal Pradesh	India	Iss. 4/2015, Iss. 1/2016, Iss. 3/2016, Iss. 4/2016, Iss. 1/2017
Prof. <b>Vincenzo D’AGOSTINO</b>	University of Salerno	Italy	Iss. 2/2016
Dr. <b>Claudia CIRILLO</b>	University of Salerno	Italy	Iss. 2/2016
Prof. Dr. <b>Maria SARNO</b>	University of Salerno	Italy	Iss. 2/2016

Name	Affiliation	Country	Journal issue
<b>Rosalva MENDOZA</b>	Engineering Institute, National Autonomous University of Mexico	Mexico	Iss. 2/2016
<b>Ramón DOMÍNGUEZ</b>	Engineering Institute, National Autonomous University of Mexico	Mexico	Iss. 2/2016
<b>Gerardo ACUÑA</b>	Engineering Institute, National Autonomous University of Mexico	Mexico	Iss. 2/2016
<b>Vikaram SINGH</b>	Indus International University, Himachal Pradesh	India	Iss. 3/2016
<b>Sujoy NAIR</b>	Indus International University, Himachal Pradesh	India	Iss. 3/2016
Prof. Dr. Ing. <b>Genovevo MOREJÓN VIZCAINO</b>	Superior Polytechnic Institute “José Antonio Echeverría” (Cujae), Marianao	Cuba	Iss. 3/2016
Ing. <b>Julio Ernesto HERNÁNDEZ MARTÍNEZ</b>	Superior Polytechnic Institute “José Antonio Echeverría” (Cujae), Marianao	Cuba	Iss. 3/2016
<b>Sanjay SINGH</b>	Indus International University, Himachal Pradesh	India	Iss. 4/2016
Prof. Dr. <b>Podalyro Amaral de SOUZA</b>	Escola Politécnica / USP, São Paulo	Brazil	Iss. 1/2017
<b>Dr. Eber Lopes de MORAES</b>	Escola Politécnica / USP, São Paulo	Brazil	Iss. 1/2017
<b>Dr. Maritza Liliana Arganis Juárez</b>	Universidad Nacional Autónoma de México	Mexico	Iss. 2/2017
<b>M. A. Juan José Baños Martínez</b>	Universidad Nacional Autónoma de México	Mexico	Iss. 2/2017
<b>M. I. Margarita Preciado Jiménez</b>	Instituto Mexicano de Tecnología del Agua	Mexico	Iss. 2/2017
Ing. <b>Cecilia González Correa</b>	Universidad Nacional Autónoma de México	Mexico	Iss. 2/2017
Assist. Prof. PhD. Stud. Eng. <b>Nikolett FECSER</b>	Széchenyi István University , Győr	Hungary	Iss. 2/2017, Iss. 4/2017

